Innovative Intelligent Sensors to Objectively Understand Exercise Interventions for Older Adults

By

Jianjia Ma

A Doctoral Thesis

Submitted in partial fulfillment of the requirements

for the award of

Doctor of Philosophy of Loughborough University

May 2019

To my dear wife, Xiang Chen

Abstract

The population of most western countries is ageing and, therefore, the ageing issue now matters more than ever. According to the reports of the United Nations in 2017, there were a total of 15.8 million (26.9%) people over 60 years of age in the United Kindom, and the numbers are projected to reach 23.5 million (31.5%) by 2050. Spending on medical treatment and healthcare for older adults accounts for two-fifths of the UK National Health Service (NHS) budget. Keeping older people healthy is a challenge. In general, exercise is believed to benefit both mental and physical health. Specifically, resistance band exercises are proven by many studies that they have potentially positive effects on both mental and physical health. However, treatment using resistance band exercise is usually done in unmonitored environments, such as at home or in a rehabilitation centre; therefore, the exercise cannot be measured and/or quantified accurately. Despite many years of research, the true effectiveness of resistance band exercises remains unclear.

A possible method to objectively quantify the effectiveness of these exercises is to use sensors systems. There are many motion capture systems available, such as smart wristband, full-body motion capture suit based on Inertial Measurement Unit (IMU), and camera-based motion capture systems. However, they are either too simplified and therefore cannot accurately measure specific exercises, e.g. smart commercial wristbands fit onto one hand but provide inaccurate step count to the user, or too complicated to set up before measuring, e.g. full-body motion capture suits or camera-based motion capture systems. As such, existing systems are not sufficient in measuring resistance band exercise remotely. A customised sensor system needs to be developed which capable of measuring remote exercise. Specifically, the goal is to answer the three main questions about remote exercise: “When was the exercise done?”, “What kind of exercise has been done?” and “How was the exercise done?”

In order to achieve the above goals, a sensorised resistance band system (called WBR-SH2) was developed, which aims to measure the resistance band exercise remotely and accurately. The design was based on the “nearable” concept to improve the technology acceptance among older adults and provide a user-friendly interface for novices to operate. The WBR-SH2 system uses two sensorised handles (based on IMU and load cell) and a smartphone to monitor the exercise objectively.

In a multiple sensors network, such as WBR-SH2 system, synchronisation is fundamental. The available synchronisation methods are either not accurate enough or require hardware modification on the smartphone. A novel synchronisation method is proposed in this thesis based on time-aligned transactions of Bluetooth Low Energy messages. This method was tested with a few Android devices in a network, including five sensor nodes, and achieved sub-millisecond accuracy. Which is around 150 times better than generic BLE time service.

Sensor nodes can generate massive data during the measurements, which results in the need for a lot of wireless bandwidth and power to transmit for post-analysis. Alternatively, doing data processing entirely or partially in the sensor nodes reduces the need for an external receiver. Neural networks are good at aggregating information and reducing the data dimensions but are also computationally expensive. The recent developments in complex neural network structure allow higher power efficiency and a reduction in the size of memory which makes memory-constrained platforms (such as microcontrollers) capable of running complex neural networks. However, there is no library currently available for microcontrollers which can support complex network structures. Therefore, a high-level Neural Network on Microcontroller (NNoM) framework was developed. NNoM organises the complex structure model by using a compiler to identify the connection and running sequence in between layers. It also provided a user-friendly interface, optimised performance and a set of validation tools for developers to develop and deploy their models onto microcontrollers.

As a proof of concept, experimental tests were undertaken both in the UK and in Italy to investigate the effectiveness of the proposed resistance exercise. The results proved that the WBR-SH2 system can recognise different types of exercises on its own without any external input from skilled operators, and can synchronise with Bluetooth Low Energy networks. A valuable resistance exercise dataset has also been collected, which can potentially help future researchers to understand and evaluate the resistance band exercise.

In conclusion, this work presents research and development of an intelligent sensor system, capable of answering all three questions in remote resistance band exercises: “When”, “What” and “How”. This work has the potential of contributing to future research in understanding the interventions with exercise, as well as other research fields requiring similar motion measurements, such as optimising athlete performance through objective exercise measurements, or help surgeons during their training and careers.

Acknowledgements

Foremost, I would like to express my sincere gratitude to my supervisor Prof. Massimiliano Zecca for the continuous support of the research, the insistent inspiring direct me to solve research problems, and his confidence in my ability to complete the PhD. He encouraged me to develop not only the skills of doing research great but also the skills to express ideas and being an independent thinker.

Besides my supervisor, I would like to thank Prof. Eef Hogervorst and Dr Vassilios Chouliaras for their encouragement, supports and comments which keep inspiring me thought out the PhD.

During the period of my PhD, the advice and guidance from Dr Daniele Magistro did much to help me to solve my research problem from the health science perspective. I would like to sincerely thank my colleagues Mr Ryan Sers, Mr Stephen Ward, Mr Junchen Ren for the discussion and their on-going support.

My sincere thanks also go to all my friends and family members for the generous help and the fun at all time.

In particular, I am grateful to thank my wife Xiang Chen for her closest supports and insisting. Last but not least, I would like to thank my parents Xianqiu Ma and Zujiao Huang, who are supporting me spiritually throughout my life.

Table of Contents

Abstract ..... **ii**

Acknowledgements ..... **v**

Table of Contents ..... **vi**

List of Figures ..... **xii**

List of Tables ..... **xix**

List of Acronyms ..... **xxi**

Chapter 1 Introduction **1**

1.1 Background 1

1.1.1 Ageing 1

1.1.2 Mental and Physical Health of Older Adults 2

1.1.3 Exercises Intervention Model 9

1.1.4 Couch Potatoes Resistance Exercise for Older Adult 14

1.1.5 Remote Exercise Measurement 14

1.1.6 Synchronisation in Wireless Sensor Network 19

1.1.7 Exercise Recognition with Machine Learning 20

1.1.8 Rethinking of Wearable Technology 20

1.1.9 Summary of Background 22

1.2 Problem Statement 24

1.3 Goals of this Thesis 25

1.3.1 Aims 25

1.3.2 Novelty 27

1.3.3 Contribution of this Research 27

1.4 Thesis Outline 28

Chapter 2 Preliminary Objective Exercise Measurement using Arm Curl Test 31

2.1 Introduction 31

2.1.1 Background 31

2.1.2 Problem Statement 35

2.1.3 Objectives 35

2.2 Methodology 36

2.2.1 Revised Arm Curl Test 36

2.2.2 Experimental Sensorised Resistance Band System 36

2.2.3 Experimental Setup 40

2.2.4 Available Measurements 42

2.2.5 Data Processing 43

2.3 Experiment 47

2.3.1 Results 47

2.3.2 Summary of Results 56

2.4 Discussion 57

2.5 Conclusion 58

Chapter 3 Development of the Sensorised Resistance Band System 60

3.1 Introduction 60

3.1.1 Background 60

3.1.2 Problems Statement 62

3.1.3 Objectives 66

3.2 Design of WBR-SH2 System 66

3.2.1 System Specification 66

3.2.2 Design Concepts 68

3.2.3 WBR-SH2 System Overview 71

3.2.4 Hardware Development 72
3.2.5 Mechanical Design 81
3.2.6 Firmware Development 86
3.2.7 Android App Development 89
3.3 Evaluation 90
3.3.1 Sensor Calibration 90
3.4 Overall System Performance of WBR-SH2 94
3.5 Preliminary Public Patient Involvement 96
3.6 Discussion 97
3.7 Conclusion 100

Chapter 4 Sub-millisecond Synchronisation of Bluetooth Low Energy Network 103

4.1 Introduction 103
4.1.1 Bluetooth Low Energy Overview 104
4.1.2 Related Works 107
4.1.3 Problem Statement 108
4.1.4 Objectives 109
4.2 Methodology 109
4.2.1 Synchronisation Method 110
4.2.2 Evaluation Method 116
4.3 Experiment 116
4.3.1 Experimental Setup 116
4.3.2 Evaluations Method 118
4.3.3 Experiment Protocols 119
4.3.4 Resources Consumption Analysis 119
4.4 Results 120
4.4.1 Test 1: Time Stability Test 120

4.4.2 Test 2: Network Initiating Stability Test 122
4.4.3 Computational Cost 122
4.5 Discussion 123
4.6 Conclusion 125

Chapter 5 Development of a Compact Neural Network Framework for Microcontroller 126
5.1 Introduction 126
5.1.1 Background 126
5.1.2 Problem Statement 128
5.1.3 Objectives 131
5.2 Methodology 131
5.2.1 Model Development Process 131
5.2.2 Quantisation 133
5.2.3 Deploy Quantised Mode to MCU 136
5.2.4 Development of NNoM 137
5.3 Experiment 148
5.3.1 Experiment Protocol 148
5.3.2 Data Processing 149
5.3.3 Convolutional Neural Network Classifier 150
5.3.4 Results 154
5.4 Discussion 157
5.5 Conclusion 158

Chapter 6 Resistance Band Exercise Recognition with Older Adults 161
6.1 Introduction 161
6.1.1 Background 161
6.1.2 Objectives 162
6.2 Methodology 162

6.2.1 Hardware Capability of WBR-SH2 162
6.2.2 Data Selection 163
6.2.3 Compact Classifier for Microcontroller 165
6.3 Experiment 170
6.3.1 International Experiment with WBR-SH2 170
6.3.2 Data Pre-processing 171
6.3.3 Evaluation 172
6.4 Results 173
6.5 Discussion 177
6.5.1 Results 177
6.5.2 Neural Network Power Efficiency on WBR-SH2 178
6.5.3 International Experiment 179
6.5.4 Reflection of WBR-SH2 179
6.6 Conclusion 180

Chapter 7 Conclusion and Future Directions 182
7.1 Backgrounds 182
7.2 Conclusions 183
7.3 Highlights of Outcomes 187
7.4 Future Directions 188
7.4.1 WBR-SH2 in Comprehensive Assisted Environments 188
7.4.2 Motion Diagnosis for Mental Health 189
7.4.3 Technical Improvement 190
7.4.4 Exploring New Research Fields 190

References 193

Appendix A Couch Potatoes for Cognition 204
A.1 Tummy Rotation 204

A.2 Straight Arm Pull 205
A.3 Cross and Pull 206
A.4 Leg Press 207

Appendix B Experimental Sensorised Resistance Band System 209
B.1 Design of Experimental Sensorised Resistance Band System 209
B.1.1 Objectives and Requirements 209
B.1.2 Hardware Design 209
B.1.3 Microcontroller 212
B.1.4 Sensors 213
B.1.5 Wireless Communication 215
B.1.6 Power Management & Battery Charger 216
B.1.7 Battery 216
B.1.8 Firmware 217
B.1.9 Mechanical Design 219
B.1.10 Working Prototype 222
B.1.11 Software Design 222

Appendix C Data Format for WBR-SH2 225

Appendix D Sensor Calibration of Experimental System 226
D.1 Sensor Calibration 226
D.1.1 Inertial Measurement Unit 226
D.1.2 Magnetometer 229
D.1.3 Load Cell Sensor 229

Appendix E Schematics and Layouts of WBR-SH2 231

Appendix F User Feedback of WBR-SH2 and Resistance Band Exercise 241

Appendix G List of Publications 242

List of Figures

Figure 1-1 Percentage of population aged 60 years or over by region, from 1980 to 2050 [1]. 1

Figure 1-2 Change in cognitive performance during the 2-year intervention (NTB=neuropsychiatric test battery.) [23]. 6

Figure 1-3 Box plots of raw data for Alzheimer's disease assessment scale-cognitive subscale (ADAS-cog) at baseline and six and 12 months. Data are median (central line), interquartile range (box margins), adjacent values (whiskers), and outliers (dots) [34]. 8

Figure 1-4 Traditional exercise intervention model. Patients do exercise at home and frequently visit the hospital for assessment. 10

Figure 1-5 Wristband Approach example. User does exercise (walking), whilst the wearable sensor (wristband) measures and quantitates the exercise (step counts). It is user's options whether to use the feedback or not or how to use the feedback. 11

Figure 1-6 Improved Wristband Approach. Instead of leaving feedback to user, this approach involves an expert to generate a personalised report for the user. 12

Figure 1-7 Improved model using remote assessment. The measurement was in the hospital is extended to the user's home by remote sensors..... 13

Figure 1-8 Exercise intervention with remote exercise measurement tools [48]..... 13

Figure 1-9 Weight lifting with sensorised weights and wearable IMUs. [61] 19

Figure 1-10 The overall thesis structures. 30

Figure 2-1 Traditional Arm Curl Test [83]. 33

Figure 2-2 A set of resistance bands equipment. Different colours on the resistance band indicate different strengths. There are also some accessories, including handles, for various exercises. 34
Figure 2-3 Resistance band with a handle 35
Figure 2-4 Side by side comparison of the traditional handle and experimental sensorised handle. 40
Figure 2-5 Revised Arm Curl Test. The band is fixed by foot, and the user lifts the handle from waist to shoulder then release to the initial position..... 41
Figure 2-6 Raw data plotting and distractions (marked by the red circle)..... 44
Figure 2-7 Peak force associated with zero crossings of rotation..... 45
Figure 2-8 Start point estimation of the first curl. 46
Figure 2-9 Subject 1 segmented force data..... 47
Figure 2-10 Subject 2 segmented force data..... 48
Figure 2-11 Example of the 4 key timing points..... 49
Figure 2-12 Rising time of each repetition. 50
Figure 2-13 Falling time of each repetition. 50
Figure 2-14 Duration of each repetition..... 51
Figure 2-15 Standard error of rising time. 51
Figure 2-16 Standard error of falling time..... 52
Figure 2-17 Standard error of duration. 52
Figure 2-18 Peak force..... 53
Figure 2-19 Standard error of peak force..... 53
Figure 2-20 The frequency trends..... 54
Figure 2-21 Maximum rotation of lifting..... 54
Figure 2-22 Standard error of maximum rotation of lifting..... 55
Figure 2-23 The potential energy. 55
Figure 2-24 The average power in lifting. 56

Figure 3-1 Conventional wireless sensor system structure. Consist of a few sensor nodes, a wireless adapter, a dedicated PC and customised software. 61

Figure 3-2 New sensor system model. Instead of using a customised wireless adapter, the sensors send the data to the user's smartphone through a standardised wireless network, such as Bluetooth. The data is then processed on the remote servers. 63

Figure 3-3 Concept of the experimental system. The system is consist of the mainboard, battery, extension wires, remote load cell and load cell driver. 65

Figure 3-4 Concept 1: All electronics placed in one customised box. This concept aims to minimise the customised parts and to reuse most commercial part handles. 69

Figure 3-5 Concept 2: Redesign the casing of the experimental system. The handle housing will be rebuilt completely. 70

Figure 3-6 The WBR-SH2 system overview. The system is consist of a set of sensorised resistance band handle and a smartphone with a customised App. (Not scaled) 72

Figure 3-7 Block diagram of WBR-SH2. 73

Figure 3-8 Main circuits of WBR-SH2 (version 2.0). 74

Figure 3-9 Radio Frequency circuits layout. The RC components are marked in red rectangle C23, L3, C22, L4, L5 and the ceramic chip antenna..... 78

Figure 3-10 Luggage weight scale disassembly. The red square indicated the customised load cell. 79

Figure 3-11 One of the two halves housing. The three compartments are separated by the highlighted wall and the supporting wall under the main circuit. 82

Figure 3-12 Assembly view of the housing. The housing mostly consists of flat surfaces and perpendicular walls. Two halves are secured by M3 screws and nuts. 83

Figure 3-13 Load simulation using ABS materials (half view). 84

Figure 3-14 Load simulation using ABS materials (assembly view). 85
Figure 3-15 Comparison of WBR-SH2 prototype (left) and commercial off-the-shelf handle (right)..... 86
Figure 3-16 Working flow of WBR-SH2. The working flow includes many parallel tasks. These asynchronous tasks are scheduled by different priorities to ensure the most time-critical task is completed in time. 87
Figure 3-17 Load cell calibrations set up. 92
Figure 3-18 Cross-sensor stability of load cell. 93
Figure 4-1 (a) Connectionless-oriented BLE network. (b) Connection-oriented BLE network. 105
Figure 4-2 Simplified BLE structures involving Android and microcontroller. Layers marked by green shades are time-critical while others may not. Radio events are available in some microcontrollers which allows applications to access low-level timing. 106
Figure 4-3 Connection Event in BLE connection. 107
Figure 4-4 A completed Transition using WRITE transaction. 114
Figure 4-5 System view. (a). A connection-oriented BLE networks, consisting of one Android smartphone and 5 WBR-SH2. They are performing synchronisation. (b). The external testing device to capture pules and calculate sync error. 117
Figure 4-6 Distribution of synchronisation error for 5 sensors across tested Android Devices. 121
Figure 4-7 The distribution of synchronisation error in 12 initialling repetitions. 122
Figure 5-1 Example of latency in responding vs. processing platform. 129
Figure 5-2 Timeline of ML research outcomes for general purposes computers [130] compared to the implementation of MCUs, which is struggling at complex structures. 131

Figure 5-3 An example of developing NN classifier for edge device with a PC. The process contains 3 steps. 1). Collect a dataset for training the model. 2). Train the model. 3). Deploy the model into MCU for real-life data classification. 132

Figure 5-4 Working flow of training with the quantised output. 136

Figure 5-5 Framework of NNoM. NNoM provides three types of APIs for developers and supports two types of backends. Local backend is a pure C language implementation of NN functions while *CMSIS-NN backend [136] provides up to 5x performance for ARM Cortex-M MCUs. 138

Figure 5-6 NNoM layer-based showing an Inception structure. Each operation, i.e., convolution, dense, etc., is wrapped inside a layer. The multiple sub-paths are achieved by multiple Hooks..... 139

Figure 5-7 Layer structure. (a) Base layer class. (b) Extended layer classes..... 140

Figure 5-8 Basic topology for model structures and the corresponding construction APIs (a) micro-branch-structure, single layer's output data is sharing with multiple layers. (b) merging-structure, single layer takes multiple layer's output data as its input. 143

Figure 5-9 Layer compiler (*compile_layer()*) working procedure..... 144

Figure 5-10 Couch Potatoes for Cognition. The red arrow shows the movement of each activity..... 148

Figure 5-11 Sliding windows. Each segment overlapping the previous segment by two thirds. 149

Figure 5-12 Position-switched segment..... 150

Figure 5-13 Convolution Neural Network Architecture (ReLu layers are hidden)[75]. 151

Figure 5-14 Quantised model summary printed by NNoM (Rotated)..... 154

Figure 5-15 Confusion matrixes. (a) Original classifier using floating-point arithmetic on PC. (b) Quantised classifier using fixed-point arithmetic deployed to MCU. 155
Figure 6-1 The Inception structure contains multiple parallel paths which take the same data as input. The results are concatenated on channel-wises [120]..... 165
Figure 6-2 The Residual net structure contains skipping links from the input to the output of a block. The input data and output data of a residual block are merged by point-wise addition. [121], [122] 166
Figure 6-3 Dense Net contains a set of dense connection between each layer in a dense block. Data is concatenated on channel-wise. [123]..... 166
Figure 6-4 Compact classifiers with Inception structures..... 169
Figure 6-5 Age distribution among participants 171
Figure 6-6 Accuracy comparison. Training with the floating-point model, testing on the floating-point model, and testing on the fixed-point model. 174
Figure 6-7 Confusion matrix comparison of the floating-point model on the PC and the fixed-point model on the MCU. Model size in the small configuration... 175
Figure 6-8 Confusion matrix comparison of the floating-point model on the PC and the fixed-point model on the MCU. Model size in the medium configuration. 175
Figure 6-9 Confusion matrix comparison of the floating-point model on the PC and the fixed-point model on the MCU. Model size in the large configuration.... 176
Figure 6-10 Confusion matrix comparison of the floating-point model on the PC and the fixed-point model on the MCU. Model size in the classic configuration. 176
Figure A-1 Tummy rotation [49]..... 205
Figure A-2 Straight arm puling [49]. 206
Figure A-3 Cross and pull [49]. 207

Figure A-4 Leg press [49]. 208
Figure B-1 Board layout (top view) 210
Figure B-2 Board layout (bottom view) 210
Figure B-3 Configuration block diagram 212
Figure B-4 Load cell sensor. 215
Figure B-5 Working flow of the experimental system. 218
Figure B-6 Upper half of handle housing. 220
Figure B-7 Lower half of handle housing. 221
Figure B-8 Housing of load cell sensor. 221
Figure B-9 Side by side comparison of the traditional handle and sensorised handle. 222
Figure B-10 Data recorder. 223
Figure E-1 Circuit schematics of WBR-SH2 motherboard (1/5). 233
Figure E-2 Circuit schematics of WBR-SH2 motherboard (2/5). 235
Figure E-3 Circuit schematics of WBR-SH2 motherboard (3/5). 236
Figure E-4 Circuit schematics of WBR-SH2 motherboard (4/5). 237
Figure E-5 Circuit schematics of WBR-SH2 motherboard (5/5). 239
Figure E-6 Top-layer layout of WBR-SH2 motherboard. 239
Figure E-7 Ground-layer layout of WBR-SH2 motherboard. 239
Figure E-8 Power-layer layout of WBR-SH2 motherboard. 239
Figure E-9 Bottom-layer layout of WBR-SH2 motherboard. 240
Figure E-10 Assembly of WBR-SH2 motherboard. 240

List of Tables

Table 1-1 A comparison of tracking technologies....23
Table 2-1 List of key parameters can potentially quantitate the ACT 37
Table 2-2 Sensorised resistance band handles of the experimental system 38
Table 2-3 The available sensors on the experimental system 42
Table 2-4 Extracted features 42
Table 3-1 Product Design Specification of WBR-SH2....66
Table 3-2 Comparison of the two concepts.....71
Table 3-3 Main characteristics of sensors in WBR-SH2 74
Table 3-4 1mm thickness 7268 4-layer PCB structure by JLCPCB [95] 77
Table 3-5 Linear regression parameters.....93
Table 3-6 Performance comparison of the experimental system and WBR-SH2.....95
Table 4-1 Selected Android Device (Ranked by CPU performances)....118
Table 5-1 Available software packs in different platforms 130
Table 5-2 Pre-Built Layers....141
Table 5-3 Layer structures of the Neural Network Classifier 151
Table 5-4 The Q-format of output and trainable parameters....152
Table 5-5 Top-1,2 accuracy comparison 155
Table 5-6 Summary of comparison....156
Table 6-1 Summary of available data in WBR-SH2....163
Table 6-2 Trainable layer configuration of the classifier 169
Table 6-3 Complexity and performance comparison in different configurations.....173
Table B-1 Main Characteristics of the Sensors....211
Table B-2 Communication protocol between sensorised handle and PC 224
Table C-1 Raw data frame structures.....225

Table C-2 CSV file recorded by SmartBand App 225

Table D-1 Calibration results for gyroscope and accelerometer 228

Table D-2 Magnetometer calibration results 229

List of Acronyms

AAHPERD	American Alliance for Health, Physical Education, Recreation & Dance
ABDC	Advance Battery Data Char
ABS	Acrylonitrile Butadiene Styrene
ACT	Arm Curl Test
ADC	Analog to Digital Converter
AI	Artificial Intelligence
AME	Address Matched Event
AP	Anchor Point
API	Application Programming Interfaces
BLE	Bluetooth Low Energy
BMI	Body Mass Index
CAIDE	Cardiovascular Risk Factors, Aging, and Dementia
CAN	Controller Area Network
CC	Config Char
CCM	Core Coupled Memory
CE	Connection Event
CI	Connection Interval
CNN	Convolutional Neural Network
CPC	Couch Potatoes for Cognition
CPU	Central Processing Unit
CSV	Comma Separated Values
CT	Computed Tomography
DAPA	Dementia And Physical Activity
DMA	Direct Memory Access

DMP	Digital Motion Processor
DoF	Degree of Freedom
dps	Degree Per Second
EMG	Electromyography
FDM	Fused Deposition Modelling
FIFO	First-In-First-Out
FLOP	Floating-Point Operation
GAP	Global Average Pooling
GPIO	General-Purpose Input/Output
GSP	Global Sum Pooling
HAR	Human Activity Recognition
I2C	Inter-Integrated Circuit
IC	Integrated Circuit
IMU	Inertial Measurement Unit
IoT	Internet of Things
kNN	k-Nearest Neighbour
LDO	Low-dropout Regulator
LPF	Low-Pass Filter
MAC	Media Access Control, Multiply-Add/Accumulate
MCU	Micro Controller Unit
MEMS	Micro-Electro-Mechanical System
MRI	Magnetic Resonance Imaging
NHS	National Health Service
NN	Neural Network
NNoM	Neural Network on Microcontroller
ODR	Output Data Rate
PCB	Printed Circuit Board
PDS	Product Design Specification

PDU	Protocol Data Unit
PLA	Polylactic Acid
PLA	Polylactic Acid
POSIX	Portable Operation System Interface
PPG	Photoplethysmogram
PPI	Public Patient Involvement
ppm	parts-per-million
PWM	Pulse Width Modulation
RACT	Revised Arm Curl Test
RAM	Random Access Memory
RBS	Reference Broadcast Time Synchronisation
RCC	Raw Ctrl Char
RRDC	Real-Time Raw Data Char
RTOS	Real-Time Operating System
SDIO	Secure Digital Input Output
SDK	Software Development Kit
SoC	System-on-Chip
SPI	Serial Peripheral Interface
SVM	Support Vector Machines
TAM	Technology Acceptance Model
TPSN	Timing-sync Protocol for Sensor Networks
UART	Universal Asynchronous Receiver-Transmitter
USB	Universal Serial Bus
WBAN	Wireless Body Area Network
WHO	World Health Organization
WSS	WBR Sensor Service

Chapter 1 Introduction

1.1 Background

1.1.1 Ageing

The global ageing issue now matters more than ever. According to the reports of the United Nations in 2017 [1], about 12% of people are aged 60 years or over globally. Figure 1-1 shows the projected percentage of older adults. In 2050, older adults are projected to account for one in five people globally. Europe is the most critical area in which over 25% of the population is predicted to consist of older adults by 2020. The ageing problem in the UK is also significant, there were a total of 15.8 million (26.9%) people over 60 years of age in 2017, and the numbers are projected to reach 23.5 million (31.5%) by 2050.

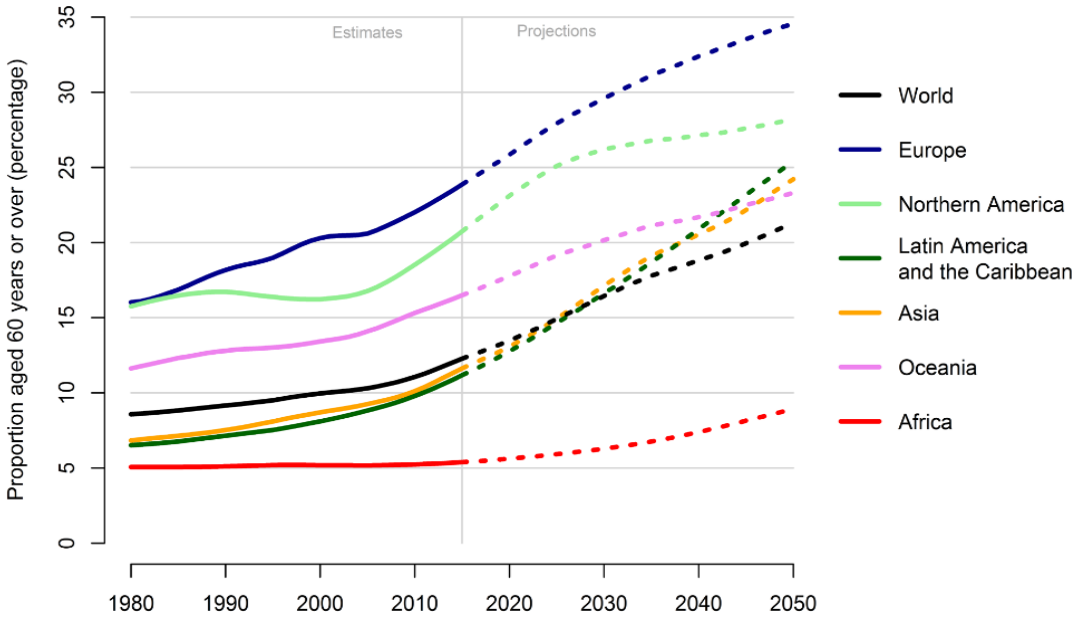

Figure 1-1 Percentage of population aged 60 years or over by region, from 1980 to 2050 [1].

An ageing society impacts many aspects such as pensions, healthcare, economics, taxes, and so on. Especially in the UK, the spending on medical treatment and healthcare for older adults takes two-fifths of the NHS budget [2]. Health spending per

person steeply increases after the age of 50, with people aged 85 and over costing the NHS an average of £7,000 per person per year. Although the impact on the NHS is tremendous, it is only a small part of the significant costs of which the majority is carried by older people and their families themselves. The health of older adults is also directly linked to the cost of medical help and healthcare. It is always more effective and cost-efficient to prevent instead of cure diseases.

1.1.2 Mental and Physical Health of Older Adults

1.1.2.1 Physical Health

Older people often suffer from poor physical health. Half of the people over the age of 80 was reported having long-standing physical problems in the survey of Adult health in Great Britain [3]. The survey revealed that 69% of people aged 75 and over reported having a long-standing illness compared with 15% of people aged 16–24. The WHO reports that those with physical health conditions, such as heart disease, have higher rates of depression than those who are physically well [4]. Results of a World Mental Health Survey published in 2007 highlighted that the risk of depression was over seven times more common in those with two or more long-term physical health conditions [4].

These age-related changes affect a broad range of physiological functions, such as muscular, cardiovascular, pulmonary, body composition and in general the physical functional capacities. Cumulatively, this could impact the preservation of the activities of daily living and independence in older adults [5], [6]. In general, a decrease in muscle functionality, that can compromise muscle mass, regional adiposity, muscle strength, and motor control is considered one of the most important physiological change during the ageing process [7]. This decrease is involved in the pathogenesis of frailty and disability that leads to decreased autonomy in the activities of daily living, increasing the risk of falls, and the consequent risk of morbidity and mortality [8], [9]. However,

muscle strength can be improved in older adults through strength training exercises [7], [10].

1.1.2.2 *Mental Health*

In 2015, over 20% of adults aged 60 and above were suffering from a mental or neurological disorder according to the report from WHO [11]. The two main issues affecting older adults' mental health are dementia and depression.

Dementia is caused by pathologies, such as Alzheimer's disease, consisting of plaques and tangles. Dementia affects people differently, especially in the early stages; how others respond to the person and how much support they get from their surrounding will greatly affect their quality of life [12]. Dementia is a rising global issue, widely affecting the lifestyles of older adults, with annual global costs in excess of $ 800 billion USD. It was estimated that 46.8 million people worldwide were living with dementia predicted to increase in 2015. This number is increasing to 74.7 million by 2030 [13], [14]. In the UK, dementia costs society an estimated £26 billion a year or on average £32,250 per person with dementia, this is more than the costs of cancer, heart disease or stroke combined [15].

Depression is another common issue among older adults which could lead to suffering and impaired functioning in daily life. Depression is characterized by sadness, loss of interest or pleasure, feelings of guilt or low self-worth, disturbed sleep or appetite, tiredness, and poor concentration [16]. Unipolar depression occurs in 7% of the general older population [11]. In England, depression affects around 22% of men and 28% of women aged 65 years and over [17], yet it is estimated that 85% of older people with depression receive no help at all from the NHS [18].

1.1.2.3 *Exercise Treatment for Mental and Physical Health*

The benefit of physical exercise for health is well known and documented. However, there are many studies which have not found this. Ageing is a complex

process that may lead to a decline in physical functions. The following sections will discuss both positive and negative evidence.

1.1.2.4 Positive Evidence of Exercise

Progressive resistance training using weight resistance devices is a popular approach for strength and conditioning. Previous studies showed that the use of weight resistance devices improved muscle strength, power, functional skills and muscle mass in older adults [6], [7], [19], [20]. Resistance band training could be defined as progressive strength training, where the workout is against an external force that is increased as strength increases [7]. Considering that in general, the older adult's population comprises of untrained or frailty older adults with functional limitations, i.e. with muscle and joint disorder, they may not be able to use the necessary weight required to produce positive muscle adaptation, due to the general physical inability, and decrease in motor control. Resistance-training program using resistance bands or tubing (e.g. TheraBands) to enhance their strength may offer a safe, inexpensive, and practical method for older adults [21].

The study done by Loughborough University with sedentary older participants (40-65 years old) showed that resistance exercise (30 min, 3 times a week for 12 weeks using resistance bands at home) had high adherence (88%) and improved memory, when compared to yoga exercises of a similar duration in an order, balanced cross over design [22]. However, the objective measurement and quantification of the exercises were limited to the number of repetitions and time. Also, the effectiveness of the form of exercise (such as how much, how long, how intense) in the exercise treatment was unknown.

The influence of exercise interventions is more significant in the long-term than the short-term. A large scale random-controlled 2-year multi-domain intervention with diet, exercise, and cognitive training to prevent cognitive decline in at-risk (Cardiovascular Risk Factors, Aging, and Dementia (CAIDE) with a Dementia Risk

Score of 6 points or higher) older adults was done by Ngando et al. in Finland [23]. 1260 elderly subjects were included in this study, with subjects separated randomly into 2 groups. One group was assigned to the intervention plan, while the other group was without intervention. Assessments of cognitive performance were done once a year, which was assessed at the beginning of the experiment, 1 year after the experiment began, and 2 years after the experiment began. The results are shown in Figure 1-2. It was clearly demonstrated that the long-term diet, exercise, and cognitive training intervention can slow down the cognition decline in at-risk older adults. Figure 1-2 shows the estimated mean change in cognitive performance from baseline until 12 and 24 months (higher scores suggest better performance) in the modified intention-to-treat population. Error bars are standard errors. Mixed-model repeated-measures analyses were used to assess between-group differences (group × time interaction) in changes

from baseline to 24 months based on data from all participants with at least one post-baseline measurement.

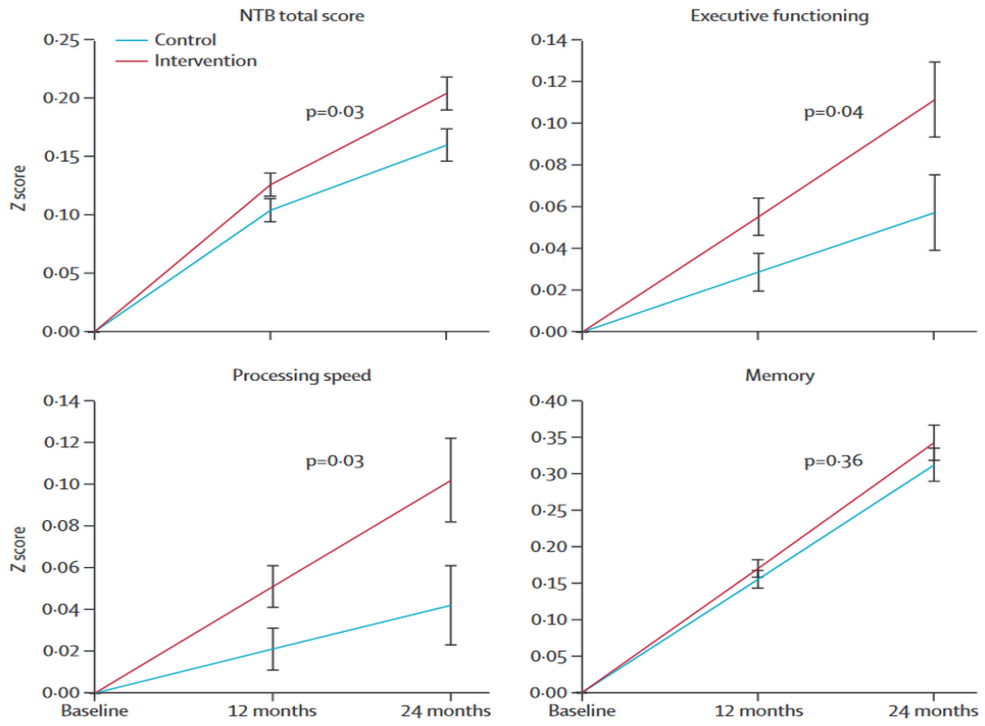

Figure 1-2 Change in cognitive performance during the 2-year intervention (NTB=neuropsychiatric test battery.) [23].

Many authors have also proposed that participating in physical and cognitive stimulating activities may improve memory, cognitive abilities and physical functions [24]–[27], in particular using resistance bands exercises [22], [28], [29].

In summary, exercises could have a positive influence on mental health among older adults in different aspects. However, it is not clear what kind of exercise is effective on what aspects of health specifically. In addition, many reviews have not shown constant beneficial effects of exercise for dementia or depression [30]–[32].

1.1.2.5 *Neutral or Negative Evidence of Exercise*

Although the above studies and others show that exercise benefits mental and physical health, there is limited definition of the intensity of exercise and the effectiveness of the exercise. A more recent study shows that exercise does not always benefit older adults with dementia [33].

The Dementia And Physical Activity [33] (DAPA) trial of moderate to high-intensity exercise for older adults was a long-term experiment involving abound 500 dementia subjects [33]–[35]. DAPA is an exercise intervention protocol which was developed for improving cognitive functions in older adults with mild to moderate dementia. Many experiments were done using DAPA with different configurations.

The experiment was done with 494 subjects in the timespan of 12 months [33], [35]. Two-thirds of the subjects were assigned with exercise intervention as an experimental group, while the others remained with normal care as the control group. The exercise intervention in this experiment was divided into 2 sessions, a supervised session and a un-supervised session. The supervised session required the subjects to attend a 1-hour exercise class twice a week for 4 months. The exercise performed during the class were targeting at 50 minutes' moderate-intensity to achieve a total of 150 minutes per week. The exercises performed were a combination of aerobic and resistance exercises. The second session lasted for 8 months, in which the subjects performed all 150 minutes' moderate-intensity exercise unsupervised. Phone calls were made approximately 2 to 3 weeks in the second session, and a single face-to-face meeting was completed during the second session to provide encouragement and assistance. The subjects were assessed before the experiment, at 6 months of the experiment, and at 12 months of the experiment using ADAS-cog score [34] which total scores ranging from 0–70, with higher scores ($\geq$ 18) indicating greater cognitive impairment. The result of the study is shown in Figure 1-3, where the middle lines of 2 groups in all assessments are similar, with the experimental group growing a little faster than the control group. Meanwhile, the diversity in the scores of the experimental group is larger than the control group.

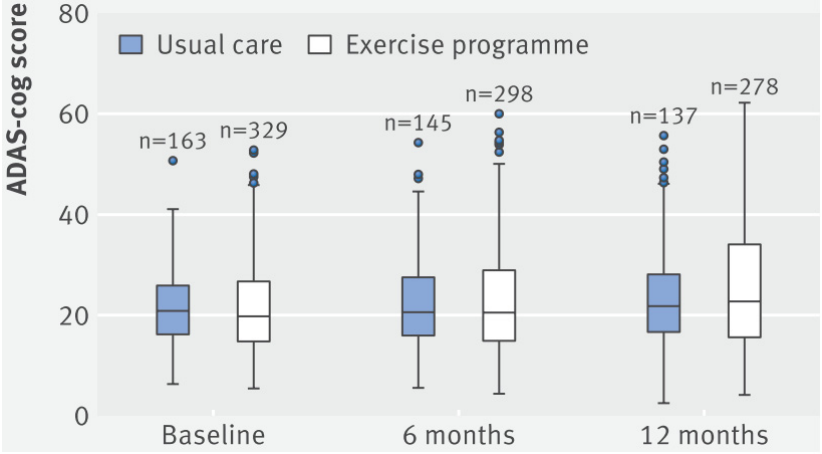

Figure 1-3 Box plots of raw data for Alzheimer's disease assessment scale-cognitive subscale (ADAS-cog) at baseline and six and 12 months. Data are median (central line), interquartile range (box margins), adjacent values (whiskers), and outliers (dots) [34].

DAPA was developed from the guidelines produced by the WHO, and the study completed a large-scale experiment including almost 500 subjects and 1-year timespan. However, the result shows that the effectiveness of DAPA intervention for some people with dementia is null or even slightly negative. The diversity of results is larger in the exercise group compared to the normal care group which indicates that some people have benefited from the exercise intervention, while others did not.

Reviews of exercise intervention for older adults with or without dementia are showing similar null effects for cognitive functions [30], [31], [36]. The reasons for the null or negative effects for some people in these studies might be due to the lack of personalised intervention plan for each individual.

1.1.2.6 Summary of Exercise Treatment

In general, exercise is believed to be good for young or older adults. However, without knowing the exact types and intensities of exercise which leads to positive effects, partaking in exercise could also be harmful to some individuals. Therefore, personalisation is necessary for optimal exercise treatment. Understanding the true effectiveness of exercise is the first step to generate a personalised exercise plan. This is a challenging multi-discipline problem, for which the research has received

innumerable effort and resources, but which remain uncertain. In most of the studies mentioned above, the two major difficulties encountered are, how to measure the exercise objectively, and how to quantitate the exercise. This is especially challenging when the subjects return home and do the exercises unsupervised.

In the resistance exercise intervention, the exercise is always done by subjects remotely in their home without direct observation by researchers or monitors. Some studies used self-reporting from the subjects to evaluate the adherence between agreed exercise plan and actual exercise completed [37], [38]. However, researches also point out that self-report is not reliable when it comes to exercise[39], [40]. Normally, studies with exercise intervention for older adults assessed the subjects on weeks or months basis [34], [41], [42], the development progress within the assessment interval are missed.

In summary, the major limitations of the above studies are the loss of exercise tracking during the exercise intervention. Thus, the key points to understand the exercise effectiveness is to be able to answer the three questions of “when”, “what” and how the exercise has been conducted remotely.

1.1.3 Exercises Intervention Model

In most of the previously mentioned studies, the tested subjects are assessed periodically either in hospital, a care home or in a laboratory environment, whilst most the exercises are done remotely at home. A review by Ashworth et al. [43] pointed out in most of the studies, home exercises are less effective compared to centre-based exercise in lab or hospital.

The traditional intervention models used by the studies discussed in section 1.1.2 are summarised in Figure 1-4. In this model, a comprehensive assessment of the person will be done periodically with instruments available in the lab or hospital. However, when the person goes home, all of the therapy trackings is completely lost until the next time the person visits the doctor. The exercise that the person at home has done at home

is unsupervised and unmonitored. When the doctor wants to know how the exercise was completed during this time to adjust the intervention plan, they must rely on the self-reporting from the person. However, self-reporting has been proved to be unreliable, especially for evaluating exercise [44].

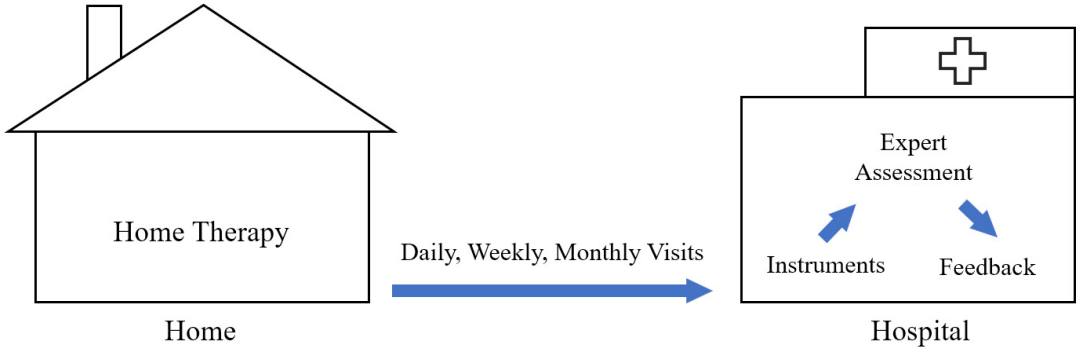

Figure 1-4 Traditional exercise intervention model. Patients do exercise at home and frequently visit the hospital for assessment.

Wearable sensors have become increasingly popular in recent years. The most represented devices are commercial smart wristbands and smartwatches. These wearable devices implement many sensors, including motion sensors to measure activities, heart rate sensors to measure heart rate and SpO2 to monitor oxygenated haemoglobin. They not only provide a more frequent measurement compared to the traditional model (shown in Figure 1-4) from daily/weekly/monthly to minutes/seconds but also provide quantitative exercise feedback to the user such as step-count, heart rate and so on. This model can be summarised as the "Wristband Approach" which is shown in Figure 1-5. In the Wristband Approach, exercise is objectively measured, and the aggregate information is provided to the user.

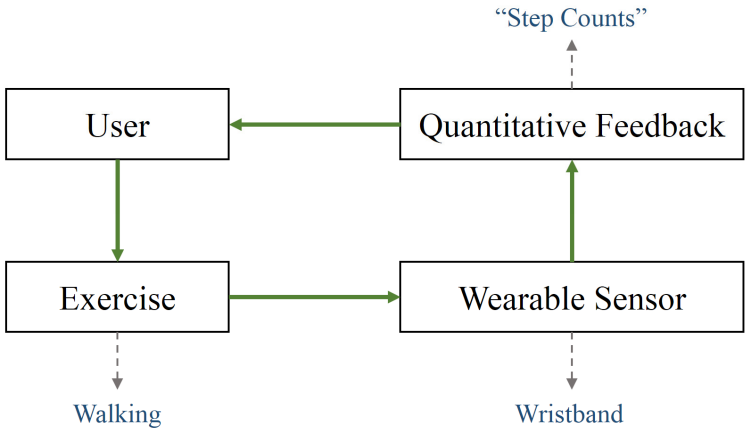

Figure 1-5 Wristband Approach example. User does exercise (walking), whilst the wearable sensor (wristband) measures and quantitates the exercise (step counts). It is user's options whether to use the feedback or not or how to use the feedback.

The objective measurement and aggregated feedback provided by the Wristband Approach should help people optimise the exercises, as they can get feedback about the exercise from the wristband directly. However, a recent study shows different results. A 2-year long-term experiment was done with 471 overweight volunteers (Body Mass Index (BMI) 25 to <40, age 18-45 years) who were asked to diet and do more exercise [45]. Half of the volunteers were given a fitness tracker to help themselves to monitor their exercise. The study results show the group which was given a tracker lost less weight than the other group. In summary, the devices which offer monitoring and feedback on physical exercise might not offer an advantage over standard behavioural weight loss approaches.

The reasons for the Wristband Approach failing could be summarised by:

1) The quantitative information is still meaningless for common users. Without involving the expert into the loop, the feedback to the user is less motivated and less reliable.
2) The activities information from these sensors is too generic. It is not feasible to determine whether a particular exercise plan has been completed to the required standard or if the exercise plan is effective.

3) Minimalist commercial motion sensors such as wristband, smartwatch or smartphone couldn't provide accurate enough measurement to assess the person and the exercise.

The improved Wristband Approach is shown in Figure 1-6, which can solve the above problems by involving an expert to assess and analyse the exercise and then provide the personalised reports to the user. In addition, the feedback and reports should be more convincing to the user if the reports and feedbacks are endorsed by the expert.

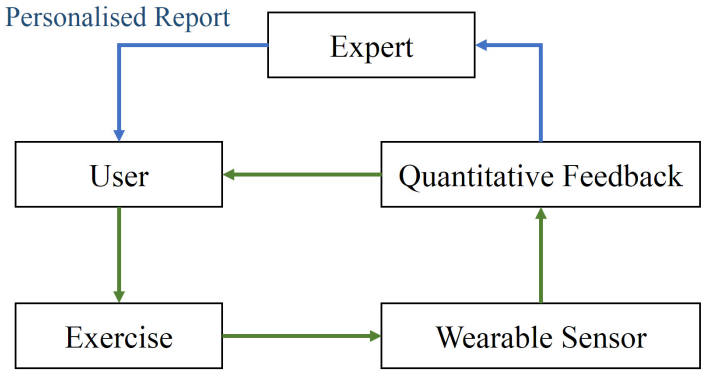

Figure 1-6 Improved Wristband Approach. Instead of leaving feedback to user, this approach involves an expert to generate a personalised report for the user.

An improved remote exercise intervention model is proposed in Figure 1-7. This model uses modern technologies such as sensors, data links, and artificial intelligence, to remotely assess the patient, therefore reducing the need to visit an assessment centre and improve the assessment duration. The remote measurement tools are one of the key components in this model, which extended the assessment from the hospital to the patients' home. This model takes advantage of the embedded sensors in people's home or the portable sensorised devices to allows remote assessment. With this model, the patient can be assessed in their home in real-time, therefore, the requirement to visit the hospital is reduced and improved continuous assessment can be achieved. The main challenge of this model is to miniaturise the assessments tools without losing the accuracy and functionality compared to what has provided in the hospital.

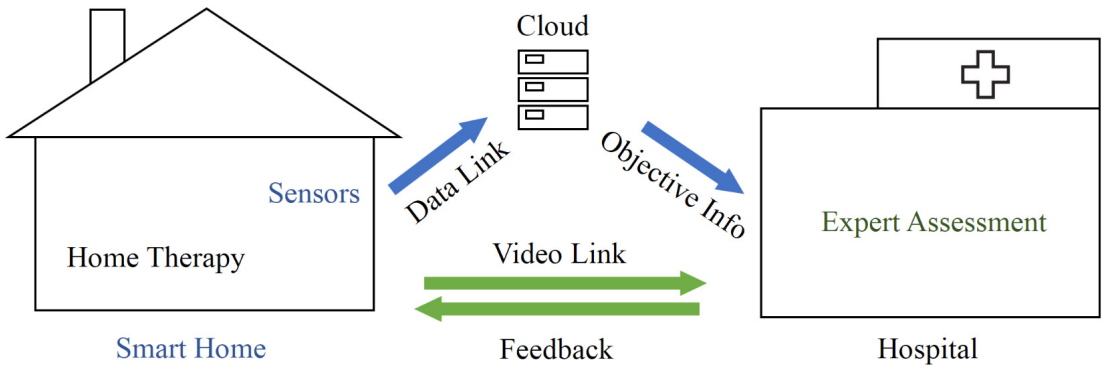

Figure 1-7 Improved model using remote assessment. The measurement was in the hospital is extended to the user's home by remote sensors.

A similar model (shown in Figure 1-8) was first introduced a decade ago (in 2009 by Waseda University [46], [47]). However, there is no effective implementation based on this model until now. The reasons why are easily seen. Accurate exercise measurement needs comprehensive tools, which are still expensive and require professional skills to operate, no matter if they are put in a patient's home or are located in a hospital. Novices or less capable older adults may have difficulty to operate the instruments.

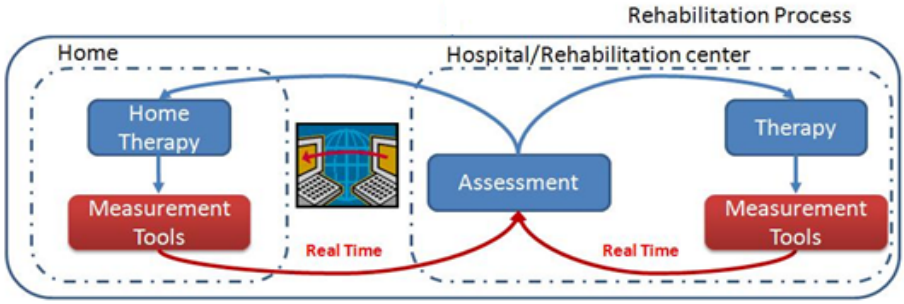

Figure 1-8 Exercise intervention with remote exercise measurement tools [48].

To summarise, the exercise interventions could not be done if any one of the following factors cannot be fulfilled: 1) remote objective exercise measurement, 2) involving experts, and 3) quantitative feedbacks. Above all, the remoted objective exercise measurement is the cornerstone of the exercise interventions. Although there are plenty of off-the-shelf products that could measure the exercise very accurately, they are still not suitable to be implemented into a user's home due to their complexity.

A few typical products using different technologies for motion tracking are discussed later in section 1.1.5.1. However, none of them can measure exercise while fulfilling all the needs at the same time. Thus, the purpose of presenting these approaches is to discuss the major limitation of the different types of technologies when applied to the exercise intervention model for long-term exercise measurement, real-time data collection, assessment and feedback. Further to establish the technological environment of building the exercise-specified nearable motion tracking sensors (in this case, the sensorised resistance band for resistance exercise) and evaluation tools which are proposed in the thesis.

1.1.4 Couch Potatoes Resistance Exercise for Older Adult

An existing exercise protocol called Couch Potatoes for Cognition (CPC) was selected for the focus of this thesis. CPC is a sitting resistance band exercise protocol for older adults was provided by Loughborough University [49]. The exercise protocol has been proved to have a positive effect on cognition functions for people with dementia [22]. The CPC protocol aims to improve the upper and lower body strength for older adults. The CPC provides benefits for working, climbing stairs, standing from a chair, holding items and the coordination of the arms and hands in daily tasks. The only 2 instruments needed for doing the workout is a set of resistance bands and a comfortable chair. CPC suggests that the workout should be undertaken at least twice a week, for 30 minutes each session. CPC includes 4 types of activities. Each activity was developed for the help of particular daily tasks, including climbing stairs, standing, coordination, getting dressed, preventing falls, shopping, washing/taking a shower, standing from a chair and gardening. The full protocol can be found in Appendix A.

1.1.5 Remote Exercise Measurement

Remote exercise measurement is the cornerstone to the implementation of the remote assessment model mentioned in section 1.1.3. The key aspect is to accurately

and continually track the motion of users while they are doing exercise at home. In this section 1.1.5, a few types of motion measurement system will be compared.

1.1.5.1 A Survey of Motion Tracking System

In order to measure remotely, a motion tracking system is required to operate independently in the user's home. Currently, there are a variety of commercially available products or systems in the markets for motion tracking. Depending on the technology of the tracking method, the available measurements are different, and the limitations are different.

1) Mechanical Trackers

Mechanical trackers have been developed and used for a very long time, and are still being widely used due to their high accuracy and low latency. The most significant characteristic of mechanical trackers is the subjects must wear a mechanical frame similar to exoskeleton without support from motors. Waseda University developed a Bioinstrumentation System WB-1 Motion Capture Systems for human-robot interaction [50]. The WB-1 system includes 12 Degree of Freedom (DoF) angular measurement per arm, with a total weight of 2.2Kg. The authors claim that the system has sufficient accuracy to measure human consciousness direction in an interaction between a human and a robot, in which application, motion tracking is the necessary condition.

However, mechanical measurement systems are relatively heavy, adding extra load to the user while they are partaking in exercise, and they potentially restrict the natural motion.

2) Camera-based System

Camera-based systems can be separated into marker-based or markerless systems. Intuitively, the difference between them is whether the system requires some visual makers to be worn on the human body to help the systems to capture the motion.

Marker-based camera systems (such as VICON [51]) are capable of tracking the motion of body accurately, however, the capture volume is limited, and the complexity of the system is high due to the requirement of multiple cameras and worn markers. On the contrary, markerless systems (such as Kinect [52], computer vision with regular RGB camera [53]) do not require the user to wear special marker for skeleton capture. Therefore, they are more feasible than a marker-based system in exercise. However, markerless motion capture has less accuracy if the line of sight is blocked. Additionally, both camera-based systems require subjects to do the exercise in a specific sensing volume, which is within the valid operating parameters of the capturing camera.

Due to the of reduced wearability in maker-based systems or accuracy with markerless systems, camera-based systems are not feasible for the remoted exercise measurement in people's home.

3) IMU-based Measurement

In the last decade, the development of Micro-Electro-Mechanical Systems (MEMS) technology has reduced both the size and the cost of small Inertial Measurement Unit (IMU) sensors. An IMU consists of a 3-Axis gyroscope, a 3-Axis accelerometer, and sometimes also a 3-Axis magnetometer. IMUs are motion sensors which measure motion directly. IMUs are already widely used in a variety of research areas including gait measurement, skeleton motion extraction, surgical training, rehabilitation training and so on.

Commercial products such as Perception Neuron can provide out-of-box solutions, one of which is a motion capturing suits which consist of multiple miniature IMUs, and the software for complete skeleton capturing [54]. The WB-2R/3/4 suit is a lightweight motion tracking suit developed by Waseda University, which provides flexible configuration of IMUs and biological signal sensors. The system was evaluated by multiple studies [55]–[57] for different motion tracking tasks, and the accuracy and functionality are outstanding. Those own-built IMU systems are event more flexible

compared to commercial systems in sensor configurations and different scenarios, such as having synchronised Electromyography (EMG) sampling and IMU sampling.

There are also variable products including smartphone and wrist band which implemented a small amount of IMUs (usually one) for simple motion capturing and analysis. They are capable of providing aggregated information on some common metrics, such as steps counting, sleeping monitoring and activity timing. Due to the number of IMUs (normally one in each product) inside the device is small, these products are not accuracy when monitoring exercises.

The largest advantage of IMU systems is flexibility. The scale of the IMU system range is from the complete full-body measurement, such as skeleton capturing, down to only one IMU measurement such as wristband or smartphone.

1.1.5.2 Summary of Motion Tracking System

The remote measurement of the exercise done by the person is still a challenge utilising the systems shown above. Mechanical systems are not feasible due to the distraction for natural movement. Marker-based camera systems are highly accurate but bulky and complex to operate. The markerless camera system is more portable but less accurate in motion tracking.

The IMU-based system is a balanced method for remote exercise measurement, due to its flexible configuration in between system complexity and usability. It allows researchers to customise the system, using different numbers of IMUs and position of IMUs.

However, the configurations of the off-the-shelf IMU-based systems are polarised, either full-body capturing suits with tens of IMUs or oversimplified with only one IMU. The full-body IMU suits are still too complex for novice and less capable older adults to operate, while the simplest one IMU devices are not capable of measuring the required detailed exercise data.

1.1.5.3 Exercise Assessments with IMU

IMUs have been widely used during research into different types of exercise evaluation, recognition, and quantisation. This is due to their miniature size, accuracy, and low latency measuring, and the flexible system size. In the previous discussion, some studies use IMU and traditional cognitive scores for cross-assessment of people with mental impairment, and the results show the clear relationship between the gait disorder and mental impairment [58]–[60].

The study done by Velloso et al. [61] focused on qualitative activity recognition of weight lifting exercises by a few wearable IMU units and an IMU attached to a dumbbell. The configuration of the experiment is shown in Figure 1-9. In total, 4 IMUs are used to capture the motion of the parts of interest, which was the upper arm, forearm, waist, and dumbbell. The data analysis is separated into 3 parts, detecting mistakes, specify exercises (exercise recognition), and providing feedback to subjects. 6 young subjects were asked to perform one set of 10 repetitions of the Unilateral Dumbbell Biceps Curl in five different fashions. The first class (Class A) is exactly following the exercise specification, the rest classes (B, C, D, E) are 4 different common mistakes, throwing the elbows to the front (B), lifting the dumbbell only halfway (C), lowering the dumbbell only halfway (D), and throwing the hips to the front (E). In the data pre-processing, 17 features are selected for 10-trees random forest classifier. The results show a 98.2% accuracy in all the data with 2.5second of sliding windows; however, when they trained the classifier with one subject for testing while other subject's data for training, the accuracy drop to only 78.2 %. A repetition counter together with the features extracted previously is modelled and provide to the user as feedback. In general, with the help of the feedback provided by the researchers, the subjects make 79.22% fewer mistakes in completing the biceps curl exercise.

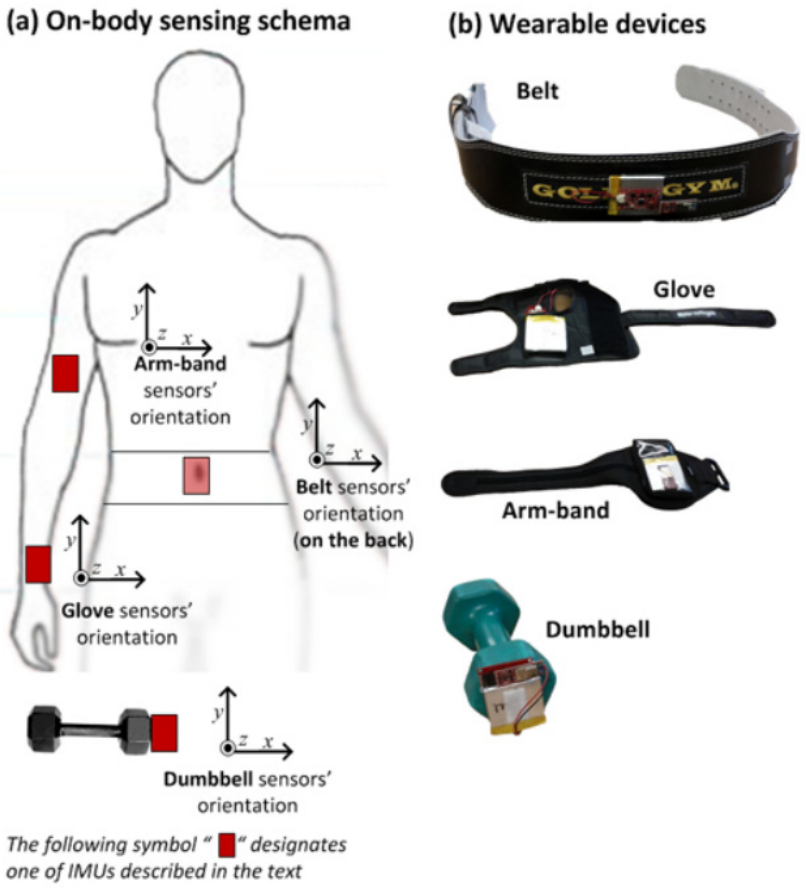

Figure 1-9 Weight lifting with sensorised weights and wearable IMUs. [61]

1.1.6 Synchronisation in Wireless Sensor Network

The proposed system should consist of multiple sensor nodes for detailed measurement in CPC resistance band exercise. Thus, the synchronisation between sensor nodes is fundamental to ensure the measurement in every sensor node is aligned on the same clock.

In a customised network with both ends (sensor end and central end) have fully MAC-layer (MAC) timestamp accessibility, the sensor network can be synchronised down to a few microsecond level accuracy [62]–[64]. When one of the ends has no access to MAC-layer timestamp, the synchronisation accuracy is unknown. This situation is very common when the sensor system involving a standardised device instead of a customised device as a data receiver, such as a smartphone.

1.1.7 Exercise Recognition with Machine Learning

Exercise recognition of IMU data is basically a feature classification application. A review by S.B. Kotsiantis [65] compared multiple supervised machine learning techniques including Decision Trees, Neural Network (NN), Bayesian Networks, k-Nearest Neighbour (kNN), Support Vector Machines (SVM). The author suggested that SVM and neural network tend to perform much better when dealing with multi-dimensions and continuous features, which is similar to the data produced by an IMU-based motion capture system.

Among SVM and NN techniques, NN classifiers have been proved to be effective in with IMU data for Human Activity Recognition (HAR) [66], as well as the implementation in gait analysis [67]. There are large quantities of studies on NN for different scenario IMU data classification [68], [69].

Normally, data from IMU is continuous measurements which then being segmented using a sliding windows technique. These segments then can be used as a training dataset to train a NN classifier, or as a testing dataset to evaluate the performance of a trained NN classifier. Public domain datasets are available, such as Human Activity Recognition Using Smartphones Data Set (UCI HAR [70]) which contains labelled 6-Axis IMU measurement (accelerometers and gyroscope data) in 6 different types of daily activities which were captured by a waist-worn smartphone. These datasets allow studies to validate and assess the performance of the customised classifiers before putting efforts for doing an experiment in similar scenarios.

1.1.8 Rethinking of Wearable Technology

Do wearable sensors really work in a real-life scenario? The question leads to another very important factor, which is the user's (the older adults') acceptance of using the wearable sensors. A study by Mercer et al. [71] recruited 32 older adults (ages over 60) to evaluate the acceptance of a few motion trackers using the Technology Acceptance Model (TAM). Among the participants, 31% had never used a smartphone

or tablet, while the others used one every day. This is already much lower than young people; 85% (age below 50) of them use a smartphone or a tablet every day [72]. In the analysis, many participants have suggested that the presented tracking devices are only for young people because those sensors are not easy to understand or operate. The authors claim that it is a barrier to the actual system use and can imply to the user that they should be able to use the device and that difficulties are a personal failing. Many participants also claim that they are only interested in the numbers, graphics but not motivated by them. This comment is similar to the limitation discussed earlier in the Wristband Approach (1.1.3 and Figure 1-5) which is the lack of involvement with experts making the data less understandable for the user or less convincing.

Further, the actual acceptance of the wearable devices is still questionable. The study done by Kim et al. [37] investigated the acceptance of two wrist bands in 20 older adult participants aged 55 years old. 80% of them accepted a non-screen wrist band (Xiaomi Mi Band), while only 50% of them accepted a screen writs band (Microsoft band). The results show a large portion of older adults might simply refuse to use these devices. Additionally, the screen with numbers (information) might not attract older adults as there is a concern that excessive information will expose their defects and their ability to be compared to others.

The concept of “nearable” might be a solution to the potential low acceptance problem among older adult. Nearable is an idea that implements sensors into a person’s environment instead of being worn by the person (wearable concept) [73]. Sensors using this concept could be fitted into the improved model for remote assessment (Figure 1-7) like the idea of “smart home”. Nearable sensors are not cumbersome to the end user since the nearables do not alter the objects they represent. The idea is a very promising solution to the acceptance problem among older adults who tend to stay in their comfort zone of conventional equipment and not like to interact with “fancy” and “smarts” sensors and equipment.

1.1.9 Summary of Background

Ageing is a global issue but of particular concern in the UK due to the higher portion of older adults (26.9% people over 60 in 2017 [1]). The consequences of an ageing society can be summarised greater burden on a variety of aspects such as social services, healthcare, and labour shortage. Keeping older adults physically and mentally healthy is a big challenge, but will effectively lower the impact on society. Exercises are proven to be effective for not only physical health but also to potentially benefit mental health in improving cognitive functions and alleviating depression in older adults. However, exercise can also be harmful if it has not been done correctly. Many studies have tried to investigate the relationship between exercise intervention and mental health, and the effectiveness of exercise intervention in improving mental health or benefiting neurological disorder such as dementia, to date, these have not provided a definitive conclusion.

Investigating the effectiveness of exercise and mental health is difficult due to the multidisciplinary nature of the problem itself. In most of the studies mentioned above, subjects are assessed over a long period (4,6,12-month interval). These long periods cannot provide the details of a disease's development or progression in shorter periods. Most of the studies have used supervised training at the beginning of their experiment, then followed by an unsupervised exercising plan. In the unsupervised session, researchers must encourage the subjects to follow the exercise plan by calling and visiting. To evaluate if the exercise has been done correctly, these studies have to rely on self-reporting from the subjects. Furthermore, it has been noted that self-reporting is not reliable in exercising scenarios [40].

Motion tracking remotely in people's home is a potential method to quantitate the exercise and provide a continual patient assessment. Potentially, the development progress of the mental disease can be assessed through motion measurement. It is therefore foreseeable that, a motion capturing system which can measure the exercise

continually in patient's home will help in both to investigate the true effectiveness of exercise intervention and the progress of the disease.

Many commercial (VICON, Kinect, Perception Neuron etc.) and customised motion tracking systems (WB-2R/3/4 etc.) shown previously in section 1.1.5.1, none of them is feasible for remote exercise measurement. Table 1-1 summaries the performance and limitations of the different technologies.

Table 1-1 A comparison of tracking technologies

	Accuracy	*Price*	*Wearability*	*Portability*	*Measurement volume*
Mechanical tracking	*Low*	*Low*	*Low*	*High*	*High*
Marker-based camera	*High*	*High*	*Mid*	*Low*	*Low*
Markerless camera	*Low*	*Low*	*High*	*Mid*	*Low*
Comprehensive IMU suits [a]	*High*	*Mid*	*Low*	*Mid*	*High*
Single IMU devices [b]	*Low*	*Low*	*High*	*High*	*High*
Customised IMU system [c]	*Mid*	*Low*	*Mid*	*High*	*High*

[a] Comprehensive IMU suits contain tens of IMUs which can provide a full-body measurement.

[b] Smartphones, smartwatches, wristbands and other devices contain single IMU.

[c] Customised measurement system with less than 10 IMU for interested parts measurement.

Among the listed technologies in Table 1-1, the customised IMU-based system with a small number of sensor nodes is a feasible choice for exercise measurement. The configuration of the IMU system is flexible between a comprehensive motion capturing system to simple system capturing only a few points of interest. The comprehensive system is not always required when measuring only a few certain exercises, this requires fewer measuring points to understand the exercise accurately. The IMU system can, therefore, be designed specifically for a certain type of exercise to reduce complexity. A sensor system for novice and less capable older adults must have good portability, wearability and be simple to operate. IMU systems are less environment-

dependent, which allows the system to be set-up fast and produces fewer restrictions on the subject while measuring. When using a customised IMU-based system for motion tracking, the trade-off must be made between the number of IMU nodes which correspond to the measurement accuracy of the exercise and the usability which must be easy to operate for novice and less capable user. Additionally, the mobility of transferring the system must be considered.

Finally, the gap between the acceptance of wearable sensors by older adults and the functionality of wearable sensors are still large. Wearable sensors can measure very useful data whilst many older adults refuse to use them. The reasons are sometimes very different, such as the sensor/APP/instructions are not easy to understand by older adults, or older adults are more inclined to stay in the comfort zone without electronics devices. The concept of nearable sensors brings undistracted measurement to the users which could be the solution of exercise measurement among older adults.

1.2 Problem Statement

Among studies discussed previously, there is a common need to measure exercise remotely, objectively and continually. Home exercise requires much less in time and resources costs compared to traditional centre-based intervention. Unless the exercise is supervised and instructed correctly at home, the home exercise is less effective than centre-based exercise. Therefore, objective and remote assessments are needed. Continuous measurement potentially provides tracking of the development progress in physical and mental disease. Once the exercise can be measured remotely, the experts could monitor the execution of the intervention continually. Commercial motion tracking systems are limited on measurement capabilities which require many preparations in setting up the system. For example, the VICON system requires the subject to wear retroreflective markers and calibrate cameras before the experiment can start. IMU systems could be feasible to undertaking the exercise measurement remotely, however, there are some limitations:

A) The comprehensive measuring tools, such as motion camera-based system or IMU-based motion tracking suits are too complicated to operate, while consumer wearable products such as a wristband, smart shoes, or smartphone itself are less capable of measuring exercise accurately. Nevertheless, most of the commercial measurement systems are for general measurement, which is too generic, so the operations of the systems are complicated (such as IMU suits) or inaccurate (such as smartphones, wristbands).

B) Getting data is only the first step of the complete intervention model. The raw measurement from sensors is meaningless for an expert or the user to read. Data processing and quantitative reports must be generated. There still a lack of analysis tools for specific exercises such as resistance band exercise.

C) The acceptance of new technologies (such as smartphone and wristband) among older adults is lower than younger adults. The sensor system or the sensorised instruments might be contradicted by the end-users (older adults).

D) The megatrend of informatic decentralisation indicated that the sensors should be capable of processing the collected data and only provide aggregated information to an upper receiver instead of raw data. Many commercial tools for exercise measurement are still sending raw data which cost more power, results in less battery time.

1.3 Goals of this Thesis

1.3.1 Aims

A less-general measurement tool designed for a specific exercise not only reduces the complexity of the system, by reducing the unnecessary sensing node and simplify the human-machine interfaces but is also superior to consumer wearable products (such as wristbands) by providing much more detailed data and higher accuracy. In the previous reviews, resistance exercise has the potential benefit for the older adults in both mental and physical health, and it comes with standard exercise protocols (Couch

Potatoes for Cognition [49], section 1.1.4). The resistance band is a common, portable, and standalone exercise instrument which does not require users to “wear” it. Making resistance band sensorised fit the idea of nearable, which does not disturb the user when unnecessary. Thus, resistance band exercises are chosen as the focus exercise in this thesis.

Therefore, the goal of this thesis is to research and develop an IMU-based sensor system for measuring resistance band exercise remotely and to research and develop the corresponding assessment methods for data collecting, processing, and exercise assessment. The goal can be separated into a few aims:

1) To develop a robust IMU-based sensorised resistance band system which can measure exercise objectively and remotely. Use the concept of nearable instead of wearable to improve the acceptance of older users. The sensor must be with the minimum operating difficulty, user-friendly interfaces, and provide very detail raw data.
2) To develop the methods and tools using the data provided from the sensorised resistance band for resistance exercise classification and exercise quantitation.
3) To implement the above assessment methods into the sensorised resistance band to provide more real-time feedback to the user, and to provide aggregated information directly from the sensor to reduce the dependency of the additional data receiver, such as a PC or smartphone.
4) To develop a time synchronisation method for the distributed sensor networks involving smartphone based on standardised communication protocols.
5) Finally, the sensorised resistance band and tools must be verified by real end-users, which are the older adults, with a complete exercise protocol to evaluate the functionality, the usability, and the limitations.

1.3.2 Novelty

This thesis demonstrates the general model for exercise intervention and the methodology for remoted exercise measurement and assessment.

The studies exploring exercise interventions are unreliable due to the lack of remote exercise measurement tools. This thesis proposes a sensorised resistance band system and related tools to allow exercise to be measured remotely.

The design of the sensorised resistance band system uses the concept of nearable instead of wearable. The wearable concept is to put sensors on the human body, while nearable is to implement sensors on the environment to reduce the interference of the user's daily life. Therefore, sensor acceptance by older adults might be higher than traditional wearable sensors.

A neural network on microcontroller framework has been developed (NNoM). It enables the possibility of not only the sensorised resistance band but also a wide range of edge devices to perform machine learning locally.

Two sets of Couch Potatoes for Cognition resistance band experiments were completed locally in the UK and in Italy with the developed sensor system. The dataset is the first to record the motion in the resistance band exercises with 50 participants.

1.3.3 Contribution of this Research

This thesis presents the research and development of a sensorised resistance band system for remoted exercise measurement which is not commercially available [74], [75].

Two sets of experiments were done with the sensorised resistance band system. The system fulfilled the requirements of remote resistance band measurement in varying degrees. It provides rich and real-time raw data and aggregated information for data processing [74], [75]

A neural network classifier was developed for resistance band exercise classification based on the experiment data [75]. The classifier achieves significant accuracy in variable testing data.

A novel synchronisation method based on Bluetooth Low Energy has been proposed with continuous synchronisation and no interference to original bandwidth [76].

A user-friendly neural network framework designed specifically for microcontroller called Neural Network on Microcontroller (NNoM) is developed. NNoM is capable of running state-of-the-art and complex NN models on a microcontroller with little effort.

Two datasets of resistance exercise are collected by the sensorised resistance band system. Both datasets record the exercise in detail with a wide range of participants, which are valuable for further research.

1.4 Thesis Outline

The thesis contains seven major chapters. The background information has been shown in this chapter. The reminders of the thesis chapters are listed below.

- Chapter 2 describes the preliminary resistance band experiment with Arm Curl Test using an experimental sensorised resistance band system.
- Chapter 3 introduces the development of the sensorised resistance band system (labelled WBR-SH2). The WBR-SH2 system has the same sensor configuration of the experimental system, however, the usability is improved dramatically.
- Chapter 4 presents a novel synchronisation method to synchronise multiple WBR-SH2s by an off-the-shelf Android phone based on generic Bluetooth Low Energy (BLE) protocols.
- Chapter 5 shows the development of the compact Neural Network on Microcontroller (NNoM) framework, the implementation of the framework to

Microcontroller Unit (MCU), and the evaluation of the neural classifier on the MCU.

- Chapter 6 presents the international experiment using WBR-SH2 with the range of people, including older adults, who is the real end-users of the system. The experiment data are analysed, and the feedback of the system are summarised.
- Chapter 7 finally concludes the contribution and limitation of this thesis and propose the futures research directions.

The structure of the thesis is shown in Figure 1-10.

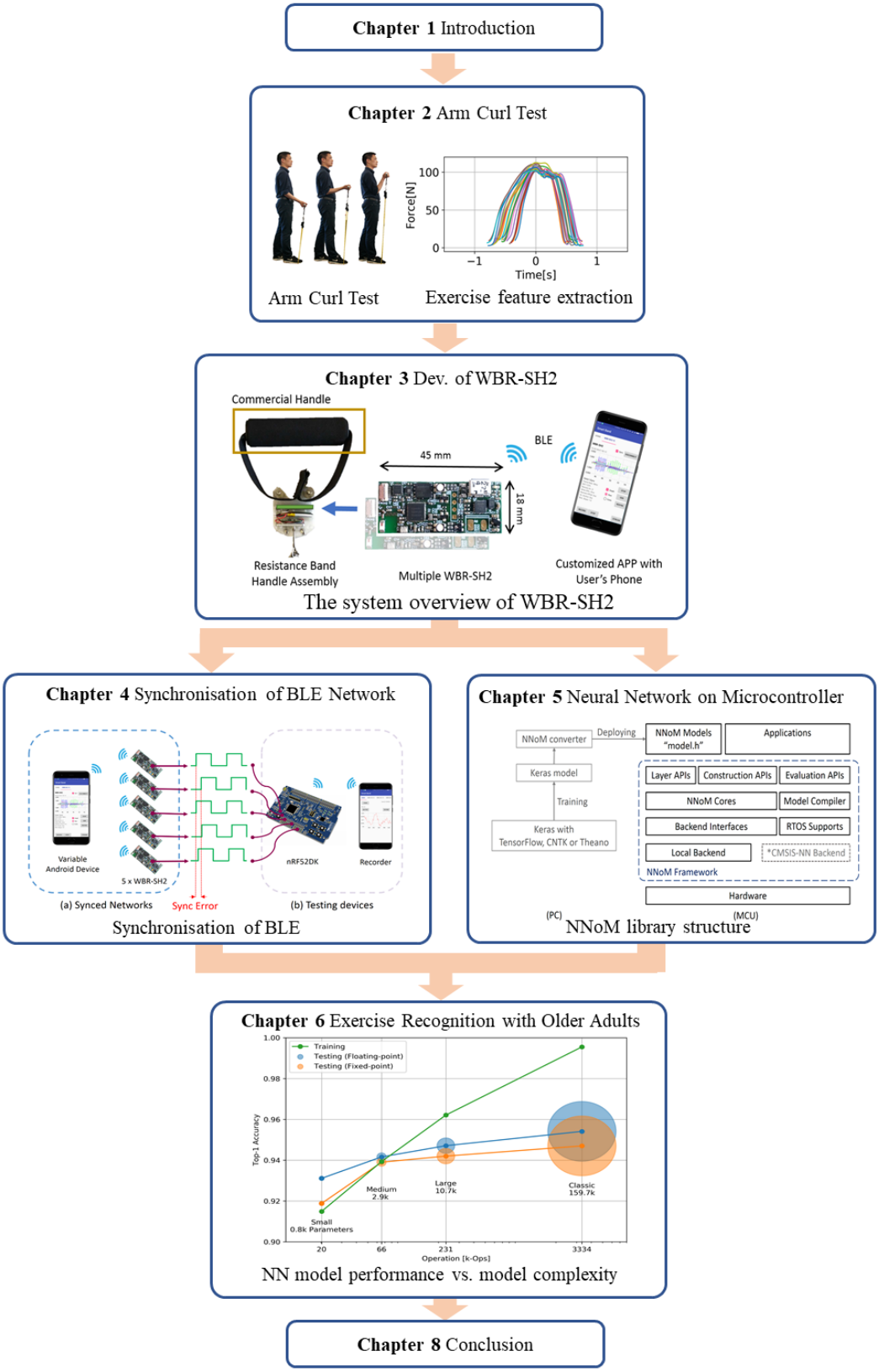

Figure 1-10 The overall thesis structures.

Chapter 2 Preliminary Objective Exercise Measurement using Arm Curl Test

2.1 Introduction

2.1.1 Background

2.1.1.1 Lack of Objective Exercise Measurement

Several scientific studies discussed in Chapter 1 have shown that resistance or strength training is beneficial in slowing the cognitive and physical decline of people suffering from mental problems, such as cognitive decline and depression. Resistance band exercise seems to be a potential intervention for older adults that suffer from memory and cognitive decline [22], [77], [78]. However, there are some critical limitations among these studies:

- The adherence between the agreed exercise plan and the actual exercise has been done is low. The evaluation of remote exercises is based on self-report, which is highly unreliable.
- The effectiveness of exercise is hard to measure due to the lack of objective exercise assessment.
- The development progress of the mental disorder cannot be tracked because the assessment intervals are long (4 months, 6 months or 12 months)
- No instant feedback to the person during unsupervised intervention sessions.

Compared to the drug treatment [23], [79], the exercise interventions on cognitive rehabilitation usually takes a longer time to be effective in many studies (normally months to show cognitive changes). Due to the relatively longer reaction time in exercise treatment, the studies in exercise intervention are less time-efficient, therefore, take longer periods to seem.

In general, the quantification of the resistance bands exercises is limited to the number of repetitions and total time. However, due to the variable loading patterns of resistance bands (greater stretch produces greater resistance) and other variants, simply counting the number cannot assess the performance accuracy. Ideally, the exact strength, intensity and speed can be used to identify the volume and intensity of training [80], therefore, to quantitate the exercise. Especially for older adults, there are large physical differences between individuals; it is fundamental to optimally assign tailored training programs to them. Prescribed resistance bands exercise could be too weak or too hard for some people, and consequently, they may be negatively affected. To understand the effectiveness of exercise, shorter assessment interval or continuous assessment is required, and objective exercise measurement is required.

2.1.1.2 *Arm Curl Test*

Arm Curl Test (ACT) is a part of the American Alliance for Health, Physical Education, Recreation & Dance Functional Fitness Test (AAHPERD), shown in Figure 2-1. This Chapter select ACT for the experiment protocols due to it is simple and well researched. The Functional Fitness Test was designed for adults over the age of 60 years[81], [82]. Compared to the more recent and more specific Couch Potatoes for Cognition (CPC) [49]), the ACT is much simpler but has been developed for a longer period and has rich studies for comparison.

Figure 2-1 Traditional Arm Curl Test [83].

The aim of ACT is to test the strength of upper body muscle using weights (dumbbell). The ACT is widely used in both research and fitness. However, the traditional ACT protocol is lack of detail assessment due to the assessment method is too simple, which is a score based on how many curl repetitions done in 30 seconds. The weights are different for men and women (5 lb for women, 8 lb for men) and a score table is used to assess the performance [84]. The performance and limitation have been discussed in many types of research [83], [85].

2.1.1.3 Resistance Band Equipment and Exercises

Resistance bands are portable exercise equipment which has been widely used in different fitness and rehabilitation. Figure 2-2 shows one type of resistance band (with specific design handle). There are normally 5 different strength of resistances, which differed by the colour of the resistance bands.

Figure 2-2 A set of resistance bands equipment. Different colours on the resistance band indicate different strengths. There are also some accessories, including handles, for various exercises.

The lightest strength starts from the yellow band, while the heaviest resistance is the black band. There are some intermediate resistances in between the yellow and the black; they are the red, green and blue band.

The use of a resistance band can be accompanied with a specific handle, which can reduce the force applied on hand and for easier gripping. The handle is made with a hard-plastic hollow cylinder and covered by soft foam material to provide a buffer between handle and hand. A nylon band goes through the hollow cylinder and the 2 ends of the band are hooked together by a metal ring. Then a range of resistance band can be hooked to the handle with a quick hook. Figure 2-3 shows the setup of a resistance band with handle. The selected yellow band is hooking on the handle by the fast hook.

Figure 2-3 Resistance band with a handle

2.1.2 Problem Statement

2.1.2.1 Limitation of Traditional Arm Curl Test

The limitation of ACT the assessment only based on only one score, which is the number of completed cycles in 30 seconds. Although some studies have expanded the scores by adding the ages and gender, it still seems insufficient. The score will then be classified into three levels broadly, such as below average, average, and above average. The more representative features such as frequency, power, energy, the timing of each repetition, the effects of the fatigue are completely ignored.

The detailed measurement in resistance band exercise is not available. For example, the ACT measures the performance based on only one score, and the CPC did not provide an evaluation method. These metrics are not enough to measure resistance band exercise or quantitate the exercise accurately.

2.1.3 Objectives

Develop an experimental sensorised resistance band system for measuring resistance exercise. The system should have multiple sensors embedded into the resistance band handle to measure exercises objectively.

Process the raw data and provided an evaluation method to quantitate the exercise objectively. Also, investigate the most related parameters in the performance and exercise quantitation.

2.2 Methodology

2.2.1 Revised Arm Curl Test

A Revised ACT (RACT) protocol is proposed which replaces the dumbbells by a range of resistance bands, therefore, allows the experiment performed by a resistance band. In addition, the subjects are required to do the exercise in standing positions.

2.2.2 Experimental Sensorised Resistance Band System

Multiple potential sensing parameters are discussed in the following sections, which capable of measuring the measure the resistance band exercise. A few types of sensors, including gyroscope, accelerometer, magnetometer, barometer and a load cell, are discussed and implemented into the handle. The development and sensor calibration are shown in Appendix B and Appendix C individually.

2.2.2.1 Potential Sensing Parameters

Different sensing technology can measure the exercise from their perspectives. In this section, three types of parameters are discussed, which could be potentially meaningful to quantitate the exercise; they are motion data, human body data, and timing data.

First of all, the movement of the handle is potentially related to the exercise, including orientation, accelerations, rotations, and the features extracted from them. The physical status of the user is also essential, including power, heart rate, and blood pressure. The timings of exercises are also important. These data should be capable of answering the three questions of exercise proposed in Chapter 1: “when”, “how” and “what”.

The list of the key parameters is shown in Table 2-1:

Table 2-1 List of key parameters can potentially quantitate the ACT

Parameters	*Camera-based*	*IMU*	*Load Cell*	*Barometer*	*PPG*
Orientation of hands	Y	Y			
Rotation of hands	Y	Y			
Acceleration of hands	Y	Y			
Heading	Y	Y			
Relative Height	Y	E		Y	
Force on band			Y		
Gripping force			Y		
Power	E	E			
Heart rate					Y
Timing	Y	Y	Y	Y	

Y: direct measurement; E: can be estimated; Blank: not able to measure

To conclude Table 2-1, most of the key parameters can be measured by the 5 types of sensors. In some of the parameters, such as orientation, rotation, acceleration, heading, and timing can be measured by 2 or more kinds of the sensor. The sensor selection will be discussed in detail in the following section.

2.2.2.2 *Sensor Selections for Sensorised Handle*

As discussed in Chapter 1, other than camera-based systems, motion-sensing can also be done by IMU sensors. IMU normally consists of gyroscopes, accelerometers, and possibly magnetometers; they can measure the 3-Axis rotations speed, 3-Axis accelerations, and magnetism on the sensor's location directly. These sensors are already commonly used in a smartphone to provide the orientation and motion data for gaming, Virtual Reality and other applications to provide the orientation of the devices. In addition, these MEMS IMUs are already widely used in many commercial wearable smart devices in fitness and healthcare, for example, wristbands are normally used to

record the step counts, exercise, sleep qualities and sometimes heart rate (recorded by photoplethysmogram (PPG) sensor).

Similar to wearable devices, the design of the experimental system is focused on implementing sensors into resistance band handle, therefore, the resistance exercise can be measured in the same way as these wearable devices. An IMU will be implemented into the handle for measurement of orientation, acceleration, and rotation. A barometer is also put in the handle to measure the atmospheric pressure and the temperature, which can be converted to the absolute height above sea level. Also, a load cell sensor is put in between the resistance band and the handle for measuring the force applied to the resistance band directly. An external housing is needed for the load cell sensor in between the main housing and resistance band.

To measure the heart rate of the exercise, a PPG sensor can be used. PPG sensors are widely integrated into many modern smart wristbands. PPG sensor is also considered to be put into the experimental system but has not yet implemented into the experimental system since, at the preliminary test, the experiment is more focus on exercise instead of the human body.

As a result, the selected sensors in the experimental system are IMU, barometer, and load cell.

2.2.2.3 *Overall Performance of the Experimental System.*

The specification of the experimental system is summarised as below in Table 2-2.

Table 2-2 Sensorised resistance band handles of the experimental system

Parameters	*Value*
Size [mm]	L130 x D32 (cylinder), L50 x W24 x 18H (load cell housing)
Weight [g]	120 Included Battery
Working Current [mA]	153
Power consumption [mW]	0.56
Sensor	9-Axis motion sensor, barometer, load cell

Parameters	*Value*
Sampling rate [Hz]	500Hz
Charging time [hour]	3
Battery durability [hour]	8
Communication method	Bluetooth LE 4.2, Sub-1G wireless
Communication distance [m]	10 with Bluetooth Low Energy 4.2, 100 with Sub-1G
Data recording time	Max 6 hour with 32G microSD card.
MicroSD card capacity	Up to 32GB
Cost [GBP]	~70

The size of the sensorised handle is similar to the conventional non-sensorised handle. The sampling frequency can be up-to 500Hz, which is enough for human exercise measurement. The 1400mAh battery allows it to measure exercise continually for 8 hours. The comparison between the traditional handle and the sensorised handle is shown in Figure 2-4. The mechanical parts were built by Fused Deposition Modelling (FDM) 3D printer with Polylactic Acid (PLA) materials.

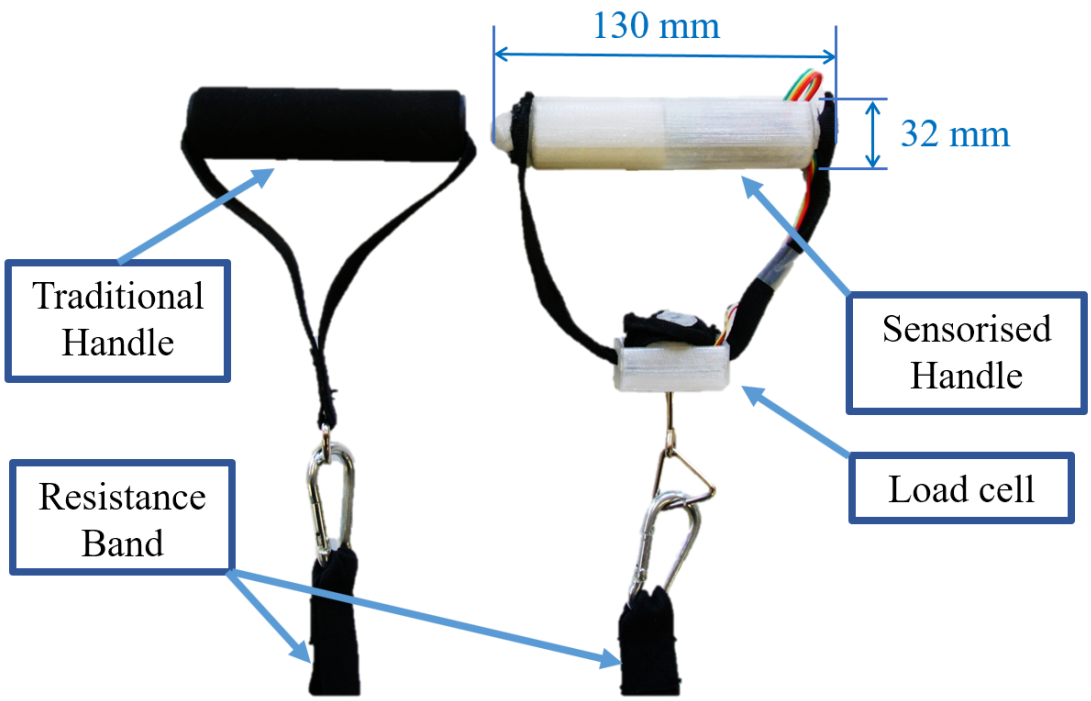

Figure 2-4 Side by side comparison of the traditional handle and experimental sensorised handle.

2.2.3 Experimental Setup

Two healthy volunteers participated in the preliminary experiments. Both were male, aged 24, and both were right-handed. The subjects were asked to do RACT in 30 seconds for four times which each hand performed two times using two levels of resistance bands. The two levels are differed by the colours of the band in black or yellow. The black band (22 lb) is stronger than the yellow band (8 lb). The subjects were asked to complete every cycle by pulling the resistance band from waist to shoulder and then releasing to the initial position. In between each test, there was 10 minutes' interval for rest to avoid the effect of fatigue across the exercise. However, the protocols need to be revised for older adults who might be weaker in physical strength.

The data is recorded into the internal microSD card Comma Separated Values (CSV) file during experiments. The recording was started by pressing the push button which located on the face of the handle. In the recording state, the sensorised handle blinked the onboard LED at 10Hz, to shows the user that the data is recording correctly.

The button is pressed 3 seconds before the subject start to do the exercise to create a new data logging file in SD card. The data recording is stopped by pressing the button again.

Additionally, the subjects are asked to do one more curl after the 30 seconds. Which will provide the redundancy for data analysis. The recorded files are copied to PC after each test is finished and the subject is on rest.

The sensorised handle and conventional handle, shown in Figure 2-4, are similar in dimensions to avoid the unnatural feeling to the user. However, during the exercise, the load cell housing might collide to the user's hand when the resistance band handle is lifting to the top position. The collision might lead to some different feeling compared to the traditional handle.

Figure 2-5 Revised Arm Curl Test. The band is fixed by foot, and the user lifts the handle from waist to shoulder then release to the initial position.

The experiment setup is shown in Figure 2-5. The selected handgrip the handle and the lower end of the resistance band are fixed by the same side foot. The length of resistance band is adjusted differently according to the height of the subject. The

resistance band should be initially tightened slightly. In the test, the subject followed the procedure of lifting the handle from waist to shoulder, after reaching the shoulder, the handle is released to the waist.

2.2.4 Available Measurements

Multiple sensors are available in the experimental system. These data are listed in Table 2-3. Besides, the timestamps of the sampling were recorded in millisecond resolution.

Table 2-3 The available sensors on the experimental system

Sensors	*Measurement*	*Axis / Channel*	*Resolution*	*Ranges*
Gyroscope	Angular velocity	3	16 [bit]	±125/±250/±500/ ±1000/ ±2000 [dps[a]]
Accelerometer	Acceleration	3	16 [bit]	±2/±4/±8/±16 [G]
Magnetometer	Magnetism	3	16 [bit]	±4/ ±8/ ±12/ ±16 [Guass]
Barometer	Air Pressure	1	24 [bit]	450 to 1100 [mBar]
	Air Temperature	1	24 [bit]	-40 ~+85[°C]
Load Cell	Force	1	24 [bit]	0~500[N]

[a]dps, Degree Per Second

With the timestamping and the raw data listed above, many features and timings can be extracted.

Table 2-4 Extracted features

Types	*Features*	*Notes*
Timing	Duration of each repetition	Measured by the start of the repetition to end.
	Time of lifting	The time taken for pulling the resistance band
	Time of falling	The time taken for releasing the resistance band
Energy	Potential Energy of lifting	The energy absorbed by the resistance band while pulling

Types	*Features*	*Notes*
Power	Average power	The mean power while pulling
	Peak power	The peak power while pulling.
Frequency	Frequency changes	The change of frequency in each repetition during 30 seconds.

The features shown in Table 2-4 are some parameters potentially meaningful to evaluate the performance using RACT. The timings are very sensitive parameters which might be affected by fatigue and strength of muscle. For example, the weaker hand might take longer to curl than the stronger hand. The timing of each cycle might take longer at the end of the test compared to the beginning due to fatigue. Potential energy and power indicate the changes during the process of exercise. The frequency change is also interested, which can use to describe the trend of curling.

2.2.5 Data Processing

The raw data lists in Table 2-3 was recorded both onboard and on a PC. The data was post-analysed by Python after the experiments. To reduce the noise, a Butterworth Low-Pass Filter () with 10Hz cut-off frequency was applied to the raw data: force, rotations, acceleration, magnetism. An LPF with 5Hz cut-off frequency was applied to air pressure.

The raw data was read out and segmented into single repetitions for further feature extraction. Python programming language and several open-source scientific libraries including NumPy, Pandas and Matplotlib were used for the data analysis and plotting. NumPy is the fundamental package for scientific computing with Python, which provides different data types, multiples data processing method, and matrices mathematics [86]. Pandas provide high-performance, easy-to-use data structures and data analysis tools [87]. It contains many other features such as a powerful N-dimensional array object, sophisticated (broadcasting) functions, tools for integrating

C/C++ and Fortran code, linear algebra functions, Fourier transform functions, and random number capabilities. Matplotlib is a plotting library which produces publication quality figures in a variety of hardcopy formats and interactive environments across platforms [88].

2.2.5.1 *Data Segmentation*

The data from each repetition (lifting from waist to shoulder then back to waist) needs to be segmented from the continuous measurement signals. Each repetition starts from where the resistance band is lifted from the waist (bottom position) to shoulder (top position) and ends by the resistance band is released back to the waist. The force applied on the resistance band is increasing through the elevating, reaching the peak forces while it is lifted to the shoulder, and then decreasing associated with the band releasing. Thus, the method to segment the data can be straight forward. Simply find out where is the peak force (the band lifted to shoulder) and where is the smallest force (the band at the waist). Thanks for the load cell sensor, the force applied on the resistance band is measured directly. Therefore, the data segmentation can base on the peak and minimum force data. However, by looking into the raw data, there were many peaks and distraction in some repetitions, which affect reduces the reliability of segmentation. The distraction is shown in Figure 2-6, marked by the red circle. The distractions are worse when exercising with a heavier band.

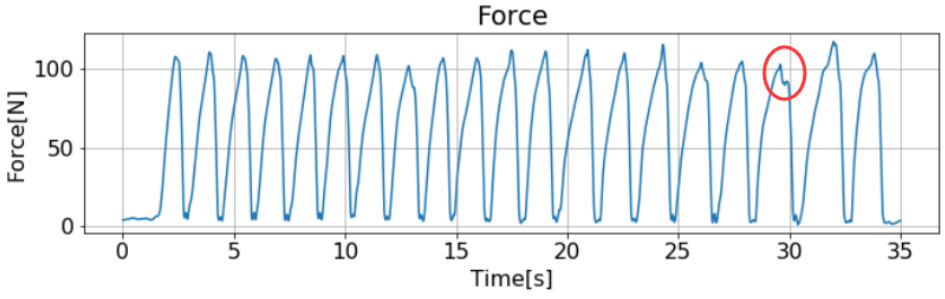

Figure 2-6 Raw data plotting and distractions (marked by the red circle).

Therefore, a more reliable segmentation method is needed. Besides, the top position, the start position and the end position should be considered individually for

each repetition. Due to the distractions shown in Figure 2-6, the force data alone cannot be used along to locate the top position. By plotting the force data with the rotation of the resistance band handle together, we found that the actual peak of the force is always associated with the zero-crossings of rotation (from negative to positive or reversed). For example, Figure 2-7 shows the first 2 repetitions of the ACT; the zero-crossing of the rotation is at the same timing (which is identified by the red lines) when the force reaches to the peak. The combination of both rotation's zero-crossing timing and peak force detection can be the more robust method for identifying the top position in segmentation.

To compare, by using peak detection with the force data along, the number of repetition detected is more than the trust of observation due to the small peaks around the main peak. By using the combined method only the main peaks are detected. Therefore, the segmentation relied on the combined method.

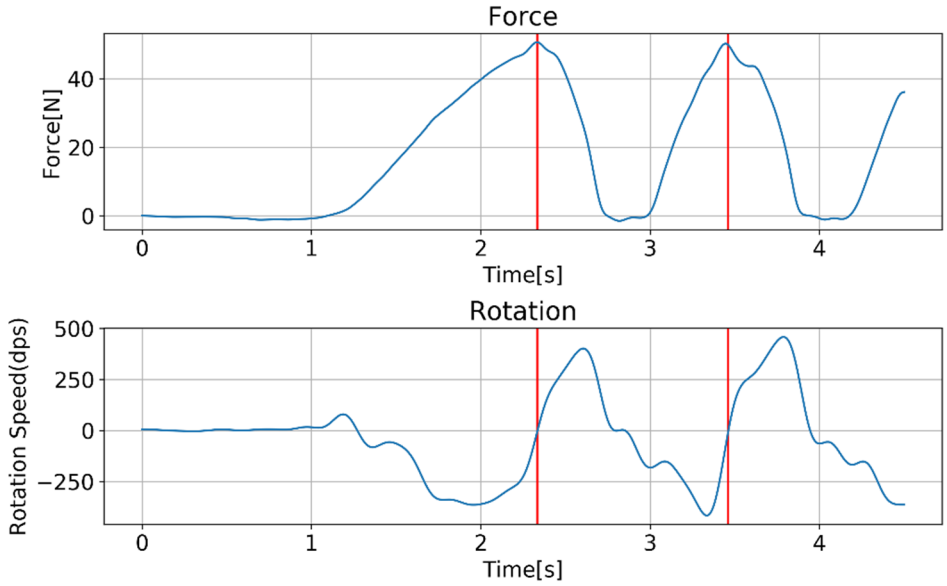

Figure 2-7 Peak force associated with zero crossings of rotation.

The combined method above has located the top position of the segmentation. However, the top position alone is not enough for data segmenting. The start and end position is also needed, where the subject just starts to lift the band and where the handle just arrived at its start position. The method to locate the cutting point between the two

peak forces is to find the middle time from the 30% force of the last repetition to the 30% force of the next repetition.

Specifically, an estimated starting point is used at the very first raising and an estimated cutting point is used after the last falling. In these cases, the estimated cutting point will be calculated separately from the other middle repetitions. Usually, the force before the first raising is at an initial position, where the subject standstill and the resistance band tighten in a light force. The data before the first repetition started is not concerned. During the ACT experiment, the time of the initial position was not controlled. The time before the first curl was related to the subject's preparation and their own decision.

The start point cutting does not need to be accurate, because the aim to segment the repetition is to separate each repetition from a continuous data sequences, not to identify the length of the repetition or to extract the features. To estimate the start point, we find the points that the force rises from idle (could be non-zero) to 30% of the peak force. Then identify the time from 30% force to the top position (peak force). After that, we estimate the start point will be within the range of half time that from 30% to peak force ahead of the 30% force. Figure 2-8 shows how the start point is estimated in real data.

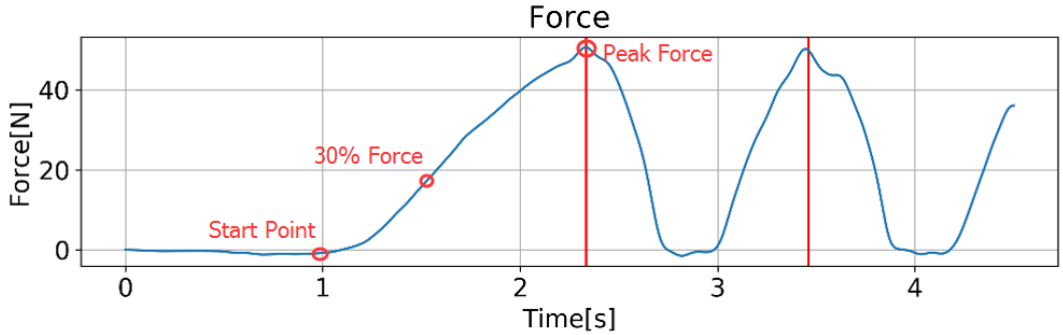

Figure 2-8 Start point estimation of the first curl.

The same estimation is applied to the segmentation of the last repetition. Correspondingly, the estimated point is located after the top position and the 30% to peak force in the falling phase.

2.3 Experiment

The experimental sensorised resistance band system was used during the experiment to measure the exercise. The data is plotted and discussed in the next few sections. The result shows a significant improvement in understanding of the exercise by using the experimental system to measure the RACT compared to the traditional ACT scores.

2.3.1 Results

After the data segmentation, the details of each repetition are plotted and analysed from a different perspective. The segmented force data for both subjects are shown in Figure 2-9 and Figure 2-10.

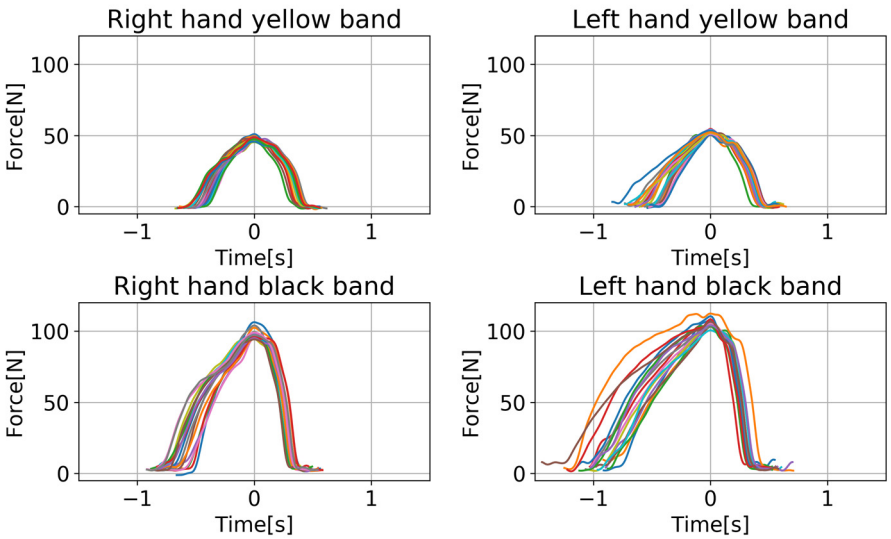

Figure 2-9 Subject 1 segmented force data.

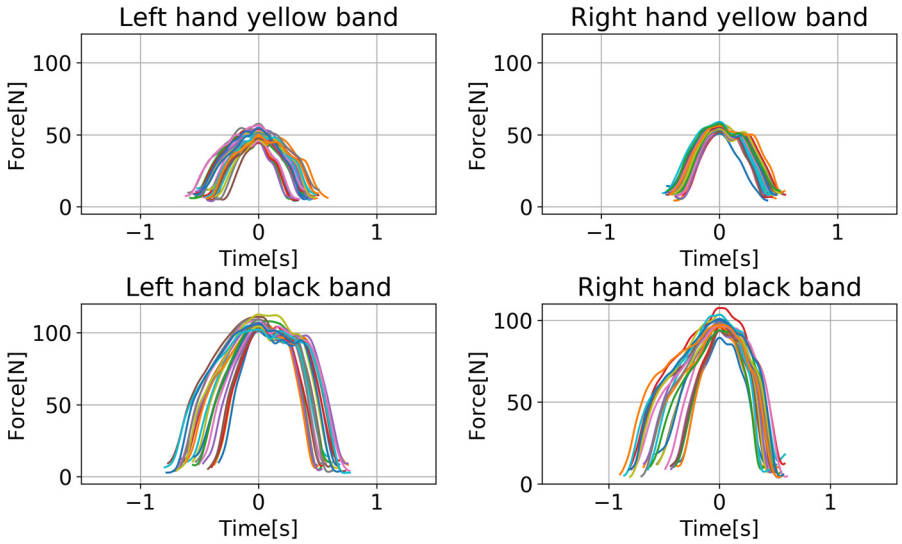

Figure 2-10 Subject 2 segmented force data.

2.3.1.1 *Timing*

In each repetition, 3 different timings are extracted, they are:

- the lifting time t_{rise}, from 10% of the peak force to 90% of the peak force during the rising phase.
- the falling time t_{fall}, from 90% of the peak force to 10% of the peak force during the falling phase.
- the duration $T_{duration}$, which is measured from 10% of the peak force during raise phase to 10% of the peak force during the falling phase.

The timings are extracted from force measurement only. The example of timings extraction in one complete repetition is graphically shown in Figure 2-11. The blue curl represents the percentage of the peak force. The red dots represent the timing which should be captured. They are 10% of the peak force and 90% of the peak in both lifting and falling phases. These timings are captured and recorded separately for more feature extractions.

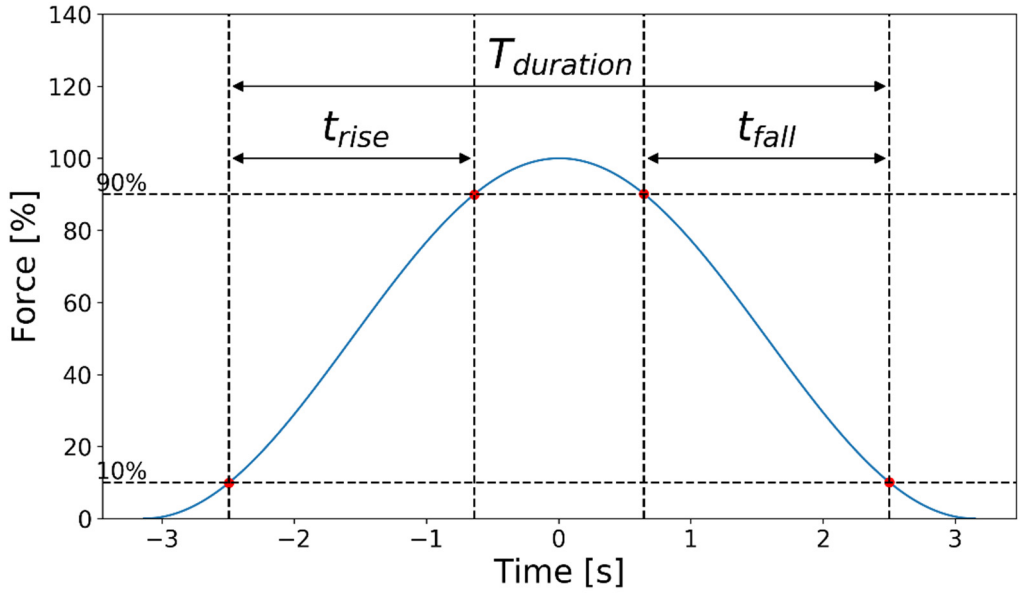

Figure 2-11 Example of the 4 key timing points.

After the timings are captured, the t_{rise}, t_{fall}, and $T_{duration}$ can be calculated individually. The method is to find the peak force of each segment, then find the time that the force reaches 10% and 90% of the peak force. Additionally, the force that considered is the delta force. Because the resistance band was tightened at the initial state before the subject started to do RACT. Therefore, a small amount of force is applied even in an initial state, which means the 10% peak force might be larger than the initial force. To avoid this problem, the timings are extracted by the delta of the force (from initial force to peak force). The initial force of each repetition is calculated individually, which is set to the minimum force of the specific segment.

The three parameters (t_{rise}, t_{fall}, and $T_{duration}$) are plotted with the number of repetition and the regression lines. The figures from the two subjects are placed side by side in Figure 2-12, Figure 2-13 and Figure 2-14. The lifting time t_{rise} and the duration of repetition $T_{duration}$ clearly show the impact of fatigue, where the timings have increased associated with the number of repetitions. In both subjects, the tests with black band (heavier band) are quicker to be affected while the tests with the yellow band (lighter band) performed more insistently.

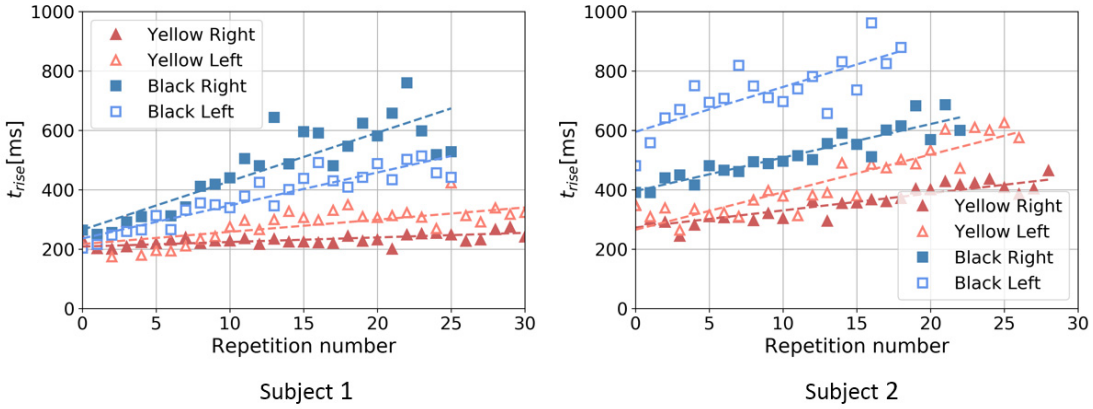

Figure 2-12 Rising time of each repetition.

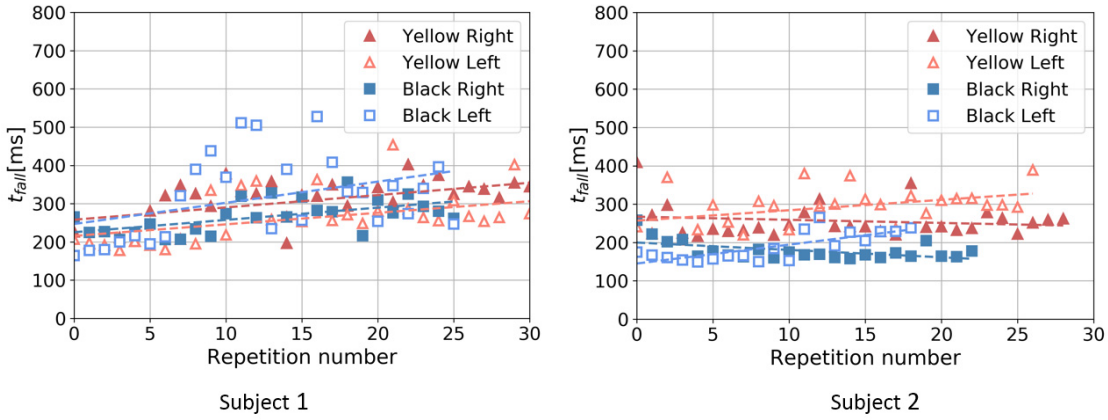

Figure 2-13 Falling time of each repetition.

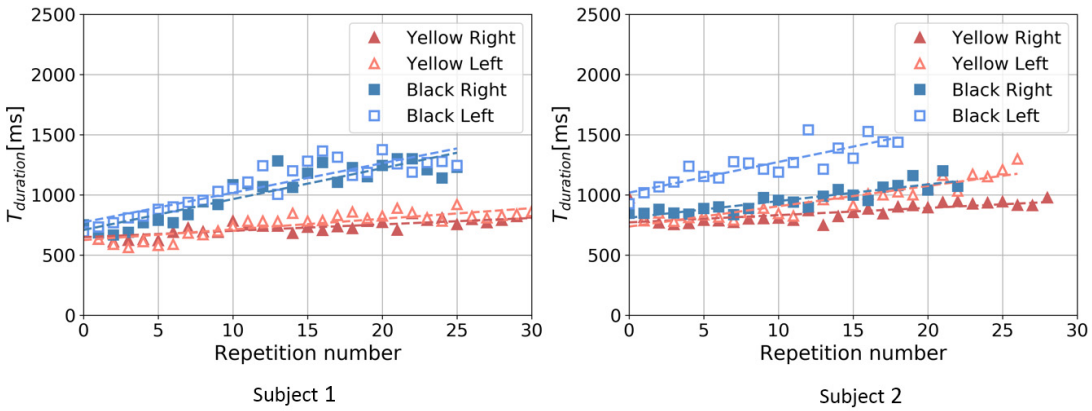

Figure 2-14 Duration of each repetition.

The distributions and standard errors of the timings in each repetition in the rising phase, falling phase, and the total timing are shown in Figure 2-15, Figure 2-16, and Figure 2-17. The standard error charts show the same results as above; the test with the yellow band is more constant than the black band.

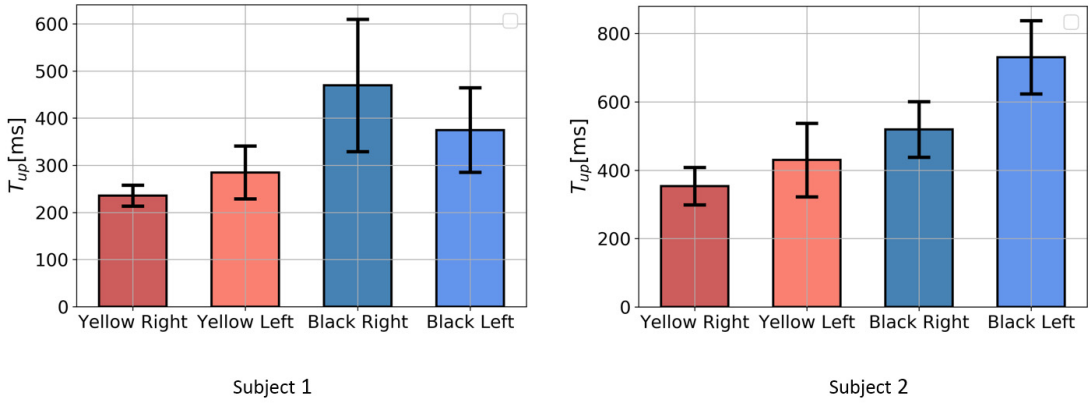

Figure 2-15 Standard error of rising time.

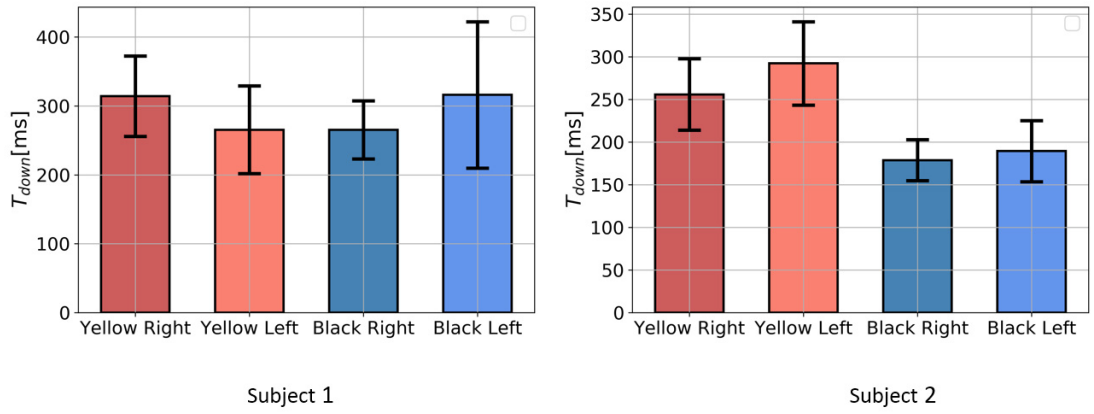

Figure 2-16 Standard error of falling time.

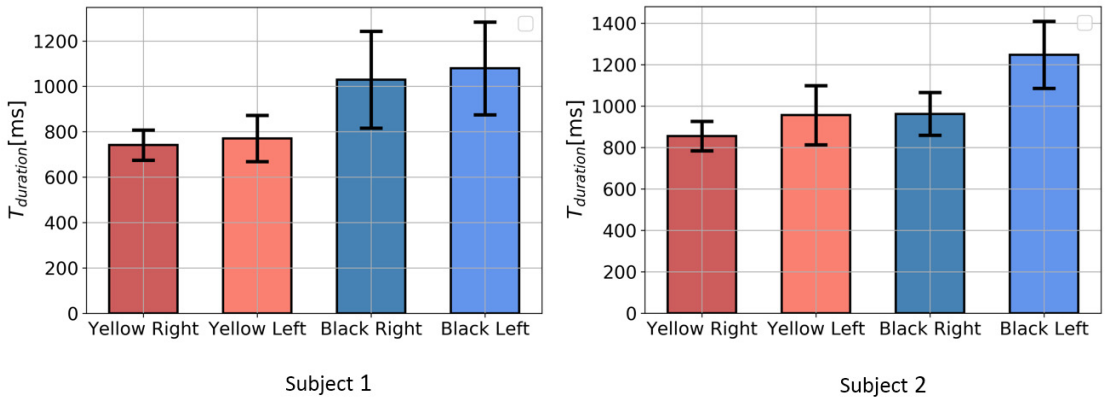

Figure 2-17 Standard error of duration.

2.3.1.2 *Peak Force*

The maximum forces measurement during each repetition is peak forces. Different weight levels of the resistance bands provide a different tensile force when extended to the same length. The force data is measured by a load cell sensor directly which was calibrated before the experiment. After the segmentation, the peak force of each segment is extracted by the maximum measurement. The peak forces are plotted with the repetition number to show the trends through the repetitions, which is shown in Figure 2-18. The peak force measurement should be reached around the shoulder which is the position top position. The tests with the yellow band in both subjects have proven the argument. Unexpectedly, with subject 1, the peak forces with the black band on both

hands are increasing with the number of repetitions. The maximum increase is over 10% when the subject 1 was doing exercise with the black band using the right hand. This might indicate the incorrect postures which might be affected by the fatigue.

The standard errors are shown in Figure 2-19. The graph from both subjects shows a stable peak forces measurement.

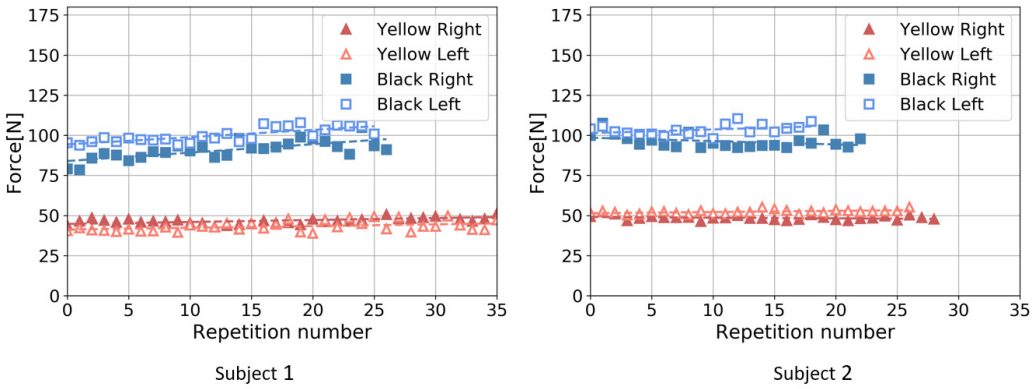

Figure 2-18 Peak force.

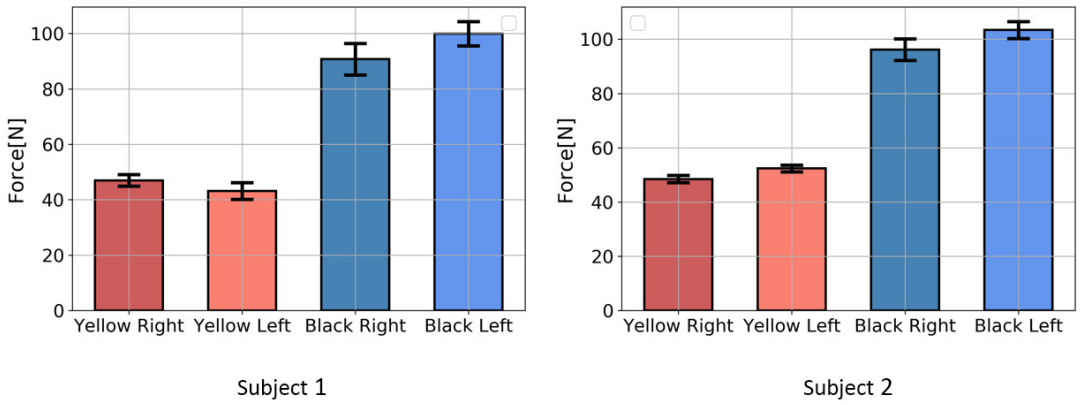

Figure 2-19 Standard error of peak force.

2.3.1.3 *Frequencies*

The frequencies are calculated by the reciprocal of the timing in between two adjoining repetition's top position. The reciprocal of the frequency is different from the $T_{duration}$ but very similar to the traditional ACT score, which is the number of repetitions done in 30 seconds. The results are plotted in Figure 2-20. The frequency of

both subjects is decreasing during the test. The subject 1 was curling faster than the subject 2 in the test with a black band at the beginning, later, they were reaching the same frequency at the end of the test at around 0.6 Hz.

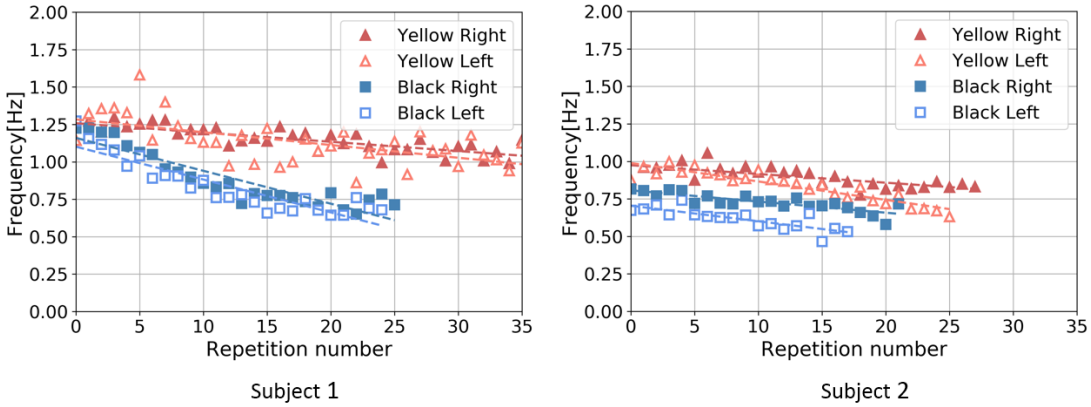

Figure 2-20 The frequency trends.

2.3.1.4 *Maximum Rotation Speed of Lifting*

The maximum lifting rotation speed is the maximum rotation measurement in the handle during the lifting phase. The results are shown in Figure 2-21 and Figure 2-22. Both subjects performed differently in the maximum rotation speed. In the tests with the yellow band, the maximum rotation speeds are more varied than the black band in both subjects.

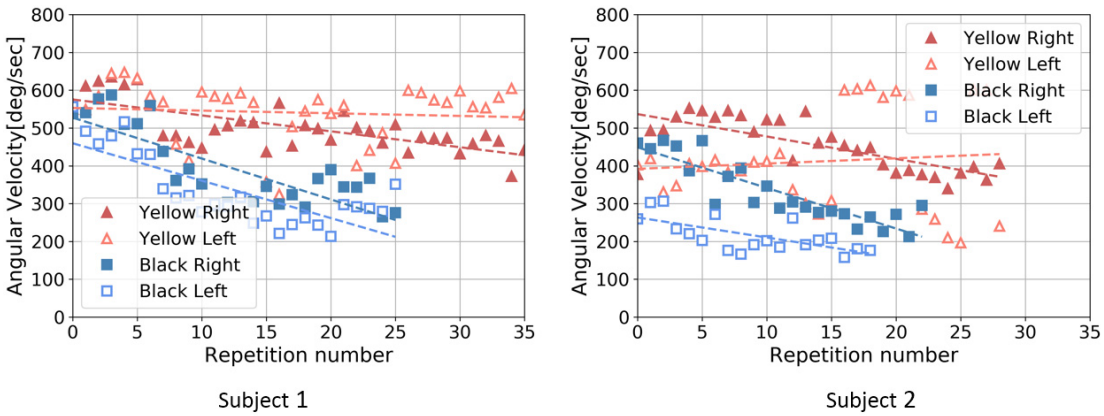

Figure 2-21 Maximum rotation of lifting.

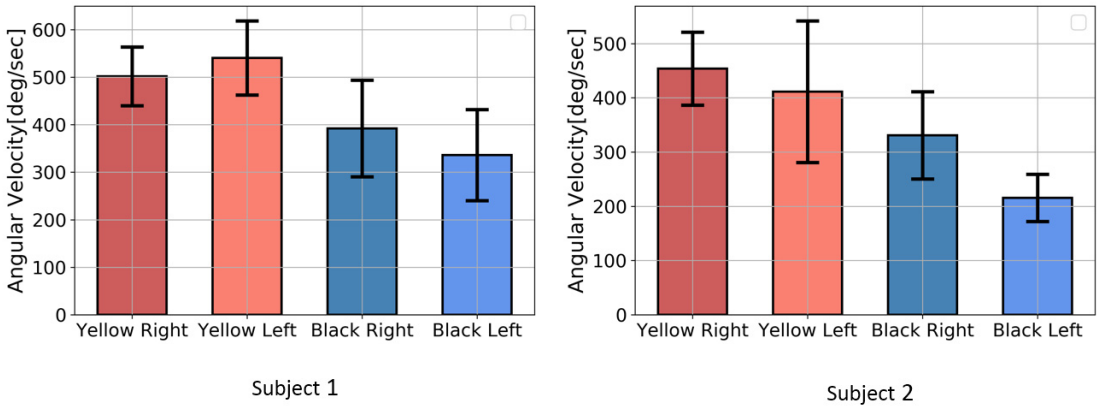

Figure 2-22 Standard error of maximum rotation of lifting.

2.3.1.5 *Potential Energy*

The potential energy represents the energy absorbed by the resistance band while it was being pulled. The resistance band can be described by a spring model $l = f/k$. Where the k is the resistance band's elastic coefficient, which is calibrated before the experiment, and f is the force applied to the resistance band. The energy in each repetition is calculated independently by (2-1). The results are shown in Figure 2-23. The energy plotting is similar to the peak forces due to they are all based on the force measurements.

$$E_p = \frac{1}{2}kl^2 \tag{2-1}$$

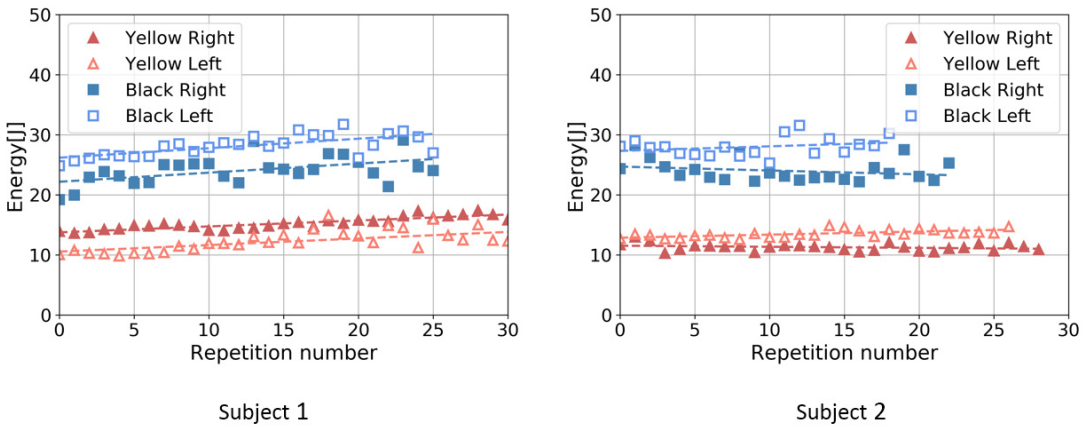

Figure 2-23 The potential energy.

2.3.1.6 *Average Lifting Power*

The average power is calculated by $p = E_p/t_{rise}$, where E_p is the potential energy that absorbed by the resistance band during the lifting phase, and the t_{rise} is the lifting time from 10% peak force to 90% peak forces. The results are shown in Figure 2-24. The power shows a similar argument to the frequency measurement, which is subject 1 can output more power than subject 2 at the beginning, but subject 1 is easier to be affected by fatigue than subject 2.

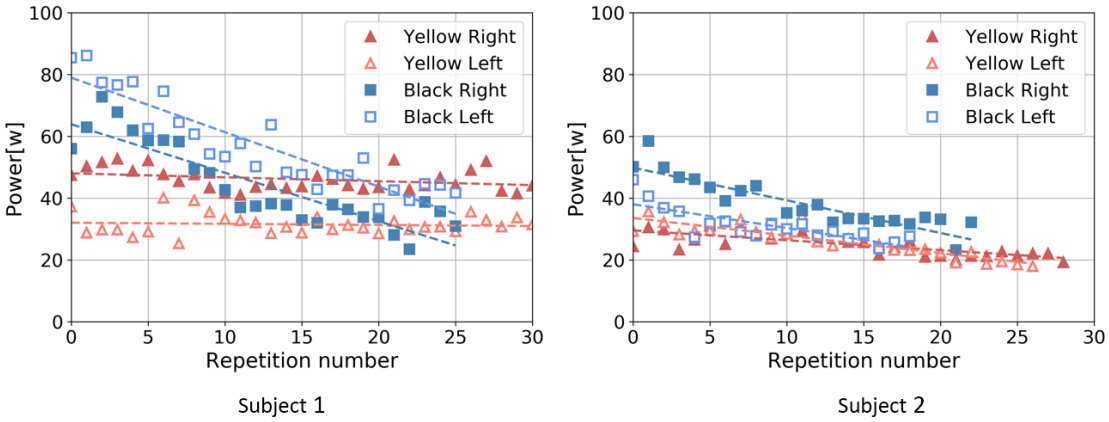

Figure 2-24 The average power in lifting.

2.3.2 Summary of Results

The results above show a few parameters and features that were extracted from the raw data collected by the experimental system. The selected features show a comparison between the 2 subjects and 4 configurations in different perspectives.

Some of the features have clearly shown the effect of fatigue, such as the average lifting power, the frequencies, the lifting time, and the repetition duration. The trends of these data are decreased with the number of repetition done while the other parameters show less correlation to the fatigue.

2.4Discussion

The experimental sensorised resistance band system was the first trial to develop a sensorised exercise instrument specifically for resistance band exercise. Meanwhile, the application scenarios are narrowed; thus, the measurement is less general than the existing commercial motion trackers. The benefit of the narrowed application is it is more straightforward in the designing and potentially have a more accurate measurement for the specific exercise. The reduced number of sensor nodes (only requires two sensor nodes) compared to other comprehensive systems has avoided the interference on the user's natural movement.

The experiment and the results show the advantages of using the sensor system in RACT while compared the traditional ACT. Basing on the detailed exercise data, the assessment of the subject's performance can be achieved from different perspectives, which is superior to the only one score assessment in the traditional ACT.

Among the experiment results, more comparisons can be made. For example, the average lifting power shows both subjects have declined performance during the number of repetitions. Beyond these, it shows that the performance of subject 1 is declined more than subject 2, which can be concluded in subject 1 is more explosive while subject 2 is more endurable. Another example is the data of peak forces and the potential energy in each repetition. Subject 1 has increased force measurements in the black band (heavier band) during the number of repetitions. It can be inferred that the subject 1 might involve more muscles including the waist and shoulders, which is not a correct motion.

Besides the above measurements, some data seems less correlated to the performance, such as the peak rotation speed of the handle. Also, there are still some features that have not been extracted from the raw data, such as the orientations, the rotation of other axes, the accelerometer's measurements and others. Those features

also describe the exercise from their perspectives but have not been investigated during the data analysis.

During the experiment, the experimental system has shown its capability of objective resistance band exercise measurement. The data recording was robust, and the raw data certainly have fulfilled the requirement of objective exercise measurement.

2.5 Conclusion

To conclude, exercise treatment on cognitive rehabilitation normally takes a longer time to be effective compared to other treatments like drug treatment. Which brings many difficulties for understanding the effectiveness of exercise intervention. These problems are lack of objective exercise measurement, lack of intermediate data while subjects are doing exercise remotely. To understand the effectiveness of exercise, a shorter assessment interval or even continuous assessment is required, and objective exercise measurement is required.

Therefore, this chapter has presented the resistance band experiment (revised of Arm Curl Test) which is objectively measured by an experimental sensor system.

In this chapter, the traditional ACT protocol is revised to use the resistance band instead of weights. By analysing the raw data, a few features are selected and plotted for analysis. Some features, such as timing and energies, has a strong relation to the fatigues. Some features, such as peak forces, potentially capable of tracing the mistakes in exercise. However, the findings above are still preliminary, further study with a larger number of participants is needed.

The functionalities of the experimental system are validated during the experiment and the data analysis, which has fulfilled the needs of objective resistance band exercise. However, there were some major limitations which prevent it from wider applications and further data analysis, including the IMU placement and the lack of multi-sensor networking.

In the next chapter, the limitations of experimental systems will be further discussed, and the development of a robust sensorised resistance band is presented.

Chapter 3 Development of the Sensorised Resistance Band System

3.1 Introduction

3.1.1 Background

Motion tracking systems have been widely used in recent years. Some of them are highly accurate and complex for professed applications, such as marker-based cameras system, VICON [89], and full-body IMU suit [54]. First, accurate measurement can be achieved in a lab with nessesary instruments, but they are too cumbersome for users to bring home. Second, the measurement from commercial wearable sensors such as wristbands is too simplistic and less accurate. As discussed in Chapter 1, customised IMU-based measurement system (containing only a few sensor nodes) can balance the system complexity, measurement accuracy and usability. In Chapter 2, an experiment using the experimental sensorised resistance band system shows the objective measurement capability using IMU and a load cell in resistance exercises. Multiple sensors were placed inside the resistance band handle to measure the motion and force. The experimental system has achieved a very detailed measurement, which was capable to measure the Arm Curl Test objectively and has provided much more details compared to the single scores in traditional Arm Curl Test. However, the experimental system was not designed for remote measurement but to validate the capability of objective measurement using IMU. It is not feasible for long-term remote measurement.

Many wireless sensor systems, such as WB3/4 motion tracking suit (by Waseda University [55]–[57]) and the experimental system used in Chapter 2, can be described as Figure 3-1. These systems usually consist of multiple sensor nodes, a wireless adapter, a dedicated PC and customised software. These systems also require professional skills to operate, which is not simple for novices or less capable older adults.

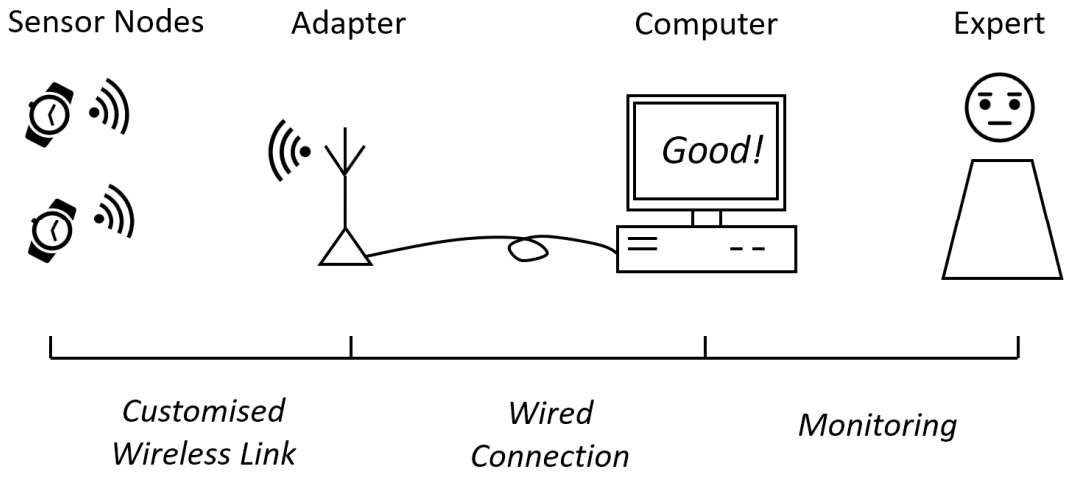

Figure 3-1 Conventional wireless sensor system structure. Consist of a few sensor nodes, a wireless adapter, a dedicated PC and customised software.

3.1.1.1 ***Concept of "Nearables"***

Wearable sensing technology is already widely used by the public. Nowadays, smart devices such as watches, wristbands, clothes, shoes, glasses, helmets and so on implemented battery, multiple sensors, and wireless communication are commercially available in the markets. They can be classified into the concept of wearable technologies, which aims to be worn as close as possible on the human body. These products are normally placed close to the human body, which allows the embedded sensors to capture bio-electro signals, motion, temperatures, and others from the closest distance to bodies. However, these wearable sensors are required to be small, flexible, low power, wireless, and easy to maintain, thus, to be less burdensome to the natural movement and natural feeling. But even with the state-of-the-art of wearable technology, the user can still feel the existing of these wearable sensors while they are wearing them. The wearable devices are still not small enough, some people simply refuse to wear these wearable devices because of the cumbersome feeling. Especially with older adults, the acceptance of these wearable devices is questionable as discussed.

On the contrary, instead of putting sensors into wearable devices, putting them into the surrounding environments might be a better solution to solve the acceptance

problem among older adults. While these sensors are embedded into the exercise instrument, which will have the same functionality and the same method of usage, but with the extra capability to sense and analyses the exercise, the instrument might be more acceptable than the wearable sensors for them. For users who tend to stay in the comfort zone of conventional instruments, these sensors could be easily ignored during exercise and can then be neglected after exercise. This discussion is the main idea of a new concept which introduced in 2014 by Estimote Inc (https://estimote.com/) called "nearables". In this thesis, the developments of sensorised devices are following the concept of nearable. Specifically, sensors will be integrated into the resistance band other than being worn by the user to avoid encumbrance to the natural feeling and the natural movement when doing exercise.

3.1.2 Problems Statement

3.1.2.1 Limitation of the Experimental Systems

The desired sensor system should be simple enough for novices and accurate enough in measurement. For example, the preparation of the system should be simple enough for novices or older adults to operate during the exercise. As discussed in 3.1.1, a sensor system with more sensor nodes provides more data that leads to a better understanding of the motion, while the fewer sensor nodes provide better usability for the users. The number of sensor node needs to be compromised for accuracy and usability.

The new system is required to be:

- Capable of working remotely.
- Capable of recognising what resistance band exercise has been done.
- Capable of quantitating resistance band exercise.
- User-friendly.

According to the requirements above, a new sensor system structure is proposed, which is shown in Figure 3-2. Comparing the conventional structure (Figure 3-1) and new structure (Figure 3-2), the new structure requires the sensor to communicate with a smartphone directly with the standardised wireless communication protocols, such as Wi-Fi and Bluetooth. In the new structure, the smartphone collects the data from sensor nodes and send the data to a cloud server for the Artificial Intelligence (AI) inspection and the expert assessment. The reports can be sent to the sensors or the smartphone for giving instant feedback to the user. This new structure reduces the complexity of the sensor system massively from the end-users' perspective. The simplification is achieved by avoiding the customised wireless adapter, the bulky dedicated PC and the needs of an expert around. To implement the system as shown in Figure 3-2, the very first step is to develop a suitable sensor node.

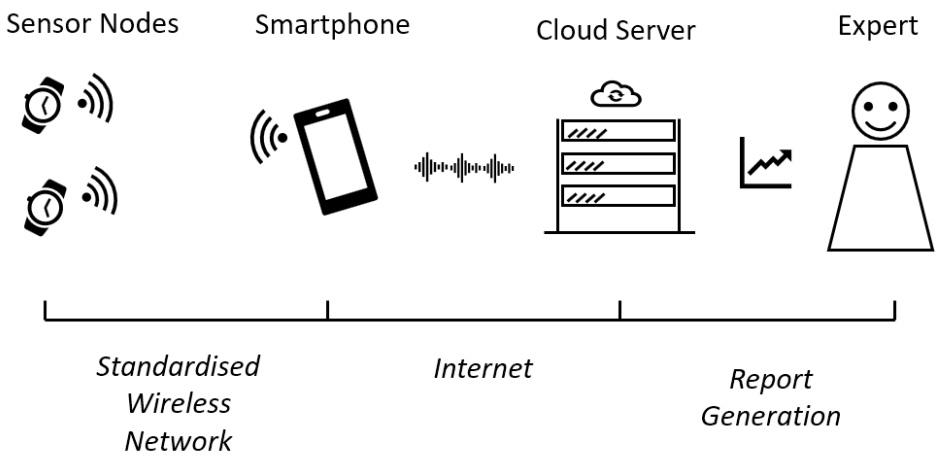

Figure 3-2 New sensor system model. Instead of using a customised wireless adapter, the sensors send the data to the user's smartphone through a standardised wireless network, such as Bluetooth. The data is then processed on the remote servers.

3.1.2.2 Reflection of the Experimental System

The new structure is desired but not implementable by previous developed experimental sensorised resistance band system.Which the system structure is similar to the conventional multi-sensor system, shown previously in Figure 3-1. The system includes a customised wireless protocol, a wireless adapter, a dedicated PC and a

researcher to monitor. Thus, the experimental system cannot fulfil the requirements listed above. There are also other limitations:

- Lack of resistance band direction measurement. The IMU was placed inside the handle, which was rotating during the exercise. Thus, the direction of the resistance band cannot be measured.
- Non-synced between multiple sensors. The experimental system is not capable of synchronising multiple sensor nodes.

The experimental system has partly fulfilled the needs for objective exercise measurement, but these limitations have appeared gradually during the previous experiment. The experimental system has redesigned the resistance band handle by a 3D-printed housing, shows in Figure 3-3. The housing is separated into 2 parts: one is the handle part which case the main electronics boards and battery; the other one is the load cell housing, which contains a load cell and its driver. The mainboard and the load cell driver are connected by a set of wires. It is unavoidable to have external wires outside of the protected structures. The wires can be broken very easily during the usages.

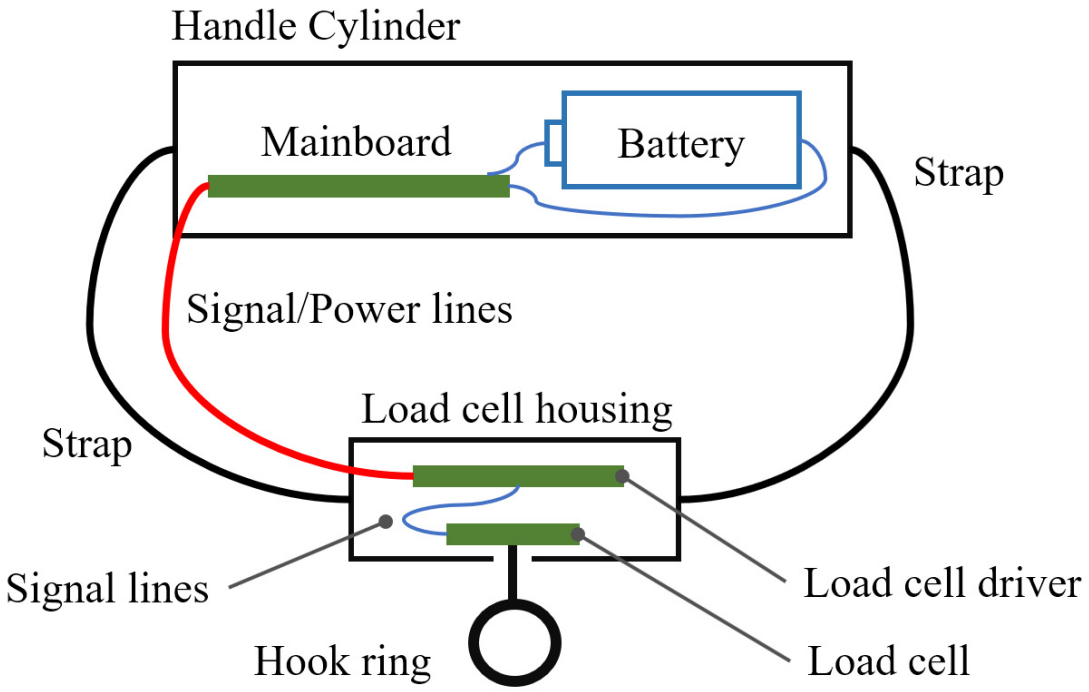

Figure 3-3 Concept of the experimental system. The system is consist of the mainboard, battery, extension wires, remote load cell and load cell driver.

The circuit design of the experimental system was not optimised for the low power consumption scenarios. It requires users to turn on and off the system manually. This operation must be repeated every time before the system is used. It increases the complexity in operation.

The experimental system also requires a customised wireless adapter to communicate with a dedicated PC for configuration and data acquisition. The extra adapter and the dedicated PC make the system complex and difficult to use.

Most importantly, many resistance band exercises require both hands to complete together. Two sensorised handles must be used in each hand individually for accurate measurement. While two devices are working independently, the synchronisation between the devices is fundamental. Without synchronisation, due to the minor difference inside the device's local clock, the sampling timestamp error will drift randomly and finally makes the data unusable.

3.1.3 Objectives

The objectives of the new sensor system focus on overcoming the limitations of the experimental system. The new sensor system should fulfil the requirement of:

- Similar sensor set-up as the experimental system (IMU, barometer and load cell).
- A durable structures.
- The physical dimension should be similar to commercial handles.
- At least 2 devices could be synchronised.
- Further improvement in usability.

This chapter design a new sensorised resistance band system named WBR-SH2 (Wearable BioRobotics – Sensorised Handle version 2). The overall requirements of WBR-SH2 should be user-friendly and straightforward for a wide range of people to use at home, and working remotely but can still provide accurate measurement of the resistance band exercises.

3.2 Design of WBR-SH2 System

3.2.1 System Specification

In the design of WBR-SH2 system, user-friendly interface is one of the requirements that less considered in the experimental system. The Product Design Specification (PDS) is listing the ideal, realistic and minimum requirements of WBR-SH2 system. The requirements are separated into a few subtypes, which shown in Table 3-1.

Table 3-1 Product Design Specification of WBR-SH2

Parameter	*Ideal*	*Realistic*	*Minimum*
Usability:			
Measuring Operation for user	No extra operation needed before and after exercising.	Use APP on a smartphone to start measuring.	User must turn on / off the sensor, retrieve data manually.

Parameter	*Ideal*	*Realistic*	*Minimum*
Power	An internal rechargeable battery can be charged automatically through wireless charging	And internal rechargeable Li-ion battery with micro USB charging	Use standard disposable batteries
Battery Life	6+ Months Larger than traditional assessment interval (6 months)	A few hours measuring with standby for weeks.	40 minutes (about 1 set of resistance exercise)
Data Acquisition	Sensor automatic upload to the cloud	Onboard storage and upload through a smartphone	Store in SD card, retrieve manually to PC
Exercise Reports	Real-time report, visualization.	Real-time raw data visualization with afterwards report.	Afterwards reports
Technical Spec.:			
Operational in high thermal exposure	-20 ~ +80°C	0 ~ +50°C	0 ~ +45°C
Weight	<20 grams	<100 grams	<200 grams
Dimensions and appearance	Sensorised handle should have the same dimensions and appearance as the non-sensorised handle	Same dimensions, but with a minimum different appearance.	The dimension changed for placing measuring devices. Different appearance
Functional in wet environments	Water & dustproof	Dustproof	None
Communication	Multiple wireless protocols	Single wireless protocol	Physical wires connection

Parameter	*Ideal*	*Realistic*	*Minimum*
Casing	Free from burrs, sharp edges or projections	Free from burrs, sharp edges or projections	Temporary case
Internal Electronics	Compact, all-in-one board design	Reasonable separate boards	Consist of separate modules
Sensor	IMU, Barometer, PPG, Temperature, Load cell	IMU, Barometer, PPG, Load cell	IMU, Load cell
Sampling frequency	200Hz	25Hz	10Hz
Feedback to user	Visual, Sound, and Vibration	Visual and Sound	None
Onboard data storage	A few hours' 100 Hz raw data storages	40 minutes (about 1 set of resistance exercise)	40 minutes (about 1 set of resistance exercise)
Others:			
Cost	Commercial wristbands ranges (20~100 GBP)	Commercial smartphone ranges (100~500 GBP)	Over 500 GBP

3.2.2 Design Concepts

Two concepts ranked out from a few drafting designs. Concept 1 is shown in Figure 3-4. The main idea of Concept 1 is putting all the electronics into a single box to reduce the complexity and improve the reliability. This design is reusing the most commercially available parts, which can be purchased in the market. The foreseeable disadvantage is the internal space left for electronics is small, which brings difficulty in hardware design. Also, due to the motion sensors are placed remotely to the user's hands, the measurements are not presenting the motion of the hands but the motion of the box. The soft connection between the sensor box and the cylinder also increase the difficulty to measure the exact hand movement. For example, the rotation of the handle

cannot be measure. However, the result of Chapter 2 rotation measurement shows that the rotation is less significant compared to other data, such as force and timing.

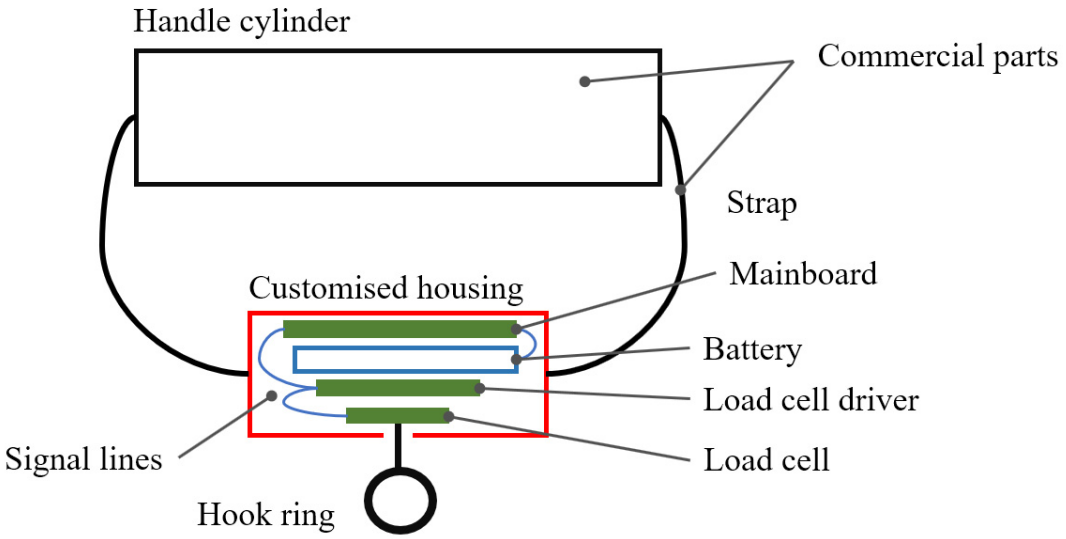

Figure 3-4 Concept 1: All electronics placed in one customised box. This concept aims to minimise the customised parts and to reuse most commercial part handles.

Concept 2 is an improved design of the experimental system, shown in Figure 3-5. This concept tries to use a hard case to protect the easily broken extension wires. In this concept, the load cell and its driver are placed remotely to the main circuit board. These extension wires are mandatory to measure the force applied to the resistance band. This design leaves the largest spaces for electronics and battery. The box should keep small for not extend ing the length of the commercial handle too much. However, it increases the difficulty in mechanical design.

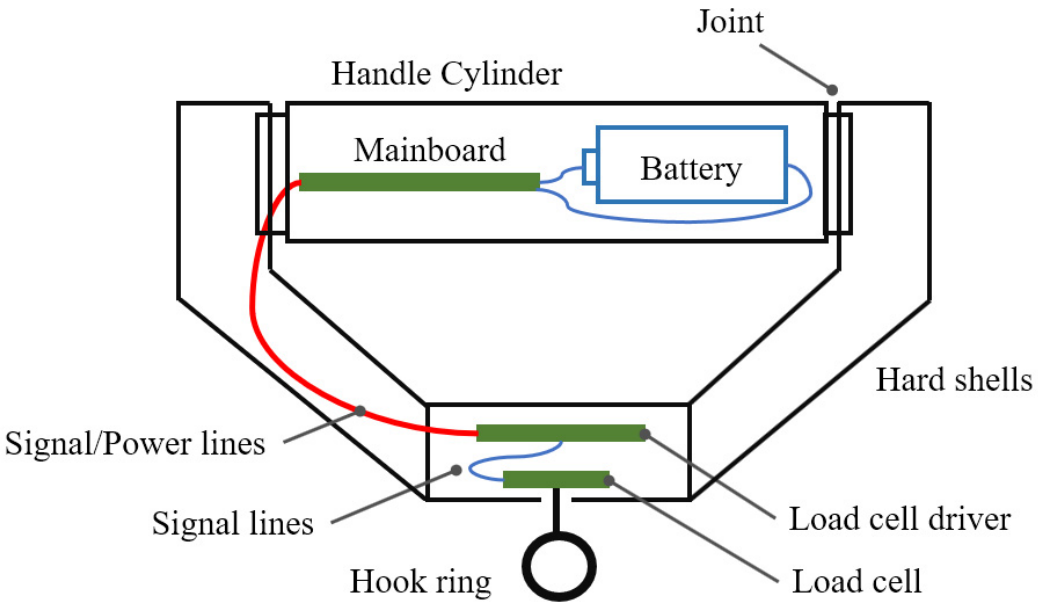

Figure 3-5 Concept 2: Redesign the casing of the experimental system. The handle housing will be rebuilt completely.

The two concepts are compared in a matrix for decision making, which is shown in Table 3-2. Each concept is scored from 5 to 1, larger numbers indicate better performance in the category. In most of the comparison, concept 1 is superior to concept 2. The only downside for concept 1 is the space limitation for electronics. However, the space limitation is the most significant factor. It is depended on whether the electronics design is small enough to be put into the small space. With the current electronics from the experimental system, it is impossible to put all the sensor into the customised box in Concept 1 without making the box bulky. To use the design of Concept 1, the electronics need to be redesigned to reduce the size, and the electronics need to be lower power consumption to reduce the size of the battery.

Table 3-2 Comparison of the two concepts.

	Concept 1 *One-Box design*	*Concept 2* *Improved design of the experimental system*
Durability	5	3
Reliability	5	3
Ease of manufacturing	4	1
Ease of mechanical design	3	1
Housing weight	4	2
Internal space for electronics	2	5
Total Score	23	15

To summarise the comparison, Concept 1 is selected for WBR-SH2. With the latest Bluetooth Low Energy 5 System-on-Chip (SoC) nRF52832, it is possible to achieve low power consumption, high performance (225 CoreMark), fast wireless link speed (2 Mbit/s data rate), and compact size (6x6x1mm) [90]. The new design based on Concept 1 will be presented in the following sections.

3.2.3 WBR-SH2 System Overview

The system overview of WBR-SH2 is shown in Figure 3-6. The WBR-SH2 system consists of a few sensor nodes (typically 2 sensor nodes) and an Android phone with a customised App. Although the WBR-SH2 can measure and store data individually, it can work with an Android smartphone for better data acquisition, recording, processing, real-time visualisation and continuous synchronisation. WBR-SH2 communicate with a mobile phone through BLE. Different from the experimental system which put most of the electronic components into the handle, the WBR-SH2 uses one-box design. All of the electronics are placed and covered by a single housing. During measurement, this box is attached between a commercial handle and resistance

band. The design details among hardware, firmware, and the software will be discussed in the following sections.

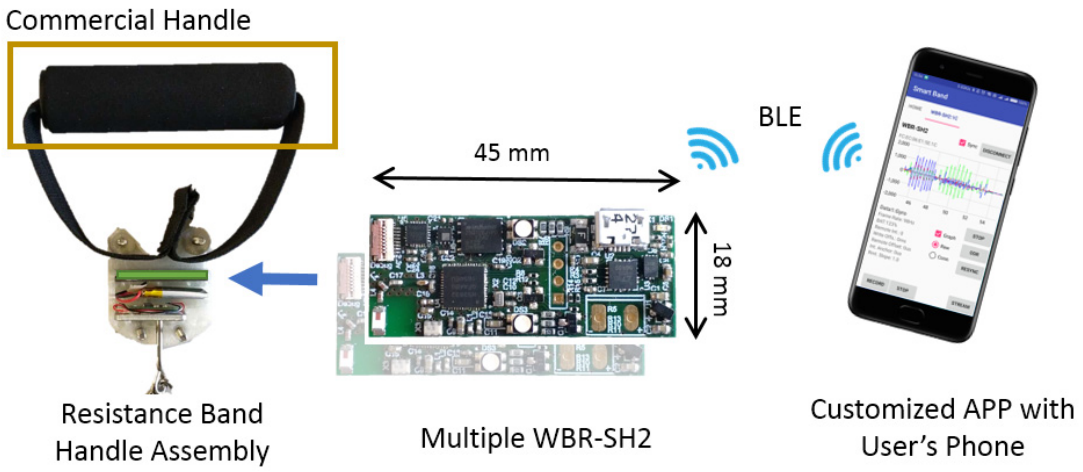

Figure 3-6 The WBR-SH2 system overview. The system is consist of a set of sensorised resistance band handle and a smartphone with a customised App. (Not scaled)

3.2.4 Hardware Development

Hardware development is a challenge due to space limitation and the low power consumption requirement in Concept 1. The block diagram of WBR-SH2 is shown in Figure 3-7. The overall design is more compact and low-power consumption-oriented.

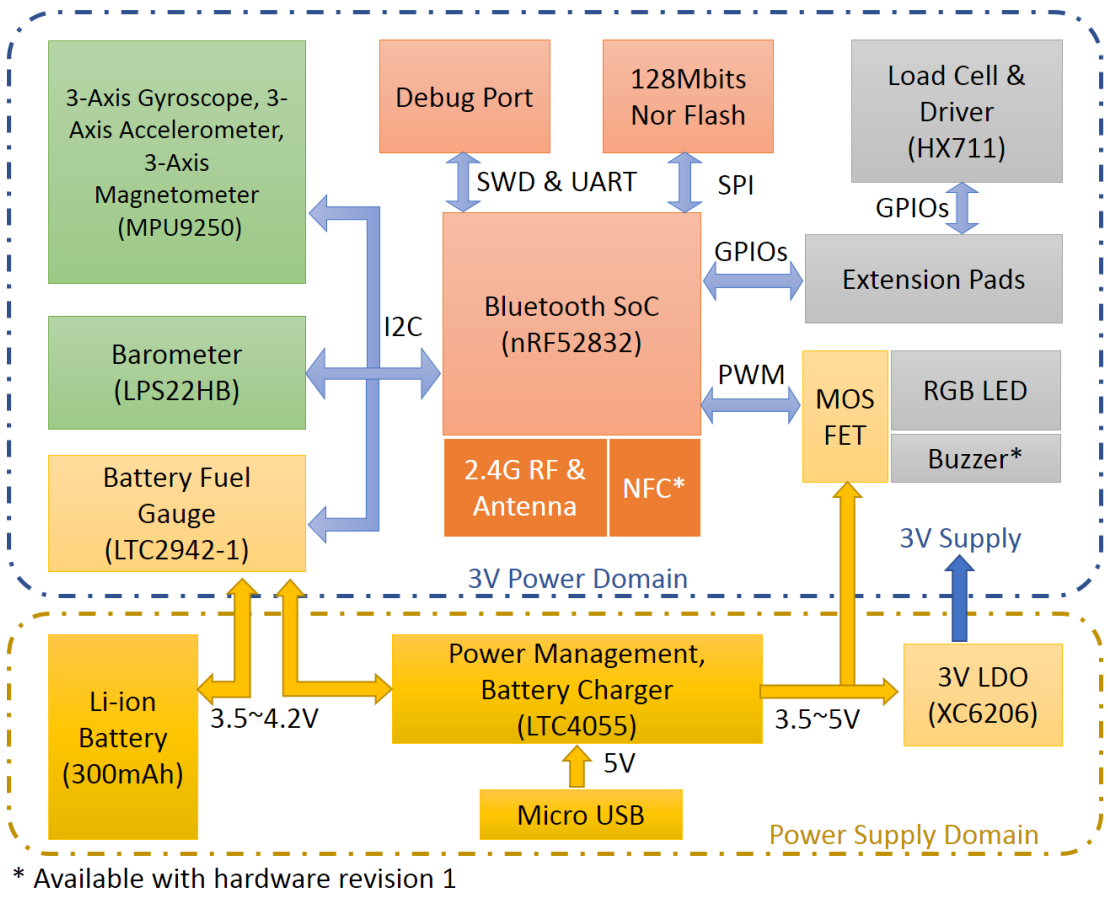

Figure 3-7 Block diagram of WBR-SH2.

The circuit board is separated into 2 domains, the main circuit domain (3V Domain) and the power supply domain. The power supply domain is responsible for supplying the main domain with proper voltages and managing the charging and discharging of the Li-ion battery. The power domain consists of a micro USB socket for the input power source, a power management IC for automatic power switching and battery management (Linear, Inc. LTC4055), a 3 V Low-Dropout Regulator (, XC6202) to supply 3 volts power source, and a battery fuel gauge for precise battery measurement (Linear, Inc. LTC2942-1).

The main domain (3V Power Domain) is responsible for presenting the functionalities of WBR-SH2. It consists of a BLE 5 SoC (Nordic, Inc. nRF52832) for control logic and radio communication, a customised debug port for hardware debugging, 128Mbits Nor Flash for local data storage, an extension pad for connecting

load cell driver (Avia Semiconductor HX711) for force measurement, a set of MOS-FETs for driving RGB-LEDs and a Buzzer, and the following sensors: a 9-Axis motion sensor (InvenSense MPU9250 integrated 3-Axis gyroscope, 3-Axis accelerometer, and 3-Axis magnetometers), and a high-resolution barometer (STMicroelectronics. LPS22HB).

The Printed Circuit Board (PCB)) and the placement of the components are shown in Figure 3-8. The PCB is designed using CircuitMaker (Altium, Inc). It contains 4 copper layers for signalling, power and ground to keep the size compact. All components are placed on the top side of the PCB. The main characteristics of the sensors are shown in Table 3-3. The schematics and layouts are shown in Appendix B.

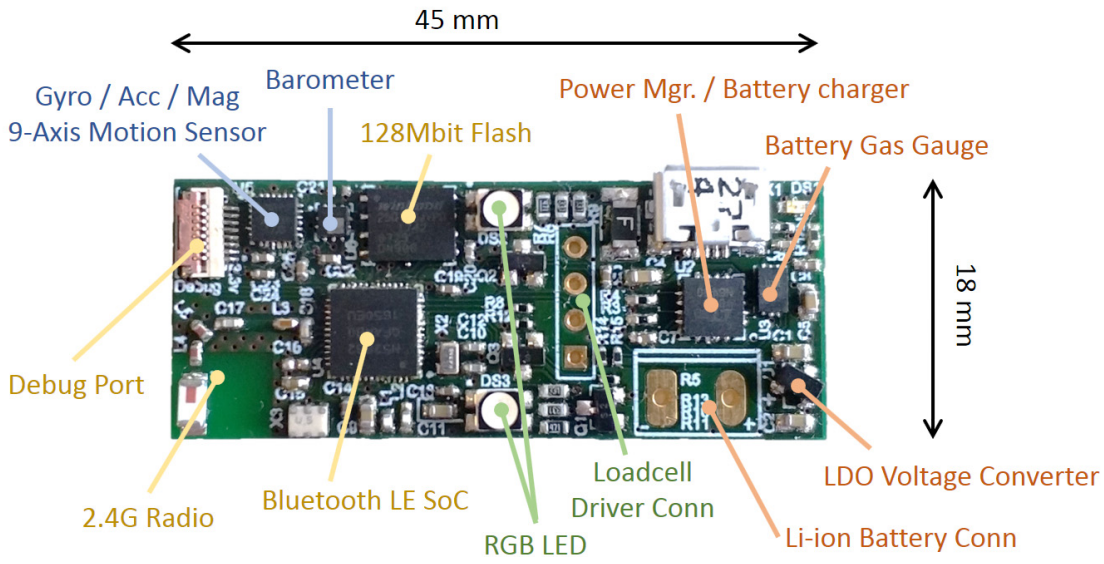

Figure 3-8 Main circuits of WBR-SH2 (version 2.0).

Table 3-3 Main characteristics of sensors in WBR-SH2

	MPU9250			*LPS22HB*	*HX711*
Category	*Gyro*	*Accelerometer*	*Magnetometer (embedded AK8963)*	*Barometer*	*Full bridge driver (Load cell)*
Num. of Axis (channel)	3	3	3	1	2

	MPU9250			*LPS22HB*	*HX711*
Category	*Gyro*	*Accelerometer*	*Magnetometer (embedded AK8963)*	*Barometer*	*Full bridge driver (Load cell)*
Voltage	2.4-3.6V			1.7-3.6V	2.7-5.5V
Working Current	3.2mA	450μA	280μA @ 8Hz	12μA @ ODR=1Hz*	<1.5mA
Power down Current	8μA			1μA	< 1μA
Temperature	-40 ~ +85°C			-40 ~ +85°C	-40 ~ +85°C
Resolution	16 bits	16 bits	14 bits	24 bits	24 bits
Range	±2000º	±16g	±4800μT	260~1260hPa	
Sample rate	4~8000Hz	4~4000Hz	130Hz (7.2ms)	1~75Hz	10 or 80Hz
Linearity	±0.1%	±0.5%			
Noise (RMS)	0.1º/s	8mg		0.75Pa	90nV

*ODR: Output Data Rate

3.2.4.1 Power Management Circuit

The power management circuit consists of a micro USB socket, a power switch & Li-ion battery charger Integrated Circuit (IC), an LDO and a battery fuel gauge. The power supply domain in Figure 3-7 shows the structure of the power management circuit. LTC4055 [91] (4 x 4 x 0.75mm) is a power switch and Li-ion battery charger, which supports up to 1 Amp charging current. A 1.5Amp fuse is placed in between micro USB and the power switch. The power switch automatically changes the power sources between USB and battery automatically depending on the availability. A small LED is also connected to its charging state pin to indicate the charging states. A battery fuel gauge (LTC2942-1 [92]) is placed between battery and charger to measure the voltage, the current, and the accumulated battery charge and discharge. The SoC

communicate to the fuel gauge by the I2C interface. A small LDO (XC6206 [93]) voltage regulator takes the power output from the switch and converts to the 3V power domain. Due to the small package size, the maximum current of the LDO is limited to 150mA. Thus, to reduce the load of LDO, the power supply circuit also output the unregulated voltage to higher current demanded and less voltage-sensitive parts, such as MOS-FET drove RGB-LEDs and a buzzer.

3.2.4.2 Bluetooth Low Energy (BLE) SoC and Radio Frequency (RF)

To keep the circuit small and low-power, a BLE SoC nRF52832 (Nordic, Inc. [90]) is selected to undertake both logic controlling and wireless communication. This SoC has implemented a high-performance ARM-Cortex-M4F core which runs at maximum 64MHz with Floating Point Unit. The 64kBytes Random Access Memory (RAM) and the 512kBytes embedded flash memory are capable of undertaking complex operation and signal processing. The QFN-48 (6x6x1mm) package is compact while keeps enough General-Purpose Input/Output (GPIO) for multipurpose applications. It also contains a range of embedded peripherals, including multiple Analog to Digital Converter (ADC), Serial Peripheral Interface (SPI), Secure Digital Input Output (SDIO), Universal Asynchronous Receiver-Transmitter (UART), Direct Memory Access (DMA), Universal Serial Bus (USB). The power supply voltage from 1.7V – 3.6V with automatic embedded LDO and DC/DC regulator which is suitable for an embedded system with limited battery.

More importantly, the SoC has embedded a built-in high-efficiency 2.4GHz transceiver, with -96 dBm sensitivity and -20 to +4 dBm TX power, supports the up-to-date Bluetooth 5 Low Energy and other protocols. Thanks to the on-chip radio and Balun circuit, the size of PCB and the RF circuit complexity are reduced.

The design of the RF circuit (included: C23, L3, C22, L4, L5 and the antenna on the left) is shown in Figure 3-9. A ceramic 2.4G mini antenna 2450AT18B100 [94] (Johanson Technology, Inc.) is used to minimise the size and increase the connectivity

performance. The feed line from SoC to the antenna is designed to be 50 Ω impedance according to the material and capabilities of the selected PCB manufacturer (JLCPCB Ltd.. The PCBs were manufactured by the 7628 structure [95], which is shown in Table 3-4). The width and clearance of the feed line are calculated by AppCAD (Agilent Technologies). The Antenna matching circuit (L4, L5, C22) is designed per the antenna's recommendation. Due to the lack of radio testing instruments, the RF design is only guaranteed by calculation. Antenna tuning is available by PCB manufacturer or special service when mass production is needed.

Table 3-4 1mm thickness 7268 4-layer PCB structure by JLCPCB [95]

Layers	*Structures*	*Materials*	*Permittivity*	*Thickness[mm]*
Top Layer-1		Copper		0.035
Pre-impregnated composite fibers	7628	FR-4	4.6	0.2
Medium layer-2		Copper		0.0175
Core	core	FR-4	4.6	0.465
Medium layer-3		Copper		0.0175
Pre-impregnated composite fibers	7628	FR-4	4.6	0.2
Bottom Layer-4		Copper		0.035

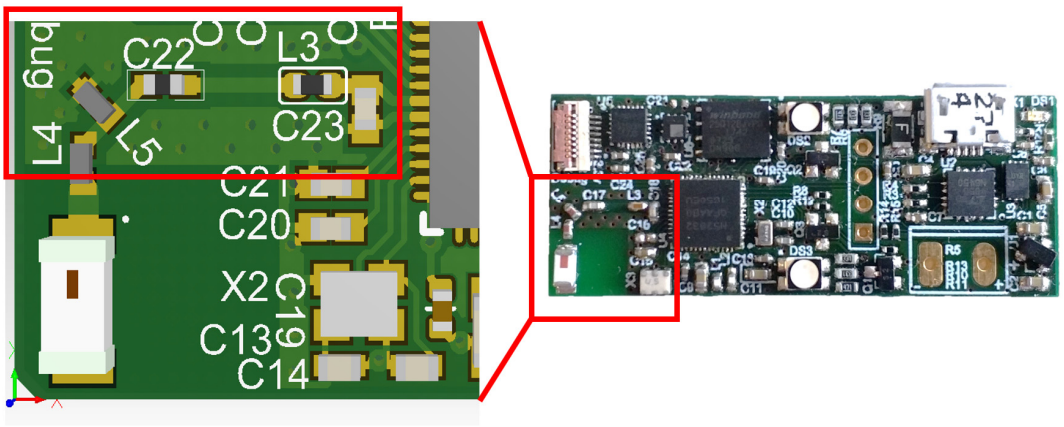

Figure 3-9 Radio Frequency circuits layout. The RC components are marked in red rectangle C23, L3, C22, L4, L5 and the ceramic chip antenna.

3.2.4.3 *9-Axis Motion Sensor*

MPU-9250 [96] is a 9-Axis MEMS motion sensor which combines a 3-axis gyroscope, a 3-axis accelerometer, a 3-axis magnetometer and an embedded Digital Motion Processor™ (DMP), while keeping the size small (3x3x1mm). The gyroscope has a range of ±2000°/sec and an embedded 16-bit ADC, with factory calibrated scale factor. The gyroscope is capable of sampling up to 8kHz. The accelerometer has a range of ±16g and an embedded 16-bit ADC. The accelerometer is capable of sampling up to 4kHz. The embedded magnetometer is a separate die of AK8963 [96] provided by Asahi Kasei Microdevices Corporation. It has a maximum measurement range of ±4800μT, with a 14-bit embedded ADC. The minimum sampling time is 7.5ms. The additional features include FIFO, auxiliary I2C, digital temperatures sensor, programmable digital filters for each sensor, I2C and SPI interfaces, supply voltage from 2.4-3.6V, low power mode, and DMP.

3.2.4.4 *Barometer*

The LPS22HB [97] (STMicroelectronics, Inc.) is a small size (2x2x0.76mm), low power (down to 3 μA), high resolution (24-bit pressure data). The barometer is factory calibrated to provide accurate out-of-box pressure measurement. The absolute pressure

accuracy after one-point calibration is 0.1hPa. Supply voltage range from 1.7V - 3.6V. The maximum output data rate is 75Hz.

3.2.4.5 *Load Cell and Driver*

Accurate load cell sensors usually are costly; however, there are much low-cost luggage weigh scales (under £5 per each) available on the market. These scales are using customised load cell for weight measurement. The disassembly is shown in Figure 3-10. The range of the scale is defined as 0 to 50kg, which contains the range of resistance band exercise (<10kg), and the size of the load cell (35x18x2.8mm) is small enough to be embedded to the resistance band housing. Therefore, for testing purposes, WBR-SH2 uses the load cell taken from the language weigh scales. The actual ranges and linearity are tested and calibrated after the PCB is built.

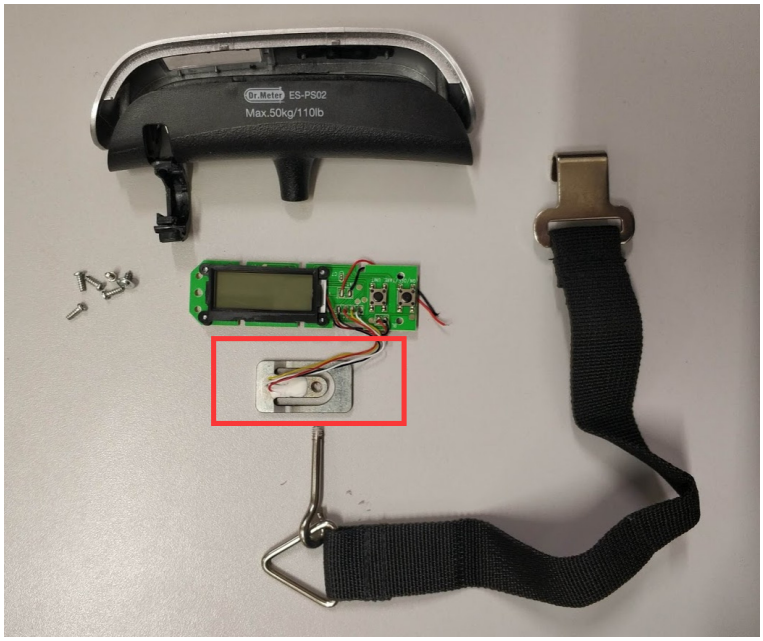

Figure 3-10 Luggage weight scale disassembly. The red square indicated the customised load cell.

The load cells disassembled from the weigh scale are a type of Wheatstone bridge bending beam load cell. A specific driver circuit is needed to drive the resistance bridge and getting the fore measurement. Thus, a highly integrated 24-bit Analog-to-Digital Converter for weight scales (HX711 [98], Avia Semiconductor, Inc.) module is selected. HX711 is a low power, high accuracy IC designed specifically for weight scales. It has

2 sets of input channels which allows it to measure 2 load cells respectively. The supply voltage ranges from 2.6V to 5.5V, with working current less than 1.5mA, and power-down current less than 1μA. It has a maximum sampling frequency of 80Hz. The communication between SoC and HX711 is not a standardised interface. It uses 2 wires for communication, one is the bit clock signal (PD_SCK) while the other is the data output signal (DOUT). The channel and gain selections are controlled by the number of PD_SCK in each sampling. The 2 signals are connected to 2 GPIOs on SoC to sample the load cell.

3.2.4.6 MOS-FETs Drove RGB-LED and Buzzer

The RGB-LEDs (Avago Technologies, ASMB-MTB1-0A3A2) and a buzzer are used for runtime visual and sound feedback to the user while they are doing exercise. Four N-Channel small sizes MOS-FETs (SI2302 [99], Vishay Siliconix, Inc.) are implemented to the circuit board. One of the four is for driving external passive buzzer (through connector), the other three are for driving each colour of the LED. The gates of the MOS-FETs are driven by SoC's Pulse Width Modulation (PWM) signal through 4 selected GPIOs. These RGB-LEDs and buzzer are powered by the unconverted power supply (3.5V to 5V) to reduce the load of the 3V power domain, which has mentioned in 3.2.4.1.

3.2.4.7 Conclusion of Hardware Development

The hardware design is low-power consumption oriented. All the components are capable of being shut down or set to low-power mode. Thus, it is not necessary to completely disconnect the power while WBR-SH2 is not in use. Therefore, the WBR-SH2 is always connected to the battery without a physical power switch. In total, the circuit board size of WBR-SH2 has reduced 50% from the main circuit board of the experimental system.

3.2.5 Mechanical Design

Concept 1 requires the housing to be mounted in between the commercially available resistance band handle and the band. There are a few considerations for designing the housing of WBR-SH2:

- The load cell sensor is direction sensitive; it should be placed with the direction of the resistance band.
- The housing structure should be strong enough to support the load from the resistance band.
- The housing can collaborate with the commercial resistance band handle and its handle, which maximise the use of the commercial parts.
- It should provide good protection for internal electronics.
- The housing should be short enough to avoid adding too much extra length compared to the original setup.
- It should be 3D-Printing-friendly to reduce the difficulty in prototyping.

The prototype design is shown in Figure 3-11 and Figure 3-12. The housing is designed to be two halves. There are many round corners in the design to reduce the potential stress concentration. The two halves are fixed together by four standard M3 hexagon socket head screws, M3 nuts, and wall guides. The housing is mounting to the commercial handle by two-cylinder bars at the top, which also shortens the total length. The inner space is separated into three compartments by some supporting walls. There are through holes between each compartment for wiring. The three compartments are arranging from top to bottom. The top compartment is designed for the main circuit of WBR-SH2. Two windows on the side walls are reserved for LED. The middle compartment (46x20x7mm) is reserved for the battery. The bottom compartment is reserved for the load cell and the load cell driver module. The structures around the load cell have been reinforced. The most surfaces are flat and perpendicular walls.

Which makes the housing are friendly to FDM 3D-printer for low-cost and fast prototyping.

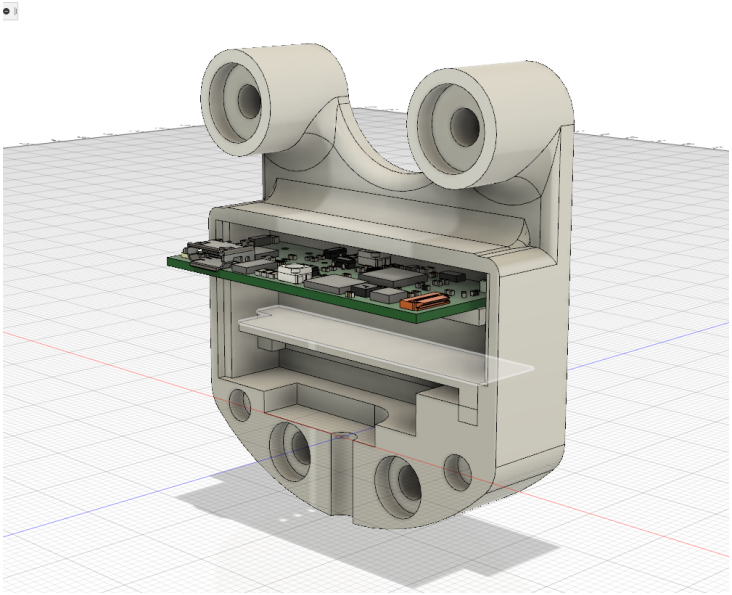

Figure 3-11 One of the two halves housing. The three compartments are separated by the highlighted wall and the supporting wall under the main circuit.

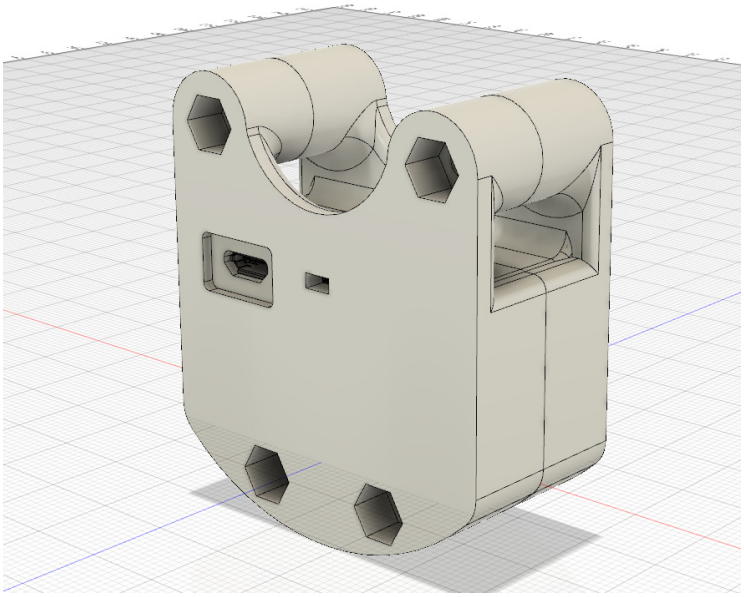

Figure 3-12 Assembly view of the housing. The housing mostly consists of flat surfaces and perpendicular walls. Two halves are secured by M3 screws and nuts.

The housing is designed by using Fusion 360 (Autodesk, Inc.). Then the 2 halves of housing are built separately with a 3D-Printer, using transparent PLA materials. The housing is estimated to consume 36g PLA material in 3D-printing.

The housing is simulated by software to determine whether it can undertake the maximum force. Two pull-up forces marked as the blue arrows are applied to each half which shows in Figure 3-13, while the plate for supporting load cell is locked to its position. Each force is 100N, together 400N is applied to the assembly. This force is 2 times larger than the heavy load resistance band. The simulation of the assembly is done by finite element analysis using Fusion 360, shown in Figure 3-14. The results show the stress and deformation with visible adjustment (not the actual deformation). Acrylonitrile Butadiene Styrene (ABS) is selected for simulation, which is normally used for manufacturing instead of PLA for prototyping. However, the property of both materials is similar in 3D-printing scenarios [100]. The maximum stress is in the holes reserved for charging socket. However, the maximum stress at 6.6MPa is still acceptable for the selected materials with a safety factor larger than 3. Due to the

simulated force is already 2 times of the maximum force, the safety factor, in this case, is larger than 6.

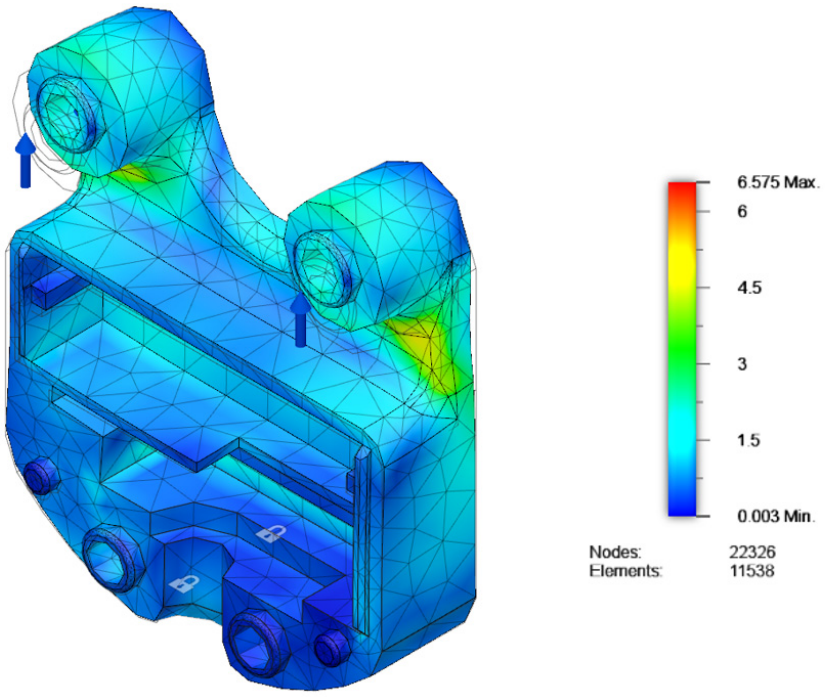

Figure 3-13 Load simulation using ABS materials (half view).

#

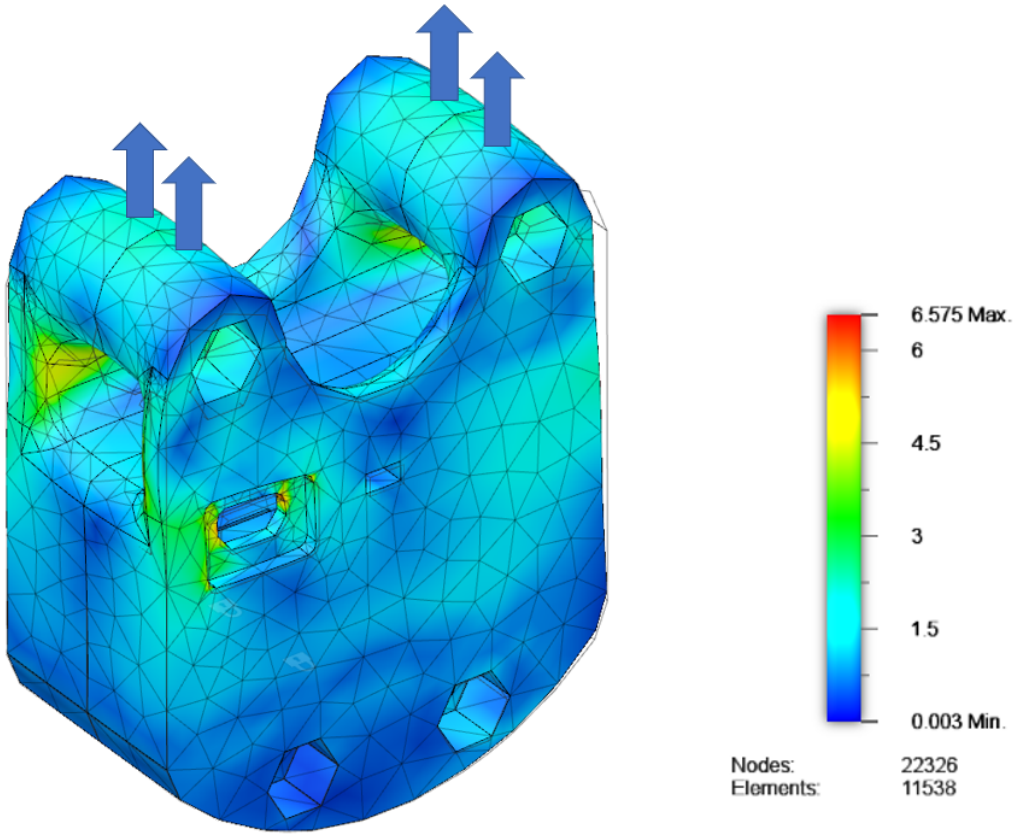

Figure 3-14 Load simulation using ABS materials (assembly view).

The comparison of prototype WBR-SH2 handle, and the commercial off-the-shelf handle is shown in Figure 3-15. The length of the prototype is similar to the commercial handle. However, it is foreseeable that the prototype housing will bring some restrictions to the user while doing exercise due to the physical interaction from the sensor. Also, the extra weight might affect the feeling of exercise.

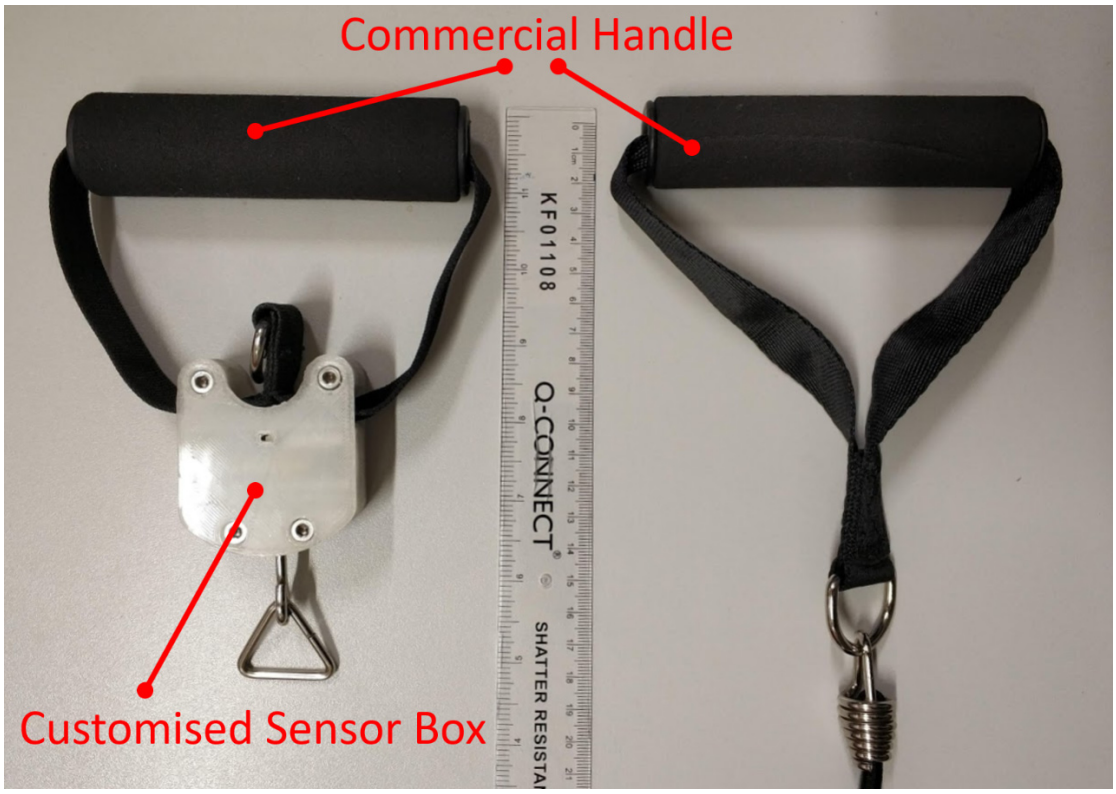

Figure 3-15 Comparison of WBR-SH2 prototype (left) and commercial off-the-shelf handle (right)

3.2.6 Firmware Development

The firmware development is based on a Real-Time Operation System (RTOS) named RT-Thread v2.1 for better multi-task scheduling. RT-Thread is a community-maintained open-source RTOS design for the Internet of Things (IoT). Using an RTOS will reduce the design firmware complexity, especially for sharing resources and low power scheduling. The working flow of the main tasks is shown in Figure 3-16. Due to the nature of multi-threading, each operation is running individually in their cycle. The inter-threading operations like mutexes, semaphores, message queues, mailbox, and events are widely used in the firmware. The main tasks are the BLE task, the sampling

task, the recording task, and a few miscellaneous tasks. Each of these tasks contains a single worker thread or multiple worker threads.

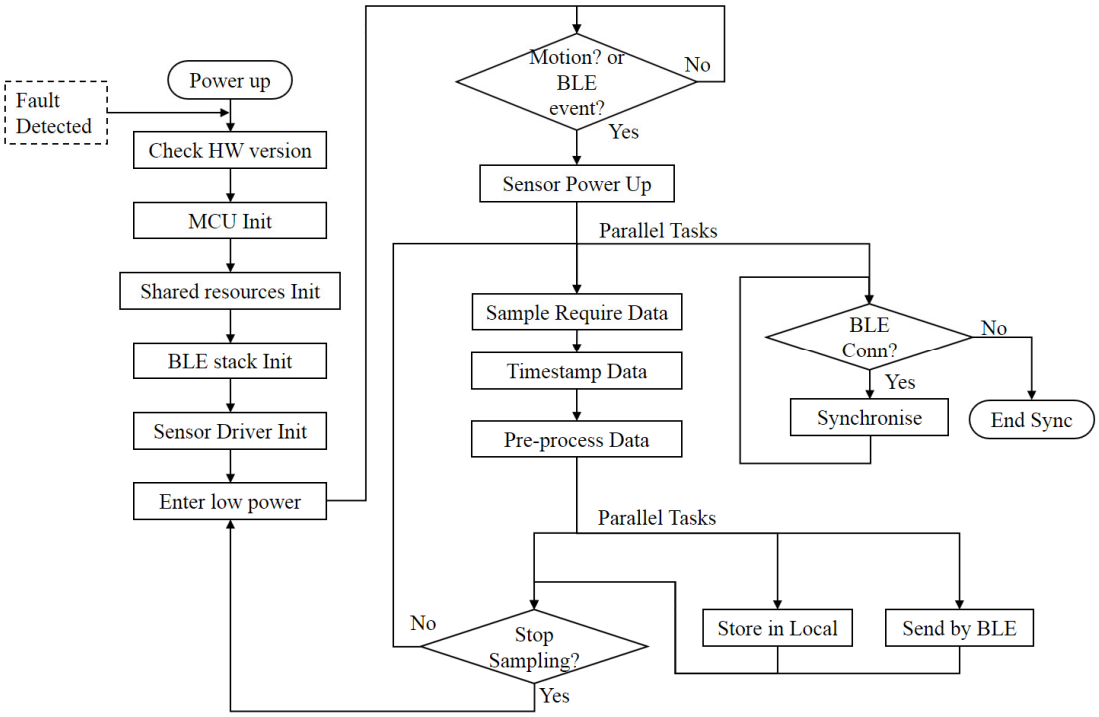

Figure 3-16 Working flow of WBR-SH2. The working flow includes many parallel tasks. These asynchronous tasks are scheduled by different priorities to ensure the most time-critical task is completed in time.

The design of WBR-SH2 hardware has avoided unnecessary hardware interaction to the user (buttons, data cables) to reduce the system complexity, which results in the BLE is the only method to control and acquire data. This function is achieved by setting up a customised BLE service, called WBR Sensor Service (WSS). A service in BLE acts as a data provider, which provides data input and output interfaces for clients. The WSS is consist of many customised characteristics (Char), including Config Char (CC), Real-Time Raw Data Char (RRDC), Advance Battery Data Char (ABDC) and Raw Ctrl Char (RCC). Among those characteristics, CC is for the general setting of WBR-SH2. The client can set and read the status of WBR-SH2 through CC. ABDC is for the client to read the battery details, such as the remaining battery volume, the voltage, the current, and the temperature. RCC is to control the output data, such as sampling frequency,

data source selection of real-time data or recorded data. RRDC is for output the raw data only, which will be described in detail below.

The value in RRDC contains one or more raw data frame(s). Each data frame includes a sampling timestamp, calibrated raw data from each sensor, and the orientation's quaternion representation. The format is shown in Appendix C. To maximise the data rate by BLE's new feature, the Date Length Extension (4.2 and later, allows maximum 251 Bytes PDU instead of 31 Bytes [101]), the length of RRDC value is variable. Each raw data frame is 64 bytes fixed length (with a few reserve bytes for future uses), and each RRDC value might contain 1 to 3 frames depending on the queueing data.

While offline measuring is required, the raw data frame can be recorded into the onboard SPI nor flash memory, then acquire later. The memory in the selected nor flash (W25Q128 [102]) is separated into blocks (64KB), sectors (4KB) and pages (256 Byte). The memory needs to be erased before writing data. The minimum erase size is one sector and the minimum write size is one page. To reduce the complexity, raw data frames are stored in a bundle of 4 frames which is the same size as one page (256 Byte). While the sampling rate is relatively high (such as 100Hz), the erase operation (erasing one sector takes 45ms normally and up to 400ms in the worst case) might not be completed before a new data frame arrives. Thus, the data recording is asynchronised to sensor sampling to avoid blocking. The asynchronisation is implemented by using a First-In-First-Out (FIFO) message queue between the sampling thread and the recorder thread. The sampling thread pushes a new raw data frame into the message queue and continues its work immediately, while the recorder thread takes out the available frames and write to the flash memory. The message queue with a size of 40 frames (relevant to 400ms @ 100Hz) is maintained by the RT-Thread. The capacity of the selected flash (W25Q128) is 16,777,216 bytes, therefore, the maximum frame number that can be recorded without overwriting previous data is 262,144. When the sampling frequency

is set to 100Hz, the maximum recording time is about 43 min. When the sampling frequency is set to higher than 100Hz, a full-chip erase needs to be performed prior to data recording. A prior full-chip erase will avoid the sector erase delay which potentially causes the loss of frames, but this operation will take about 40 secs usually and up-to 200 secs in the worst cases [102].

WBR-SH2s are usually operated in pairs; the time synchronisation between 2 separate wireless sensors, such as WBR-SH2, is fundamental but also a challenge. A novel synchronisation method for BLE sensor network using unmodified Android phone will be presented in Chapter 4. When a few WBR-SH2s are synchronised, data is only captured when the timestamps are an integer multiple of a reciprocal of the sampling frequency. The synchronisation is to align the capturing moments in every device. For example, if the sampling frequency is set to 100Hz, then, its reciprocal is 10ms; the WBR-SH2 only sample when the local timestamps are integer multiple of 10ms, such as 30 or 1,518,438,268,990 (when WBR-SH2s are synchronised with UTC 64-bit millisecond timestamps).

3.2.7 Android App Development

The new wireless sensor model is discussed in Figure 3-2. In the model, the smartphone is the key bridge which collects the data from the sensors and sends them to the remote cloud server. In the preliminary prototype without a cloud, the smartphone acts as a data recorder. WBR-SH2 only support BLE as communication. Thus, it is needed to develop application software (App) to acquire the data. Therefore, an Android App called SmartBand2 is developed specifically for interaction with WBR-SH2. SmartBand2 is written by JAVA programming language in Android Studio. SmartBand2 can run on variable Android devices which has BLE hardware available and Android version 5.1 or later. The App supports multiple WBR-SH2 (tested up to 8) connection and synchronised data recording [76]. While receiving data, a few selections of data can be plotted on screen in real-time. The data from multiple WBR-SH2 is converted

into metric units and recorded into one .csv file. The data from different sensors can be distinguished by the sensor's BLE physical addresses recorded in each frame. The data format record by SmartBand is shown in Appendix C.

3.3 Evaluation

3.3.1 Sensor Calibration

Some of the sensors come with factory pre-calibration and/or runtime calibration, for those sensors, no offline calibration is needed. Those sensors include the gyroscope, the magnetometer and the barometer. The gyroscope is factory-calibrated during manufacturing and runtime calibration is available in its Software Development Kit (SDK) [96][103]. The magnetometer is runtime calibrated by its SDK [103]. The barometer is factory calibrated, however, performing a one-point calibration will increase the relative accuracy [97].

The load cell used in the WBR-SH2 (as well as the experimental system) has no specifications available. So, the calibration of the load cell is needed. The accelerometer has not been calibrated during manufacturing. Therefore, the calibration for accelerometer and load cell is needed.

3.3.1.1 Load Cell Calibration

The load cells used in experimental system & WBR-SH2 are disassembled from a low-cost commercial weight scales, which is unbranded. Thus, the calibration for the load cell is not only to eliminate the measurement errors but also to develop a model to fit the sensor. The load cell in the experimental system was calibrated by using a linear model (3-1), described in Appendix D.1.3. The calibration which has been done in the experimental system is a 2 points calibration (weights applied by 0 and 5kg). The calibration results for the specific load cell used in the experimental system are: gain G=5835.92, bias b=8265300. In the previous calibration, the non-linearity and the cross-sensor stability are not evaluated.

$$d_m = G(d_r - b) \tag{3-1}$$

During the use of the experimental system, the bias of the load cell was found that is not fixed. Therefore, an auto-zero calibration for bias is implemented in the WBR-SH2's firmware to calibrate the bias automatically while the non-motion state is detected. The calibration uses the previous calibrated gain G=5835.92 and the previous linear model provided by an experimental system to verify the cross-sensor stability.

The calibration with WBR-SH2 is similar to the experimental system, but with more devices (2x WBR-SH2s), more precise (calibration-level weights compared to regular weights) and more calibration points (5 calibration points: 100g, 200g, 500g, 1000g, 1500g, compared to 2 points, 0 and 5kg). The calibration set up is shown in Figure 3-17. The WBR-SH2 was left still and unloaded for a moment until the auto-zero calibration performed, which compromised the weight of the loading box. Then the calibration weight is applied immediately. Thus, only the increment of force is recorded. The sample rate is set to 100Hz, however, the actual update rate from the load cell is 80Hz. The data is recorded for 3 secs after the weight is applied and the loading boxed is stable. The procedure is repeated for 3 times for each weight.

Figure 3-17 Load cell calibrations set up.

The results are shown in Figure 3-18. All the test points from both devices are plotted into the same graph. The linear regression lines are calculated by data from each sensor individually. The linear regression results are shown in Table 3-5. The regression line matched well, and the linearity is high.

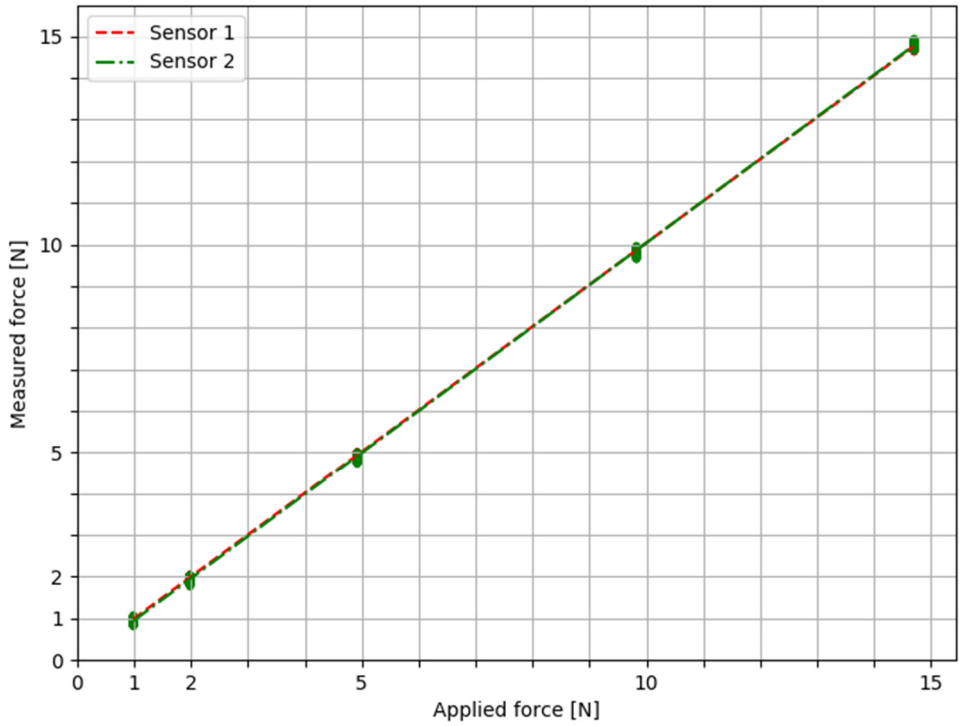

Figure 3-18 Cross-sensor stability of load cell.

Table 3-5 Linear regression parameters.

	Slope	*Intercept*	*Correlation Coefficient*	*p-value*	*Std. error*
Experimental System*	1.0*	0*			
WBR-SH2 #1	1.0053	-0.0104	0.999977	0.0	0.00009967
WBR-SH2 #2	1.0101	-0.0612	0.999959	0.0	0.00013233

*Using the results of the previous calibration for the experimental system as the reference

Thus, the load cells are approved to have high linearity, low noise level and stability for a range of resistance band measuring. The gain is stable across sensors. While with auto-zero calibration, the force measurement is accurate across two WBR-SH2 systems.

3.3.1.2 Accelerometer Calibration

The calibration of accelerometers on WBR-SH2 is the same as the accelerometer calibration on the experimental system, which shown in Appendix D.1.1. Each WBR-

SH2 has been calibrated individually and the calibration parameters are written into their firmware.

3.4 Overall System Performance of WBR-SH2

The sampling frequency for WBR-SH2 is adjustable from 1Hz to 200Hz to adapt to the variety of requirements in different scenarios. The provided sampling rates should be compatible with the resistance band exercise monitoring. If only raw data is needed (onboard sensor fusion is not needed), the WBR-SH2 can sample and transfer real-time raw data up to 800Hz with a single sensor node or 2 x 500Hz with the double sensor nodes to the same receiver in real-time (the receiver must support BLE 5.0 or later).

Thanks to the low-power oriented design, the sensorised handle in WBR-SH2 system can support up to 12 hours' full sensor sampling with a small 300mAh battery (@100Hz full sensor sampling, visual feedback, and real-time data acquisition or onboard recording), or up to 90 days standby. The handle will last at least four weeks with a single charge in a typical exercise intensity in resistance band intervention plan (e.g. Couch Potatoes for Recognition, three days per week, 40 minutes each day). Also, the battery life might extend further in the actual application. Because in real-life scenarios, only the aggregated information is necessary to transfer to a smartphone, the data size is much smaller than raw data. The SoC in the sensor is capable of processing data. Also, the sampling frequency can be lower to reduce power. The low-power neural network classifier for exercise recognition which runs on the SoC directly will be discussed later in Chapter 5.

Benefiting from the ultra-miniaturised design, the powerful onboard SoC, and the flexible configuration, the main circuit of WBR-SH2 also can measure the motion as a conventional motion sensor in variable applications. A comparison between the experimental system and WBR-SH2 is listed in Table 3-6. The specification which WBR-SH2 is superior to its predecessor is highlighted.

Table 3-6 Performance comparison of the experimental system and WBR-SH2.

	Experimental System	*WBR-SH2 System*
Circuit Size [mm]	55x28x5	45x18x1
Circuit Weight [g]	15	4
Working Current [mA]	130	22
Standby Current [mA]	15	< 0.1
Battery Capacity [mAh]	1400	300/400
Storage	Micro SDHC Card (up to 32GB)	Onboard Flash 16MB
Working Time [hour]	8	12/16
Standby Time [day]	2.5	90
Sampling Rate (Local storage) [Hz]	100, 200, 500	1, 10, 20, 50, 100
Sampling Rate (Over-the-Air) [Hz]	500	1, 10, 20, 50, 100, 500*
Offline Data Download Speed	1x (100Hz)	13x (100Hz)
Sensor Types	Gyroscopes, Accelerometers, Magnetometers, Barometer, Load cell	Gyroscopes, Accelerometers, Magnetometers, Barometer, Load cell
Synchronised Sampling	None	Yes
Interaction with user	None	RGB-LED, Buzzer*
NFC	None	Yes*
Communication	CAN Bus, UART,	UART (debugging only),

	Experimental System	*WBR-SH2 System*
	Sub-G wireless, BLE 4.2 UART module	BLE 5.0
Maximum Over-the-Air Bandwidth [kbps]	250	1300*
BOM Cost [GBP]	~70	~35

* support with the first revision.

3.5 Preliminary Public Patient Involvement

As discussed in Chapter 1, the acceptance of the real end-users (older adults) is equally important to the performance of the devices. Thus, a preliminary Public Patient Involvement (PPI) with mild dementia patients was done involving the WBR-SH2 system. The PPI was led by Professor Eef Hogervorst at Loughborough University to investigate the acceptance of new technologies in people with dementia. The WBR-SH2 system presented in the PPI as one feedback tools for the exercise interventions.

During the PPI, the sensorised handles are configured to light up using its onboard RGB LEDs according to the force applied to the resistance band. The LEDs were lighted up from 5 newtons force measurement with blue colour, gradual changed to green and stopped with red at 35 newtons measurement. In total three sessions were done. In each session, a patient and his/her carer were invited to a special room decorated with different kind of technologies which would be potentially helpful in interventions for dementia. WBR-SH2 system is one of the equipment that researchers discussed with the participants. The patients and their carers were asked the questions about usability, appearance, and suggestions. The feedback related to WBR-SH2 is shown below.

In the general feedback, all subjects (including carers) showed their acceptance and approval to the visual feedback. One carer pointed out that the colour encoding should be clearly informed to the carer who could explain this later to the patient during the

intervention because the patient might not be able to understand the meaning of different colours. Besides visual feedback, a carer also suggested a simple “beeping” sound feedback to the patient. Then, the patient would not need to look at the resistance band all the time.

Another feedback was the lack of motivation for doing exercises. One patient has successfully built a routine with cycling because “the exercise is very simple and there is a physical piece of apparatus” (as said by the carer). The carer also mentioned that if there is no one around to motivate the patient, the patient will not do the exercise. Possibly, built-in voice reminder with comments to encourage people of the resistance band when the band has not been moved for some time could be included.

One patient showed more interests in seeing data as he mentioned his background is a software engineer. He claimed the numeric feedback (data showing on screen) is more attractive to him, while colour feedback is more for other peoples.

Overall, most feedback on WBR-SH2 was positive. with some neutral feedback on motivations, the band selection and the colour of the bands.

3.6 Discussion

One of the improvements from WBR-SH2 system to the experimental system is the optimised power consumption, the better integration and the simplified operations. These improvements finally result in less complexity and better usability.

The ultra-compact BLE SoC, which comes with the built-in radio transceiver, primarily reduce the needs of space on the PCB. The onboard storage provides just enough space for 43 minutes of raw data measurement (@100Hz sampling rate), but the PCB size is reduced dramatically.

This new design reduced the size of PCB, reduce the operational complexity, and avoid the connector which could potentially be broken during exercise. The experimental extension pads on the experimental system have been abandoned to reduce the size.

The power strategies of WBR-SH2 system is low-power oriented. The working power consumption and standby power consumption are the key parameters for component selection. The layout and the passive component design of PCB are also low-power oriented. Comparing to the experimental system, the sensorised handle in WBR-SH2 system has 5 times lesser working current and 150 times lesser standby current, which allows it to work on a much smaller battery (300mAh compared to 1300mAh) but still capable of performing. The standby time is also increased from 2.5 days to about 90 days.

WBR-SH2 uses BLE as the only communication method. With a large amount of supported smartphone, WBR-SH2 can communicate with a wide range of existing Android device, including the end user's Android phones. It reduces the cost of the system and improves the usability dramatically while compared to the conventional wireless sensor system, which requires a wireless adapter and bulky software for data acquisition. The use of BLE also allows multiple WBR-SH2s to connect to the same Android device and transfer real-time data simultaneously. The novel synchronisation method (will be presented in Chapter 4) allows multiple sensors are working with sub-milliseconds synchronisation accuracy, which is enough for body motion measurement.

The completely redesigned housings have improved the reliability massively. The hardware and firmware designs are button-less and always-power-on. The design of the housing has avoided the movable part and reduced the numbers of holes which can weaken the structures. The 2 halves housing is fixed by standard M4 screws and nuts, and the prototype design comes with a large flat surface which is 3D-Printing friendly. The cost of mechanical parts is lower and the manufacturing is easier compared to the experimental system.

However, in the WBR-SH2 system, the IMU is placed in a remote position (the sensor box) to the user’s hands, where the IMU cannot measure the movement of the

user's hand directly. This limitation should be considered in experiments and data analysis in the following studies.

Thanks to the good computational power and rich memory resources in the selected BLE SoC, the firmware is multi-functional. The use of RTOS reduces the complexity to manage the shared resources and multi-thread scheduling. Taking advantage of the computational power, WBR-SH2 can not only act as a measuring unit (data provider) but also a processor (data consumer). The sensor calibration, data filtering, and orientation computing are done by the device directly instead of a dedicated computer. The data output from WBR-SH2 is calibrated and normalised, which is readable for researchers or experts without doing extra data processing. As the data consumer, a neural network classifier is also implemented into the SoC for exercise recognition, allowing the sensor to aware of what kind of exercise is performing by the user (will be discussed in Chapter 5 and Chapter 6).

Although the preliminary PPI is not widely covered by the number of participants, it is very valuable to the development of the WBR-SH2. The results have proven the overall design of WBR-SH2 is successful in many aspects such as usability and the acceptances. The sound feedback which was produced by the PPI has been added to the WBR-SH2 in the first revision. The PPI also pointed out that with the nearable concept, WBR-SH2 might be easier to be forgotten by the user because of the lesser motivation compared to traditional exercise instruments. A better instruction of the sensor, local group exercise, or online community and doctor's endorsement might help to improve the motivation.

Overall, the WBR-SH2 is superior to the experimental system in most aspects and as well as the real-life application. The WBR-SH2 is the key component of the resistance band intervention model, which discuss in 3.1. The prototype has fulfilled most of the requirements in PDS and the objective described in 3.2.1, and it is proven that design concept 1 is achievable.

3.7 Conclusion

The limitations in the experimental system prevent it from being widely used in a further experiment. Therefore, a new sensor was built to overcome these problems. A development process of the new WBR-SH2 system is then shown in this chapter, including the problem statement, objectives, system specifications, initial design concepts, hardware (PCB) development, firmware (embedded software) development, Android App development, evaluation with load cell and accelerometer calibrations.

In the problem statement, the problem and limitations of the experimental system are summarised and shown. They are:

- Lack of band direction sensing.
- Power shortage.
- No synchronisation between multiple sensors.
- Required extra wireless adapter.

The general objective of building a new resistance band system (WBR-SH2) are discussed. They are:

- Similar sensor set-up as the experimental system (IMU, barometer and load cell).
- Durable structures.
- At least 2 devices could be synchronised.
- Improve usability.

The design of WBR-SH2 is shown in 3.2. Starts from providing a PDS, which list the minimum, realistic and ideal requirement of the new sensors. Following the PDS, 2 main concepts of WBR-SH2 are ranked out for the final decision. Concept 1 is a completely new concept with one-box design; Concept 2 is an improved design of the experimental system. The decision is made to Concept 1 in the comparison. Concept 1 has many advantages such as robust housing, less mechanical design difficulty, reused commercial handles to reduce the cost, and can measure resistance band direction. The challenge of Concept 1 is the space for electrics and battery are limited.

The limited space challenge is solved by low-power oriented hardware design and optimised compact multi-layer PCB design. The former reduces the size of the battery dramatically, while the latter reduces the size of PCB. To have better interaction with the end-user, WBR-SH2 also includes a set of RGB-LED and a buzzer, which provides visual and sound feedback to the user. The optimised hardware design reduces 50% in PCB area, 5 times lesser working current and 150 times lesser standby current.

The mechanical part of the housing is designed to be 2 halves, which assembly together by the standard screws and nuts. The housing is 3D-printing friendly, allowing fast and low-cost prototyping.

The firmware is designed to be multi-threading. Thanks to the rich computational and memory resources available in the selected SoC, the WBR-SH2 can not only measure data but also process the data. The built-in high-speed BLE radio allows fast real-time raw data transmitting to Android phone up-to 500Hz with a pair of WBR-SH2s. Synchronisation in a distributed sensor network is fundamental but challenging, especially with a wireless sensor system. A novel synchronisation method is implemented into the firmware and Android App to ensure multiple WBR-SH2s are synchronised within 1ms.

The load cell on WBR-SH2 is calibrated by using the linear model. The linear model is validated with WBR-SH2s, and the accuracy and range are for resistance band exercise measurement.

The overall performance indicates that WBR-SH2 is capable of undertaking the works done by the experimental system with much better usability and functionality. The PPI has proven the acceptance of WBR-SH2 with the real-life end users to a certain extent.

The development of WBR-SH2 is only the first step for remote exercise measurement. The following Chapter 4 will describe the problem of synchronisation in BLE sensor network and provide a novel method to overcome the problem using an

unmodified Android device and multiple WBR-SH2. The latter Chapter 5 presents the development of a high-level neural network framework for microcontrollers, and it is successfully implemented into WBR-SH2 in Chapter 6.

Chapter 4 Sub-millisecond Synchronisation of Bluetooth Low Energy Network

4.1 Introduction

During the last 2 decades, wearable inertial sensors are widely used by researchers to investigate the potential risks and the motor function of human bodies. In the past, most sensor systems are scanning measurement through physical wired connections which links up all sensor nodes. These sensor systems usually consist of one central device and multiple sensor nodes [104], [105]. Data are exchanged through physical wires by serial communication interfaces (CAN, RS485, I2C). The wired systems are capable reliable but also have some clear limitations: (1) Physical interference between sensors. (2) Complex to set-up. (3) Uncomfortable wearing. Recently, many sensor systems are basing on wireless communication and distributed powered nodes [54]. Wireless sensors aim to avoid the needs of physical wires. Those wireless sensor systems are taking advantages of less inconvenient and less interference by physical connections between each sensor node. However, wireless sensor systems are always suffering from unstable communication latency and power shortage in remote nodes.

Back in 2010, the first Bluetooth Low Energy (BLE) was introduced in Bluetooth 4.0 specifications. BLE aims to provide low data latency, reliable data transmission and low energy consumption features, which makes BLE an ideal wireless network protocol for Wireless Body Area Network (WBAN). Most importantly, BLE is already widely implemented in most of the smartphones which released after 2011 [106]. If a WBAN could be formed with a smartphone and many sensor nodes, the cost of the system will be lower and usability will be improved dramatically. In this ideal WBAN, wireless

sensors nodes responsible for measuring, while smartphone acts as a central device to process data.

To accurately measure motion data, other than the sensor accuracy, the timing of the measurement is also important. Timestamping the data on the receiver side is inaccurate due to the possible loss of messages or delayed by retransmission in a crowded wireless environment. The ideal method is to timestamp the measurement immediately on the sensor node before being sent out to the data receiver. This method requires the sensor node is synchronised and has an accuracy local clock. Once the data is timestamped, no matter whether the data is delayed or not, the timestamps on the data are still accurate when the master receive it.

Therefore, the sensor needs to be synchronised before starts sampling and during the sampling. This chapter presents a novel method to synchronise the timing between sensor nodes in a connection-oriented BLE network by using an Android phone. It is implemented by an unmodified off-the-shelf Android phone as a central device and multiple embedded systems as sensor nodes. A specific Android App to perform the necessary operation on the Android side is installed on the testing smartphones. The results show a maximum synchronisation error within 1.2ms across 5 sensors with variable unmodified Android Device.

4.1.1 Bluetooth Low Energy Overview

In the view of transmitting data using BLE, there are mainly two methods of doing this: advertising and scanning (connectionless-oriented) or connection (connection-oriented). Figure 4-1 shows the difference between both methods.

In connectionless-oriented BLE network, there are 2 kinds of devices, “beacons” and “scanners”. Beacons broadcast messages occasionally, while the scanner keeps scanning whenever it is available. In this network, data will be broadcast in limited length messages by beacons. Acknowledgement from the scanner to beacons is not available. This method can easily achieve multiple TX to multiple RX topology because

no connection and synchronised channel hopping are required. However, there are some limitations, including (1) limited length of the payload. (2) limited data bandwidth (3) single direction communication. (4) no acknowledgement, i.e. messages are not guaranteed to be received [101].

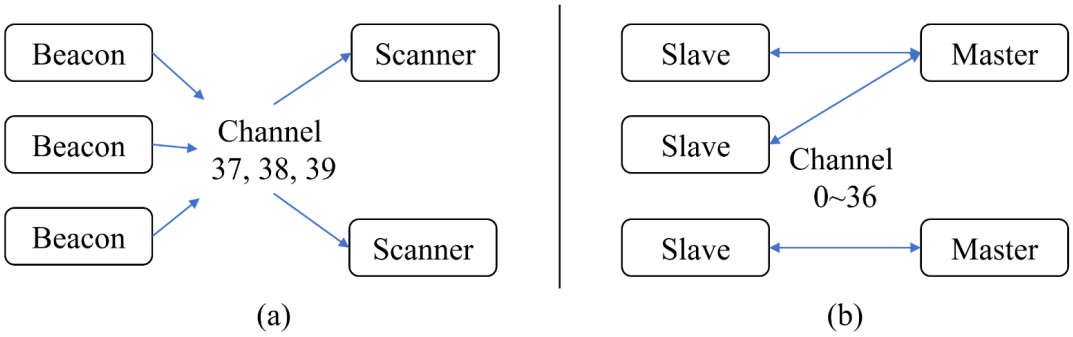

Figure 4-1 (a) Connectionless-oriented BLE network. (b) Connection-oriented BLE network.

In connection-oriented BLE network, there are two kinds of devices, “master” and “slaves”. Typically, in one connection-oriented BLE network, there is only one master and one, or multiple slave(s). In contrast to connectionless-oriented BLE, a connection is established after an advertising device broadcasts connectable advertising message, and a scanning device initiates a connection with it. After initialisation, the advertising device will perform the slave role, and the scanning device will perform the master role. Data will be exchanged by one of the 37 physical channels with channel-hopping technology. In the connection state, the master is responsible for organising the timing of communication with each slave, while the slaves follow the timing strictly. Communication only happens when the timing is agreed. When not actively communicating, the slave will enter radio idle or system sleep state, to reduce power consumption. In connection-oriented BLE, each slave is invisible to others.

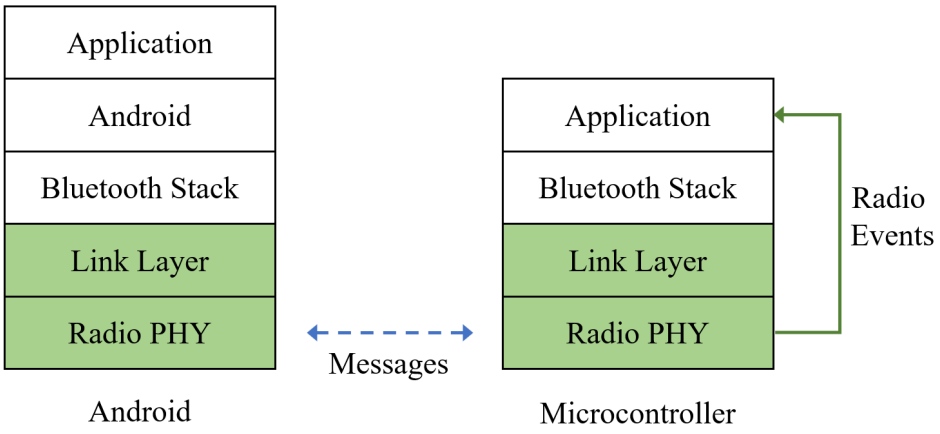

Figure 4-2 Simplified BLE structures involving Android and microcontroller. Layers marked by green shades are time-critical while others may not. Radio events are available in some microcontrollers which allows applications to access low-level timing.

In connection-oriented BLE network, the low-level timing is critical. The Structure of the BLE stack is shown in Figure 4-2. The timing is guaranteed by Link Layer in both ends; any upper-layer has no access to the timing information. Figure 4-3 shows a typical BLE network contains one Master and two Slaves. A timeslot that Master and Slaves exchange message called Connection Event (CE). A CE is started at a specific timing point called Anchor Point (AP), which is controlled by Master and strictly followed by Slave. The AP is triggered at a fixed interval called Connection Interval (CI). The length of the CE is not fixed. It might be ended by the Master or Slave actively or passively. However, a CE is always started at the AP. At the AP, the Master will always transfer the first message to the Slave to indicates a start of CE as well as for Slave to recalibrate the AP. There is an optional Slave Latency indicating a maximum number that Slave could ignore (not respond to Master) the number of CE without being considered that the connection is lost. The AP is resynchronised in Slave's Link Layer whenever a new message is received (where a CE is started). To be noticed, if there is no data to transmit, an empty Protocol Data Unit (PDU) will still be transferred from Master to Slave to start a CE.

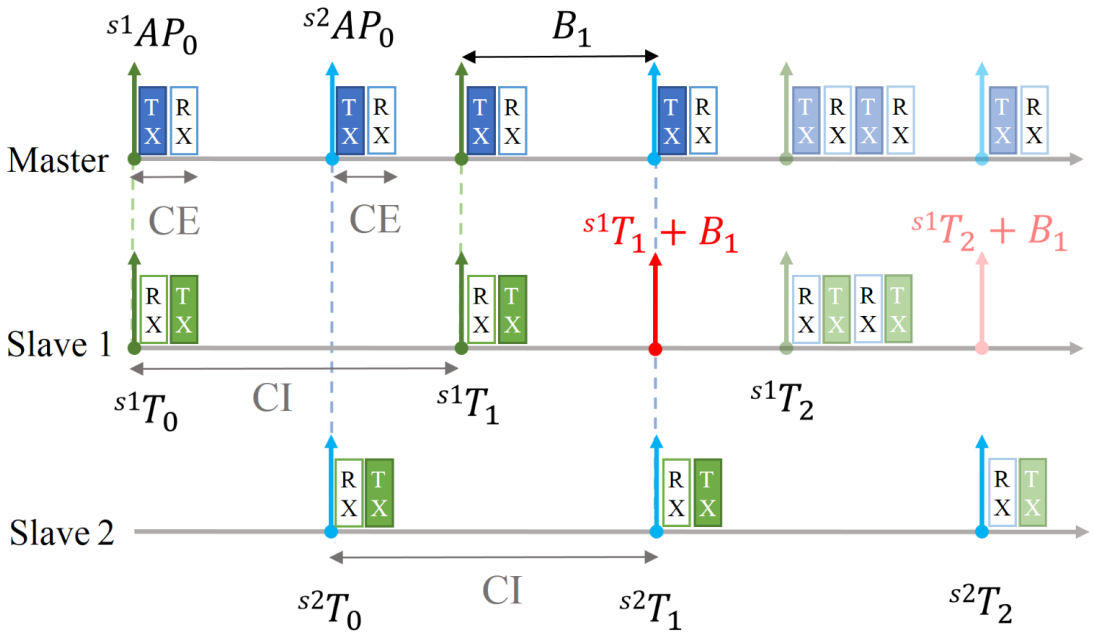

Figure 4-3 Connection Event in BLE connection.

4.1.2 Related Works

Synchronisation for distributed sensor system has been researched and implemented for decades. However, those distributed systems that use BLE do not benefit from the existing works, such as the Reference Broadcast Time Synchronisation (RBS [107]) and the Timing-sync Protocol for Sensor Networks (TPSN [108]). Many studies have explored the synchronisation of BLE sensor network since the first BLE version was released.

Accurate synchronisation using BLE can be achieved when both ends could access the accurate timing information in the BLE stack. Some of them are implemented in connectionless-oriented BLE networks. BlueSync [109] focuses on synchronising a Beacon with a Scanner by timestamping the fixed-length advertising message on both sides. A similar setup by CheepSync [110] used modified Android phones and beacon units. The authors modified Android firmware to access timing information down to the device driver to avoid the unpredictable delay that causes by BLE stack. Both methods

require accessing very low-level timing, and both reach almost the same level of accuracy at about 10μs.

There are some studies that focus on the synchronisation in connection-oriented BLE network. A study by Dian et al. [111] has further assessed the method provide by Bideaux et al. [112]. Their method is to timestamp the "connected-event" that is generated on both sides while a new BLE connection is established. In Bideaux's method [112], two embedded BLE modules were used to perform the synchronisation. One module acts as an advertiser and the other acts as a scanner. The scanner initialises a connection with the advertiser, then both wait for the "connected-event". Once the event is triggered, both devices output pulses to an oscilloscope, and a microcontroller for data logging. The results show the accuracy of the synchronisation during connection establishment is around ±750μs. Since this method can only be applied at the beginning of each connection, it cannot continually calibrate the clock drift in sensor nodes.

There are also some studies that use external measurement methods for synchronisation. A study by Somaratne et al. [111] uses the current consumption pattern during the connection to synchronise the device, with an accuracy of 19μs being achieved.

To conclude, the results of the methodologies described above are good enough for some limited distributed sensor network application. Some of the methods focus on reaching the low-level timing information to avoid unpredictable stack accessing delay, whilst, others require external hardware for capturing radio power pattern. The methods described are incompatible with BLE sensors systems using an off-the-shelf stock smartphone.

4.1.3 Problem Statement

In wireless sensors systems, synchronisation between sensor nodes is a fundamental issue. Especially when the system is involving a user's smartphone for the

only method of data acquisition and control. In these cases, only standards protocols (such as Bluetooth, WiFi) can be used by the sensors, while they are reliable in transmission but less time-critical.

In Chapter 3, BLE is selected as the only communication method for WBR-SH2. When there is a need to involve both hands for resistance exercise, the two WBR-SH2s must be synchronised. However, the accuracy of generic BLE Time Service is not accurate enough (Time Service resolution is 1/8 secs)[113]; while the motion sensing is always requiring higher accuracy [114]–[116]. The methods discussed in 4.1.2 have tried to solve the problem from different perspectives, but all require modification of the user's smartphone, which is not suitable in our application scenarios.

4.1.4 Objectives

The objective is to develop a synchronisation method for typical applications involving customised sensors and off-the-shelf smartphones. The study should fulfil the requirements of:

- The method must base on the standard BLE protocols.
- The method can synchronise at least 2 sensors at a time.
- Able to synchronise sensor with miniature impact on the original bandwidth.
- The synchronisation accuracy must be less than 10ms (at 100Hz sampling rate).

4.2Methodology

It is essential to capture the system time as time-critical as possible when synchronising networks. The more critical usually means better synchronisation accuracy. The targeting BLE network consists of two kinds of non-equivalence devices, one Android device, and multiple customised sensor nodes. The major difference between the two types of devices is the accessibility of the BLE stack. Without modification on Android firmware, the programming is restricted to the very top App-level, which is less time-critical. On the contrary, the programming on sensor nodes (embedded system) could be more time-critical. Although the Android application level

is less time-critical, the timing is still guaranteed in the Link Layer which is always time-critical as required by the Bluetooth core specification [101].

The method proposed in this chapter is based on the accurate timing within the Android's Link Layer, even though the time is not accessible to the App-level. Sensor nodes use their time-critical programming to synchronise with Android's Link Layer timing. Whilst the Android device identifies the biases between sensor nodes by timestamping BLE transaction callbacks in App-level programming.

To clearly explain the method, the principle of connection-oriented BLE needs to be introduced first. The principle and related background information of BLE is described in section 4.1.1. In section 4.2.1, the detail of our approach and the evaluation method is discussed.

4.2.1 Synchronisation Method

The key to synchronising the network is to identify the biases and clock rate in every slave. As mention in 4.1.1, while in the connection state, the timing of AP is already guaranteed by the Link Layers at both sides. Therefore, it is ideal to calibrate the Slave's local clock by referencing AP. The principle of our method is to use captured AP on the slave side as a time reference, by adding bias to the AP to match the other slaves. Once AP and bias are known in a slave, the networks it can adjust its local clock to match the network's clock.

For example, in Figure 4-3, assuming the two slaves are connected to the master with the same CI, once the bias (B_1) and AP are known by slave 1, then slave 1 can add the bias to its AP (${}^{s1}T_1 + B_1$) to match the other slave's AP (${}^{s2}T_1$). Then, the two sensors are synchronised.

Due to the nature of the BLE connection, each connected slave is invisible to other slaves, the master is then responsible for identifying the biases between slaves.

Beside the biases, the clock rate is also calibrated in the slaves to improve the accuracy. This is done by using linear regression with multiple APs in the slave.

4.2.1.1 *Clock Calibration Model in Slaves*

A clock calibration on Slave can be described as a linear model referring to (4-1). If we assume that the clock of the network is based on the master's Link Layer, then $T_{Network}$ represents the time of Master, T_i is the local time of the slaves, CR_i is the clock rates in the slaves, and B_i is the bias for the slaves.

$$T_{Network} = CR_i \cdot T_i + B_i \tag{4-1}$$

4.2.1.2 *Slave (Sensor Nodes)*

In the Slave side, the slope $A_{1,2,3\ldots}$ could be calculated by using the local timer to capture the local timing of AP. Each Slave needs to know when is the AP for its connection. Although the Link Layer is calibrating AP automatically, there isn't access to this information if the BLE stack is close-sourced or pre-compiled.

However, there is a possibility to estimate when is the AP from variable aspects. In many of the commercial BLE chips or SoCs, there is an interrupt indicated that the next CE is started in a range of time ahead. Specifically, with Nordic BLE SoCs, there are a few RF events can be used to capture the radio hardware directly by linking them to its specific designed Programmable Peripherals Interface. A comparison of different events is described in this study [117]. Although one of them could capture the AP directly, the timings of them are related to AP. For example, the Address Matched Event (AME) is triggered whenever the RF PHY capture the Access Address, which is always triggered at the beginning of receiving a message. As mention at 4.1.1, no matter there is data to send or not, the Master will always send a message to Slave at the AP to initiate a new CE. Therefore, an AME is always triggered when a CE is started unless there is interference in the environment resulting in hardware failing to capture the message. We assume the timing of Address Event to AP is relatively fixed, then the slope can be calculated using Address Matched Event.

4.2.1.3 *Master (Android Device)*

As discussed previously, the Master is responsible to identify the biases across each Slave. Considering the complexity of the Android system and the limited information in App-level programming, it is hard to know when is the AP exactly. One of the previous studies, CheepSync, modified the USART driver to timestamp the messages in HCI, which are transferred between Link Layer and upper BLE stack. This has avoided the delay of processing package through upper BLE stack. However, without modifying Android firmware, this method cannot be done. In this chapter, we timestamp transaction's callbacks to estimate the biases between different Slave's AP. Specifically, a Write transaction and its callback are used to calculate these timings. The procedure of transaction is shown in Figure 4-4. For each Slave, the Master sends a WRITE transaction and timestamp right after the Write callback is called. By comparing the timestamps delays across Slaves, the bias of each Slave can be estimated.

4.2.1.4 *Bias Estimation*

In the previous discussion, biases can be identified by the APs of different Slaves, and the biases estimation must be done in Master side. In the Android App-level programming, there is no access to the timing of AP directly. By using BLE transactions, there is a chance to estimate the bias, because the *Response* of transaction is always close to one of the APs. In our method, a default *Write transaction.* The transaction is performed by Master write a characteristic on Slave which requests acknowledgement (*Response*) from the Slave. The *Response* is then used to estimate bias. The transaction is shown in Figure 4-4, where clearly shows how a *Response for Write transaction* is related to an AP. In Android, receiving a *Response* will trigger a callback to App-level. Then, these callbacks are timestamped individually according to different Slaves. Due to Android's multiple task and nonpreemptive nature, the delay from the actual AP to the callback is unpredictable. If we assume the delay is standard distributed and the

mean delays are equal across Slaves, then the actual biases can be estimated by linear regression.

In the practice, a *Write transaction* is started with App sets up a message and uses *BluetoothGatt.writeCharacteristic()* to write the message into Android's Bluetooth stack, where timestamped as T_{ms}. The message must wait for the next available CE to be sent out. When the message is transmitting, an Address Matched Event (AME) will be triggered in the embedded system (Slave) at the very beginning of transmitting with minor fixed delay to AP [101]. After the message is received and the CRC (Cyclic Redundancy Check) is checked, a *Response* is sent from the embedded system to acknowledge the message. The *Response* must wait for the next available CE to be sent out. In the next CE, an empty PDU or a new message will be sent from Android to indicate a new CE started. The empty message takes t_s to for transmitting. Then both sides will wait for an Inter Frame Space (T_IFS: t_{IFS}). After T_IFS, Slave sends out a *Response*. The transmission takes t_r to complete. When Android receives the *Response*, it takes t_p to process the *Response* within Android and its Bluetooth stack, and then trigger a write-completed call-back, *BluetoothGattCallback.onCharacteristicWrite(),* where timestamped as T_{mr}.

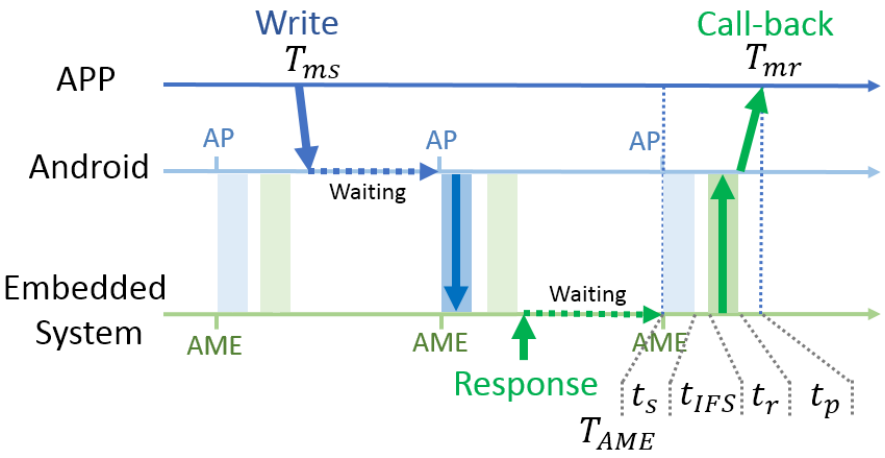

Figure 4-4 A completed Transition using WRITE transaction.

In Android App-level programming, only T_{ms} and T_{mr} is known. The relationship between AME timestamp (T_{AME}) and T_{mr} is shown in (4-2). Per BLE spec [101], the t_s , t_p and t_r are relatively constant. The length of the message, Empty PDU and Response PDU are known and can be estimated by over-the-air bitrate, and the T_IFS is also fixed to 150μs. The Response processing time $t_p$is the only unpredictable parameter. We assume $t_p$is normally distributed. If the transaction has been repeated many times, then the average $\bar{t}_p$ should be stable.

$$T_{AME} = T_{mr} - (t_s + t_{IFS} + t_r) - t_p \tag{4-2}$$

In BLE network with multiple Slaves, if we select one of the Slave's T_{AME} as clock reference T_{ref}. Then the bias of other Slaves could be calculated by (4-3).

$$B_i = T_{mr_i} - T_{ref} \tag{4-3}$$

However, the process that described above is valid only when:

1) The connection is idle, but only the synchronisation transactions are transmitting.

2) No interference leads to message retransmitting.

While there is some interference in the environment, retransmission will be performed by the Logical Link Control and Adaptation Protocol Layer (L2CAP, one of the BLE layers above Link Layer) without notifying the upper layers and App. Retransmission leads to an unpredictable time delay, which could be an integer of CI.

To detect the retransmission, a Write-to-Response delay should be identified which can be calculated by $t_{wr} = T_{mr} - T_{ms}$.

While a Write-to-Response is delayed, it is unclear whether the delay happens on sending *Write message* or on receiving *Response*. Due to this uncertainty, the procedure described above cannot be performed. Therefore, the transaction should be considered as invalid. The Write-to-Response delay of the last operation will be included in the next Write message and sent to the slave.

On the Slave side, it is never known whether the current message is valid until the next message arrives. While calibrating the local clock, Write-to-Response delay (t_{wr}) that are larger than two times the CI will be excluded. Linear regression is used to estimate the next AP when the transaction is delayed.

Due to the nature of BLE, it is important to note that the connection parameters are set by the master and will not tend to change unless required. Once the estimated biases are steady, the continuous bias estimation is not necessary. The link resources occupied by the synchronisation can, therefore, be released.

4.2.1.5 Clock Rate Calibration

To reduce the power consumption, BLE devices could use low power, low accuracy clock source (maximum 500 parts-per-million [ppm] on each side) for sleeping clock [101]. In our method, the clock drifting is eliminated at each AME once a new CE is established. The clock synchronisation period is the same as CI. Therefore, when a CI (from 7.5ms to 4s [101]) is relatively long, Slave Latency is enabled, or interference that leads to an unsuccessful transaction, the synchronisation period will increase respectively. In these cases, the clock drifting within one synchronisation period might be significant. To reduce the clock drifting within a synchronisation period, the clock rate in Slave needs to be calibrated to match Master's clock rate. The calibration is done by linear regression with multiple AME timestamps. The slope of the regression line is the Slave's clock rate.

4.2.2 Evaluation Method

To evaluate the effectiveness of the synchronisation, we need to measure the local timing on each Slave. The Slave was configured to output a pulse signal per its calibrated timer. The pulse interval was set larger than BLE interval to avoid misunderstanding. An external development board will be used to record the pules.

4.3 Experiment

To validate the method performance, the method was implemented into a small network which included a stock Android device. Two tests have been done to evaluate the effectiveness of synchronisation. The cost of computational resources and memory is recorded.

4.3.1 Experimental Setup

In the practice, the synchronisation method is evaluated in a small BLE network, which is consist of 5 customised sensor nodes (WBR-SH2 [75]as slaves) and one of the variable Android smartphones (as the master). WBR-SH2 is an embedded sensor node designed for exercise monitoring using multiple sensors. The WBR-SH2 is controlled by a high-performance low-power Bluetooth SoC, Nordic nRF52832. In the previous study, the clock drifting of WBR-SH2 was measured and was found to be as large as 1.5% base on its low power clock source [76]. The inaccurate clock makes WBR-SH2 an ideal device for evaluating this synchronisation method. In the experiment, WBR-SH2s were configured to output pulses per its local clock though a GPIO (General Purpose Input/Output). Additionally, an nRF52DK development board was physically connected to these WBR-SH2s to capture the pulses. The experimental setup is shown in Figure 4-5.

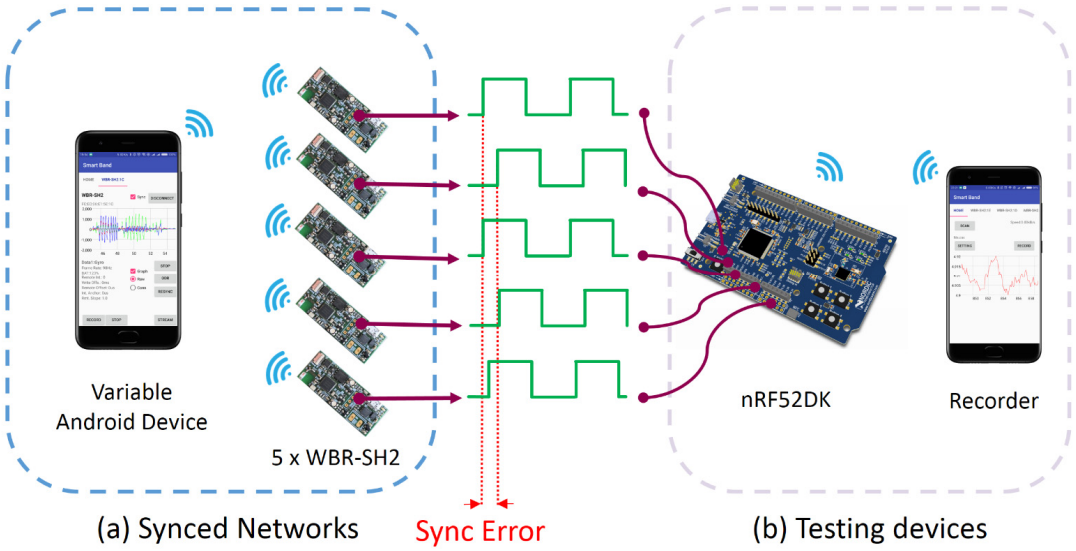

Figure 4-5 System view. (a). A connection-oriented BLE networks, consisting of one Android smartphone and 5 WBR-SH2. They are performing synchronisation. (b). The external testing device to capture pules and calculate sync error.

To be simplified, the same BLE connection parameters are set for each Slave during the experiments:

1. Connection interval: 25ms
2. Slaver Latency: 0

The tested clock source in Slave was set to the default 1MHz low-power clock source in each sensor node. The resolution of the timers was set to 1μs.

On the smartphones (Master), a customised App was installed to perform the time synchronisation. The screen on all smartphones was set to remain on during the tests. When all slaves are connected to the master, the master started to send *Write messages* to every Slave with a fixed interval of 100ms. The slaves then outputted the pulse signal with a frequency of 5 Hz, and 50% duty per its calibrated local clock. Ideally, after synchronisation, the edges of output signals from the 5 devices should be closely matched.

The selected Android device are listed in Table 4-1 with Bluetooth version from 4.0, 4.2, and 5.0, the SoCs from low-end to flagship, and the variable Android versions including 5.1.1, 6.0, 7.1.1, 8.0. AnTuTu is a benchmarking tool commonly used to

benchmark phones and devices. The Central Processing Unit (CPU) performances of AnTuTu Benchmarks for each device are listed for performance comparison, the higher the score, the better the performance [118].

Table 4-1 Selected Android Device (Ranked by CPU performances)

Phone Model	*AnTuTu Benchmark (CPU)*	*Android*	*BLE*	*Test*
One Plus 5T	72541	8.0	5.0	1
Xiaomi Mi 6	72454[a]	8.0	5.0	1/2
Xiaomi Mi 6	70193	7.1.1	5.0	1
One Plus 3T	54053	8.0	4.2	1
Sony Xperia Z2	33132[a]	5.1.1	4.0	1/2
LG Nexus 5	22393[a]	6.0.1	4.1	2
Galaxy TAB Active T365	15578 [a]	5.1.1	4.0	1/2

[a] Benchmarking is done by the tested devices with AnTuTu 7.1.0.

4.3.2 Evaluations Method

The evaluation of the synchronisation effectiveness is based on the pulses output from 5 Slaves. As shown in Figure 4-5, the Slaves continually output the pules through one GPIO per its local clock. Each of them is connected directly to one of the GPIO on the nRF52DK. These GPIOs on nRF52DK are configured to captured both rising and falling edges of the input signal. A set of Programmable Peripheral Interconnect channels are used to link GPIOTE event with timer capturing task. The clock source for the capturing timer is set to high accuracy (20ppm) onboard crystal. Once an edge of the pules was detected, the timer captured the current counter to the corresponded channels' register. The values in the register were read, stored and then transferred to another phone for data recording. Finally, values were saved in the recorder (another smartphone) using a .csv (Comma-Separated Values) formats for post-analysis.

4.3.3 Experiment Protocols

The tested BLE network is consist of 5 Slaves and 1 Android Device. The selected Android device acted as the Master separately.

The experiment is separated into two individual tests.

4.3.3.1 Test 1: Time Stability Test

Test 1 evaluated continuous synchronisation effectiveness. First, the network was set up (5 Slaves were connected to the Master). Then, 30 seconds continually synchronisation followed. The 30 seconds of synchronisation allows about 300 transactions for the initial bias estimation. The synchronisation was continually performing while the pulses were recorded for 3 minutes.

4.3.3.2 Test 2: Network Initiating Stability Test

Test 2 evaluated the stability of initiating a new network. After the network was set up, the network will perform the synchronisation for 30 seconds for initiation. Then, the synchronisation was performed continually, the pulses of 5 channels were recorded for 30 seconds. Test 2 was initialled 12 repetitions for each tested Android device.

4.3.4 Resources Consumption Analysis

4.3.4.1 Master

Master is responsible for calculating the biases across Slaves. It requires the smartphone to keep a limited length queue (300 timestamps, 30 seconds) for the bias estimation for each Slave. As mentioned in 4.2, once biases are stable, there are not any other works needed for synchronisation but keeping connected.

4.3.4.2 Slave

The clock calibration is based on linear regression, which requests dedicated memory and computational power. In the experiment, Slaves maintained a queue of 256 AME timestamps and a queue of 64 *Write messages* timestamps. The cost of CPU and memory used to perform a completed calibration were recorded in the experiment.

4.4Results

Table 4-1 shows the selected devices, the benchmark, Android Version, Bluetooth Version and the test that the device did. In total, 6 devices have done Test 1 and 4 devices have done Test 2.

During data processing, the synchronisation error of each slave E_i $(i = 1,2,3,4,5)$, at each interval, was calculated by (4-4), where T_i is the timestamps of the edges of the pulses captured by the nRF52DK. The maximum network error (E_{max}) at each interval is calculated by (4-5).

$$E_i = T_i - mean(T_i) \tag{4-4}$$

$$E_{max} = max\ (T_i) - min(T_i) \tag{4-5}$$

4.4.1 Test 1: Time Stability Test

The synchronisation errors of each Slave (E_i) are shown in Figure 4-6. During the 180 seconds, about 9000 timestamps were captured for each tested Android device (5ch x 10Hz x 180sec = 9000). In the test with all the devices, the distribution of each channel at a fixed position during the 180 seconds. The actual bias of each channel does not drift. The clock drift in WBR-SH2 is eliminated by the synchronisation method.

The synchronisation effectiveness seems unrelated to the performance of the devices. The Galaxy TAB Active T365 (T365) is considered as a lower performance device (15.5k CPU scores), however, the synchronisation error is smaller than both Xiaomi Mi6s (Mi6) and the other One Plus 5T (5T), with both Mi6 and 5T being considered high-end smartphones (70k CPU scores).

The version of Android and BLE are also not linked directly to effectiveness. The Sony Xperia Z2 (XZ2, Android 5.1.1, BLE 4.0) and One Plus 3T (3T, Android 8.0, BLE 5.0) are both high-performance phones. They provide similar distribution and the errors are smaller than all other devices. The Xiaomi Mi6 with different versions (Android 7.1.1 and 8.0, different device) results in different synchronisation effectiveness. The

possible causes are different Bluetooth stack version or different power saving strategies lead to different delays in App level.

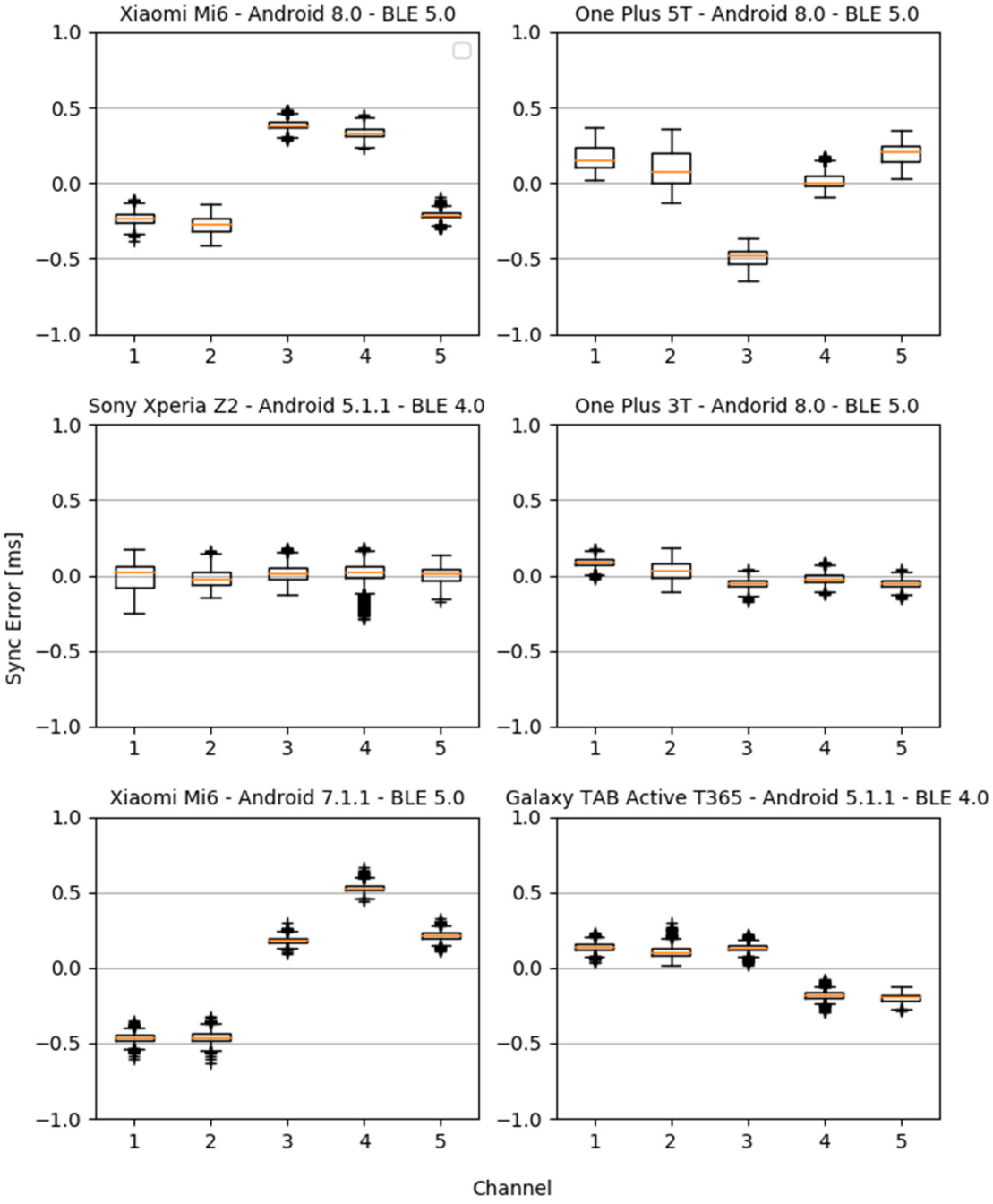

Figure 4-6 Distribution of synchronisation error for 5 sensors across tested Android Devices.

4.4.2 Test 2: Network Initiating Stability Test

The synchronisation was repeated 12 times for each of the 4 selected devices. In Figure 4-7, 5 channels and 12 repetitions (about 5 x 10 x 180 x 12 = 18000 timestamps) for each device are plotted in the same box. 3 devices (Mi6, XZ2, T365) did both tests; Nexus 5 did only Test 2. After 12 cycles of initialling and detaching networks, the overall synchronisation effectiveness of XZ2 is better than Mi6 and T365, which is similar to the argument in Test 1. The Nexus 5 comes with an Android 6.0.1, but it performs within the same range of all other Android versions.

In all the timestamps that collected in Test 2, the absolute channel error ($E_{1,2,3,4,5}$) is 0.829ms, CDF95% (Cumulative Distribution Function at 95%) of $E_{1,2,3,4,5}$ is at 0.47ms. The standard deviation of $E_{1,2,3,4,5}$ is 0.217ms. The maximum network error (E_{max}) of all collected data is 1.284ms.

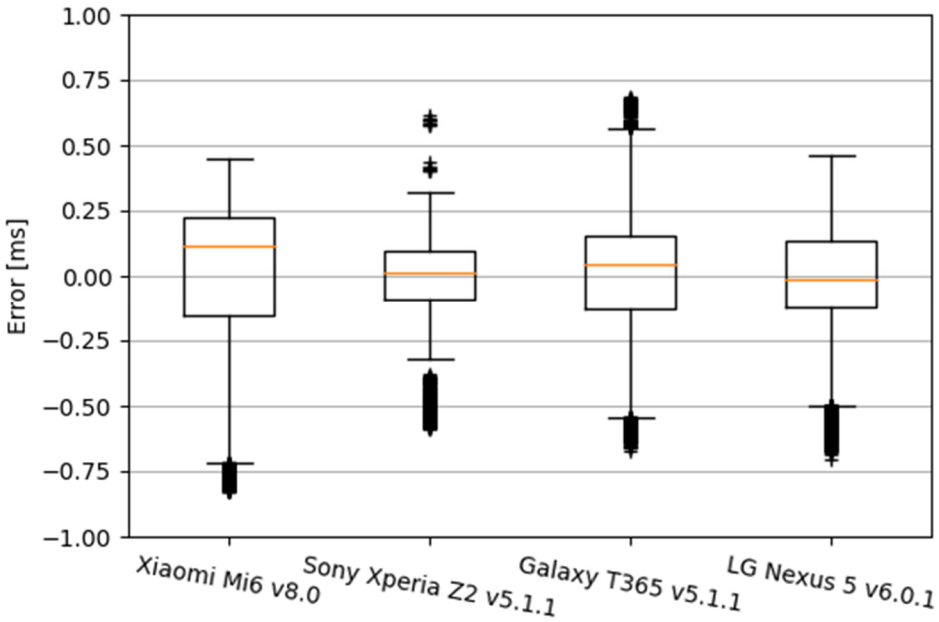

Figure 4-7 The distribution of synchronisation error in 12 initialling repetitions.

4.4.3 Computational Cost

The cost of resources was assessed individually in the smartphone and sensors. The memory and computational cost used by the App on the smartphone are small compared

to the resources available in a modern smartphone. We consider that the cost of resources in the modern Android device is, therefore, negligible. Sensors used as part of an embedded system, usually possess limited computational capabilities and limited battery power. Thus, the computational cost is more relevant.

In WBR-SH2, a set of timestamps needs to be kept in the memory for the bias estimation using linear regression. In the experiment, 256 timestamps were kept, and 64 message timestamps were kept. Each timestamp is comprised of a 32-bits unsigned integer, so the extra memory cost for synchronisation and local clock calibration were 1280 bytes. There is 64kB RAM available in the SoC, thus, the memory cost by synchronisation is about 2%.

To perform each clock calibration with 256 points linear-regression, the SoC takes average 230μs per round. The calibration is performed every CI, which is 25ms in the experiment. The computational cost in the sensors was 0.92%. It is important to note that the memory and computational costs in the sensors is highly related to the experimental setting. These parameters can be adjusted depending on the needs of the application.

4.5 Discussion

The results of both tests have proven that our synchronisation method can eliminate the clock drift in WBR-SH2 as an example. This method does not require extra hardware on both sides, so it can be implemented into generic microcontrollers which support related radio events. For other microcontrollers without radio events, this method can also be performed by using transaction callback instead of radio events. However, the accuracy might be lower since which introduce the uncertain process time in its Bluetooth stack.

In Test 1, the synchronisation error of each channel is not drifting but stable at some fixed error within 180 seconds in all the tested Android devices. The synchronisation effectiveness seems different between devices. The distribution of S2 and S5 matched

closely while S1, S3 and S6 distribute separately. However, in Test 2, after 12 times of repetition, the distribution ranges cross devices are similar. The differences between tested devices are lesser than Test 1. Thus, the argument of Test 1 can be a special case of Test 2. There is not much evidence showing the synchronisation effectiveness is irrelated the Android version, Bluetooth version or the performance.

The results show that the method has met the requirement of the objectives in 1) The method can work on a customised sensor network involving variable stock Android devices. 2) The accuracy (Std: 0.217ms, CDF95% 0.47ms, maximum network error: 1.284ms) is enough for motion sensing (100Hz, required synchronisation error below 10ms). 3) This method can provide high-frequency continually clock synchronisation without compromising for the bandwidth. Therefore, this method is superior to other methods discussed in the introduction section for WBR-SH2's typical application.

The limitations of the experiment are: 1) Did not test while the android phone is off-screen. 2) Other operating systems are not tested. 3) the method is not guaranteed in the future development of Android. These limitations are discussed below.

The tests were only done while the tested devices are screen on, and the App was on the foreground, which gave the App the highest priority to run the synchronising algorithm. Thus, the messages from the sensor nodes were responded in time. When the App was in the background or the Android device screen off to entre low power mode, the responses, which could affect the calculation of the biases at the beginning of the connection. This test only is done with Android device, other systems such as Windows, Linux, are not tested. Although the method is proposed for stock Android, it can also be used with traditional embedded wireless adapter. In this case, the accuracy will be improved because the embedded wireless adapter can normally measure the biases more accurate than Android. The method is validated with the up-to Android system (version 8.0), which could be invalided during the development of Android.

4.6 Conclusion

The synchronisation method provided by this chapter has been tested with variable off-the-shelf unmodified Android devices; the results (Std: 0.217ms, CDF95% 0.47ms, maximum network error: 1.284ms) are significant, compared to the generic time service (1/8 secs). However, the synchronisation error is larger than the previous works which including modified Android devices and SoC or using SoCs only.

This method has been proved that is working on variable Bluetooth version from 4.0 to 5.0, variable Android version (from 5.1.1 to 8.0), and it performs stable from low to high-performance device. The experiment showed a minimum performance for running this synchronisation method is AnTuTu CPU score 15k, Android version 5.1.1, BLE version 4.0.

This method does not require additional hardware or modification on the stock Android, which means the already sold sensor systems are also capable of implementing this method by On-the-Air firmware upgrade and App upgrade. The application scenario is not limited to wearable sensors. It can also be implemented in many different applications that have higher synchronisation requirement.

There are currently a few notable limitations: 1) Testing while the Android device screen is off was not conducted. 2) Other smartphone operating systems have not been tested. 3) Have not been tested in a controlled environment with radio frequency interference to validate the stability. Future work is to understand and overcome these limitations and provide a robust method.

Overall, this chapter has presented a novel synchronisation method for generic devices using BLE such as WBR-SH2 system. The following Chapter 5 will discuss a high-level neural network framework for edge devices.

Chapter 5 Development of a Compact Neural Network Framework for Microcontroller

5.1 Introduction

5.1.1 Background

As mentioned in Chapter 1, the three questions in “when”, “what” and “how” is the exercise done are the keys to understand exercise interventions. Among the questions, the “when” and the “how” can be answered by the initial data analysis from smart sensors such as WBR-SH2. However, to answer the question of “what” kind of exercise is done is still relying on the post data analysis on higher performance platform (such as smartphone and PC). As discussed in Chapter 1 neural network is effective in exercise classification. Thus, is it recognise exercise on the sensorised handle alone? In this chapter, an initial trial to run neural network classifier on small footprint microcontroller is presented.

5.1.1.1 Exercise Monitoring

The lack of remote exercise monitoring (discussed in Chapter 1) can be solved by wearable sensors or nearable devices, which continually assess exercise even the patient had left the hospital [48]. The type, the frequency and the intensity of exercise can be understood by using the motion data captured by these sensors. By sharing the information to the doctors or experts, they can assess the user remotely. The WBR-SH2 system aims to measure the resistance band exercise remotely in people’s home.

Especially, WBR-SH2 has improved in most of the specification compared to the experimental system. It provides up to 12 DoF measurement. The available sensors include 3-Axis gyroscopes, 3-Axis accelerometers, 3-Axis magnetometers, barometer, temperatures sensors, and a load cell sensor to measure the force. WBR-SH2 has not

only provided a strong measurement ability but also provided the easy-to-use human-machine-interfaces for users to measure their exercise fluently. The development of WBR-SH2 has been presented in Chapter 3 and Chapter 4.

5.1.1.2 *Convolutional Neural Network Classifier*

Convolutional Neural network classifiers for exercise recognition has been discussed in Chapter 1 briefly. Convolutional Neural Network (CNN) models have been proved to be effective in many data processing applications, including voice keyword spotting, human motion recognition and bio-signal sensing [75], [119]. Although CNNs are great tools to understand the raw data and to aggregate information out of these raw data, they also require high computational cost to run the arithmetic. For example, a NN model trained for exercise classification can take 2.8MB for storing weights and take 9.2M Floating-Point Operation (FLOP) for one inference cannot run on a typical microcontroller used in WBR-SH2 system (512KB ROM, 64KB RAM, 64MHz CPU frequency) [75].

Network efficiency is one of the diversities that attracted more and more focused. New structures such as Inception (2014) [120], Residual Net (2015) [121], [122], and DenseNet (2016) [123] has successfully improved the efficiency and performance by optimising the network structures. Some more recent achievements are also based on the above structures, such as Inception V3 [124] (further reduces the computational cost by using separately convolutional computation), and Octave-Convolution (2019) [125] (replace the traditional convolution by a low-frequency and a high-frequency subpath). However, due to the lack of higher-level library for MCU level, MCUs are not benefiting from these structures.

5.1.1.3 *Neural Network Classifier for Resistance Band Exercise*

One resistance band exercise using Couch Potatoes for Cognition has been done previously by us [75]. In the experiment, 6 healthy volunteers participated, 5 males and 1 female, aged from 23 to 40, right-handed. The participants were required to do 4

different activities, each consisting of 20 repetitions followed by 1 minute of rest to avoid the accumulation of fatigue. The experiment was measured by the WBR-SH2 system and the raw data are stored in the computer for post-analysis.

A multiple-layers neural network classifier was built for exercise data recognition. The classifier consists of 2 convolutional layer blocks and 2 layers of a fully connected layer, together with 716k weights and 9.2MFLOP. The classifier was trained using 60% of the data and then tested by the other 40% of data. The results show 97% accuracy in the test dataset. However, the classifier was too large to deploy to MCU. More detail will be discussed in the following sections.

5.1.1.4 Data Decentralisation

The trend of data decentralisation is emerging in recent days. Edge devices, which previously acted as the data provider, are now being utilised in many applications [126]. In particular, edge devices should be able to understand what it has measurement and provide precise and aggregated feedback to the upper-level receivers. WBR-SH2 is one representative of the modern edge devices which is also required to understand what has been measured. To date, this concept is known by the public by its other name, the Artificial Intelligent in Edge devices (Edge AI).

5.1.1.5 CMSIS-NN

CMSIS-NN [119] is a software library which is a collection of efficient neural network kernels developed to maximise the performance and minimise the memory footprint of the neural network on Cortex-M processor cores. The library is a fixed-point arithmetic library providing a very basic and low-level function set for NN operations. This library makes NN possible to run on low-performance microcontrollers.

5.1.2 Problem Statement

NN classifiers are performing extraordinary well on PC for post data analysis. However, transferring real-time raw data from sensor to PC is not always possible in real-life scenarios. In the model of remote exercise intervention, which was presented

in Figure 3-2 and was discussed previously in Chapter 3, the smartphone is a key bridge to collect data from the sensor then send it to the cloud server. If the smartphone is not presented during the exercise, The sensorised handle of WBR-SH2 system can only record the raw data for around 43 minutes (@100Hz sampling rate). The measurement for the last exercise could be lost if the data cannot be sent out in time due to the memory is overwritten by the new incoming data. Nevertheless, the more data transferring in between each component increase the latency of responses, reduce the reliability and reduce the security. An example of latency and the processing platform is shown in Figure 5-1. To avoid the dependency of the smartphone, as well as to solve the above problem, the raw data must be analysed locally inside the sensor.

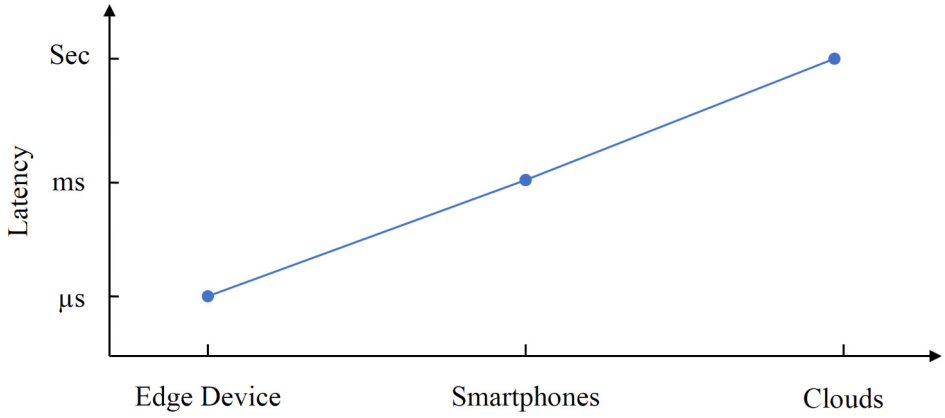

Figure 5-1 Example of latency in responding vs. processing platform.

Implementing NNs into MCUs is desirable, but there are still many barriers. Most currently available libraries for MCUs are incomplete. Some of them, such as *tinn* [127] and *uNeural* [128], support fully-connected layers only. *uTensor* [129] relies on the TensorFlow model alone. Table 5-1 lists the available NN tools/libraries comparison on three platforms. The lack of high-level libraries for MCUs increases the difficulty and time cost to implement NNs into MCUs.

Table 5-1 Available software packs in different platforms

Level	*Platform (Performance FLOPS [a])*		
	Computer / Servers (~T-FLOPS)	Smartphone (~G-FLOPS)	MCU (~k or M-FLOPS)
Higher	Keras, PyTorch, etc.		**None**
Middle	TensorFlow, Theano, etc.	TensorFlow Lite, ARM-NN, etc.	CMSIS-NN/DSP, uTensor, uNeural, etc.
Lower	cuDNN, etc.	OpenCL/DSP, etc.	

[a.] Floating-point operations per second

The lack of tools not only increase the difficulty of implementing NN into a microcontroller but also impact the motivation of trying the latest research outcomes. Figure 5-2 shows a brief timeline comparison of the research outcomes in the general-purpose computer and the implementation states in MCU level. The implementation in the MCU stays far behind to the latest models, while the recent researches are more focus on reducing the resources, the complexity and improve the power-efficiency than it was before. Those new specifications are essential, especially for the resources-limited platforms, such as the MCUs. The latest models are optimised from different aspects, one of the most effective aspects is modified structures, such as Inception uses a few parallel operations [120], [124], Residual Network uses a few skipped connections jumping over several layers [121], and the DenseNet are concatenating every layer's output and input in a single dense block [123]. These networks are mostly optimised from the perspective of modifying structures, and they achieve better power-efficiency by lower the computational complexity. However, due to the multiple links between the layers and the increased complexity in the structures, the difficulty of implementation on MCU growth dramatically while uses the currently available lower-level library to build the model, such as CMSIS-NN. Currently, building or deploying a model on an MCU is tedious work due to the lack of a higher-level framework.

Developers must manually manage the memory exchanges, the running sequences of each layer, the memory copies, and the matrix arithmetic.

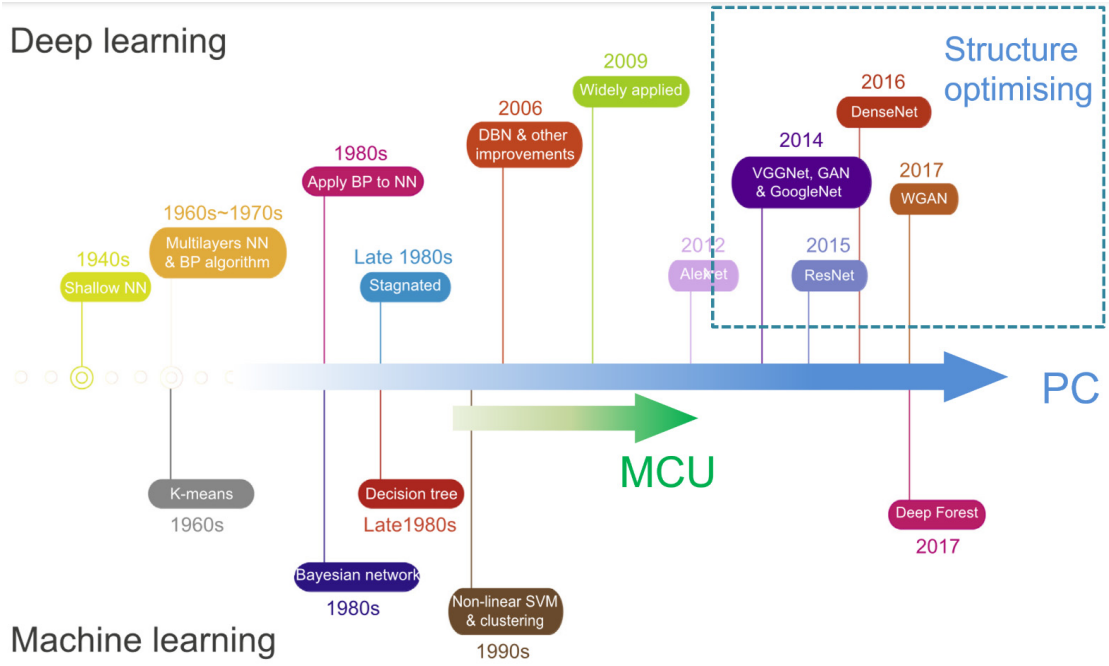

Figure 5-2 Timeline of ML research outcomes for general purposes computers [130] compared to the implementation of MCUs, which is struggling at complex structures.

5.1.3 Objectives

The objective of this chapter is to develop a high-level neural network framework for microcontrollers, which is more user-friendly, more flexible, and more capable than CMSIS-NN. Specifically, the library should allow developers to build complex models fast and conveniently. The implementation of the neural network model based on it must also be verified for performance and accuracy.

5.2 Methodology

5.2.1 Model Development Process

Currently, training NN models are computationally expensive but can be relatively low-cost when making predictions. Therefore, the development of NN models for embedded systems is usually separated into two steps [131], training and deploying. NN models are trained on higher performance platforms such as computers or the cloud

for fast training speed, then deployed to lower capability platforms such as smartphones or in this case MCUs. The development procedures to develop a NN model for an MCU is shown in Figure 5-3.

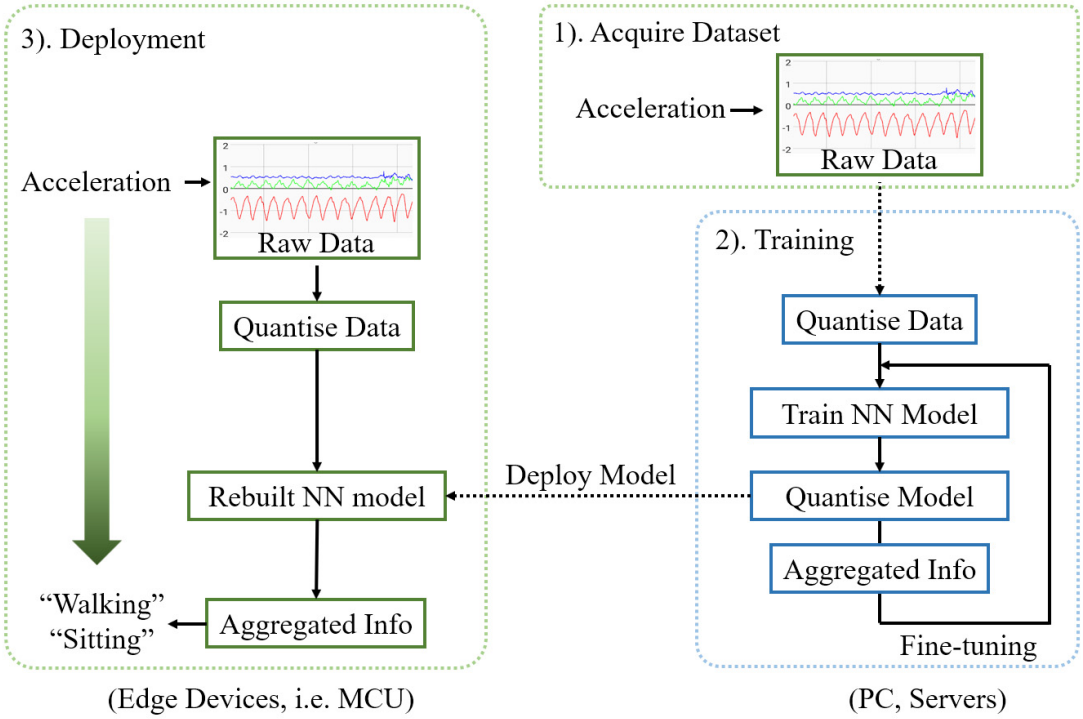

Figure 5-3 An example of developing NN classifier for edge device with a PC. The process contains 3 steps. 1). Collect a dataset for training the model. 2). Train the model. 3). Deploy the model into MCU for real-life data classification.

Training models on a PC usually use floating-point arithmetic. A floating-point calculation on MCUs is less efficient due to its lesser FLOPS (Floating-point Operation Per Second) performance compared to a PC. A conventional method to reduce the size and computational cost is to quantise the model. A floating-point model can be quantised into the fixed-point representative while deploying to MCU.

MCUs are sensitive to memory and computational cost. A larger size model may result in small improvements in accuracy but takes times of costs in memory or time while running in MCU. After quantisation, the resolution of a model has been changed so the performance of a model needs to be evaluated after deployed the model into MCU. Other sensitive performance such as computation complexity and run time also

need to be evaluated directly on the MCU. The floating-point NN tools and libraries running on the PC are lack of capabilities of simulating the fixed-point implementation on MCUs. Also, after the model has been deployed, any tuning in model structure or parameters will lead to a massive programming work in the MCU side.

5.2.2 Quantisation

The quantisation of a floating-point model can accelerate the speed especially in MCU which always suffered from limited floating-point capability [131]–[133]. The quantisation method in this chapter is adapted from the method developed by Han et al. [131]. The selected backend, CMSIS-NN [119], is a fixed-point library, therefore, quantisation is necessary to deploy an NN model into an MCU. A quantisation of a neural network model can be done with a few steps, firstly, quantise input data, secondly, training with quantised layers, and finally, quantise weights and biases and deploy.

Models are normally trained with floating-point data and parameters for better performances, while the quantised model only accepts fixed-point data and weights as input. Due to the representation range of an integer is much lesser than the same width floating-point variable, directly convert a floating-point variable to a fixed-point variable will lead to the saturation or the loss of resolution.

Q-format can be used to solve the above problem. Q-format can match variety ranges of numbers with same resolution with in the ranges. Q-formats are bit-level formats for storing numeric values [119]. In Q-format, the precision of the number can be defined by the length of total bits. The integer part can be defined according to the range required by the data. The form of a Q-format is Qm.n, where m is the number of bits before a notional binary point, and n is the number of bits that follow it. For example, an 8-bit integer (byte) can hold values in a signed Q4.3 format. This covers the range -8 to (almost) +8, with 256 unique values available in that range. The number m and n could be negative, in this case, the other part gain better range than the original same bit integer. For example, Q10.-3 gives the maximum range of -1024 to +1016 to

an 8-bit integer, which is larger than the original range of an 8-bit integer (-128 to +127). A conversion from floating-point to Q-format can be done by (5-1).

$$Q = 2^{-n}x \tag{5-1}$$

The number n can be set to an integer in Q-format, however, a good n value must maximise the use of its resolution without being saturation. The best n number must be tested with the whole dataset. The number n can be calculated by (5-2), where w is the width of bits in the Q-format, x is the set of floating-point values for conversion.

$$n = w - ceil(log_2(max(abs(x)))) \tag{5-2}$$

As shown in Figure 5-3, the quantisation process is compulsory for training and deploying a quantised model. Both input data and the weights must be quantised [134]. With the quantisation process, the NN models for MCU can be built and trained similar to they have been done in PC while the performance in MCU is acceptable with minor loss on accuracy [131]–[133].

5.2.2.1 *Quantise Input Data*

If the input data is the same width of the model's input, such as an image with RGB (8-8-8) format can be stored in an 8-bit array without losing any features, the Q-format is a particular case where n number is 0. Input data such as 32-bit floating-point time sequence signal cannot be stored into fixed-point array directly. They must be converted into Q-format using the above methods.

5.2.2.2 *Training with Quantised Layers*

An NN model usually consists of multiple operations. Each operation takes input data, does arithmetic, and output data. The operations are abstracted as layers. Training model on PC is using floating-point for better accuracy, so the data passing through layers is also floating-point. Fixed-point models, however, will only pass the fixed-point data. A model which trained with floating-point output in each layer, cannot simulate the loss of resolution and data saturation in the quantised model. Therefore, to

achieve the best performance, the training of the model must simulate the loss of resolution and saturation in the quantised model to adapt to the limitation.

To solve the above problem, a layer level quantitation needs to be performed. This can be done by inserting a quantising layer in between each of 2 layers. Practically, a Lambda layer is used to quantise the output of the previous layer, then pass the data to the next layer as its input. During the training, the weights and biases are changed after each training batch, thus the maximum and minimum ranges are variable through each training batch. After training is done, the model will run again with the training and testing dataset to get the output range of each layer. The Q-format can then be calculated through the range of the output of each layer. After new Q-format for each layer is set, the model will then need to be trained to adapt for the new resolution. The procedure will repeat until the best Q-formats for each layer are determined. The working flow is shown in Figure 5-4.

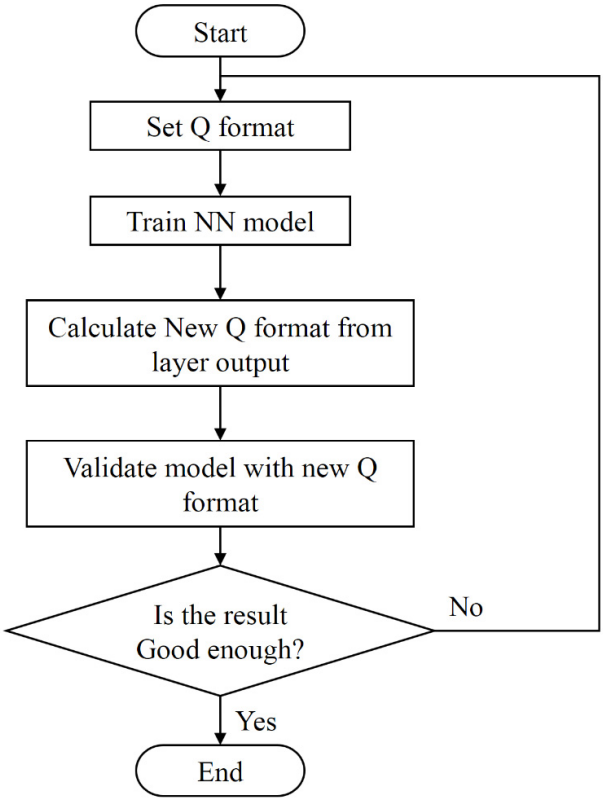

Figure 5-4 Working flow of training with the quantised output.

5.2.2.3 *Quantise Weights and Biases*

The weights and biases are generally floating-point while training. They must be quantised using Q-format to be imported into the quantised model. The weights and biases quantisation are done finally. It is optional to convert the quantised weights and biases back to the floating-point model to validate the effect of quantisation because the model can be validated in the quantised model.

5.2.3 Deploy Quantised Mode to MCU

Once the weights are quantised, the model can then be deployed into MCU's development environment by rebuilding the model with the targeted programming languages such as C programming language.

Currently, building a model on an MCU is a tedious work due to the complicated deploying process and the lack of a high-level NN framework for MCU. Developers

must figure out the structures of the model, the data format between layers, the parameters for each layer, and how the memory is passing between layers. After the model has been deployed, any tuning in the model structure or parameters will lead to a massive reworking in the MCU side.

5.2.4 Development of NNoM

5.2.4.1 Overviews of NNoM

NNoM aims to provide a higher level, user-friendly and flexible NN framework with statistics analysis abilities. NNoM releases the developer from miscellaneous low-level programming to more meaningful works such as structure and parameter fine-tuning. The interfaces of NNoM is similar to Keras (a popular and user-friendly machine learning framework written in Python [135]) but with a different implementation and adaption for C language and MCUs. NNoM is working closely with Keras and providing tools to convert Keras model to NNoM model directly. Thus, developers will not need to learn other lower-level frameworks such as TensorFlow. The structure of NNoM is shown in Figure 5-5, which consists of a few construction Application Programming Interfaces (APIs), evaluation APIs and layer APIs.

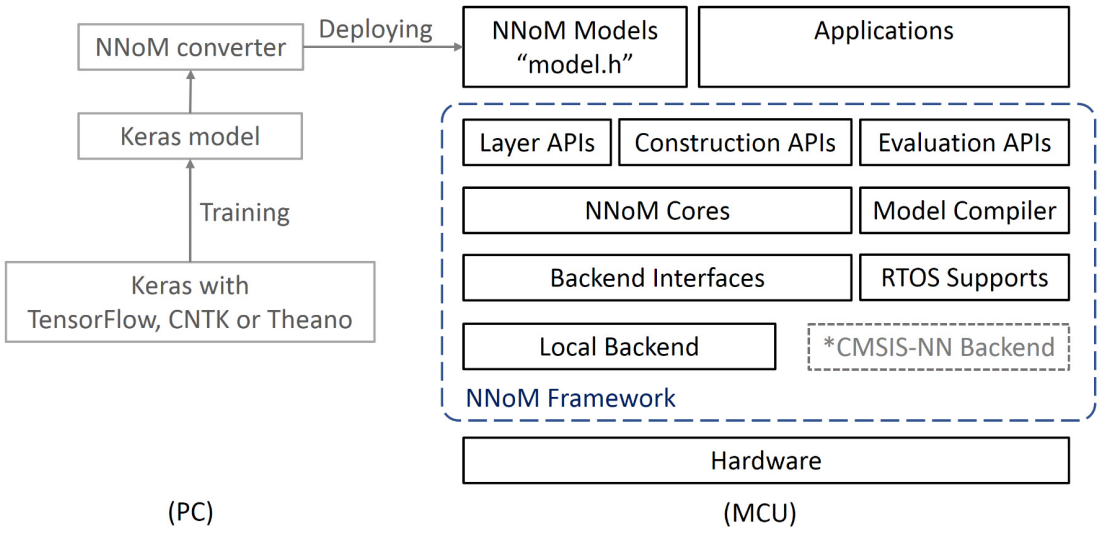

Figure 5-5 Framework of NNoM. NNoM provides three types of APIs for developers and supports two types of backends. Local backend is a pure C language implementation of NN functions while *CMSIS-NN backend [136] provides up to 5x performance for ARM Cortex-M MCUs.

5.2.4.2 *Construction-compiling Method*

The most limitation of CMSIS-NN is that there are too many user-configurable arguments to distract developers, while most of them are context-related arguments related to the output of the previous operations. To overcome this problem, NNoM must be capable of figuring out these context-related arguments for the developer, which allows the developer to focus on more important parameters and the structures.

Thus, a construction-compiling method is used by NNoM to separate the building of the model into two separate stages, which is similar to the coding-compiling procedures in many programming languages. Firstly, in the construction stage, the developer constructs the model by specifying the links between layers and setting some compulsory parameters. Secondly, in the compiling stage, NNoM is responsible to fill in the rest context-related arguments such as output shapes, type, layer buffers and the running orders.

5.2.4.3 *Layer-based Structure*

To support complex NN structures, NNoM uses a layer-based structure, shown in Figure 5-6. A layer is a container class which contains the parameters, the links to other layers, and a set of backend interfaces. The actual operations (the worker functions that actually do mathematic on the data) are wrapped by the corresponding layer. The operation can be convolution, max pooling, concatenate, and others. The data passing logic and the data buffers are stored in the Input/Output modules (I/O). Each layer maintains a list of input modules and a list of output modules.

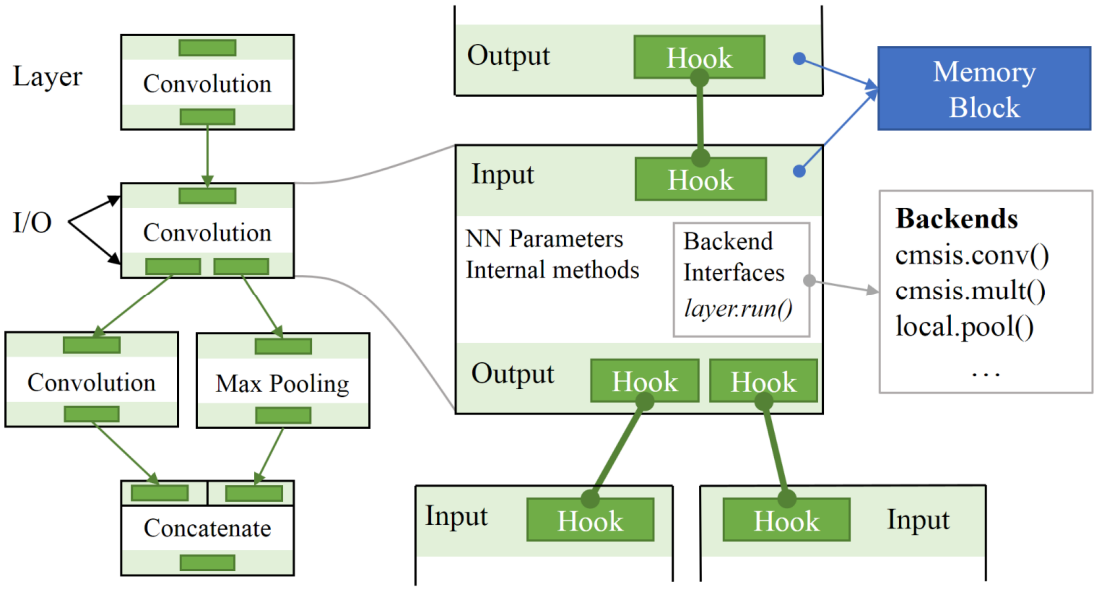

Figure 5-6 NNoM layer-based showing an Inception structure. Each operation, i.e., convolution, dense, etc., is wrapped inside a layer. The multiple sub-paths are achieved by multiple Hooks

The link between layers is defined in the Hook module. Each I/O also maintain a list of Hooks. While building a model, developers only need to specify the links by construction APIs. The I/Os and Hooks are not seen by developers and should not be configured by developers.

5.2.4.4 *Layers Classes*

To construct a fully functional model, the developers should create a few layer instances for the different operations. These layer instances are created by Layer APIs. There are two types of layer, Base Layer and Extended Layer. Every Layer API returns a layer instance in either type of classes:

- **Base Layer class** contains only necessary modules, argument and methods.
- **Extended Layers class** is a child class which inherited from the Base Layer. Besides, it includes many private arguments and/or more I/O modules.

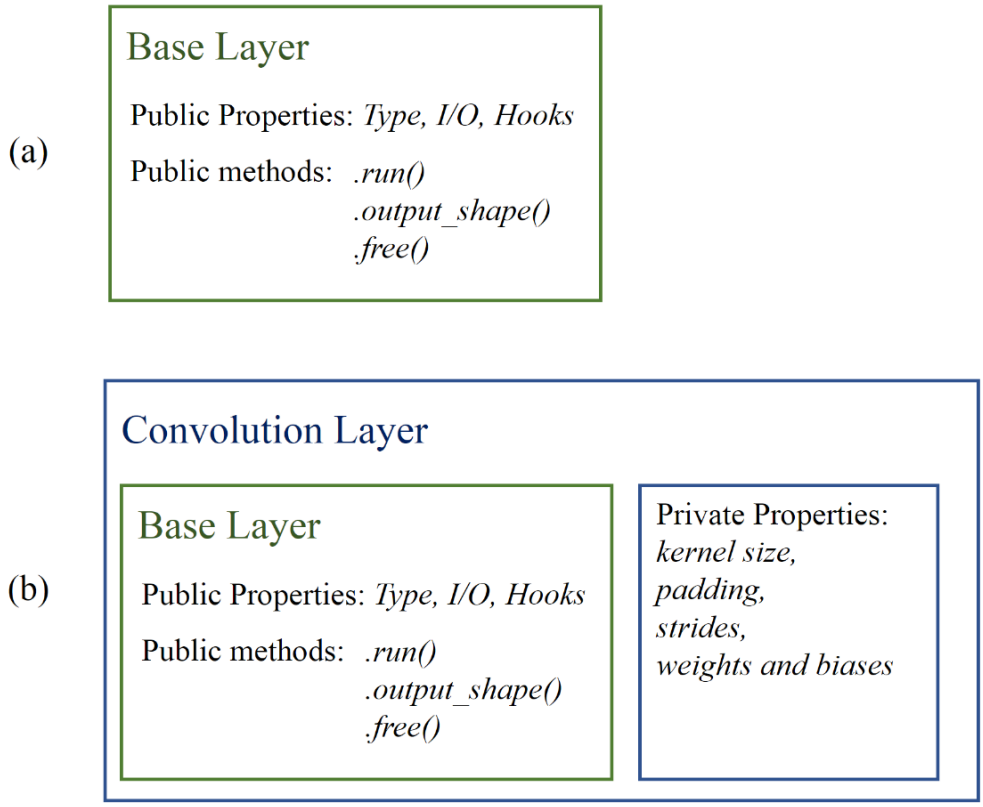

Figure 5-7 Layer structure. (a) Base layer class. (b) Extended layer classes.

A Base Layer class consists of one Input module, one Output module, and three public methods. Three methods are (1) *layer.free()* for releasing resources while the layer is deleted, (2) *layer.output_shape()* for calculating the output data shape during compiling, and (3) *layer.run()* for executing the operation which will actually call a backend worker function.

Different kinds of Extended Layers are defined by the actual operations. For example, Convolution layer containing the convolution operation and the private arguments for convolution. A list of pre-built Layers for NNoM is shown in Table 5-2. A special example for an Extended Layer is the Lambda Layer, which is an anonymous layer and brings much flexibility inside layer-level. Lambda Layer allows developers to use customised the worker functions on a standard layer interface. Thus, it can be used in the same way as other prebuilt layers to build a model.

Table 5-2 Pre-Built Layers

Layer	*Opt*[a]	*Notes*
Core Layers		
Convolutions, Pointwise Conv	Yes	
Depthwise Convolution	Yes	
Densely Connected Network	Yes	Fully-connected network
Batch Normalization		Fused to Conv
Lambda		A user-defined anonymous layer
Activation	Yes	A layer wrapper for activations
Zero Padding		
Cropping		
Flatten		
Pooling Layers		
Max Pooling	Yes	
Average Pooling	Yes	
Sum Pooling		
Global Max Pooling	Yes	
Global Average Pooling	Yes	
Global Sum Pooling		
Up Sampling		Enlarge the image by an integer scale.

Layer	*Opt*[a]	*Notes*
Activations Layers		
ReLU	Yes	Rectified Linear Unit
Sigmoid	Yes	
TanH	Yes	
SoftMax	Yes	
Merging Layers		
Concatenate		Concatenate two input on the specified axis.
Multiplier	Yes	Elementwise multiplication
Addition	Yes	Elementwise addiction
Subtraction	Yes	Elementwise substraction

[a]The layer is optimized for ARM Cortex-M core when CMSIS-NN backend is selected.

5.2.4.5 *Model Construction*

The Layer-based structure allows developers to build and modify the model quickly and conveniently using standard construction interfaces. In a complex structure model, if every operation is wrapped into a layer, then complex network topologies can be broken down into many microstructures basing on the 2 basic structures, branch-structure and merging-structure. The basic structures are shown in Figure 5-8. Thus, any complex model can be built by the corresponding construction APIs of the 2 basic structures. A branch-structure or single line topology can be built with *model.hook()*. A merging-structure is constructed using *model.merge()*.

The Layer-based structure allows developers to build and modify the model quickly and conveniently. Based on the layer-based structures, NNoM provides two types of model, sequential and functional model, which is similar to Keras. The construction can be done by the construction APIs. On the one hand, sequential models are built by *model.add(),* which is a simple interface to avoid manually specify the links between layers. On the other hand, the functional model can be built by *model.hook()*

and *model.merge()*. These APIs are more flexible, which allows the developer to manually build complex structures, such as Inception structures are with several sub-paths [120] or Residual Network with skipped connection jumping over several layers [137]. This simple interface allows developers to focus on improving model structures and critical parameters.

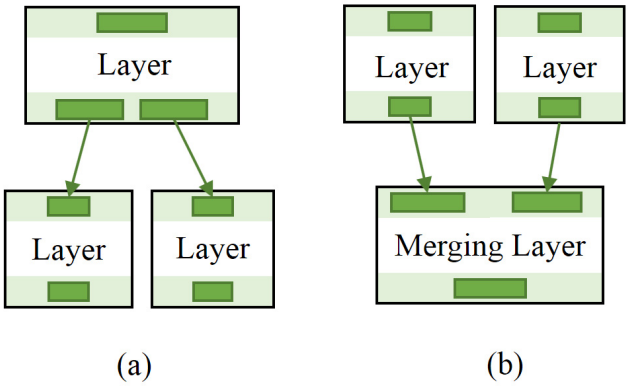

Figure 5-8 Basic topology for model structures and the corresponding construction APIs (a) micro-branch-structure, single layer's output data is sharing with multiple layers. (b) merging-structure, single layer takes multiple layer's output data as its input.

5.2.4.6 *Compiler and Memory Management*

The compiling stage is done by a compiler. The compiler is to complete the miscellaneous works left by the developers. To compile a model, call *model.compile()*. The compiling is done by nested calling a layer compiler, named *compile_layer()* method. The job of the layer compiler is to analyse the topology of the models, create an interlayer shortcut lists, to calculate the output shapes of each layer, to fill in relevant parameters, to analyse the memory lifetime, and finally to assign the memory for each layer.

The layer compiler will start from the first layer of a model, which usually is the Input Layer. The working flow is shown in Figure 5-9. Firstly, it checks whether the current layer's input buffer(s) are all fulfilled by another layer (s). The multiple input buffers checking is for the layers using merging-topology. Secondly, it calls the *output_shape()* method to calculate the current layer's output shape and the needs for

the extra buffer (i.e. buffer for arithmetic), and then it allocates the memory for the layer. Thirdly, it will check whether the layer has multiple hooked layers to its output buffer. The multiple hooks are for the layers with micro-branch-topologies. If the layer is hooked by multiple layers, then a new nested call to the layer compiler will be performed for each of the hooked layers.

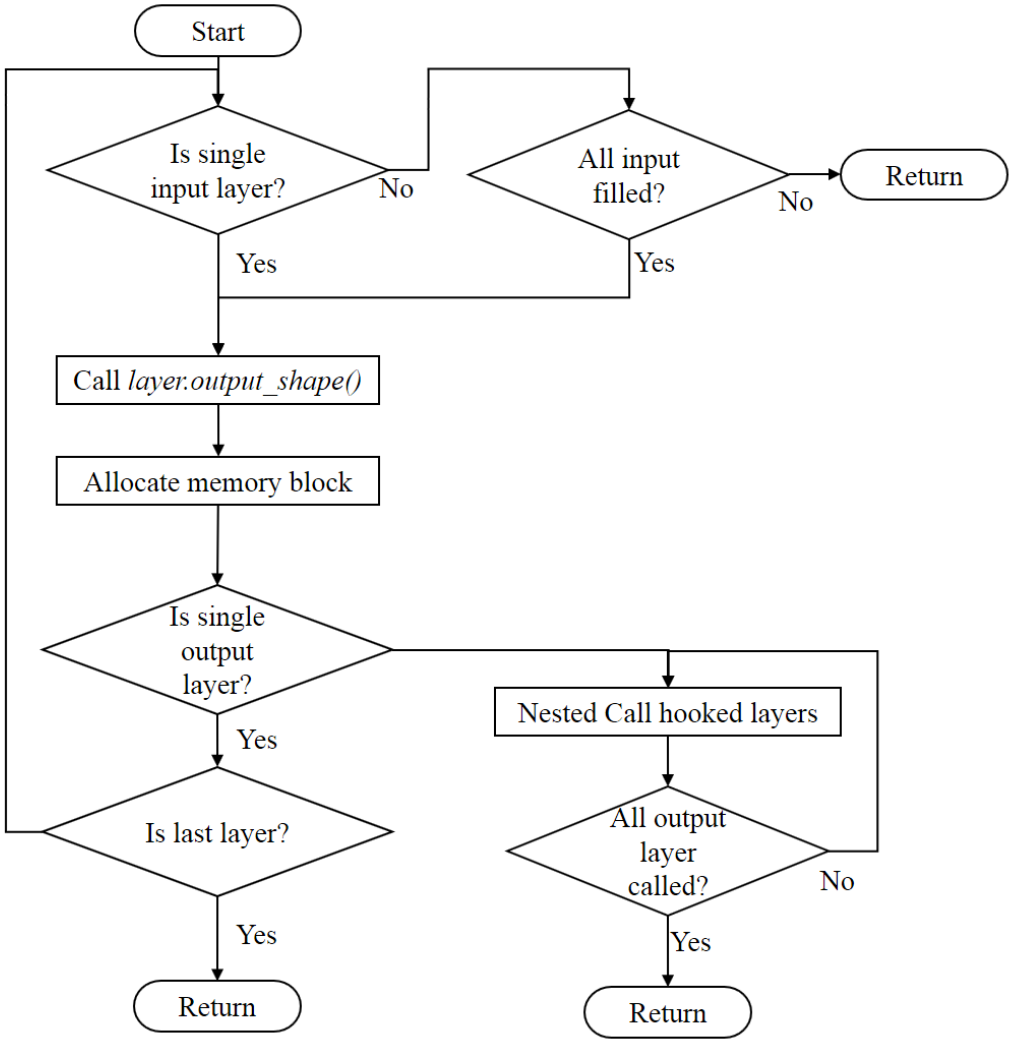

Figure 5-9 Layer compiler (*compile_layer()*) working procedure.

To analyse the model topology, the compiler starts with the Input Layer and iterates each layer which is hooked on the current layer's I/O module. After all the layers are iterated, the running order of these layers is fixed. The compiler creates an interlayer shortcuts list by the running order. To run a model, instead of analysing topology again, simply iterate the list to avoid the impact of the performance.

layer.output_shapes() method is called during the compiling which is responsible to calculate the layer's output shape according to its input shape and the related arguments, such as the output shape of the convolution layer is depended on the kernel size, filter size, padding method, and the input shape. The input shape of a layer is inherited from its hooked previous layer.

The memory management is performed simultaneously with the topology analysis. To avoid runtime memory allocation, the requirement of memory in each layer is calculated beforehand in compiling stages. To minimise the memory cost of the model, memory is reused across layers. The minimum memory unit is a block. Each layer is permitted to take one private memory block for arithmetic if needed and several blocks for I/O buffer(s). These memory blocks can be marked as temporary or reserved by the layer. A temporary block is released after the layer finished its job and will be reused by the next layers; while a reserved block is reserved for the specified layer and will not be reused by other layers or released after an epoch ended. To avoid memory copy in between layers, the block used by the current layer's output is shared to the input of "next layers". The "next layers" means those layers' input modules are hooked to the output module of the current layer. When there are multiple layers which are hooked to the current layers' output, the lifetime of the output block will be retained until the last hooked layer is called. The maximum required size for each block is recorded while compiling and the memory is assigned after compiling.

The RAM complexity in space is $o(n) + o(0)$, where $o(n)$ is the memory cost by instancing layers, which is relatively small (100~200 bytes per layers), and where $o(0)$ is the maximum reserved memory block size plus the maximum temporary retained memory size.

5.2.4.7 Backend Functions

As mention previously, backend functions are the functions which complete the computation. When the model is compiled, the run-order for layers is fixed. Before a

layer.run() is called, the input data for this layer is prepared. The backend functions are called inside of *layer.run()* to do the actual calculation. With NNoM, porting a backend is relatively straightforward; the corresponding backend function is put into each layer's *layer.run()* and the configuration from layer's parameters are passed to it. There is no need for the developers to organise buffers or to calculate the parameters manually.

NNoM currently supports two different backends. NNoM by default runs on a local pure C implementation backend which completely supports every operation in NNoM. The second backend is CMSIS-NN backend which is optimised for ARM cortex-M microcontrollers. CMSIS-NN is not completely supporting every available operation in NNoM, thus, the local implementation is called when the setting or the operation is not supported in CMSIS-NN.

5.2.4.8 *Automatic Converter*

NNoM was designed to have a similar user interface to the Keras, which is popular by its ease to use. However, due to the necessary process of quantisation the model, it is still complicated for developers. Therefore, an automatic converter has been developed to convert Keras model to NNoM directly. The converter is written by Python which can be called directly after a model has been trained with Keras. To convert a Keras model to NNoM model, firstly, it calculates the Q-format of each layer's output range. Secondly, it performs the quantisation of each layer's weights and bias. Also, it merges the Batch Normalisation layer's parameters to the previous convolution layer. Thirdly, it automatically generates a C language header file in a readable form. This C header is the only files contains the NNoM model which includes necessary parameters, weights, biases and a model creating method. The developer can call this method in their embedded developing environment to create and run the model in the MCU.

5.2.4.9 *Evaluation Functions*

Evaluation of the quantised model is also necessary since the model's resolution has been changed and the runtime is sensitive on MCU. NNoM provides the evaluation method of the model directly on the target devices. When connecting MCU with a terminal, the evaluation can be done online with NNoM. Thanks to the CMSIS-NN and NNoM are compliance with ISO/IEC 9899:1999 (known as "C99"), the framework can be compiled for PC and validated the quantised model directly on PC.

1) Layer-by-layer Analysis

The layer-by-layer analysis is a part of the compiling process. The result includes the running order of layers, the output shape of each layer, the estimated computational cost fused Multiply-Add/Accumulate (MAC) count for each computational layer, the required memory for each layer, and which memory block is assigned in each layer. Besides, a summary of memory cost and maximum memory required for each block is printed.

2) Runtime Statistics

The runtime statistics are measured by the time cost required to run each layer. The time for running layers is recorded individually for each layer. *stat()* can be used to print the statistics. Runtime statistic also lists the MAC ops/us, which indicate the efficiency of the layer. A summary of statistic lists the total MAC number, the total running time for a model, the MAC ops/us of the model, and the average running time of the model for a period.

3) Prediction on MCU

To validate the implementation, during the training, the test data set is exported into a binary file. This file can be used to evaluate NN implementation. NNoM provides a prediction API *predic()* to use those data for prediction. The prediction result from MCU can be compared side-by-side with the result from PC to validate the

implementation. The prediction API provides Top-k accuracy, as well as a confusion matrix. In addition, it also summarises the runtime statistics during the test.

5.3 Experiment

5.3.1 Experiment Protocol

The Couch Potatoes for Cognition [49] is produced by Loughborough University specifically for older adults and dementia people, and it consists of 4 types of low-intensity resistance band activities, shown in Figure 5-10. The detailed protocol has been discussed in Chapter 2 and shown in Appendix A. These activities are mainly focussed on improving the upper body muscle strength, as the previous studies have proven that training of the upper body will slow down the process of dementia [49], [138]. During the exercise, subjects were asked to sit on a chair to minimise the chance of falling.

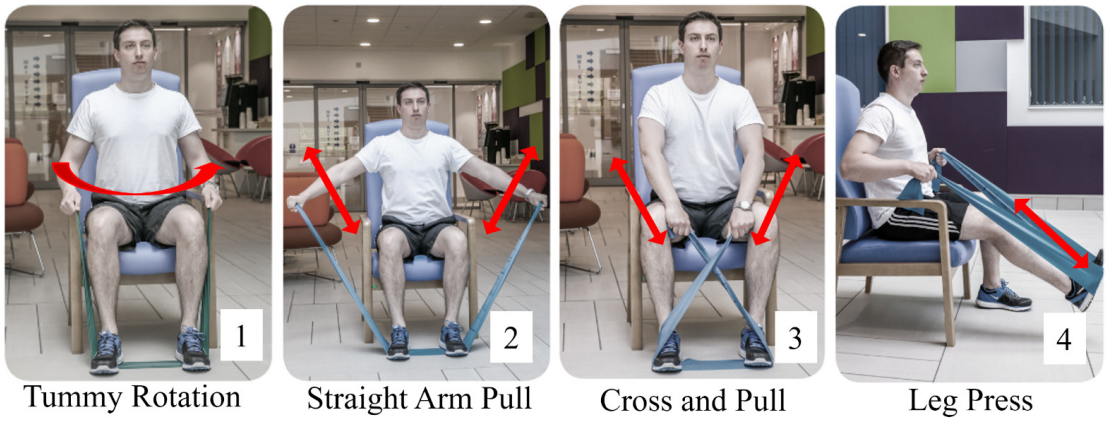

Figure 5-10 Couch Potatoes for Cognition. The red arrow shows the movement of each activity.

In the preliminary experiment, six healthy volunteers participated, five males and one female, aged from 23 to 40, dominated on right-hand. The experimental procedures involving human subject described in this chapter were approved by the Institutional Review Board. The participants were required to do four different activities, each consisting of 20 repetitions followed by 1 minute of rest to avoid the accumulation of fatigue.

5.3.2 Data Processing

5.3.2.1 *Raw Data Frame*

During the experiment, all data were collected at a frequency f = 100Hz and stored in a CSV file for further processing. 12 DoF data were available including 3-Axis accelerometer, 3-Axis gyroscope, 3-Axis magnetometer, barometer, load cell and temperature. In this preliminary experiment, only accelerometer data is used. Each frame consists of 3-Axis acceleration data from both left-hand and right-hand sensors. No filtering of raw data is required while using a CNN [139].

5.3.2.2 *Overlapping Windows*

Sliding windows technique are widely used by many classifiers to split data into small segments [140]. In data processing, an overlapping windows technique is used to segment the raw data. Each segmented data size of 2.5 seconds (including 250 frames) with 2/3 window overlapping [140]. The sliding windows are shown in Figure 5-11.

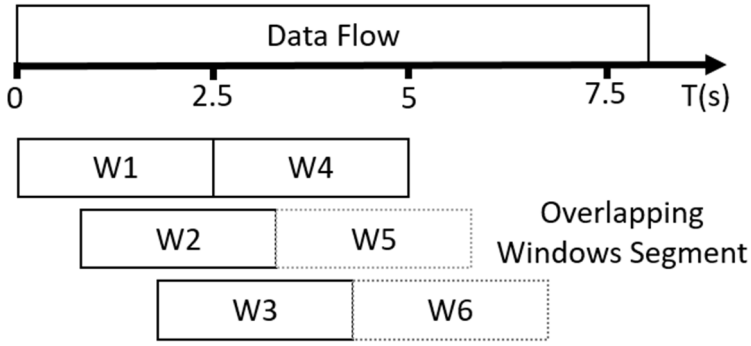

Figure 5-11 Sliding windows. Each segment overlapping the previous segment by two thirds.

5.3.2.3 *Sensor Position Switching*

Each frame consists of two sets of acceleration data from the two handles. However, in real-life scenarios, the allocation of the resistance band handles to the hands is randomised. To reduce the correlation, the position is switched in the segmentation process. This position switching generates another set of segmented data. Both segmentations are put into the same neural network for training. Figure 5-12 shows the segmented raw data and position-switched data.

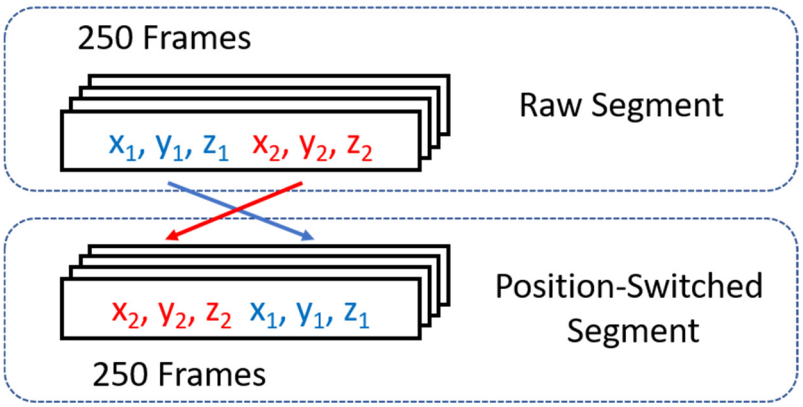

Figure 5-12 Position-switched segment.

5.3.2.4 *Training and Testing Dataset*

The training dataset and testing dataset were randomly picked from the segmented data with a ratio of 60% and 40%, respectively. In total, the training dataset contains1919 segments, while the testing dataset contains 1271 segments.

5.3.3 Convolutional Neural Network Classifier

The neural network classifier is built using Keras with Tensorflow backend. The structure of the classifier is shown in Figure 5-13, and the layer's structure is shown in Table 5-3. The classifier consists of 2 convolutional layers, 2 fully-connected layers, a few functional layers between and finally a SoftMax layer for the probability of the prediction. To be noticed, the quantised layers (using Lambda layer) are inserted after some layers (highlighted in Table 5-3) which potentially changed the range of the output data.

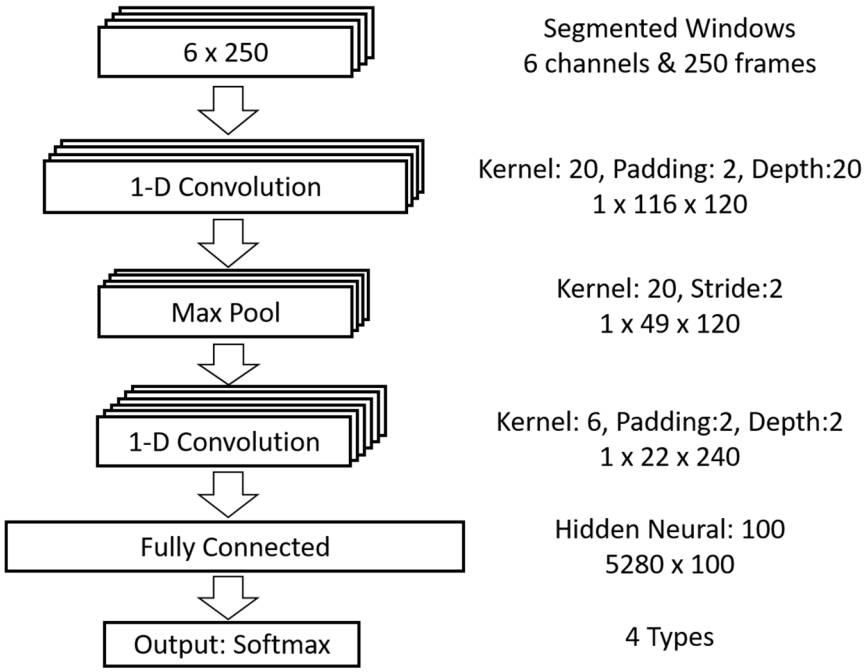

Figure 5-13 Convolution Neural Network Architecture (ReLu layers are hidden)[75].

Table 5-3 Layer structures of the Neural Network Classifier

Layer	*Output shape (W×C)*	*Kernel*	*Stride*	*Parameters*	*Operations (MAC)*
Input	250×6				
Conv_1	113×120	25	2	18120	2.034M
Quantised (Lambda)	113×120				
Max Pool_1	56×120	2	2		
ReLU_1	56×120				
Conv_2	25×240	7	2	201840	5.04M
Quantised (Lambda)	25×240				
Max Pool_2	12×240	2	2		
ReLU_2	12×240				

Layer	*Output shape (W×C)*	*Kernel*	*Stride*	*Parameters*	*Operations (MAC)*
Flatten	22800				
Dense_1	100			288100	228.8k
Quantised (Lambda)	100				
ReLU_3	100				
Dense_2	4			404	400
Quantised (Lambda)	4				
SoftMax	4 types				
Total				508.5k	7.36M

The dataset (range -13.11 to +11.67) is quantised to 8-bit Q-format representative with n = 3, thus, the quantised dataset range is -105 to + 93.

The classifier is trained with the quantised dataset using CPU (Intel i5 3475S). Adaptive Moment Estimation (Adam [141]) optimisation algorithm is used for training and the training was stopped at the 20th epochs; the accuracy and confusion matrix was stored after the training was done. The final output Q-format of the quantised layer was determined and listed in Table 5-4 together with the Q-format of weights and biases. All arithmetic and intermediate data are using 8-bit quantisation.

Table 5-4 The Q-format of output and trainable parameters

Layers	*Output Q-Format(n)*	*Weights Q-Format (n)*	*Biases Q-Format(n)*
Input	3	N/A	N/A
Conv_1	1	10	11
Conv_2	0	10	11

Layers	*Output Q-Format(n)*	*Weights Q-Format (n)*	*Biases Q-Format(n)*
Dense_1	1	10	11
Dense_2	0	8	12

An STM32L476-Discovery board is used to experiment. The MCU (STM32F476, STMicroelectronics) is based on an ARM Cortex-M4F core which running on 80MHz with the performance of 3.42 CoreMark/MHz or 1.25 DMIPS/MHz (Drystone 2.1) [142]. STM32L476 is a typical configuration of MCU in edge devices provided high-performance and high power-efficiency.

After the classifier has been trained on PC, the model was deployed to the MCU projects using NNoM framework by the model converting tools. The Q-formats, weights and biases were written into a C language header file to be compiled into the MCU project. The discovery board was connected to the PC through a serial port. The quantised model summary was printed to a terminal through the serial port, shown in Figure 5-14. After the model is compiled, the testing dataset was sent to the MCU for NNoM to validate. The prediction results including Top-k accuracy and confusion matrix were printed to the terminal.

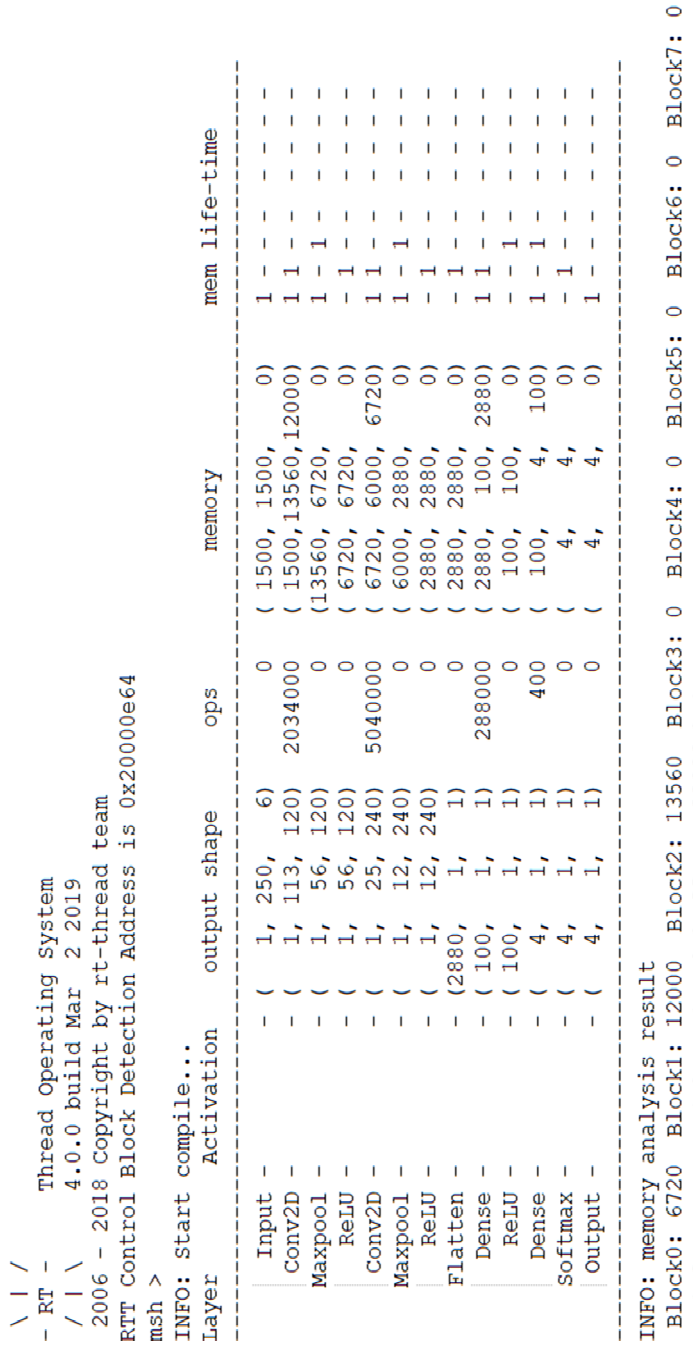

Figure 5-14 Quantised model summary printed by NNoM (Rotated).

5.3.4 Results

The evaluation of MCU is done by using the evaluation APIs provided by NNoM. The Top-k accuracy and confusion matrix from both quantised and floating-point model will be compared in this section. The performance of the two models will be compared and discussed in the later section.

5.3.4.1 *Accuracy and Confusion Matrix*

The Top-k (k=1) accuracy of the original classifier and NNoM classifier are shown in Table 5-5. Both models have the same accuracy for Top-k accuracy. The confusion matrix is shown in Figure 5-15. The difference between the distribution is very minor across all the classes.

Table 5-5 Top-1,2 accuracy comparison

Accuracy	*Classifier*		
	Floating Point Original (on PC)	*Fixed-Point Quantised (on MCU)*	*Difference*
Top-1	99.45%	99.45%	0.0%

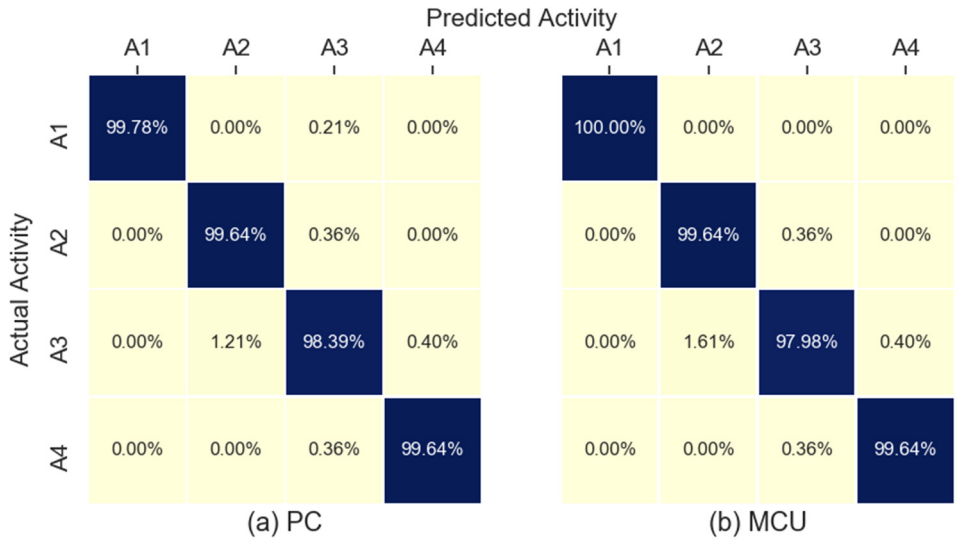

Figure 5-15 Confusion matrixes. (a) Original classifier using floating-point arithmetic on PC. (b) Quantised classifier using fixed-point arithmetic deployed to MCU.

5.3.4.2 *Performance*

The time for a single prediction was recorded in both MCU and PC sides. The prediction time on MCU was 290ms, while on the PC was 405us, which is~716x faster.

The memory utilisation is separated into two parts, non-volatile memory and volatile memory. Non-volatile memory is for storing weights and biases which are fixed

after the model is trained, located in embedded Flash. Volatile memory is occupied by the data buffers and arithmetic buffers, which is located in RAM. The classifier built previously takes 508.5KB for weights and biases and 32.28KB for volatile memory. Besides, NNoM also took a small amount of memory for the layer instances and APIs. In the classifier, 13 Layer instances were created and took 1704 bytes of volatile memory. The non-volatile memory can be seen by the map file which presented the compiling summary of the MCU project. The total non-volatile memory cost by NNoM files was 7744 bytes.

The summary of the comparison of the implementation versus PC is shown in Table 5-6.

Table 5-6 Summary of comparison

Item	*Neural Network Libraries*		
	Keras with TensorFlow backend (PC or Server)	*NNoM with CMSIS-NN (MCU)*	*CMSIS-NN (MCU)*
Platform	Intel i5-3475S 4 cores 2.9-3.6 GHz	STM32L476VGT6 Single code Cortex M4F 80MHz	
Data format	32bit-float	8bit-int	8bit-int
Code Length	13 lines[a]	13 lines	20 lines[b] (1.5x)
User configured parameter	~19	30 (1.5x)	86[b] (4.5x)
Weights / bias memory [bytes]	2.034M	508.5k (0.25x)	508.5k (0.25x)
Complexity	14.72M-FLOPS	7.36M-MACOPS	7.36M-MACOPS
	Model Performance		
Top 1 Accuracy	99.45%	99.45%	N/A
Top 2 Accuracy	99.92%	99.92%	

Item	*Neural Network Libraries*		
	Keras with TensorFlow backend (PC or Server)	*NNoM with CMSIS-NN (MCU)*	*CMSIS-NN (MCU)*
Prediction time	404us	290ms (717x)	
Efficiency [MAC ops/Hz]	6.28	0.317 (~20x)	
	Implementation on MCU		
Code size [byte]	N/A	Baseline + 7.7k bytes	Baseline
RAM cost [byte]		32.28k (NN buffer) +1.7k (NNoM instances)	51.2k (without manual memory optimisation)
Interlayer switching time		<1us	N/A

[a] Exclude the training only operation, such as dropout and fake clips

[b] Estimated per CMSIS-NN/CIFAR-10 example

5.4 Discussion

In the experiment, the classifier was built on PC then deployed to MCU using quantised arithmetic. The results showed the completely same accuracy thought the testing dataset. However, there are minor differences in the comparison of the confusion matrix, shown in Figure 5-15, which indicates that the fixed-point implementation of the floating-point classifier has not completely reproduced the same results. The difference is due to the resolution has changed during the quantisation process. Considering the difference are minor, the methods discussed in section 5.2 for neural model training and deploying is effective in real-life implementation.

One of the most concerns is whether the MCU is capable of undertaking the computational requirement of neural network models. Although quantisation and fixed-point neural network have reduced the computational complexity dramatically[134], [143], it still requires massive computational power (~Mops per prediction) and relatively large memory to run. In the experiment, the quantised model implemented with NNoM took 508.5KB ROM and 32.28KB RAM. It took 7.36MOPS for single prediction which results in nearly 0.3sec on the selected STM32L476 @ 80MHz (1MB Flash, 128KB RAM). The classifier has occupied over half of the available embedded flash and 1/4 RAM in the MCU, which might be less feasible to implement into those applications already required large memory. However, the classifier built in this chapter is a classic single path feed-forward network designed for PCs or other higher power platform, which could be overkill for the exercise classification. Further optimisation on structures and configuration might bring down the requirement of resources.

On the positive side, NNoM largely simplifies the development process of quantising a neural network model, and it makes the implementation on MCU more flexible and convenient, with a small trade-off in code size (7.7KB) occupying extra non-volatile space. From the developer's perspective, NNoM has provided similar interfaces to Keras, which is famous for its usability. Comparing to CMSIS-NN, NNoM has much lesser (3x lesser) parameters which must be configured by the developer. Most importantly, NNoM provides the functionality to build complex model structures, though it is not presented in this chapter.

5.5 Conclusion

To conclude, CNN classifier has shown its potential in data analysis. The trend of data decentralisation is pushing edge devices to undertake more works than before. Those edge devices now need to know what has measured by themselves and only send the aggregated information, such as WBR-SH2 must know what exercise is the user

performing. These required the neural network being implemented into MCU. However, neural networks tend to be bulky in both memory utilisation and computation cost, which restrict the implementation into MCU. Model compressing methods such as fixed-point quantisation help to reduce both memory and computation complexity, which allows the neural network to run on MCU. Unfortunately, there are very limited available neural network lib or implementation on MCU level programming. Moreover, most of them are either has limited supported operation or less user-friendly due to its low-level APIs. There is a significant need for a higher-level framework, specifically for MCU level programming.

Therefore, this chapter shows the development of Neural Network on Microcontroller framework, which is a higher-level framework designed specifically for microcontrollers using fixed-point arithmetic. It provides a layer-based structure for building complex network topology, minimises the user-configurable parameters, the abstracted layer interfaces, and the necessary methods for evaluating the implementation directly on MCU. NNoM is written with C programming language which is compliance with ISO/IEC 9899:1999 allows it to be implemented to other platforms such as PC or other embedded systems.

A multi-layer convolutional neural network classifier was built, and it was trained and validated with the dataset from resistance band exercise using WBR-SH2. Then classifier is then quantised and implemented into MCU using NNoM framework for validation. Both models provide the same prediction accuracy on the same test dataset, with little difference in the confusion matrix.

However, there are limitations to this experiment:

1. The model is still too large for many MCU application. The classifier tested in this chapter cannot be deployed into smaller footprint MCUs such as nRF52832, the one in WBR-SH2 contains only 512k embedded flash and 64k RAM.

2. The exercise dataset is small (data collected on six subjects), which might not be sufficient to classifier data from unseen people.

In this chapter, a preliminary experiment was done for resistance band exercise recognition. Two major limitations are 1) Lack of exercise data. 2) the classifier is not optimised for MCU. A further study will be presented in the next chapter, using more data from resistance band exercise with ranges of ages (including older adults) and a more compact classifier designed especially for MCU.

Chapter 6 Resistance Band Exercise Recognition with Older Adults

6.1 Introduction

6.1.1 Background

WBR-SH2 system is a purpose-built sensorised instrument for resistance band exercise. Together with the novel synchronisation method, WBR-SH2 can provide very detailed and very accurate motion measurement during resistance band exercise. In the previous chapter, the development of NNoM framework was presented, and it proved that MCU is possible to run exercise recognition.

To assess the performance and capability of NNoM implementation on MCU, a classic CNN classifier was developed and validated with the data from a small resistance exercise experiment. However, the CNN model was still too complex (~500KB parameters, ~32KB RAM) for the MCU in WBR-SH2 (~100KB ROM and ~8KB RAM left after other functions). Thus, to deploy the classifier into WBR-SH2, the model must be further scaled down.

NNoM, discussed in Chapter 5, provides user-friendly and flexible interfaces which make the building of these state-of-the-art structures much easier than ever before. Edge devices such as the WBR-SH2 are now free to try these new structures to improve the model performances.

After the development, WBR-SH2 were used in an international experiment to assess the resistance band exercise with older adults. Three sets of WBR-SH2s and a few types of resistance bands were sent to Italy. The experiment used Couch Potatoes for Cognition [49] as the experiment protocols. During the 2-month experiment, 40 participants with an age range from 18 to 80 have completed the test. The raw data from both hands were recorded into a smartphone and sent back for data analysis. The dataset

is much larger (40 subjects) and more diverse in ages from 18 to 80 than the previous preliminary experiment with six subjects age from 24 to 40. This dataset is surely valuable for the training of neural network classifier.

6.1.2 Objectives

The first objective of this chapter is to scale down the NN classifier to an acceptable size for the MCU in WBR-SH2. Allows WBR-SH2 to run the classifier locally, thus, to answer the question of "what" type of exercise that the person is doing.

The second objective is to use the data from the international experiment to validate the above implementation and discuss the feedbacks on WBR-SH2.

Furthermore, this chapter should prove that NNoM is sufficient for running NN classifier on a resource-constrained platform (such as WBR-SH2). Also to evaluate the performance of a few scale configurations.

6.2Methodology

6.2.1 Hardware Capability of WBR-SH2

The overall performance of WBR-SH2 has been presented in Chapter 3. It is controlled by a Bluetooth SoC nRF52832 (Nordic Inc.), with single-core ARM-Cortex-M4F running at 64MHz. The core has the performance of 215 EEMBC CoreMark (3.36 CoreMark/MHz)[90]. This MCU has 512KB embedded flash (ROM) and 64KB RAM. However, after other functions were implemented, only 100KB ROM and 8KB RAM are left for the NN classifier. In regular measuring scenario (sampling of all sensors at 100Hz, real-time data sent to a smartphone, and synchronising), other tasks take 15% of CPU time, leaving 80+% CPU time available for a NN classifier. However, the more CPU time the NN takes, the more power it will consume. In a battery-powered scenario such as WBR-SH2, less CPU occupation is always the goal.

6.2.2 Data Selection

WBR-SH2 has collected 12 DoF measurement for each hand. The raw data includes 3-axis rotations speed, 3-axis accelerations, 3-axis magnetic field, atmospheric pressure, atmospheric temperature and force applied on the resistance band. Each data series is in resolution range from 16-bit to 24-bit. Some processed data can be calculated from the raw data, such as the orientation in quaternion form, the linear acceleration without gravity components, and others. Among the data, some features that used for traditional data analysis can be extracted, such as the maximum and minimum values, the frequency range of each series, and others. Table 6-1 summarises the available data in WBR-SH2.

Table 6-1 Summary of available data in WBR-SH2

Raw data *(Low computational cost)*	*Processed data* *(Medium computational cost)*	*Features* *(High computational cost)*
Rotation	Quaternion	Frequency Spectrum
Acceleration	Linear acceleration	Cepstrum
Magnet field	Gravity vectors	
Force	Maximum, minimum	
Atmospheric pressure		
Atmospheric temperature		

In the above data, the raw data requires the least computational cost which can be read out directly from the sensors. Processed data requires medium calculation complexity, the calculation normally requires some multiplication and/or addition. Features normally require the most computational power, such a Fourier transform, and sorting. Although some studies propose that adding features in a neural network can improve accuracy [67], [145], [146], the accuracy improvement is not significant. Many studies also use raw motion data similar to what has provided by WBR-SH2, which

also achieve competitive accuracy. Therefore, to reduce power consumption, features are excluded.

Physical exercises are a set of motions, thus, motion data are promising for representing the exercise. In Chapter 5, the raw accelerometer data from both hands are selected for training classifier, and the results were accurate. The previous training of the classifier used across position method to reduce the correlation of sensor placement, for example, sensor #1 is allocated to the left hand while sensor #2 is allocated the right hand, but the exercise should be considered the same type even when the sensor position is switched. When the classifier is moved to the edge (the sensorised handle), one handle will never know the raw data from the other hands, thus the Cross-Position Method introduced in Chapter 5 cannot be applied. Although it enlarges the dataset, it is still not enough to solve the dependency problem since the data it uses are vectors (3 axis acceleration) and the dataset is too small to reproduce all the states.

To further reduce the correlation on sensor positioning and to enhance the adaptability of the classifier, vectors such as 3-axis gyroscope data and accelerometers data are not selected for training classifier. These data are sensitive to the orientation of the sensor placements. However, in real-life scenarios, each type of exercise may have many sensor placements. Instead, the magnitudes of rotation and acceleration vectors are selected in two considerations. Firstly, they are the representatives of motion, only without the orientation. Secondly, the arithmetic of them is simple enough which can be done in MCU fast and efficiently. Both rotation speed and acceleration magnitude are calculated using (6-1), where $|m|$ is the magniude and x, y, z are the vectors. Besides, the force measurement of the resistance band is also selected. Since the force is applied directly on the resistance band, the force measurement should also be a direct representation of the exercise.

$$|m| = \sqrt{x^2 + y^2 + z^2} \tag{6-1}$$

To summarise, the rotation speed magnitude, acceleration magnitude, and force measurement are selected for exercise recognition.

6.2.3 Compact Classifier for Microcontroller

6.2.3.1 Complex Structures

Recently, there are three representative feedforward neural network structures (Inception [120], Residual Network. [121], [122], and DenseNet [123]) showed their competitive results with lesser parameters and computational complexity compared to classic single path convolution. One common idea of them is they optimised from model structures (except Inception V3 and variants using separable convolution). In this thesis, those network structures have multiple connections between layers called complex structures; correspondingly, the single path networks called classic structure. The three complex structures can be summarised in Figure 6-1, Figure 6-2 and Figure 6-3.

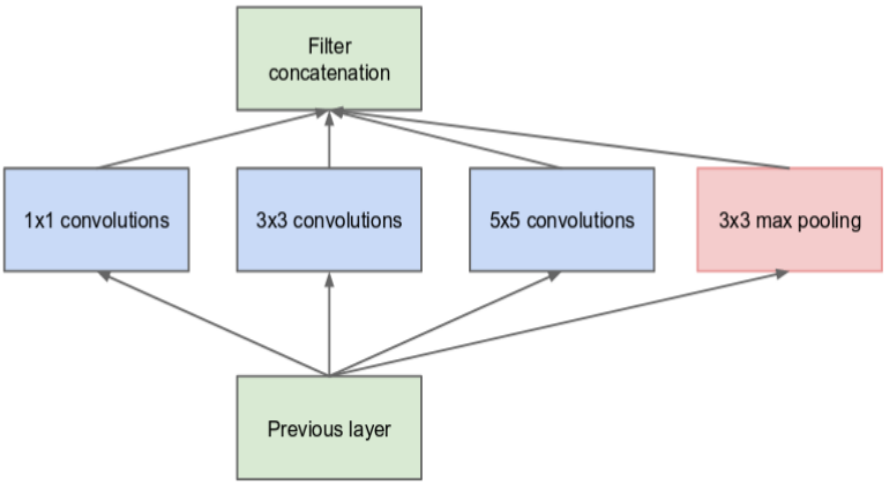

Figure 6-1 The Inception structure contains multiple parallel paths which take the same data as input. The results are concatenated on channel-wises [120].

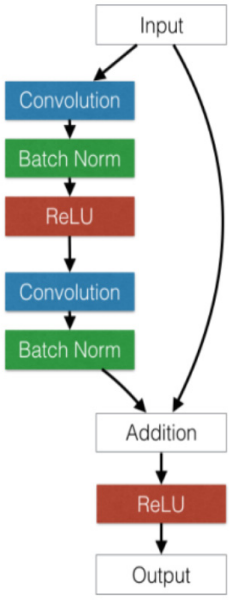

Figure 6-2 The Residual net structure contains skipping links from the input to the output of a block. The input data and output data of a residual block are merged by point-wise addition. [121], [122]

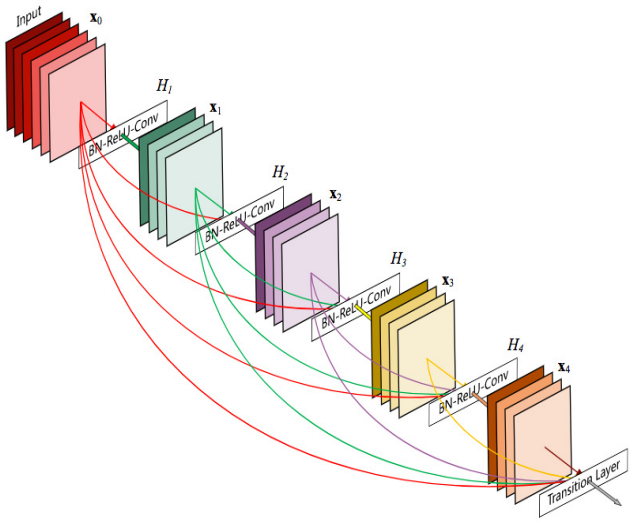

Figure 6-3 Dense Net contains a set of dense connection between each layer in a dense block. Data is concatenated on channel-wise. [123]

NNoM provided concatenate and additional layers which are necessary for these complex structures. Thus, those complex structures can be implemented into MCU with little effort.

Among the three candidate structures, Residual Net and DenseNet are designed for a very deep neural network (up-to thousands of layers [121], [123]). They are less meaningful in the edge devices which are limited by the memory. The Inception was produced for less deep neural networks (tens layers [120]) which depth is similar to the classic deep neural network. Therefore, the Inception structures are selected to build the classifier for WBR-SH2.

6.2.3.2 Compact Classifier

A CNN classifier was built with Inception structure, shown in Figure 6-4. As shown in the figure, a single block of Inception structure was embedded into the classifier. When running a NN in MCU, the size of the model needs to be considered carefully. To compare the different sizes of the classifier and its performance, the classifier was tested with 3 configurations distinguished by the size, so-called “small”, “medium” and “large”, shown in Table 6-2. Additionally, a much larger configuration, namely “classic”, was also tested to provide a ground reference on the dataset.

The classifier has multiple layers in-depth and the maximum three layers in parallel. All trainable layers were l-D, multiple channels convolutional layers. Dropout layers were added after each convolutional layer with different dropout rate (Conv-1: 0.1, Conv-2x: 0.2, Conv-3: 0.5, Conv-4: None). The Conv-1 was the initial scanning of the data. The output was then shared with the three convolutional layers named Conv-2x (x=a, b, c). The kernel sizes of the three parallel convolutions were set to 7, 3, and 1 individually. The outputs of the parallel layers were concatenated along the channel axis (called channel-wise concatenate). The concatenated output was then fed to the Conv-3 for deeper features extractions, following by a final convolutional layer Conv-4 to

compress the output channel to 4 which match the number of classifications. Finally, a Global Average Pooling (GAP) was applied to generate a size of 4 output.

Additionally, a Softmax layer was attached at last for calculating the probability. Using GAP instead of fully connected layer has many advantages [124], one of them is it avoids the massive weights contributed by fully connected layers. Without a fully connected layer, the number of weights was reduced massively.

Due to the very limited resolution of 8-bit integer, GAP layer might perform very differently in the quantised model while the kernel setting (the input size in GAP) is relatively large. Calculating average with small integer data and output into the same format results in the vanishing of the data. This defect will be even worse when the size of the average windows (kernels) is relatively large. To solve this problem, the GAP layer in the floating-point classifier will be replaced by a Global Sum Pulling (GSP) layer in NNoM. The advantage of using GSP over GAP is avoiding the integer dividing, which is the reason for the small data vanishing. The transform between GAP and GSP layer is linear. Thus, this operation will not cause a different result in the following Softmax layer. However, the GSP layer might cause data overflowing on the size of the output integer. The customised GSP layer uses a dynamic shifting method to solve the problem. Firstly, the sums will be store in a larger integer array (32-bit integer). Secondly, the maximum absolute value among the array will be sorted out. Thirdly, the best shifting number (the power of 2) which can store the maximum value without overflowing will be identified. Finally, all the sums stored in the temporary array will be shifted by the best shifting number and store to the output buffer. Thus, the massive resolution loss on GAP layer is solved by the customised GSP layer.

The different configurations of the classifier are listed in Table 6-2. They are considered much smaller than what was proposed in Chapter 5 as well as other studies [75], [147]. The memory cost and the computational complexity will be discussed in following sections.

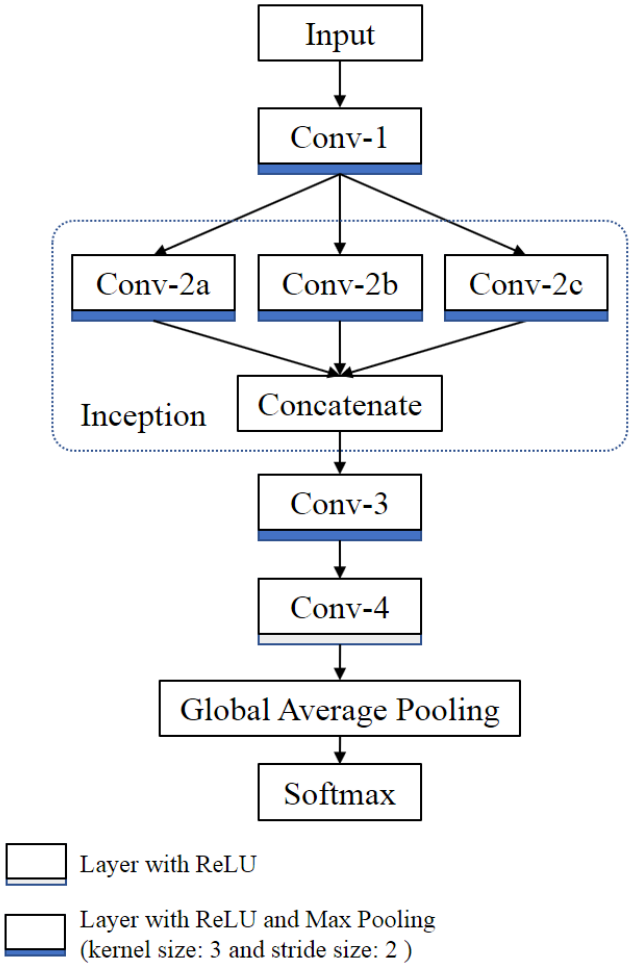

Figure 6-4 Compact classifiers with Inception structures.

Table 6-2 Trainable layer configuration of the classifier

Layers	*Kernel size **	*Small (filter)*	*Medium (filter)*	*Large (filter)*	*Classic (filter)*
Conv-1	7 (stride 2)	4	8	16	64
Conv-2a	7	4	8	16	64
Conv-2b	3	4	8	16	64
Conv-2c	1	4	8	16	64
Conv-3	3	16	24	48	192
Conv-4	4	4			

* Stride = 1 if not specified

The classifier was first built on PC using Keras with Tensorflow backend [148], then it was quantised and deployed into WBR-SH2 using NNoM framework. The training and deploying followed the procedure discussed in 5.2 Methodology.

6.3Experiment

6.3.1 International Experiment with WBR-SH2

During the development, 3x WBR-SH2 and an Android phone were sent to Italy for a collaborative experiment (the experiment involving human subjects was approved by the University of Torino Ethics Committee). The aims of the experiment were to understand the resistance band exercise in a wide range of people through the very detail data measured by the WBR-SH2 and to assess the usability and functionality of WBR-SH2 itself. The protocol used in the experiment was the Couch Potatoes for Cognition [49] which has been discussed previously. Each subject was asked to do 4 types of activities each for 30 seconds. Especially, activity 4 is done twice, on both legs for 30 seconds. Most of the subjects have done three repetitions of exercise during the experiment. In total, 40 subjects (16 males, 24 females, aged from 18 to 80) have completed the full protocol. The ages among participants were not evenly distributed, 20 people aged below 60 years old (included) and 20 people aged above 60 years old. The age distribution is shown in Figure 6-5.

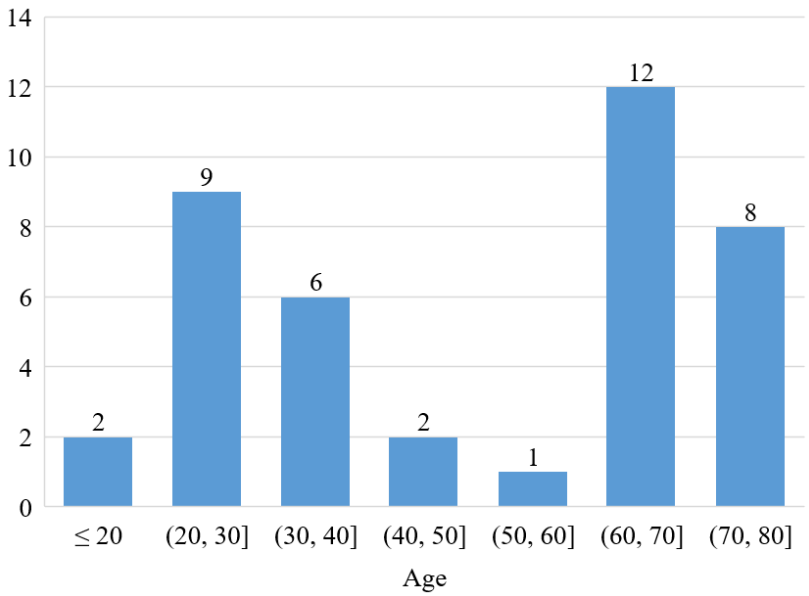

Figure 6-5 Age distribution among participants

6.3.2 Data Pre-processing

During the experiment, around 10 hours of continuous exercise data (around 18000 seconds for each hand) was recorded at a 100Hz sampling rate. Each sample contained 12 DoF measurement and a millisecond accuracy timestamp. However, not all 12 DoF measurements were used for training the classifier due to the performance of the MCU is very limited. As discussed in previous sections, three magnitude measurement sequences were selected as the dataset for training and testing the classifier. The dataset was quantised with the resolution of 8-bit integer (256 levels) to simulate the accuracy in the quantised classifier.

Testing dataset and training dataset is generated individually from the original dataset. Different from the method in Chapter 5 which was randomly select the pieces of data in the whole dataset, the training dataset and the testing dataset was selected by the subjects. Data from 30 out of 40 subjects (75%) was assigned for training dataset while the data from the rest 10 subjects (25%) (6 subjects over 60 years old, 4 subjects below 60 years old) was assigned to testing dataset. In this case, the data from testing

subjects were completely invisible by the classifier during the training. In total, the training dataset includes 71148 samples, and the testing dataset includes 5998 samples.

Both training dataset and testing dataset were sliced separately into same length pieces for feeding into the classifier. The training dataset was sliced by a sliding windows technique with a sliding rate of 1/8 window size, while the testing dataset as sliced with a sliding rate of 1/2 window size. To further reduce the size of the input data, the data were resampled at a frequency of 50Hz similar to the public domain dataset UCI HAR (Human activity recognition) [145]. The size of windows was set to 128 timestamps which corresponded to 2.56 seconds [145]. Thus, each sample of data size 128 × 3 (timestamp × channel). Additionally, the training dataset was reproduced by 4 levels of magnitudes (1x, 0.8x, 0.64x, 0.512x) to improve the generalisation of the classifier [149].

6.3.3 Evaluation

The classifier was trained with the training dataset on PC (Intel i7 4770, 4 cores @ 3.7GHz) with the four configurations shown previously. The classifier was then validated using the test dataset. The hyperparameters for training are set to epoch = 20, batch size =128, used Adam optimiser with default learning rate on categorical cross-entropy loss functions. The best classifier was saved per the test accuracy during training. Each configuration was trained for 3 times, and only the best classifier for each configuration was recorded.

The best classifier was quantised and deployed into MCU for validation. To simplify the testing, the WBR-SH2s were not used for testing directly due to the limited resources and already running multiple tasks. Instead, an STM32L476 (ARM Cortex-M4F core was set to 64MHz) was used to simulate the performance of the MCU (NRF52832, ARM Cortex-M4F @ 64MHz) inside the WBR-SH2. The performance of both MCUs is very similar since they are the same cores, with very little performance difference, 3.36 CoreMark/MHz with nRF52832 [90] and 3.42 CoreMark/MHz (1.8%

faster) with STM32L476 [142]. The optimised configuration is implemented into WBR-SH2 directly after the experiment.

The confusion matrix, the Top-k (k=1) accuracy on both training and testing sets, and the times cost for single prediction are recorded on both PC and MCU side. In addition, the total MAC operation and the memory utilisation on the MCU side are recorded.

6.4 Results

The complexity in memory and computation is shown in Table 6-3. The performance and complexity are compared through all the 4 configurations.

Table 6-3 Complexity and performance comparison in different configurations.

	Small	*Medium*	*Large*	*Classic*
Operations [MAC-Ops]	20.1k	65.6k	231.4k	3,334k
Trainable Parameters (ROM cost [byte])	868	2,948	10,756	159,748
RAM by NN buffers	912	1,440	2,880	11,520
Total RAM (Inc. memory cost by NNoM)	3,276	3,804	5,244	13,884
Run-time (PC) [us]	24	28	33	120
Run-time (MCU) [us]	2,543	5,317	13,987	149,143
Speed difference [PC/MCU]	106x	190x	424x	1242x
Efficiency [MAC-Ops/MHz]	0.124M	0.192M	0.258M	0.349M
Training Top-1 (PC)	91.49%	93.93%	96.21%	99.55%
Testing Top-1 (PC)	93.11%	94.16%	94.71%	95.41%
Testing Top-1 (MCU)	91.88%	93.90%	94.20%	94.70%

In the 4 configurations, 3 of them (small, medium, large) met the memory requirement of WBR-SH2. Figure 6-6 shows the interrelation between the configuration size and the performance of the classifier.

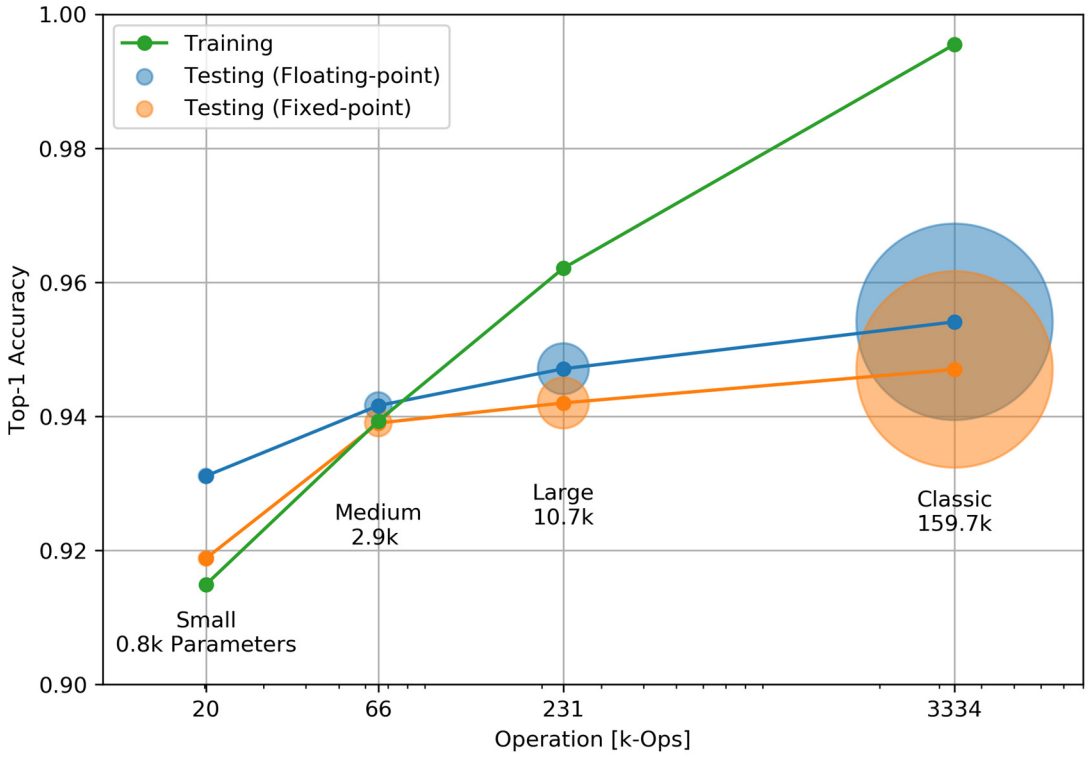

Figure 6-6 Accuracy comparison. Training with the floating-point model, testing on the floating-point model, and testing on the fixed-point model.

The confusion matrix comparisons of each configuration shown below in Figure 6-7, Figure 6-8, Figure 6-9 and Figure 6-10.

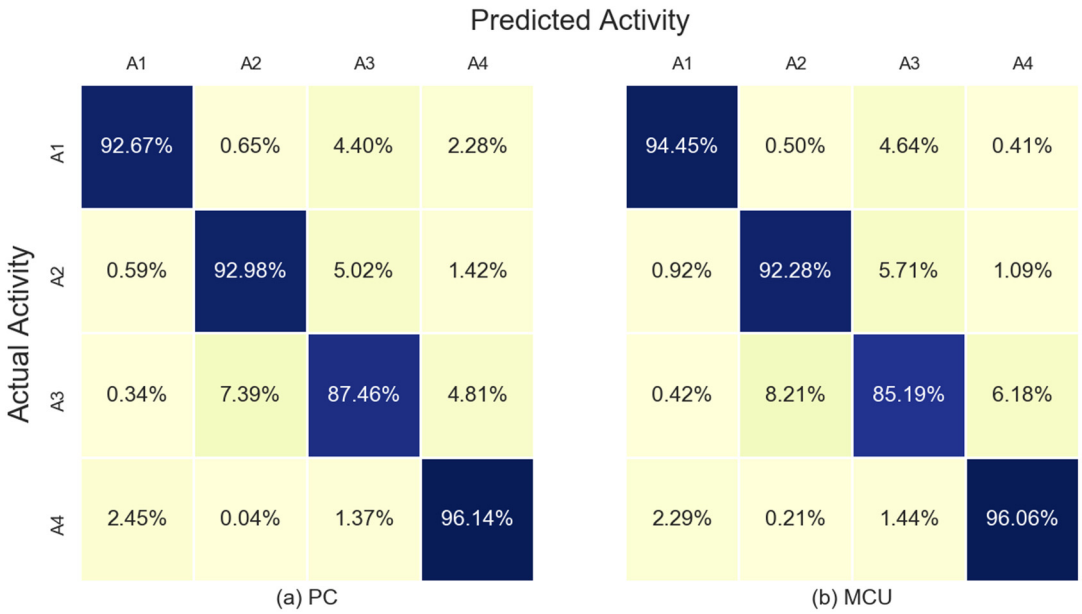

Figure 6-7 Confusion matrix comparison of the floating-point model on the PC and the fixed-point model on the MCU. Model size in the small configuration.

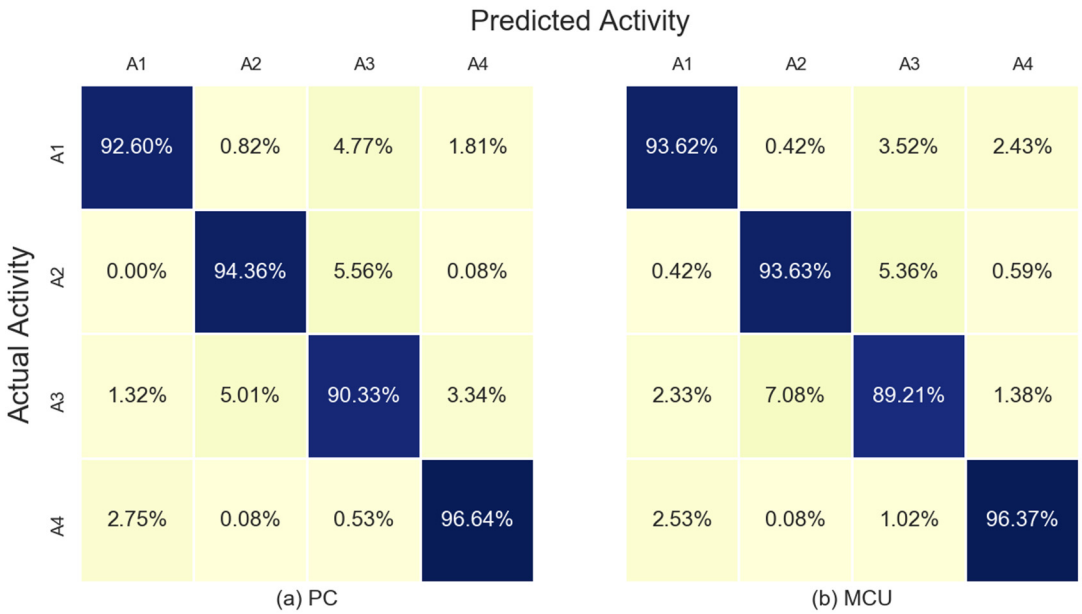

Figure 6-8 Confusion matrix comparison of the floating-point model on the PC and the fixed-point model on the MCU. Model size in the medium configuration.

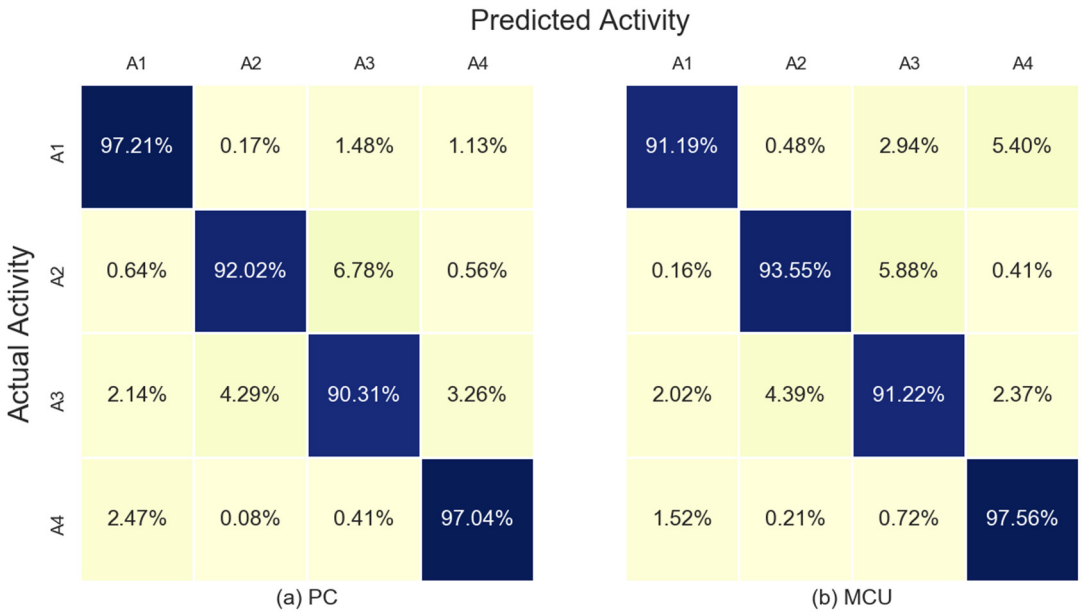

Figure 6-9 Confusion matrix comparison of the floating-point model on the PC and the fixed-point model on the MCU. Model size in the large configuration.

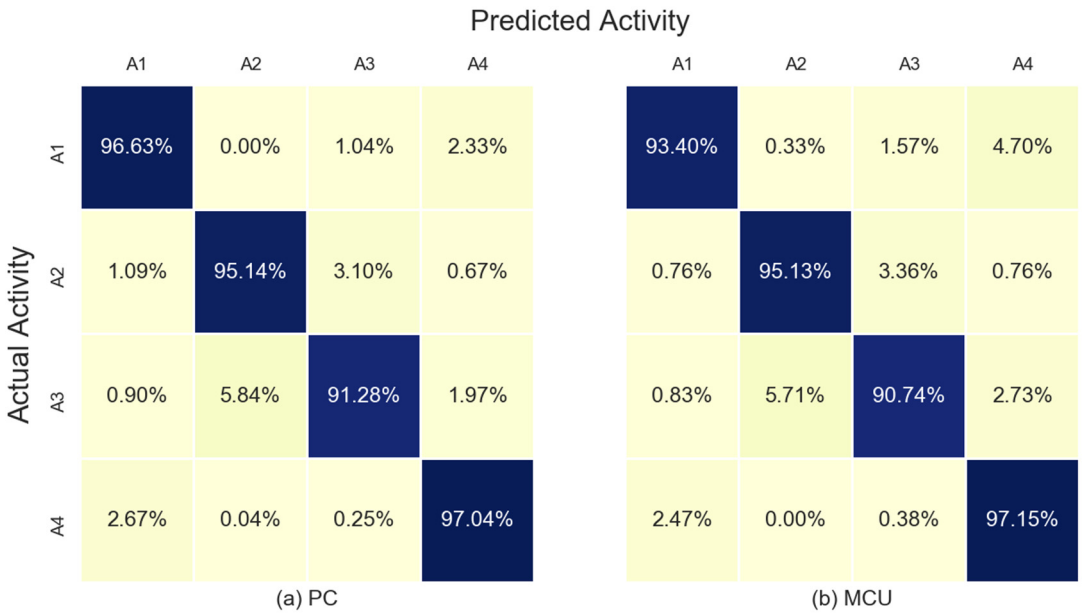

Figure 6-10 Confusion matrix comparison of the floating-point model on the PC and the fixed-point model on the MCU. Model size in the classic configuration.

6.5Discussion

6.5.1 Results

Overall, the results show that the quantised classifier can perform exercise recognition accurately and efficiently (e.g. the medium configuration achieve 93.9% accuracy only takes ~5ms for one prediction). It is generally believed the size of the neural network model is related to its recognition performance. This test result also shows the same pattern (Figure 6-6, Table 6-3). In the training accuracy comparison, the larger configuration always results in better accuracy in training. The crossing point on the accuracy of training dataset and the testing dataset is where the optimal model size for the dataset (around the medium configuration). The model size smaller than the point is insufficient to classifier the data, while the model size larger than the point is overfitting the training dataset with a little accuracy increment on the testing dataset. The increase of testing accuracy could meet the ceiling (around 95%) when further size increment no longer corresponded to better testing accuracy.

To find the optimal size of configurations, 4 different configurations have been tested (3 of them were relatively small which aimed to run on MCU, the other one was much larger for comparison). As envisioned, all the quantised classifiers were less accurate compared to its floating-point versions. Contrary to the previous conclusions in Chapter 5 (both models have the same accuracy), the difference between floating-point and the quantised classifier is larger (up to 1.23% difference in the small configuration). However, the classifier in Chapter 5 is much larger than the classifier in this chapter. The gap between floating-point and quantised classifier might shrink as the model capacity grows larger.

Although the smallest configuration achieves a 91.88% accuracy in the testing dataset, it only contains 868 trainable weights, occupies ~3.2KB RAM, and takes the minimum 2.5ms for a single prediction. In the models which is larger than the medium-size configuration, the accuracy increment no longer corresponds to the complexity of

the model. Which could be the natural difference between the training dataset and the testing dataset. The medium configuration achieved similar accuracy (93.90%) compared to the large configuration (94.20%) with 2.6x less the running time. The best accuracy was achieved by the classic configuration at 94.70%. Overall, the medium configuration is the balance configuration for WBR-SH2 considering both complexity and accuracy.

Comparing to the classifier built in Chapter 5, all the configuration tested for MCU in this chapter are much smaller (20k, 66k, 231k MAC-ops compared to 7.36M previously), that can be embedded into WBR-SH2 for exercise recognition. Thus, the final question of "what" kind of exercise the person is doing is now can be answered by the sensorised handle itself.

The experiment result has proven that the data from older adults can also be used for classification with reasonable accuracy. Though they performed differently due to weaker strength and the decreased mobility, once enough data is used to train the NN classifier, it is sufficient to recognise the exercise in most of the cases.

Finally, the type of exercises was small (only four types of exercise) and the dataset is lack of an idle status (which indicate no exercise has ever performed). Future studies should consider adding more statuses.

6.5.2 Neural Network Power Efficiency on WBR-SH2

The time for a single prediction is recorded on both PC and MCU. Even though, the quantised model requires lesser computational power than the floating-point model, due to the significant performance gap between PC and MCU, the floating-point model running on PC was still much faster than the quantised model on the tested MCU (up to ~1200x faster in the classic configuration). However, the time for one prediction with the medium configuration (5.3ms) was still faster than the default data sampling period on the WBR-SH2 (10ms). On the one hand, with the medium or small configuration, the classifier is capable of running the prediction on each new sampling for the best

performance. On the other hand, in the low-power scenarios, with sampling windows size of 2.56secs and 50% overlapping, the classifier could run as slow as 1.28secs per round without missing data. Thus, the estimated CPU utilisation by the classifier is about 0.41%. The nRF52832 consumes 3.7 mA while running in full speed with the DC/DC and cache enable [90]. In this case, the classifier only takes an average 15uA for the classification, which is ignorable compared to the working current (22mA) of WBR-SH2 (per Table 3-6).

6.5.3 International Experiment

The international experiment done in Italy is also the first time for WBR-SH2 to be operated by researchers with less engineering background. With the help of an instruction manual, they were able to operate the sensors well during the experiment. The experiment not only shows WBR-SH2 has the necessary capability to measure the exercise remotely and precisely but also shows the considerable improvement in the usability than its predecessors (the experimental system).

A list of feedback about the system and the exercise protocols was sent back from Italy, shown in Appendix F. The most comments are related to the Couch Potatoes for Cognition protocols. Firstly, the length of the resistance band was too long for the exercise. This was foreseen before the study but could not be solved. One of the challenges is to personalised the exercise instrument and the treatment. Changing the length of a band for an individual is one of the options for personalised treatment. Secondly, in activity 4, the band can easily slip out from the foot. The securing of the resistance band is also an old problem; this problem can be fixed by using a flattened resistance band instead of the current tube type resistance band.

6.5.4 Reflection of WBR-SH2

The aim of WBR-SH2 was to measure the exercise objectively. To measure the exercise, the three questions related to the exercise must be answered. With embedded sensors, WBR-SH2 can answer the “when” and “how” already. The final question of

"what" is now can be answered by the embedded neural network classifier in real-time. These features together make WBR-SH2 an intelligent standalone device for measuring resistance band exercise.

The improvement of usability is more significant than what was expected during the development. Without good usability, the experiment cannot be done easily with non-engineering background users. Even though the current system is still requiring many preparations before exercise, such as connecting the devices to smartphone manually and recording data manually.

6.6 Conclusion

This chapter presents the design of a compact and effective neural network classifier using state-of-the-art structures. The aim was to develop a neural network which is feasible to run on MCU for exercise recognition. Thus, the question of "what" type of exercise is done could be answered by the device directly. The results show the implementation was capable of recognising the 4 types of exercise with an identical accuracy at 93.9% in real-time. Although the performance was not competitive to the classic model runs on PC, the outcome was still significant which has genuinely moved the Artificial Intelligence to the edge. Thus, the dependency of having a smartphone present during exercise was reduced.

The international experiment using WBR-SH2 has proven the usability and shown the potential of real-life applications, such as exercise intervention in the user's home or rehabilitation centres. The new classifier was beneficial from the much larger dataset collected in the experiment. The feedback from the experiment is also valuable, which has pointed out the limitations and the defects in both Couch Potatoes for Cognitive exercise protocols and the sensorised resistance band.

The experiment in this chapter proved that the NNoM is sufficient of running NN classifier in WBR-SH2 and it further proved that NNoM is potentially effective in other

similar application scenarios, which use a neural network to process data in a resource-constrained platform.

However, there are some limitations: 1) Only one specific model was tested in this chapter. 2) No supports for Recurrent Neural networks.

Chapter 7 Conclusion and Future Directions

7.1 Backgrounds

More and more evidence shows the potential benefits of exercise to a portion of diseases. There are already massive efforts put into the field to investigate the true effectiveness of the exercise. However, the interrelation remains unclear. Both positive and negative evidence was shown in previous studies. Without the understanding of precisely what kind of exercise with how much intensity is positive and how much is negative, the exercise intervention cannot be performed with confidence. Most of the studies were restricted by the lack of long-term objective measurement tools, resulted in relatively long assessment period (4, 6, or 12 months).

Nevertheless, follow-up experiments usually are unsupervised and unmonitored. The quantity and quality of the remote exercise were never known. Thus, there is a clear need for a sensing system which can measure exercise remotely, objectively, and accurately, especially for the studies with long-term exercise intervention.

By using some remote measurement tools, the proposed models in Chapter 1 can be achieved. However, the current measurement devices in the market are either too simple (such as wristband and smartphone contains only one IMU sensor) that are unable to measure exercise accurately or are too complex to use (such as motion capture suits) which requires professional skills to operate. A simple, user-friendly and accurate measurement device is needed for exercise measurement remotely and continually.

The acceptance of wearable devices among older adults is also relatively lower than in younger people. Which means they tend not to use that new technology when the appearance of the sensor systems is prominent. While designing new sensorised devices, the acceptance of the sensor must be the priority. The concept of nearable might

be the potential solution to improve the acceptance which hides the sensors, pretends to a conventional instrument and brings less cumbrance to the user.

Therefore, this thesis presented the development of the innovative intelligent sensors system as the solution for remote exercise measurement. The system implements multiple state-of-the-art technologies and the nearable concept. The outcomes of this thesis (the WBR-SH2 system) have achieved the requirements above. WBR-SH2 can provide very detail measurement of resistance band exercise remotely by its onboard sensors. It reused most of the parts from a commercial resistance band handle to avoid the distraction of the natural motion while doing exercise. The robust mechanical design protects internal electronics in typical usage scenarios, which also dramatically reduces the needs of maintenance. The concept of nearable brings less disturbance to the user's natural feeling of exercise compared to existing sensor systems. Finally, the embedded neural network makes WBR-SH2 an innovative and intelligent device.

7.2 Conclusions

In this thesis, the road towards monitored exercise intervention has been presented. After the review of the state-of-the-art, the model of remote exercise intervention with older adults was proposed. The cornerstone of the model is a system which is capable of measuring the exercises remotely, objectively, and accurately. The three major questions about remote exercise ("what", "when" and "how") must be answered to assess the exercise objectively. Thus, an innovative intelligent sensor system (WBR-SH2) based on motion sensing and force sensing has been proposed. It provides promising results on both functionality and usability. The state-of-the-art neural network implementation fit the megatrend of pushing the AI to the Edge. Most importantly, the WBR-SH2 is generally acceptable by the real end-user (older adults) from the functionality and usability aspect. Overall, the sensor is very promising for remote exercise interventions with resistance band exercise.

The thesis is divided into seven chapters. The recalled messages for every chapter are discussed below.

Chapter 1 has generally discussed the ageing problem, the links between exercise and the health among older adults, and the current limitation on most of the studies. After that, the goals, the novelty and the structures of this thesis are presented.

Chapter 2 has shown the preliminary experiment using an experimental sensorised resistance band system to do the Arm Curl Test. The experiment aimed to validate the capability of using IMU and load cell sensor to measure resistance band exercise objectively. The experiment was done with two young subjects. The data analysis on the raw data already shows much more detail compared to the traditional method, which only counts the repetitions done in 30seconds. Parameters such as the power, peak forces, frequency and their changes over time have proven that the exercise can be understood in detail. The limitation of the experimental system has been discussed, which can be concluded to 1) unable to measure the direction of the resistance band, 2) the usability is still not enough for novices. Therefore, a new sensor must be built to overcome these limitations.

Chapter 3 has presented the development of the new sensorised resistance band system, named WBR-SH2. This system aimed to fulfil the principle goals shown in Chapter 1 and overcome the limitations found in the experimental system during Arm Curl Test experiment (Chapter 2). An all-in-one box design concept was selected as the final design. WBR-SH2 uses Bluetooth Low Energy 5.0 for the only communication method to reduce the complexity in usage. The sensors in WBR-SH2 are capable of measuring the orientation of the resistance band. The low-power design dramatically improves the working time (12/16 hours compared to 8 hours) as well as the standby time (90 days compared to 2 days in the experimental system). By using the low-power motion wake-up function, WBR-SH2 can measure the exercise only when it is needed. It saves power and reduces the operations needed by the user. Thus, a single charge

allows the sensor to work for at least four weeks in an exercise plan with the recommended intensity (120~150 min per week). After the development, a preliminary PPI was done with the real end-users (older adult with mild dementia and their carers). The results suggested that acceptance was high, and the simplified RGB colour feedback was understandable and attractive to them.

Chapter 4 has discussed the principled problem of synchronising multiple sensors nodes in a wireless network. The solution was focused on the wireless network with BLE, which has been widely implemented into most of the smartphones. A novel method to synchronise sensors nodes based on the generic BLE protocol without modifying the Android devices have been proposed and tested with five sensor nodes (WBR-SH2). The results are significant with Std: 0.217ms, CDF95%: 0.47ms, Maximum Network Error: 1.284ms. The result is much better compared to the generic time services in BLE (resolution at 1/8 sec). This result is accurate enough for human body sensing. Moreover, this method can be implemented to other sensors even those already sold to the customer by updating the firmware, since it does not require modification on the sensor node's hardware or user's smartphone. Finally, this method improved the WBR-SH2 synchronisation accuracy for measuring resistance band exercises.

Chapter 5 has presented the development of the Neural Network on Microcontroller framework, which designed for a wide range of small footprint platforms. With the new megatrend of data decentralisation, edge devices are pushed to understand what has been measured instead of transferring raw data to the remote servers. The neural network has shown its ability for data classifications or other precession. However, there are still many barriers such as limited resources with MCU and lack of higher-level tools which make the implements of AI into edges more difficult than other platforms. Therefore, this chapter showed the development of a high-level Neural Network on Microcontroller (called NNoM). The details of the ideas,

the model quantisation technique, the framework structures, and a preliminary experiment for comparing the classifier on PC and MCU have been discussed. The experiment results showed that the MCU implementation (fixed-point arithmetic) has the same accuracy (99.45%) as the model trained on PC with floating-point arithmetic. The classifier takes 508.5KB ROM and 32.28KB RAM on the MCU and 7.36Mops for single prediction which results in nearly 0.3sec on STM32L476 @ 80MHz. Even though the tested classifier is still too large to be implemented into WBR-SH2, it shows the possibility to optimise further and scale down the model for lesser resources.

Chapter 6 has presented the evaluation of the NN model in the small footprint as same as WBR-SH2. It also discussed the actual usage of WBR-SH2 in an international resistance band exercise experiment using WBR-SH2 for measurement and Couch Potatoes for Cognition as protocol. In total, 40 subjects (20 of them aged above 60) participated, and a large dataset was collected. By using this dataset, four different size configurations of neural network classifier have been tested and discussed. The optimal configuration is 2.9k weights, 3.9k RAM, and 66k MAC ops, which has achieved an accuracy of 93.90% on MCU (94.16% on PC). This classifier took only 5.3ms for one prediction. Due to the difference in dataset and data processing method, the accuracy between Chapter 5 and Chapter 6 are not comparable. However, the size (508k to 2.9k) and the running time (300ms to 5.8ms) were reduced dramatically while both of them can achieve similar (same) accuracy level. Nevertheless, the experiment also collected valuable feedback to the protocols and the system which has approved the efforts in improving the usability of WBR-SH2. Overall, this chapter presented the real-life application of the works done in previous chapters, and the promising results allow WBR-SH2 to answer the three major problems of “when”, “what” and “how” is the exercise done remotely by its own, which has achieved the concept of edge AI.

Chapter 7 finally concludes the thesis and points out the possible future direction after this work.

7.3 Highlights of Outcomes

The goals proposed in Chapter 1 have been fully fulfilled by the outcomes from the above chapters. Under the remote exercise intervention framework proposed in Chapter 1 (Figure 1-7), three highlighted outcomes have been presented and validated.

Firstly, the sensorised resistance bands system have been built for remote exercise measurement. The new developed WBR-SH2 system has dramatically improved the usability while keeping a similar sensor setup as the experimental system. Both developments were following the concept of "nearable", which is none disturbed during measurement. A preliminary PPI with older adults has shown the high potential acceptance of WBR-SH2 among real end-users. Overall, this outcome can be the cornerstone of not only resistance band exercise but also wide ranges of researches requiring remote exercise measurement.

Secondly, a novel synchronisation method base on generic BLE stack has been proposed. This method did not require hardware or firmware modification on a smartphone like other existing methods. It can provide continuous and accurate synchronisation on many existing sensor systems. This method could synchronise small sensors network with an unmodified Android device without impact on BLE bandwidth. It allowed WBR-SH2 and similar sensor systems to achieve sub-millisecond accuracy synchronisation based on the user's smartphone (Std: 0.217ms, CDF95%: 0.47ms, maximum network error: 1.284ms). This outcome has solved the principled problem for every sensor network involving a user's smartphone which is not allowed to be modified.

Thirdly, a higher-level Neural Network on Microcontroller (NNoM) framework has been developed. This framework was aimed to overcome the difficulties in deploying the neural network model into edge devices (e.g. a microcontroller). The comparison has shown 3x less user-configurable parameters compared to the existing lower-level library (Chapter 5, Table 5-6). It finally made

WBR-SH2 an artificial intelligent sensor which can answer all three problems of “when”, “what” and “how” about remote exercise on its own. In the trend of “data decentralisation”, the concept of “Edge AI”, this outcome is significantly valuable for developers to deploy the neural network fast to edge devices. This framework has been open-sourced since January 2019 on GitHub. To September 2019, the repository has received 169 stars.

As the results, the outcomes above have been formed as the “Innovative Intelligent Sensors” (WBR-SH2 and its tools), which is a robust and promising device to “Objectively Understand Exercise Interventions for Older Adults” — finally completing the title of the thesis.

This thesis contributes by providing the innovative intelligent sensor for remote objective measurement. It helps not only researchers but also a variety of people who want to understand the exercise and their health better. Foreseeable, the contributions of this thesis will improve the health among older adult; therefore, benefit the global society. The technologies developed and assessed by these works will not only benefit for exercise measurement but also extensively contribute to many other fields. For example, 1) NNoM provides a unique opportunity for countless edge devices to catch up the mage-trend of data decentralisation, and finally achieve the concept of “Edge AI”. 2) the synchronisation method in BLE provide good accuracy for the sensors network using user’s devices. 3) the small design of WBR-SH2 allows it to be used in other scenarios, such as swimming and cycling, while benefited from its networking and intelligent advantages.

In the next section, the auspicious directions for future works will be discussed.

7.4Future Directions

7.4.1 WBR-SH2 in Comprehensive Assisted Environments

Although WBR-SH2 has fulfilled the needs of objective measurement, it is still not enough for exercise interventions with older adults. Measuring is only a small part of

exercise intervention. Especially with older adults and people with chronic physical or mental diseases, they need a more comprehensive environment to perform the exercise safely. Therefore, WBR-SH2 is required to cooperate with other surrounding smart devices to provide systematic supports and assistance for the user.

7.4.2 Motion Diagnosis for Mental Health

The traditional diagnoses for mental diseases are using well-developed recognition and memory testing protocols and brain scanning such as Magnetic Resonance Imaging (MRI) and Computed Tomography (CT). However, these methods are costly, complicated and time-consuming. Most importantly, the disease development process cannot be tracked continually due to the relatively longer diagnosis interval (years, month). Recently, many studies have been done to discover the potential interrelation of motor function to mental health. A portent of mental diseases can potentially be perceived under motor functional testing. A systemic review concluded that reduce limb motor functions were associated with an increased risk of developing dementia [150]. The study [24] has shown mental neurological disorders can affect the performance in motor functioning, and vice versa, it might be possible to assess the mental problems and to track their developing process continually by more frequently motor testing and motion tracking (real-time, minutes, hours, days).

If the exercise or activities can be monitored accurately and continually through the days, months of the intervention, and combined with the state-of-the-art cognitive assessment scores, the interrelation between exercise and cognitive may be clearer. Thus, the effectiveness of the exercise intervention could be clearer, and the diagnosis of cognitive functions might also be possible through exercises measurement and using the clearer interrelation of cognitive and motor functions. Although the sensor has not tested in the PPI with people with depression, people with dementia have given positive feedback during the PPI. Future work in PPI for people with depression needs to be done.

7.4.3 Technical Improvement

WBR-SH2 is the physical combination of the most significant outcomes from this thesis, which had implemented the state-of-the-art technologies by the time of development. However, the development of technology never stops. The sensor can be improved by implementing new technologies.

One example is in the wireless sensor model proposed in Figure 3-2 required a smartphone to act as a bridge to forward data from sensors to the data server. Thus, a smartphone must be present sometime during or after the sensors have collected data. Although with the neural network embedded, information and measurement are aggregated, so the size is much smaller, this aggregated information still needs to be sent out at some time. The sensor is then dependent on the smartphone. If the new 5G / Narrow Band-IoT can be implemented into the sensors, then it can access the Internet alone. The dependency of a smartphone is avoided.

Other possible technical improvements are: 1) Implement wireless charging capability to improve the usability further. 2) Improve Android App interfaces. 3) Train neural network from different aspects, such as the quality classification to see if the person is doing good or bad. 4) Improve and implement quantitative exercise algorithm into sensors. 5) Develop more general software and hardware interfaces for use in other related fields. 6) Research in better motion feature extraction with both time and frequency patterns.

7.4.4 Exploring New Research Fields

The WBR-SHx sensors and the tools have provided an unprecedented measurement tool for remote exercise, which could be a game-changer in the related fields. When countless studies are struggling in how to measure the remote exercise, the thesis has already provided a solution which has been validated by a post-experiment. This is done only because the configuration of the sensors and tools are carefully designed to be 1) Optimised in usability. 2) Using “nearable concept” to

improve acceptance by older adults. 3) Minimised but enough number of sensor nodes for accurate measurement. 4) Only understandable and straightforward feedback for older adults. Thus, any studies doing exercise measurement especially requiring one or more principles above will potentially benefit from this thesis and the WBR-SH sensors. The principles are nearly desired by all physical exercises, especially the exercise involving instruments.

An example is cycling which requires no disturbance to the user and the exercise involving standalone instruments, namely the bicycle. A preliminary configuration can be done by implementing 4 x WBR-SH2 sensors onto the bicycle with one sensor on the handle, one on the seat and two for each pedal. 1) Sensors on pedals can measure the force, rotation speed, and others, 2) sensor on the seat can measure the bicycle's orientation, acceleration and the weights on the seat, 3) and the sensor in the handle can measure the movement of the hand. All sensors are not measuring the body directly, but measuring the interface between the user and the equipment, which this thesis has shown to result in an understanding of the exercise potentially. All sensors together can give much more detail to describe the exercise better. Most importantly, this configuration has no interference to user's natural motions. Thus, a more realistic measurement can be achieved.

Other than measuring performance, further investigating mental and physical disease diagnosis through long-term exercise measurement is a direction that potential can be impactive, but has not yet been widely studied. The reviews discussed in Chapter 1 has shown that early signs can be tracked through motion assessment before they are serious enough to affect the person's lifestyle. Continuous measurement of dedicated exercise can easily extract the features and patterns changes alongside the development of the diseases. Therefore, the development of diseases might seem through the decline in exercise performance. This work has provided researchers with the necessary measurement tools to pursue their research goals.

References

[1] S. P. Beeby, G. Ensell, R. Lambert, and N. M. White, “Plucked excitation of micromachined silicon DETF resonators,” 2000.

[2] D. Robineau, “Ageing Britain: two-fifths of NHS budget is spent on over-65s | Society | The Guardian,” *The Guardian*, 2016. [Online]. Available: https://www.theguardian.com/society/2016/feb/01/ageing-britain-two-fifths-nhs-budget-spent-over-65s. [Accessed: 11-Feb-2019].

[3] Office for National Statistics, “Adult Health in Great Britain, 2012,” 2014.

[4] Mental Health Foundation, “Fundamental Facts About Mental Health 2015 | Mental Health Foundation,” London, 2017.

[5] Y. Cedervall, K. Halvorsen, and A. C. Åberg, “A longitudinal study of gait function and characteristics of gait disturbance in individuals with Alzheimer’s disease,” *Gait Posture*, vol. 39, no. 4, pp. 1022–1027, Apr. 2014.

[6] W. J. Chodzko-Zajko *et al.*, “Exercise and Physical Activity for Older Adults:,” *Med. Sci. Sport. Exerc.*, vol. 41, no. 7, pp. 1510–1530, Jul. 2009.

[7] C. Liu and N. K. Latham, “Progressive resistance strength training for improving physical function in older adults,” John Wiley & Sons, Ltd, 2009.

[8] F. Candela, G. Zucchetti, E. Ortega, E. Rabaglietti, and D. Magistro, “Preventing Loss of Basic Activities of Daily Living and Instrumental Activities of Daily Living in Elderly: Identification of Individual Risk Factors in a Holistic Perspective,” *Holist. Nurs. Pract.*, vol. 29, no. 5, p. 313, Apr. 2015.

[9] K. A. Hartholt *et al.*, “Societal Consequences of Falls in the Older Population: Injuries, Healthcare Costs, and Long-Term Reduced Quality of Life,” *J. Trauma Acute Care Surg.*, vol. 71, no. 3, p. 748, Apr. 2011.

[10] U. Olsson Möller, P. Midlöv, J. Kristensson, C. Ekdahl, J. Berglund, and U. Jakobsson, “Prevalence and predictors of falls and dizziness in people younger and older than 80 years of age-A longitudinal cohort study,” *Archives of Gerontology and Geriatrics*, vol. 56, no. 1. pp. 160–168, 16-Feb-2013.

[11] “Mental health of older adults.” [Online]. Available: https://www.who.int/news-room/fact-sheets/detail/mental-health-of-older-adults. [Accessed: 10-Apr-2019].

[12] “What is dementia?,” *Alzheimer’s Society*, 01-Jul-2016. [Online]. Available: https://www.alzheimers.org.uk/site/scripts/documents_info.php?documentID=106. [Accessed: 01-Jul-2016].

[13] “Factsheet: Assessment and diagnosis,” *Alzheimer’s Society*, 27-Jun-2016. [Online]. Available: https://www.alzheimers.org.uk/site/scripts/download_info.php?downloadID=1154. [Accessed: 27-Jun-2016].

[14] “World Alzheimer Report 2015, The Global Impact of Dementia: An analysis of

prevalence, incidence, cost and trends - WorldAlzheimerReport2015.pdf," 22-Aug-2016. [Online]. Available: https://www.alz.co.uk/research/WorldAlzheimerReport2015.pdf. [Accessed: 22-Aug-2016].

[15] A. Society, "Dementia Tax Report 2011," *Alzheimer's Society*, 18-Jun-2017. [Online]. Available: http://files/1475/110630_Alzheimers_Society_Dementia_Tax_2011_report-1.pdf. [Accessed: 18-Jun-2017].

[16] C. Leray, "Mental disorders," *Diet. Lipids Heal. Brain Funct.*, pp. 123–196, 2018.

[17] R. Craig and J. Mindell, "Health Survey for England 2005: The health of older people: Summary of key findings," Leeds, 2005.

[18] C. Smyth, "Depression in old age 'is the next big health crisis,'" *Times, The (London, England)*, 2014. [Online]. Available: https://www.thetimes.co.uk/article/depression-in-old-age-is-the-next-big-health-crisis-vkb835j05f8. [Accessed: 10-Apr-2019].

[19] J. H. S. Holviala, J. M. Sallinen, W. J. Kraemer, M. J. Alen, and K. K. T. H??kkinen, "Effects of strength training on muscle strength characteristics, functional capabilities, and balance in middle-aged and older women," *J. Strength Cond. Res.*, vol. 20, no. 2, pp. 336–344, 2006.

[20] F. Nicola and S. Catherine, "Dose-response relationship of resistance training in older adults: a meta-analysis.," *Br. J. Sports Med.*, vol. 45, no. 3, pp. 233–4, Mar. 2011.

[21] A. S. Zion, R. De Meersman, B. E. Diamond, and D. M. Bloomfield, "A home-based resistance-training program using elastic bands for elderly patients with orthostatic hypotension," *Clin. Auton. Res.*, vol. 13, no. 4, pp. 286–292, Aug. 2003.

[22] E. Hogervorst, "Exercise to Prevent Cognitive Decline and Alzheimer's disease: For Whom, When, What, and (most importantly) How Much?," *J. Alzheimer's Dis. Park.*, vol. 02, no. 03, May 2012.

[23] T. Ngandu *et al.*, "A 2 year multidomain intervention of diet, exercise, cognitive training, and vascular risk monitoring versus control to prevent cognitive decline in at-risk elderly people (FINGER): A randomised controlled trial," *Lancet*, vol. 385, no. 9984, pp. 2255–2263, Mar. 2015.

[24] G. C. Gilmore, H. E. Wenk, L. A. Naylor, and E. Koss, "Motion Perception and Alzheimer's Disease," *J. Gerontol.*, vol. 49, no. 2, pp. P52–P57, Mar. 1994.

[25] J. Stevens and M. Killeen, "A randomised controlled trial testing the impact of exercise on cognitive symptoms and disability of residents with dementia," *Contemp. Nurse*, vol. 21, no. 1, pp. 32–40, Jun. 2006.

[26] P. Heyn, B. C. Abreu, and K. J. Ottenbacher, "The effects of exercise training on elderly persons with cognitive impairment and dementia: A meta-analysis1," *Arch. Phys. Med. Rehabil.*, vol. 85, no. 10, pp. 1694–1704, Jun. 2004.

[27] J. Elliott-King, S. Shaw, S. Bandelow, R. Devshi, S. Kassam, and E. Hogervorst, "A critical literature review of the effectiveness of various instruments in the diagnosis of dementia in adults with intellectual disabilities," *Alzheimer's Dement. Diagnosis, Assess. Dis. Monit.*, vol. 4, pp. 126–148, Aug. 2016.

[28] S. Balsamo *et al.*, "Effectiveness of exercise on cognitive impairment and Alzheimer's disease," *Int. J. Gen. Med.*, vol. 6, pp. 387–391, Oct. 2013.

[29] N. Ahn and K. Kim, "Effects of an elastic band resistance exercise program on lower extremity muscle strength and gait ability in patients with Alzheimer's disease," *J. Phys. Ther. Sci.*, vol. 27, no. 6, pp. 1953–1955, Aug. 2015.

[30] D. Forbes *et al.*, "Exercise programs for people with dementia," *Sao Paulo Med. J.*, vol. 132, no. 3, pp. 195–196, 2014.

[31] G. M. Cooney *et al.*, "Exercise for depression," *Cochrane Database Syst. Rev.*, no. 9, Sep. 2013.

[32] T. Crocker *et al.*, "Physical rehabilitation for older people in long-term care," *Cochrane Database Syst. Rev.*, no. 2, Feb. 2013.

[33] D. Brown *et al.*, "Development of an exercise intervention to improve cognition in people with mild to moderate dementia: Dementia And Physical Activity (DAPA) Trial, registration ISRCTN32612072," *Physiotherapy*, vol. 101, no. 2, pp. 126–134, Jun. 2015.

[34] S. E. Lamb *et al.*, "Dementia And Physical Activity (DAPA) trial of moderate to high intensity exercise training for people with dementia: randomised controlled trial.," *BMJ*, vol. 361, p. k1675, May 2018.

[35] N. Atherton *et al.*, "Dementia and Physical Activity (DAPA) - an exercise intervention to improve cognition in people with mild to moderate dementia: study protocol for a randomized controlled trial," *Trials*, vol. 17, no. 1, p. 165, Dec. 2016.

[36] C. Groot *et al.*, "The effect of physical activity on cognitive function in patients with dementia: A meta-analysis of randomized control trials," *Ageing Res. Rev.*, vol. 25, pp. 13–23, Jan. 2016.

[37] J. Kim, "A Qualitative Analysis of User Experiences With a Self-Tracker for Activity, Sleep, and Diet," *Interact. J. Med. Res.*, vol. 3, no. 1, Apr. 2014.

[38] C. Kerner and V. A. Goodyear, "The Motivational Impact of Wearable Healthy Lifestyle Technologies: A Self-determination Perspective on Fitbits With Adolescents," *Am. J. Heal. Educ.*, vol. 48, no. 5, pp. 287–297, Jul. 2017.

[39] S. R. Chekroud *et al.*, "Association between physical exercise and mental health in 1·2 million individuals in the USA between 2011 and 2015: a cross-sectional study," *The Lancet Psychiatry*, vol. 5, no. 9, pp. 739–746, Oct. 2018.

[40] J. C. Bollen, S. G. Dean, R. J. Siegert, T. E. Howe, and V. A. Goodwin, "A systematic review of measures of self-reported adherence to unsupervised home-based rehabilitation exercise programmes, and their psychometric properties," *BMJ Open*, vol. 4, no. 6, p. e005044, Oct. 2014.

[41] A. Lampit, H. Hallock, and M. Valenzuela, “Computerized Cognitive Training in Cognitively Healthy Older Adults: A Systematic Review and Meta-Analysis of Effect Modifiers,” *PLoS Med*, vol. 11, no. 11, p. e1001756, Nov. 2014.

[42] N. Ahn and K. Kim, “Effects of an elastic band resistance exercise program on lower extremity muscle strength and gait ability in patients with Alzheimer’s disease,” *J. Phys. Ther. Sci.*, vol. 27, no. 6, pp. 1953–1955, Jun. 2015.

[43] N. L. Ashworth, K. E. Chad, E. L. Harrison, B. A. Reeder, and S. C. Marshall, “Home versus center based physical activity programs in older adults,” *Cochrane Database Syst. Rev.*, no. 1, Jan. 2005.

[44] D. R. Bassett, “Device-based monitoring in physical activity and public health research,” *Physiol. Meas.*, vol. 33, no. 11, p. 1769, Oct. 2012.

[45] J. M. Jakicic *et al.*, “Effect of wearable technology combined with a lifestyle intervention on long-term weight loss: The IDEA randomized clinical trial,” *JAMA - J. Am. Med. Assoc.*, vol. 316, no. 11, pp. 1161–1171, Sep. 2016.

[46] Z. Lin, M. Zecca, S. Sessa, L. Bartolomeo, H. Ishii, and A. Takanishi, “Development of the wireless ultra-miniaturized inertial measurement unit WB-4: preliminary performance evaluation.,” 2011, pp. 6927–6930.

[47] M. Zecca *et al.*, “Development of the Ultra-Miniaturized Inertial Measurement Unit WB3 for Objective Skill Analysis and Assessment in Neurosurgery: Preliminary Results,” Springer, Berlin, Heidelberg, 2009, pp. 443–450.

[48] S. Sessa, M. Zecca, Z. Lin, T. Sasaki, K. Itoh, and A. Takanishi, “Waseda Bioinstrumentation System #3 as a tool for objective rehabilitation measurement and assessment - Development of the inertial measurement unit,” in *2009 IEEE International Conference on Rehabilitation Robotics, ICORR 2009*, 2009, pp. 115–120.

[49] National Centre for Sport and Exercise, “Couch Potatoes for Cognition Seated Resistance Band Workout,” 2016. [Online]. Available: https://www.lboro.ac.uk/media/wwwlboroacuk/external/content/schoolsanddepartments/ssehs/documents/FINAL Resistance band workout.pdf.

[50] S. Roccella, M. C. Carrozza, P. Dario, S. Superiore, and S. Anna, “Development of a robot evaluation system in the interaction between a humanoid robot and a robot,” vol. 15, no. 06, pp. 2–5, 2006.

[51] M. Windolf, N. Götzen, and M. Morlock, “Systematic accuracy and precision analysis of video motion capturing systems—exemplified on the Vicon-460 system,” *J. Biomech.*, vol. 41, no. 12, pp. 2776–2780, Aug. 2008.

[52] Z. Zhang, “Microsoft kinect sensor and its effect,” *IEEE Multimed.*, vol. 19, no. 2, pp. 4–10, 2012.

[53] D. Mehta *et al.*, “Monocular 3D human pose estimation in the wild using improved CNN supervision,” *Proc. - 2017 Int. Conf. 3D Vision, 3DV 2017*, pp. 506–516, 2018.

[54] Perception Neuron, “Perception Neuron by Noitom | Perception Neuron motion

capture for virtual reality, animation, sports, gaming and film," 2018. [Online]. Available: https://neuronmocap.com/. [Accessed: 18-Feb-2019].

[55] M. Zecca *et al.*, "Development of the ultra-miniaturized Inertial Measurement Unit WB3 for objective skill analysis and assessment in neurosurgery: preliminary results.," *Med. Image Comput. Comput. Assist. Interv.*, vol. 12, no. Pt 1, pp. 443–450, 2009.

[56] U. Imtiaz *et al.*, "Design of a wireless miniature low cost EMG sensor using gold plated dry electrodes for biomechanics research," 2013, pp. 957–962.

[57] Z. Lin, M. Zecca, S. Sessa, H. Ishii, and A. Takanishi, "Development of an ultra-miniaturized inertial measurement unit for jaw movement analysis during free chewing," *J. Comput. Sci.*, vol. 6, no. 8, pp. 896–903, 2010.

[58] Y. Cedervall, K. Halvorsen, and A. C. Åberg, "A longitudinal study of gait function and characteristics of gait disturbance in individuals with Alzheimer's disease," *Gait Posture*, vol. 39, no. 4, pp. 1022–1027, Jul. 2014.

[59] A. S. Naidu, A. Vasudev, A. M. Burhan, E. Ionson, and M. Montero-Odasso, "Does Dual-Task Gait Differ in those with Late-Life Depression versus Mild Cognitive Impairment?," *Am. J. Geriatr. Psychiatry*, vol. 27, no. 1, pp. 62–72, 2018.

[60] M. Montero-Odasso, J. Verghese, O. Beauchet, and J. M. Hausdorff, "Gait and Cognition: A Complementary Approach to Understanding Brain Function and the Risk of Falling," *J. Am. Geriatr. Soc.*, vol. 60, no. 11, pp. 2127–2136, Nov. 2012.

[61] E. Velloso, A. Bulling, H. Gellersen, W. Ugulino, and H. Fuks, "Qualitative activity recognition of weight lifting exercises," in *Proceedings of the 4th Augmented Human International Conference on - AH '13*, 2013, pp. 116–123.

[62] M. Maróti, B. Kusy, G. Simon, and Á. Lédeczi, "The Flooding Time Synchronization Protocol," 2004, pp. 39–49.

[63] A. Vilhar and M. Depolli, "Time synchronization problem in a multiple wireless ECG sensor measurement," in *2018 14th Annual Conference on Wireless On-demand Network Systems and Services (WONS)*, 2018, pp. 83–86.

[64] F. Gong and M. L. Sichitiu, "On the Accuracy of Pairwise Time Synchronization," *IEEE Trans. Wirel. Commun.*, vol. 16, no. 4, pp. 2664–2677, Apr. 2017.

[65] S. B. Kotsiantis, I. Zaharakis, and P. Pintelas, "Supervised machine learning: A review of classification techniques," *Emerg. Artif. Intell. Appl. Comput. Eng.*, vol. 160, pp. 3–24, 2007.

[66] F. Ordóñez, D. Roggen, F. J. Ordóñez, and D. Roggen, "Deep Convolutional and LSTM Recurrent Neural Networks for Multimodal Wearable Activity Recognition," *Sensors*, vol. 16, no. 1, p. 115, Jan. 2016.

[67] O. Dehzangi, M. Taherisadr, R. ChangalVala, O. Dehzangi, M. Taherisadr, and R. ChangalVala, "IMU-Based Gait Recognition Using Convolutional Neural Networks and Multi-Sensor Fusion," *Sensors*, vol. 17, no. 12, p. 2735, Nov. 2017.

[68] N. Y. Hammerla, S. Halloran, and T. Ploetz, “Deep, Convolutional, and Recurrent Models for Human Activity Recognition using Wearables,” Apr. 2016.

[69] F. Cuzzolin *et al.*, “Metric learning for Parkinsonian identification from IMU gait measurements,” *Gait Posture*, vol. 54, pp. 127–132, 2017.

[70] D. Anguita, A. Ghio, L. Oneto, X. Parra, and J. L. Reyes-Ortiz, *A Public Domain Dataset for Human Activity Recognition Using Smartphones*. .

[71] K. Mercer, L. Giangregorio, E. Schneider, P. Chilana, M. Li, and K. Grindrod, “Acceptance of Commercially Available Wearable Activity Trackers Among Adults Aged Over 50 and With Chronic Illness: A Mixed-Methods Evaluation.,” *JMIR mHealth uHealth*, vol. 4, no. 1, p. e7, Jan. 2016.

[72] B. Y. K. Taylor and L. Silver, “Smartphone Ownership Is Growing Rapidly Around the World, but Not Always Equally,” no. February, 2019.

[73] Swaytha Sasidharan, “A New Connected World - IEEE Internet of Things,” 2016. [Online]. Available: https://iot.ieee.org/newsletter/may-2016/a-new-connected-world.html. [Accessed: 19-Mar-2019].

[74] J. Ma and M. Zecca, “Development of a Portable Sensorised Handle for the Objective Assessment of the Effectiveness and Concordance of Intervention Plans in Dementia,” *IEEE Int. Conf. Eng. Med. Biol. EMBC2017*, Jul. 2017.

[75] J. Ma, E. Hogervorst, D. Magistro, V. Chouliaras, and M. Zecca, “Development of Sensorised Resistance Band for Objective Exercise Measurement: Activities Classification Trial,” in *Proceedings of the Annual International Conference of the IEEE Engineering in Medicine and Biology Society, EMBS*, 2018, vol. 2018-July, pp. 3942–3945.

[76] J. Ma, D. Magistro, and M. Zecca, *Synchronizing connection-oriented distributed sensor network using bluetooth low energy with unmodified android device*, vol. 21. 2019.

[77] E. H. Angela Clifford, “What is the Relationship between Higher Levels of Education Delaying Age at Onset of Dementia?,” *J. Alzheimer’s Dis. Park.*, vol. 03, no. 01, Jul. 2013.

[78] A. Lampit, H. Hallock, and M. Valenzuela, “Computerized Cognitive Training in Cognitively Healthy Older Adults: A Systematic Review and Meta-Analysis of Effect Modifiers,” *PLoS Med*, vol. 11, no. 11, p. e1001756, Jan. 2014.

[79] E. Santana-Sosa, M. I. Barriopedro, L. M. López-Mojares, M. Pérez, and A. Lucia, “Exercise Training is Beneficial for Alzheimer’s Patients,” *Int. J. Sports Med.*, vol. 29, no. 10, pp. 845–850, Aug. 2008.

[80] T. C. Shoepe, D. A. Ramirez, and H. C. Almstedt, “Elastic Band Prediction Equations for Combined Free-Weight and Elastic Band Bench Presses and Squats,” *J. Strength Cond. Res.*, vol. 24, no. 1, pp. 195–200, Jan. 2010.

[81] D. Shaulis, L. A. Golding, and R. D. Tandy, “Reliability of the AAHPERD Functional Fitness Assessment across Multiple Practice Sessions in Older Men and Women,” *J. Aging Phys. Act.*, vol. 2, no. 3, pp. 273–279, Jul. 1994.

[82] M. Bottaro, S. N. Machado, W. Nogueira, R. Scales, and J. Veloso, “Effect of high versus low-velocity resistance training on muscular fitness and functional performance in older men,” *Eur. J. Appl. Physiol.*, vol. 99, no. 3, pp. 257–264, Aug. 2007.

[83] D. Shaulis, L. A. Golding, and R. D. Tandy, “Reliability of the AAHPERD Functional Fitness Assessment across Multiple Practice Sessions in Older Men and Women,” *J. Aging Phys. Act.*, vol. 2, no. 3, pp. 273–279, Jul. 1994.

[84] C. J. Jones and R. E. Rikli, “Measuring functional,” *J. Act. aging*, vol. 1, pp. 24–30, Aug. 2002.

[85] R. E. Rikli and C. J. Jones, “Development and Validation of a Functional Fitness Test for Community-Residing Older Adults,” *J. Aging Phys. Act.*, vol. 7, no. 2, pp. 129–161, Jun. 1999.

[86] E. Jones, T. Oliphant, P. Peterson, and others, “SciPy: Open source scientific tools for Python.” .

[87] W. McKinney, “Data Structures for Statistical Computing in Python.” pp. 51–56, 2010.

[88] J. D. Hunter, “Matplotlib: A 2D Graphics Environment,” *Comput. Sci. Eng.*, vol. 9, no. 3, pp. 90–95, May 2007.

[89] O. Salah *et al.*, “Sit to stand sensing using wearable IMUs based on adaptive Neuro Fuzzy and Kalman Filter,” 2014, pp. 288–291.

[90] Nordic Semiconductor, “Flexible, efficient Bluetooth 5 and Bluetooth mesh multiprotocol SoC,” no. nRF52832. 2016.

[91] Linear Technology, “LTC4055/LTC4055-1 - USB Power Controller and Li-Ion Linear Charger,” pp. 1–24.

[92] Linear Technology, “LTC2941-1 1A I 2 C Battery Gas Gauge with Internal Sense Resistor Features LTC2941-1 Absolute Maximum Ratings Electrical Characteristics.” .

[93] Torex, “XC6206 Series.”

[94] Johanson Technology, “High Frequency Ceramic Solutions, 2.4GHz Mini Antenna, P/N 2450AT18B100.” pp. 7–9, 2018.

[95] JLCPCB, “JLC PCB manufaturing specification.” [Online]. Available: https://www.sz-jlc.com/portal/t6i1339.html. [Accessed: 25-Feb-2019].

[96] InvenSense, “MPU9250 Product Specification Revision 1.1,” vol. 1, no. 408. pp. 1–4, 2016.

[97] STMicroelectronics, “LPS22HB - MEMS nano pressure sensor: 260-1260 hPa absolute digital output barometer.,” no. June, p. 49, 2017.

[98] Avia Semiconductor, “24-Bit Analog-to-Digital Converter (ADC) for Weigh Scales,” pp. 1–10.

[99] Vishay Siliconix, “Si2301DS,” no. V, pp. 1–4.

[100] T. Letcher and M. Waytashek, “Material property testing of 3D-printed specimen in PLA on an entry-level 3D printer,” *Proc. ASME 2014 Int. Mech. Eng. Congr.*

Expo. IMECE2014, pp. 1–8, 2014.

[101] Bluetooth SIG, "Bluetooth Core Specification Version 5.1," 2019.

[102] Winbond, "W25Q64Fv Serial Flash Memory With Dual / Quad Spi & Qpi." 2012.

[103] InvenSense, "Application Note Programming Sequence for DMP Hardware Functions," pp. 1–27, 2015.

[104] K. Saito *et al.*, "Assessment of walking quality by using Inertial Measurement Units," in *Proceedings of the 2012 1st International Conference on Innovative Engineering Systems, ICIES 2012*, 2012, pp. 13–18.

[105] S. Sessa *et al.*, "Walking assessment in the phase space by using ultra-miniaturized Inertial Measurement Units," 2013, pp. 902–907.

[106]Bluetooth SIG, "Bluetooth Market Update 2018 | Bluetooth Technology Website," 07-Jun-2018. [Online]. Available: https://www.bluetooth.com/markets/market-report.

[107] J. Elson, L. Girod, and D. Estrin, "Fine-grained Network Time Synchronization Using Reference Broadcasts," *SIGOPS Oper. Syst. Rev.*, vol. 36, no. SI, pp. 147–163, Nov. 2002.

[108] S. Ganeriwal, R. Kumar, and M. B. Srivastava, "Timing-sync Protocol for Sensor Networks," 2003, pp. 138–149.

[109] F. Asgarian and K. Najafi, "Time Synchronization in a Network of Bluetooth Low Energy Beacons," in *Proceedings of the SIGCOMM Posters and Demos on - SIGCOMM Posters and Demos '17*, 2017, pp. 119–120.

[110] S. Sridhar, P. Misra, G. S. Gill, and J. Warrior, "Cheepsync: a time synchronization service for resource constrained bluetooth le advertisers," *IEEE Commun. Mag.*, vol. 54, no. 1, pp. 136–143, 2016.

[111] K. Somaratne, F. J. Dian, and A. Yousefi, "Accuracy analysis of time synchronization using current consumption pattern of BLE devices," in *2018 IEEE 8th Annual Computing and Communication Workshop and Conference (CCWC)*, 2018, pp. 841–844.

[112] A. Bideaux, B. Zimmermann, S. Hey, and W. Stork, "Synchronization in wireless biomedical-sensor networks with Bluetooth Low Energy," *Curr. Dir. Biomed. Eng.*, vol. 1, no. 1, pp. 73–76, Jun. 2015.

[113] Bluetooth SIG, "GATT Services | Bluetooth Technology Website." [Online]. Available: https://www.bluetooth.com/specifications/gatt/services. [Accessed: 25-Feb-2019].

[114] S. Sessa, M. Zecca, Z. Lin, T. Sasaki, K. Itoh, and A. Takanishi, "Waseda Bioinstrumentation System #3 as a tool for objective rehabilitation measurement and assessment - Development of the inertial measurement unit," in *2009 IEEE International Conference on Rehabilitation Robotics, ICORR 2009*, 2009, pp. 115–120.

[115] X. Meng, H. Yu, and M. P. Tham, "Gait phase detection in able-bodied subjects and dementia patients," 2013, pp. 4907–4910.

[116] S. Salehi, G. Bleser, N. Schmitz, and D. Stricker, “A low-cost and light-weight motion tracking suit,” *Proc. - IEEE 10th Int. Conf. Ubiquitous Intell. Comput. UIC 2013 IEEE 10th Int. Conf. Auton. Trust. Comput. ATC 2013*, pp. 474–479, 2013.

[117] F. Asgarian and K. Najafi, “Time Synchronization in a Network of Bluetooth Low Energy Beacons,” 2017, pp. 119–120.

[118] “Ranking - AnTuTu Benchmark - Know Your Android Better,” 19-Nov-2018. [Online]. Available: http://www.antutu.com/en/ranking/rank1.htm. [Accessed: 19-Nov-2018].

[119] L. Lai and N. Suda, *Enabling deep learning at the IoT edge*. 2018.

[120] C. Szegedy *et al.*, “Going deeper with convolutions,” 2015.

[121] S. Zagoruyko and N. Komodakis, “Wide Residual Networks,” *Br. Mach. Vis. Conf. 2016, BMVC 2016*, vol. 2016-September, pp. 87.1-87.12, May 2016.

[122] K. A. Pollard, P. K. Tran, and T. R. Letowski, “A free-field method to calibrate bone conduction transducers,” *J. Acoust. Soc. Am.*, vol. 133, no. 2, pp. 858–865, Feb. 2013.

[123] G. Huang, Z. Liu, L. Van Der Maaten, and K. Q. Weinberger, “Densely connected convolutional networks,” *Proc. - 30th IEEE Conf. Comput. Vis. Pattern Recognition, CVPR 2017*, vol. 2017-January, pp. 2261–2269, Aug. 2017.

[124] C. Szegedy, V. Vanhoucke, S. Ioffe, J. Shlens, and Z. Wojna, “Inception_v3,” pp. 4278–4284, 2015.

[125] Y. Chen *et al.*, “Drop an Octave: Reducing Spatial Redundancy in Convolutional Neural Networks with Octave Convolution,” Apr. 2019.

[126] H. V. Jagadish *et al.*, “Big data and its technical challenges,” *Commun. ACM*, vol. 57, no. 7, pp. 86–94, Jul. 2014.

[127] “glouw/tinn: The tiny neural network library.” [Online]. Available: https://github.com/glouw/tinn. [Accessed: 21-Jan-2019].

[128] “Jeff-Ciesielski/libuneural: Fixed Point Neural Network library in C.” [Online]. Available: https://github.com/Jeff-Ciesielski/libuneural. [Accessed: 16-Jan-2019].

[129] “uTensor/uTensor: AI inference library based on mbed and TensorFlow.” [Online]. Available: https://github.com/uTensor/uTensor. [Accessed: 21-Jan-2019].

[130] C. Cao *et al.*, “Deep Learning and Its Applications in Biomedicine,” *Genomics. Proteomics Bioinformatics*, vol. 16, no. 1, pp. 17–32, Feb. 2018.

[131] S. Han, H. Mao, and W. J. Dally, “Deep Compression: Compressing Deep Neural Networks with Pruning, Trained Quantization and Huffman Coding,” Oct. 2015.

[132] Z. Alom, A. T. Moody, N. Maruyama, B. C. Van Essen, and T. M. Taha, “Effective Quantization Approaches for Recurrent Neural Networks.”

[133] S. Kapur, A. Mishra, and D. Marr, “Low Precision RNNs: Quantizing RNNs Without Losing Accuracy.”

[134] M. Rusci, A. Capotondi, F. Conti, and L. Benini, “Quantized NNs as the definitive solution for inference on low-power ARM MCUs?: work-in-progress,” *Proc. Int. Conf. Hardware/Software Codesign Syst. Synth.*, p. 12, 2018.

[135] F. Chollet and others, “Keras.” 2015.

[136] L. Lai, N. Suda, and V. Chandra, “CMSIS-NN: Efficient Neural Network Kernels for Arm Cortex-M CPUs,” Jan. 2018.

[137] K. He, X. Zhang, S. Ren, and J. Sun, “Deep Residual Learning for Image Recognition.” pp. 770–778, 2016.

[138] E. Hogervorst, “Exercise to Prevent Cognitive Decline and Alzheimer’s disease: For Whom, When, What, and (most importantly) How Much?,” *J. Alzheimer’s Dis. Park.*, vol. 02, no. 03, 2012.

[139] C.-C. Yang and Y.-L. Hsu, “A Review of Accelerometry-Based Wearable Motion Detectors for Physical Activity Monitoring,” *Sensors*, vol. 10, no. 8, pp. 7772–7788, Feb. 2010.

[140] S. J. Preece, J. Y. Goulermas, L. P. J. Kenney, D. Howard, K. Meijer, and R. Crompton, “Activity identification using body-mounted sensors—a review of classification techniques,” *Physiol. Meas.*, vol. 30, no. 4, p. R1, 2009.

[141] D. P. Kingma and J. Ba, “Adam: A Method for Stochastic Optimization,” pp. 1–15, 2014.

[142] STMicroelectronics, “STM32L476xx datasheet,” no. May, 2018.

[143] I. Hubara, M. Courbariaux, D. Soudry, R. El-Yaniv, and Y. Bengio, “Quantized Neural Networks: Training Neural Networks with Low Precision Weights and Activations,” Sep. 2016.

[144] J. Ma and M. Zecca, “Development of a portable sensorised handle for the objective assessment of the effectiveness and concordance of intervention plans in dementia,” in *IEEE International conference on Engineering in Medicine and Biology EMBC2017*, 2017, pp. 2337–2340.

[145] O. Steven Eyobu and D. S. Han, “Feature Representation and Data Augmentation for Human Activity Classification Based on Wearable IMU Sensor Data Using a Deep LSTM Neural Network,” *Sensors (Basel).*, vol. 18, no. 9, pp. 1–26, 2018.

[146] A. Ignatov, “Real-time human activity recognition from accelerometer data using Convolutional Neural Networks,” *Appl. Soft Comput.*, vol. 62, pp. 915–922, Jan. 2018.

[147] C. Crema, A. Depari, A. Flammini, E. Sisinni, T. Haslwanter, and S. Salzmann, “IMU-based solution for automatic detection and classification of exercises in the fitness scenario,” *SAS 2017 - 2017 IEEE Sensors Appl. Symp. Proc.*, pp. 1–6, 2017.

[148] F. Chollet and others, “Keras: The Python Deep Learning library,” *Astrophys. Source Code Libr. Rec. ascl1806.022*, 2018.

[149] J. Salamon and J. P. Bello, “Deep Convolutional Neural Networks and Data

Augmentation for Environmental Sound Classification," *IEEE Signal Process. Lett.*, vol. 24, no. 3, pp. 279–283, 2017.

[150] J. K. Kueper, M. Speechley, N. R. Lingum, and M. Montero-Odasso, "Motor function and incident dementia: a systematic review and meta-analysis," *Age Ageing*, vol. 46, no. 5, pp. 729–738, Sep. 2017.

[151] STMicroelectronics, "STM32F407xx datasheet," p. 180, 2012.

[152] Dialog Semiconductor, "SmartBond^{TM} DA14580." 26-Nov-2015.

[153] STMicroelectronics, "SP1ML SPIRIT1 868 and 915 MHz low power RF modules with integrated," no. October. pp. 1–31, 2017.

[154] STMicroelectronics, "LSM6DS33 iNEMO inertial module," vol. Rev 6, no. September, pp. 1–78, 2017.

[155] ST Microelectronics, "LIS3MDL Digital Output Magnetic Sensor," no. May, pp. 1–33, 2017.

[156] TE Sensor Solutions, "MS5611-01BA03." 2017.

[157] Linear Technology, "Battery Gas Gauge with Temperature, Voltage Measurement," pp. 1–18, 2010.

[158] T. Walter, "A Comparison of Complementary and Kalman Filtering," vol. 1975, no. 3, pp. 321–325, 1975.

[159] RT-Thread Team, "rt-thread." [Online]. Available: https://github.com/RT-Thread/rt-thread.

Appendix A Couch Potatoes for Cognition

Couch Potatoes for Cognition is a workout developed by Loughborough University that aims to improve upper and lower body strength of older adults. It consists of 4 different activities and usually takes 40 minutes to complete. The original protocols document can be found in [49]. The 4 activities are discussed below individually.

A.1Tummy Rotation

The first activity is “Tummy Rotation”, shown in Figure A-1. The tummy rotation is a training of the stomach muscles, which improve the function of the waist. This activity improves the function of co-coordination, preventing falls, and standing from a chair.

Figure A-1 Tummy rotation [49].

A.2 Straight Arm Pull

The second activity is “Straight Arm Pull”, which is shown in Figure A-2. This activity aims at improving dressing and standing from chair.

Figure A-2 Straight arm puling [49].

A.3 Cross and Pull

The third activity is “Cross and Pull”, which aims to improve standing from a chair, gardening, and washing/taking shower capabilities. The activity is shown in Figure A-3.

Figure A-3 Cross and pull [49].

A.4 Leg Press

The “Leg Press” activity is to improve the lower part muscles, which is shown in Figure A-4. This activity will benefit the climbing stairs, standing, shopping, preventing falls, and standing from chair.

Figure A-4 Leg press [49].

Appendix B Experimental Sensorised Resistance Band System

B.1 Design of Experimental Sensorised Resistance Band System

This section shows the development of the experimental sensorised resistance band system, including general objectives, hardware development, firmware development and software development.

B.1.1 Objectives and Requirements

The objective for this section is to design an experimental sensorised resistance band system that can be used in researches scenarios to investigate the needs and performances in measuring resistance band exercise. To achieve the objective, the following fundamental requirements for the experimental system should be fulfilled.

- Motion sensors (Gyroscopes, Accelerometers which can measure the motion directly) must be integrated.
- Force sensing on the resistance band. The resistance band can measure the force applied to the hands for exercise quantitation.
- Same dimensions as a traditional none sensorised handle. This new design must be similar to the commercial resistance band handle to avoid unnatural feeling to the user.
- The device must have wireless communication for real-time data collections.

B.1.2 Hardware Design

The experimental system is a highly integrated embedded system which contains multiple sensors, data recording, wireless communication and long-life battery for

resistance band exercises. An overview of the circuit board, sensor selection, component placement and the block diagram of the hardware are shown in this section.

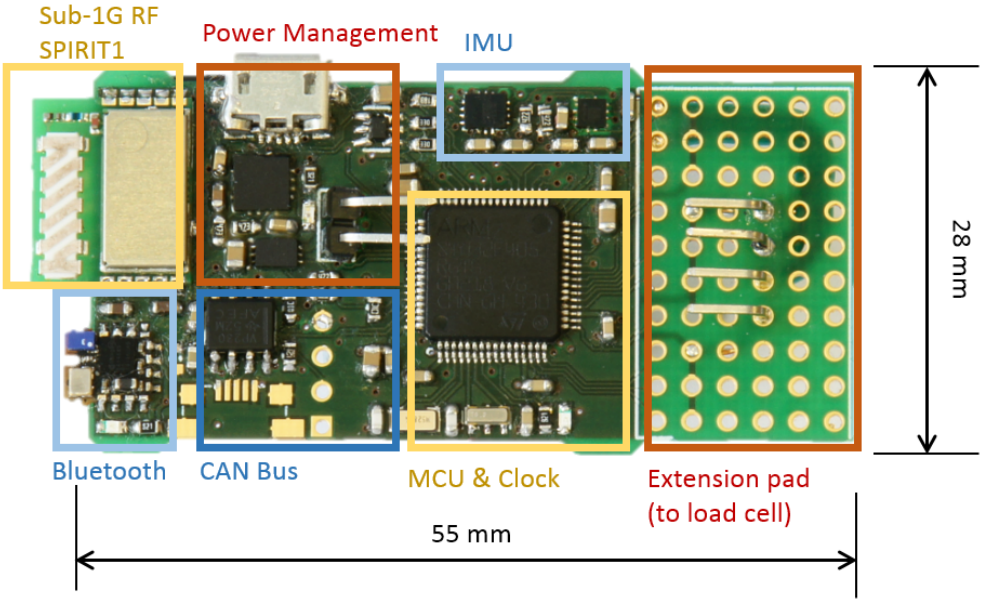

Figure B-1 Board layout (top view)

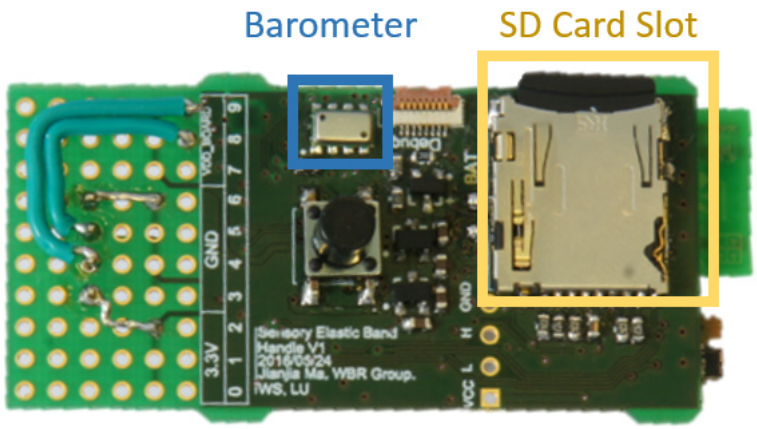

Figure B-2 Board layout (bottom view)

The main circuit board is shown in Figure B-1 and Figure B-2. The board is consist of an STM32F405RGT6 MCU [151] (or in low power configuration, a more advanced low power microcontroller is used, STM32L476RGT6 [142]), a USB power

management circuit, a Bluetooth 4.2 module DA14580 [152], a SPIRIT1 Sub-1GHz wireless module [153] and the following sensors: I-NEMO digital 3-Axis gyroscope & 3-Axis accelerometer module LSM6DS3 [154], 3-Axis magnetometer LIS3MDL [155], and Barometer MS5611 [156]. A 6x10 extension pad is reserved with 10 programmable GPIO and power ports for the possibility of adding new sensors. Currently, the load cell is connected to the board thought the extension pads. The major characteristics of the onboard sensors are listed in Table B-1. The configuration block diagram main circuit board is shown in Figure B-3.

Table B-1 Main Characteristics of the Sensors

	Sensors			
	LSM6DS3		*LIS3MDL*	*MS5611*
Category	Gyroscope	Accelerometer	Magnetometer	Barometer
Axis	3-axis	3-axis	3-axis	N/A
Size	2.5 x 3 x 0.83 [mm]		2x2x1[mm]	5x3x1[mm]
Range	±125/±250/ ±500/ ±1000/ ±2000 [dps]	±2/±4/±8/±16 [G]	±4/ ±8/ ±12/ ±16 [Guass]	450 to 1100 [mBar]
Resolution	16 [bit]	16 [bit]	16 [bit]	24 [bit]
Bandwidth	830 [Hz]	3.3k [Hz]	500 [Hz]	250 [Hz]
Current[a]	1.25 [mA]	0.24 [mA]	0.27 [mA]	1.4 [mA]

a. the maximum current during the measuring.

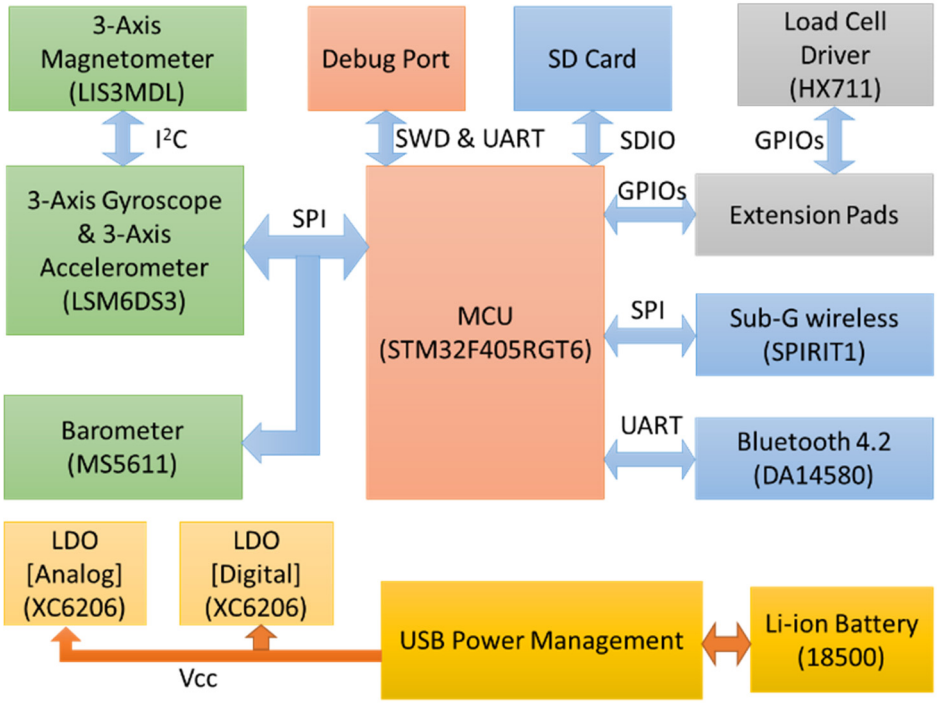

Figure B-3 Configuration block diagram

B.1.3 Microcontroller

For the prototype and lab-based short-term experiment purpose, the power consumption by MCU is not a core consideration. Instead, the MCU must be powerful enough to undertake data collection and other potential works. Thus, a high-performance STM32F405RGT6 microcontroller based on advance ARM Cortex-M4F architecture with the package LQFP48 (7x7x1.4 mm) is implemented to the board. Its high-performance ARM® Cortex™-M4F 32-bit RISC core running on 168MHz with a variety of peripherals (including multiple ADC, SPI, SDIO, UART, DMA, USB, CAN), etc.) which capable for running multiple tasks in real-time, such as data processing, data recording, and wireless communication. The memory contains 1MB programmable flash and 192KB RAM which includes 64KB single-cycle access Core-Coupled-Memory (CCM). With the operation voltage range from 2.0V to 3.6V, it is suitable for the battery used.

For a long-term experiment, the microcontroller can be replaced by a pin-to-pin compatible, low-power, high power efficiency MCU, STM32L476RGT6. This MCU contains most of the peripherals similar to the implemented one but with more advanced low-power performance and features, such as higher running power efficiency (100 μA/MHz compares to 238 μA/MHz), faster start-up clock system (Internal multispeed 100 kHz to 48 MHz oscillator), lower power standby mode (420 nA Standby mode with RTC).

B.1.4 Sensors

B.1.4.1 Gyroscope & Accelerometer

In order to measure the orientation of the resistance band handle, the measurement of 3-Axis angular velocity and 3-Axis acceleration is needed. The I-NEMO inertial module LSM6DS3 consists of 3-Axis gyroscope and 3-Axis accelerometer as well as a master I2C interfaces and sensor hub function. With the low-power feature (0.9 mA combo normal mode) and compact design (size 2.5 x 3 x 0.83 mm), it is possible to reduce both the size of the circuit board and battery compared to the existing system. The scales of the gyroscope can be selected from ±125 to ±2000 dps (degree per second) and the scales of the accelerometer can be selected from ±2 to 16G by configuring the registers inside the module. The sensor hub function enables the LSM6DS3 to act as an I2C master to collect data from other sensors by I2C. In the case of the sensorised handle, the I-NEMO model acquires data from magnetometer by its I2C interface. The communication interface between the master microcontroller and LSM6DS3 is SPI.

B.1.4.2 Magnetometer

The 3-Axis magnetometer LIS3MDL is an ultra-low-power, high-performance and small design (2.0 x 2.0 x 1mm) three-axis magnetic sensor, with a full scale of ±16 Gauss. The magnetometer could measure the magnetic field of the earth to provide a reference vector.

B.1.4.3 ***Barometer***

The barometer is the device to measure the temperatures and atmospheric pressure. With the sea level height information, the barometer will help to correct drifting of height estimation from IMUs. With the high-resolution barometer, it might be possible to identify the relative height difference between the two sensorised handles. Which could be potentially useful when the motion difference between hands are different. The barometer, MS5611, is a high-performance ultra-accurate sensor with 24-bits ADC and factory calibration, which provide height resolution in 10 cm in size of 5 x 3 x 1mm.

B.1.4.4 ***Load Cell & Driver***

The load cell is a full bridge transducer that is used to create an electrical signal whose magnitude is directly proportional to the force being measured. Load cell could be driven and measured by specified driver chips which automatically provide voltage bias and differential measurement on the load cell. HX711[98] is a low-power 24-bits ADC one-chip solution for load cell measurement, with the maximum 80 samples per second output rate. A commercial standalone HX711 development board is used and is placed close to the load cell. Combine with an unbranded 50kg range load cell which is disassembled from low cost a luggage weight (~£5/pcs on Amazon), the combination is capable of measuring the force applied on the resistance band up to 50kg, which provide the essential measurement for the quantification of exercise. The selected load cell is shown in Figure B-4.

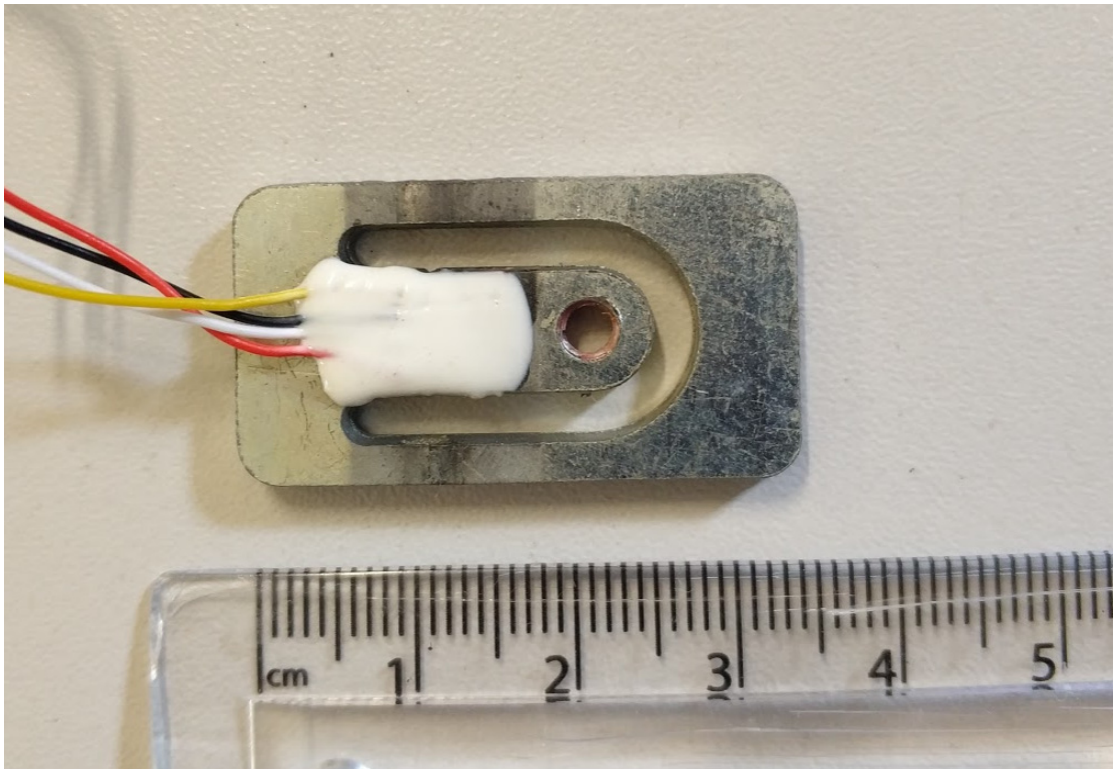

Figure B-4 Load cell sensor.

B.1.5 Wireless Communication

Two different wireless modalities are integrated into the circuit for prototyping and testing. They are BLE module and Sub 1GHz wireless module. BLE which capable of transmitting data between smartphone could be useful in the long-term monitoring. The sub 1GHz with higher bandwidth compared to BLE is for real-time data monitoring during experiments and data synchronising while two sensorised handles being used at the same time.

B.1.5.1 Bluetooth Module

The Bluetooth 4.2 module used in the sensorised handle is an ultra-small DA14580 module with a dimension of 5 x 6.2 x 1mm. The module is configured to the serial port mode during the lab-based experiment to transmit raw data to the PC. After the experiments, the module could be connected to a smartphone. The power consumption is about 5mA/3V at 0dBm output.

B.1.5.2 SPIRIT1 (Sub 1GHz) Wireless Module

Alternatively, the second wireless module SPIRIT1 is also implemented. The SPIRIT1 is a very low-power RF transceiver, intended for RF wireless applications in the sub-1 GHz band. The over-air data rate can be set from 1 to 500 kbps. It is also with low power consumption (9 mA RX and 21 mA TX at +11 dBm). The SPIRIT1 is used in an experiment for data synchronisation between two sensorised handles. The communication between handle and PC based one SPIRIT1 wireless module, the air bandwidth is set to 500kbps.

B.1.6 Power Management & Battery Charger

The power management circuit is consist of a USB power controller and Li-ion linear charger LTC4055-1, a battery gas gauge LTC2942 [157] and multiple LDOs XC6206 [93] (Low Dropout linear regulators). Due to 2 ideal diodes in the LTC4055-1[91], the power switch between USB power and the battery is smooth and fast. The maximum charging current is 500mAh with the maximum output current at 1500mAh. The analogue power supply and the digital power supply is supplied individually by separate LDO to reduce the noise interference to the analogue power supply. Additionally, the USB power controller is protected from overheating by the internal thermal switch above 105°C.

B.1.7 Battery

One standard 18500 Li-Ion battery (size of Φ18x50mm) with battery protect circuit is selected for powering the device. The maximum capability of the battery is 1400mAh while the average working current is estimated at 150mA in full data acquisition states. Therefore, the battery could support about 9 hours of working time on a single charge. Thanks to power management, the battery can be charged without taking the battery out of the handle by directly connecting the USB port to a computer or a USB power adapter.

B.1.8 Firmware

The handle can directly measure the angular velocity and acceleration by 3-Axis gyroscope and 3-Axis accelerometer. With the 3-Axis magnetometer and barometer, which measure the magnet field of the earth and the air pressure of current position, the handle capable of estimating the orientation and the relative height during time by using Complementary Filter [158].

B.1.8.1 RT-Thread Real-Time Operating System

To manage multiple tasks on the sensorised handle, an RTOS is introduced as the scheduler and base for different tasks. RT-Thread [159] is a lightweight RTOS which capable of running on the most of ARM-based CPU. It includes the necessary components of real-time embedded system, including but not limited to real-time operating system kernel, TCP/IP protocol stack, Portable Operating System Interface (POSIX) compatibility file system, libc interface, graphics interface, and so on.

In the handle, some peripherals interfaces are simultaneously used by multiple tasks as share resources. The program must avoid conflict in the use of these share interfaces (resources). With the completed and powerful driver frameworks and the objective-oriented kernel objects in RT-Thread, the hardware resources sharing (such as SPI, I2C) interfaces), CPU sharing, and data sharing can be simple achieve within critical timing. Using an RTOS not only helps with the management of multiple tasks (sharing CPU) but also reduce the difficulty in power management. When the user tasks are finished, the scheduler will switch to an always-ready task, called idle task, where an instruction for CPU to enter low-power mode can be inserted. The CPU is stopped until the next hardware event to reduce the power consumption during the idle time. The power consumption can be reduced in variable degree depending on the system loads.

The brief working flow is shown in Figure B-5. Introducing RTOS allows multiple tasks to run “simultaneously” on single CPU by time-division multiplexing. The

working flow shows the logical description of the system. The process starts from initialling the microcontroller, then initialling RT-Thread including memory initialisation, tasks initialisations, driver registrations, and filesystem initialisation. After the initialisation process, the hardware interfaces (SPI, I2C, SDIO and so on) and filesystem are ready. The next work is to do the sensor initiations and to create logging files on SD Card. After the initialisation works, the system is driven by the sensor data update event, and the firmware will run into the circle of collecting measurements, pre-processing and calculation, and storing data/sending data.

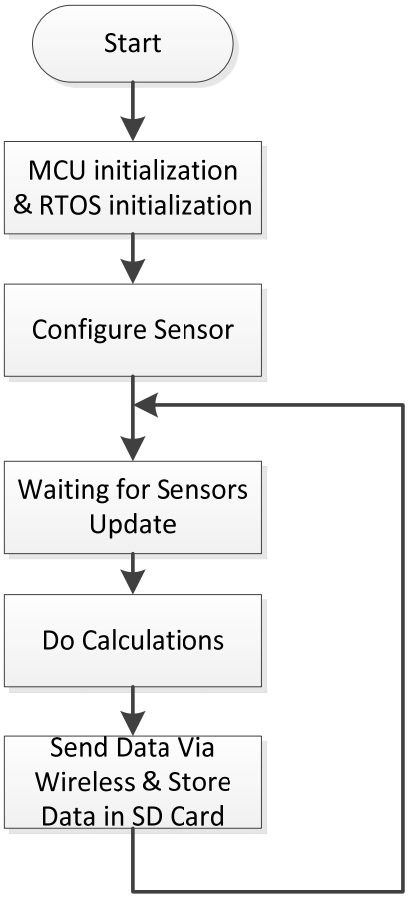

Figure B-5 Working flow of the experimental system.

The raw sensing data will be stored locally into the SD Card in a file of 100Hz and be sent out to PC up to 500Hz through SPIRIT1 wireless module.

B.1.9 Mechanical Design

The mechanical design mainly focuses on the housing of the main circuit board, which is also the handle replacement of the conventional handle. The handle (housing) is designed to be the same size as the commercial band handle to minimise the difference. The housing uses a 2-halves design for easy accessing to the circuit board during the debugging process. The housings are built by a 3D-printer using Polylactic Acid (PLA). Additionally, the housing for load cell is built separately by the same 3D-printing process.

Figure B-6 and Figure B-7 show the upper and lower half of the housing. The 2 halves are fixed together by screws. The ball heads on 2 sides are used to mount the nylon bands which will be connected to the load cell housing. The space on the right is dedicated for 18500 Lithium battery and the space on the left is dedicated for electronics and wires. There is a hole reserved for the multiple purpose button on the upper half. The circuit board is fixed inside the left space by 4 mounting hollows. The 4 mounting points around the circuit board (shown in Figure B-1) will fit into these hollows to secure the circuit board. There is also a hole in the wall of the lower half, which is reserved for the micro USB charging connector.

Figure B-6 Upper half of handle housing.

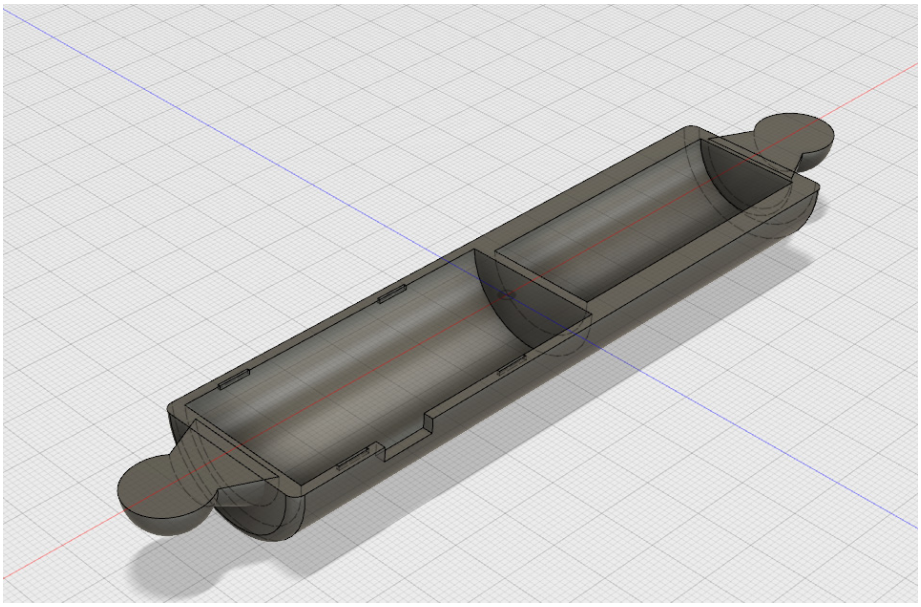

Figure B-7 Lower half of handle housing.

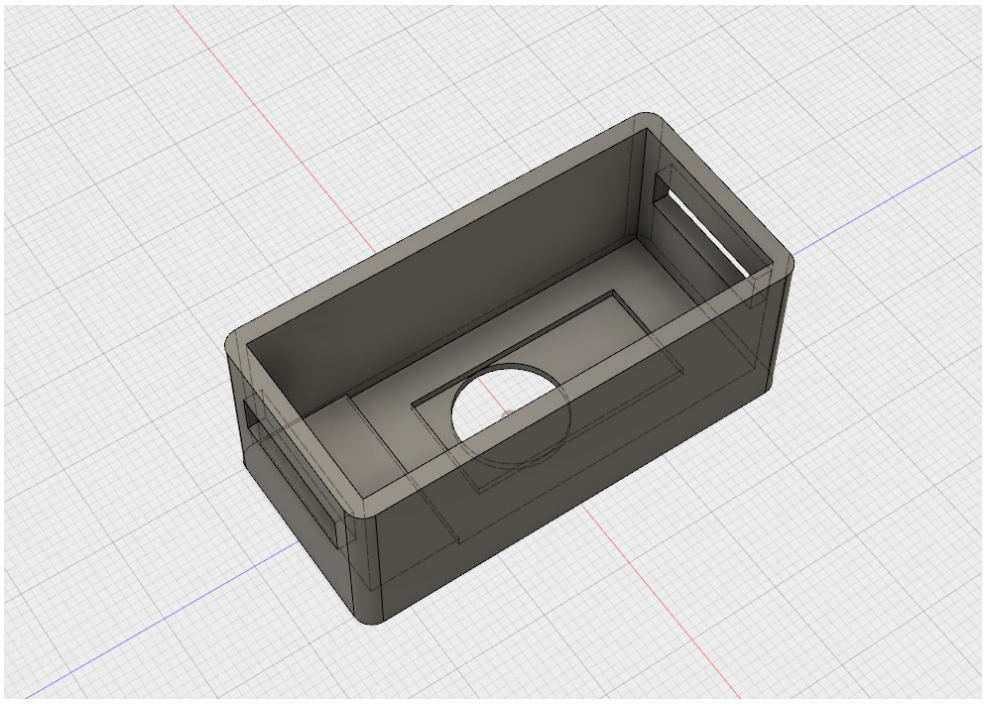

Figure B-8 Housing of load cell sensor.

The load cell sensor is placed separately to the main circuit board in its own housing. The load cell housing is to place the load cell sensor and the load cell driver. The housing is shown in Figure B-8. There are two square holes on the sidewall which

is for the nylon bands to go through. The hole on the bottom is where the resistance band is connected to the load cell.

B.1.10 Working Prototype

The housings were printed using a 3D-printer. the prototype included the main circuit board (Figure B-1 and Figure B-2), load cell sensor and its driver, battery, wires, and the 3D printed housings. Figure B-9 shows the assembly of the experimental system and the comparison of the traditional resistance band handle.

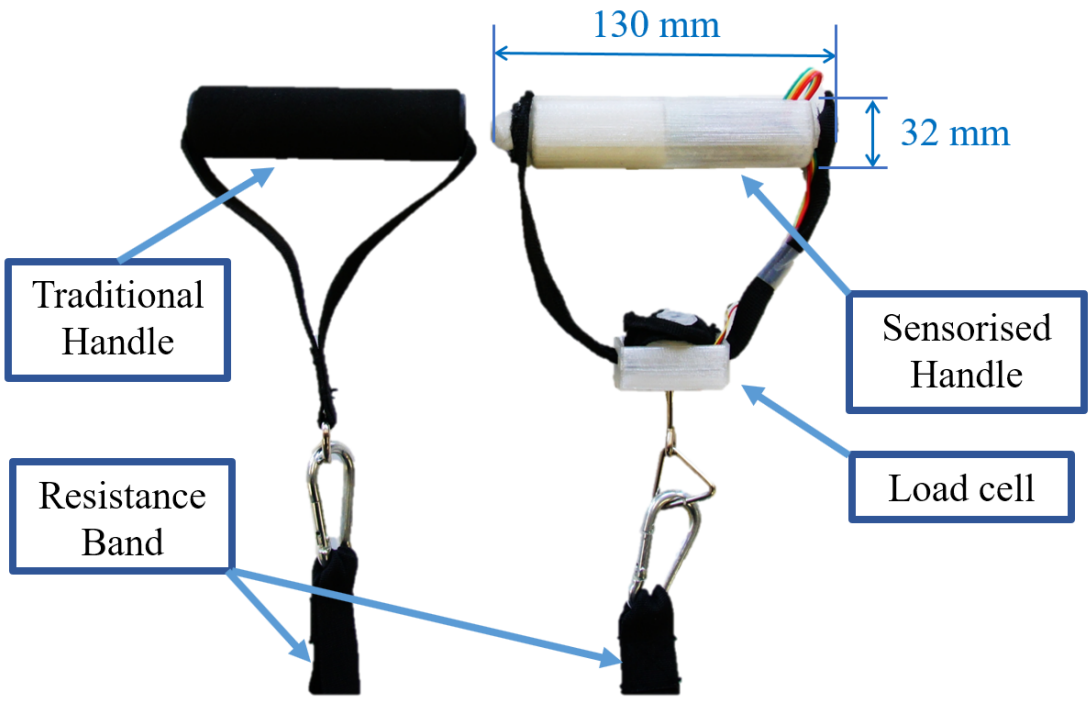

Figure B-9 Side by side comparison of the traditional handle and sensorised handle.

B.1.11 Software Design

Although the data is already recorded in the onboard microSD card by its firmware, it is still a complicated procedure to get the data from the sensorised handle. Firstly, the sensorised handle must be disassembled to take the microSD card out. Secondly, the data then can be read by plugging the microSD to the computer and copy the data file. Thirdly, the handle should be assembled again for the next experiment. To simplify the

process, the data should be sent and received wirelessly. Thus, PC software is needed to acquire data accomplished with the sensorised handle. By using the onboard wireless module, the measurement can be transferred from the sensorised handle to PC in real-time.

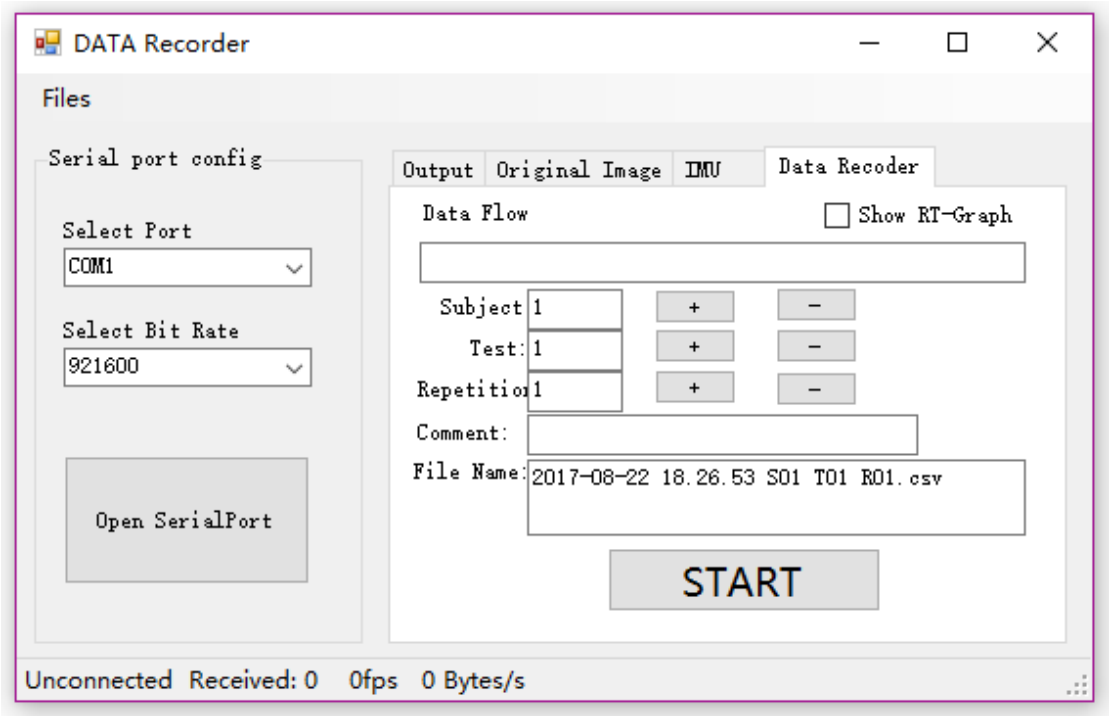

Figure B-10 Data recorder.

A software tool is explicitly written to record data from sensorised handle onto PC, shown in Figure B-10. The aims for the software are to provide a friendly interface and easy to a used tool to acquire data and to check the working state of the sensor. The wireless communication between sensorised handle and PC is done by SPIRIT1 module. The data receiving on PC is done by a customised wireless dongle, which is consist of SPIRIT1 module and an STM32 microcontroller with customised firmware. The STM32 act as a USB-to-Serial bridge. Messages received by dongle are bridged to a virtual serial port on the PC. Then, the software tool can read the message from the virtual serial port. The communication protocol is shown in Table B-2.

Data is recorded in a .csv format on the PC, which is the same as it is saved to the onboard microSD card to keep the compatibility in the data processing.

Table B-2 Communication protocol between sensorised handle and PC

	header	*ts* [a]	*gyro* [a]	*acc* [a]	*mag* [a]	*temp* [a]	*load cell*	*quaternion*	*checksum*
Size (bytes)	4	4	3 x 2	3 x 2	3 x 2	4	4	4 x 4	2
type	binary	uint 32	int16	int16	int16	float	float	float	uint16

[a] ts: timestamp, gyro: gyroscope, acc: accelerometer, mag: magnetometer

Appendix C Data Format for WBR-SH2

The raw data frame format is shown in Table C-1. Each raw data frame contains 54 bytes valid data but is padded by zero to 64 bytes in length with the last 2 bytes for CRC checksum inclusive.

Table C-1 Raw data frame structures.

*Name	ID	TS	Gyro	Acc	Mag	Res	AP	AT	LC	QT
Data Type	Uint8	Uint64	Int16	Int16	Int16	Uint8	Uin24	Int16	Uint24	Float32 x 4
Size (Byte)	1	8	6	6	6	3	3	2	3	16

*ID: device's identity number, TS: timestamps in milliseconds, Gyro: Gyroscope, Acc: Accelerometer, Mag: Magnetometer, Res: Resolution (scales) of gyroscope, accelerometer and magnetometer, AP: Atmospheric Pressure, AT: Atmospheric Temperature, LC: Load Cell, QT: orientation in quaternion.

The data format for CSV file recorded by SmartBand App is shown in.Table C-2

Table C-2 CSV file recorded by SmartBand App

Label	*Sensor addr*	*timestamps*	*gyro x*	*gyro y*	*gyro z*	*acc x*	*acc y*	*acc z*	*mag x*	*mag y*	*mag z*	*pressure*	*force*	*q1*	*q2*	*q3*	*q4*
Data Type	Strings	Uint64	Float	Float	Float	Float	Float	Float	Float	Float	Float	Float	Float	Float	Float	Float	Float

Appendix D Sensor Calibration of Experimental System

D.1 Sensor Calibration

There are many sensors inside the sensorised handle of the experimental system, most of them are based on MEMS technology, including a gyroscope, an accelerometer, a magnetometer, and a barometer. Besides, the load cell sensor, which consists of four strain gauges in a Wheatstone bridge configuration. All of them requires calibration before measuring correctly.

The IMU sensors used here are based on MEMS technology. In an ideal IMU sensor, the tri-axial cluster should be the same 3D orthogonal sensitivity axes that span in a 3D space, as well as the same scale factor. However, these low-cost MEMS sensors suffer more variance than traditional IMU sensors results in inaccurate scaling, axis misalignments, cross-axis sensitivities, and non-zero biases. Therefore, the calibration on the IMU sensor is needed. In the following section, each sensor is calibrated except the barometer which is already calibrated by the manufacturer during its production.

D.1.1 Inertial Measurement Unit

The misalignment and cross-axis sensitivities of the MEMS sensor are not mentioned in the selected sensor [154]. The bias for gyroscope is ±10 dps and the bias for the accelerometer is ±40mg. Temperatures sensitivity is relatively small with ±1% for accelerometer and ±1% for gyroscope from -40°C to +85°C. Considering the experiment environment usually is in room temperature, the sensor can be considered stable. Therefore, ignoring the misalignment error, cross-axis sensitivities and the temperatures sensitivity, the gyroscope can be described by the model:

$$\begin{bmatrix} d_{gx} \\ d_{gy} \\ d_{gz} \end{bmatrix} = \begin{bmatrix} G_{gx} & 0 & 0 \\ 0 & G_{gy} & 0 \\ 0 & 0 & G_{gz} \end{bmatrix} \left(\begin{bmatrix} d_{rgz} \\ d_{rgz} \\ d_{rgz} \end{bmatrix} - \begin{bmatrix} b_{gx} \\ b_{gy} \\ b_{gz} \end{bmatrix} \right) \quad \text{(D-1)}$$

In (D-1), d_{gx}, d_{gy}, d_{gz} represent the ideal measurement result of the sensor; d_{rgx}, d_{rgy}, d_{rgz} represent the actual output by the sensor. G_{gx}, G_{gy}, G_{gz} are the gains of each axis; b_{gx}, b_{gy}, b_{gz} are the bias of each axis. The calibration of the gyroscope is divided into 2 steps.

The first step is to measure the biases of each axis. To measure the biases in the gyroscope, the measurement is recorded for 10 seconds while the sensors are stationary. However, the temperature changed by the thermal release by other components such as power chips and microcontroller might affect the measurement. Therefore, the calibration was performed after the circuit board is powered on for 10 minutes to reduce the effect of heating. By looking into the measurement during the calibration, 10 minutes is an acceptable time to ensure the data is stable. The data is collected for 1 minute. The means of the measurements are the biases of each axis.

The second step is to calculate the gains of each axis. To calculate the gains, we need a controllable rotating platform which can rotate at a constant speed. In the calibration, a turntable is introduced to provide stable rotation as the reference. The turntable is the rotating platform of a phonograph which can provide multiple constant rotations. A 3D printed frame is then used for mounting the circuit board onto an orthogonal cube which can be fixed on to the rotating disc. In this way, we measured the positive and negative rotation of every axis in a constant rotating speed. The same power-up process in the first step is also performed in the second step. The system will first power up for 10 minutes, then the actual calibration is performed for 1 minute.

The same model is also used in the accelerometer calibration. An accelerometer is an electromechanical device used to measure acceleration forces. Such forces may be static, like the continuous force of gravity or, as is the case with many mobile devices,

dynamic to sense movement or vibrations. Acceleration is the measurement of the change in velocity divided by time.

$$\begin{bmatrix} d_{ax} \\ d_{ay} \\ d_{az} \end{bmatrix} = \begin{bmatrix} G_{ax} & 0 & 0 \\ 0 & G_{ay} & 0 \\ 0 & 0 & G_{az} \end{bmatrix} \left(\begin{bmatrix} d_{rax} \\ d_{ray} \\ d_{raz} \end{bmatrix} - \begin{bmatrix} b_{ax} \\ b_{ay} \\ b_{az} \end{bmatrix} \right) \quad \text{(D-2)}$$

In (D-2), d_{ax}, d_{ay}, d_{az} represent the ideal measurement result of the sensor; d_{rax}, d_{ray}, d_{raz} represent the actual output by the sensor. G_{ax}, G_{ay}, G_{az} are the gains of each axis; b_{ax}, b_{ay}, b_{az} are the bias of each axis. The calibration of the accelerometer was performed by an orthogonal cube and a table which is adjusted to horizontal by a level. The circuit board is mounted on the cube. After powered up for 10 minutes, in proper order, collect the accelerometer data from 6 faces, each one was faced to the ground. The biases then can be calculated by positive value plus negative value. The gain is calculated by dividing the magnitude by gravity.

After calibration, the results of the above parameters are written into the firmware. The results are listed in Table D-1. For gyroscope, the range is set to ±1000dps, thus the gains are for converting the raw data to degrees per second. For the accelerometer, the range is set to ±8G. Thus the gains are for converting raw data to unit gravity.

Table D-1 Calibration results for gyroscope and accelerometer

Gyroscope	*Value*	*Accelerometer*	*Value*
G_{gx}	3336.09214	G_{ax}	4113.2107
G_{gy}	3315.430283	G_{ay}	4090.90895
G_{gz}	3320.939663	G_{az}	4097.68905
b_{gx}	78.8308	b_{ax}	-28.3004
b_{gy}	-223.0551	b_{ay}	68.1639
b_{gz}	-156.763	b_{az}	-229.1807

D.1.2 Magnetometer

A simple calibration is performed for the soft ion distortion and hard ion distortion which is shown by (3).

$$\begin{bmatrix} d_{mx} \\ d_{my} \\ d_{mz} \end{bmatrix} = \begin{bmatrix} 1 & 0 & 0 \\ 0 & \frac{G_{my}}{G_{mx}} & 0 \\ 0 & 0 & \frac{G_{mz}}{G_{mx}} \end{bmatrix} \left(\begin{bmatrix} d_{rmx} \\ d_{rmy} \\ d_{rmz} \end{bmatrix} - \begin{bmatrix} b_{mx} \\ b_{my} \\ b_{mz} \end{bmatrix} \right) \tag{D-3}$$

In (D-3), d_{mx}, d_{my}, d_{mz} represent the ideal measurement result of the sensor; d_{rmx}, d_{rmy}, d_{dmz} represent the actual output by the sensor. G_{mx}, G_{my}, G_{mz} are the gains of each axis; b_{mx}, b_{my}, b_{mz} are the maximum measurement in all direction of each axis. The calibration of the magnetometer is similar to gyroscope and accelerometer, except the gains are different, and the biases are determined differently. The bias b_m is defined by the half of the sum of maximum and minimum measurement in each axis. In one of the axes, the gain is set to 1 constantly, while other axes use the scale of the axis for its gain. To calibrate, the sensorised handle was rotated manually in all possible direction for 5 minutes. The calibration results are shown in Table D-2.

Table D-2 Magnetometer calibration results

Parameters	*Value*
G_{mx}	1.0
G_{my}	0.991480611
G_{mz}	1.026459854
b_{mx}	402.5
b_{my}	1863.983549
b_{mz}	-2740.64781

D.1.3 Load Cell Sensor

The load cell is a full-bridge resistance network and it is measured by a specific weight driver (HX711). The load cell can be described as a linear model in (D-4).

$$d_m=G(d_r-b) \tag{D-4}$$

In the model, d_m represents the ideal result by load cell sensor; d_r is the real output of the sensor; G is the gain and b is the bias.

The calibration of the load cell sensor is to measure a constant weight. The weights that used to calibrate is 5kg. Firstly, the load cell is zero calibrated without load. After that, the 5kg weight was put on the load cell and record the measurement. Then the results were averaged and divided by the gravity of 5kg to get the gain. The calibration process was repeated for 5 times and the results were averaged to improve the accuracy. Additionally, the calibration of load cell sensor does not need to follow the 10 minutes' power-up procedure due to the load power of load cell measurement and the load cell is not integrated on the main circuit board and therefore not affected by the heating.

The calibration result shows the gain from raw data to kg $G=5835.9$ and the bias $b = 8265300$.

Appendix E Schematics and Layouts of WBR-SH2

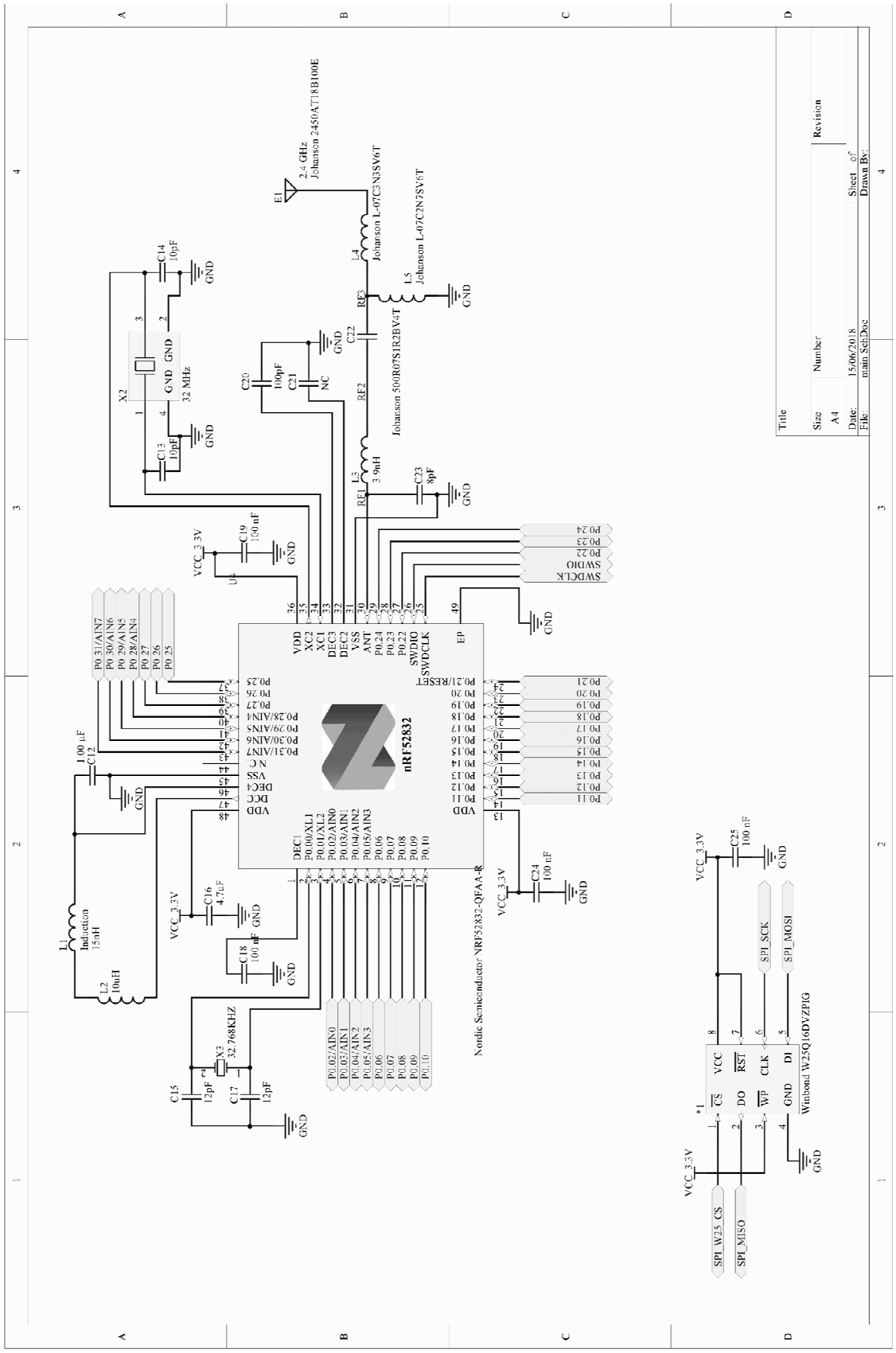
nRF52832
Nordic Semiconductor nRF52832-QFAA-R
Winbond W25Q16DVZPIG
2.4 GHz
Johanson 2450AT18B100E
Johanson L-07C3N3SV6T
Johanson L-07C2N7SV6T
Johanson 500R07S1R2BV4T
32 MHz
32.768KHZ
Induction
15nH
10uH
3.9nH
1.00 µF
4.7uF
100 nF
10pF
12pF
8pF
VCC_3.3V
GND
SWDCLK
SWDIO
SPI_SCK
SPI_MOSI
SPI_W25_CS
SPI_MISO
Title
Size
Number
Revision
A4
Date:
15/06/2018
Sheet of
File:
main.SchDoc
Drawn By:

Figure E-1 Circuit schematics of WBR-SH2 motherboard (1/5).

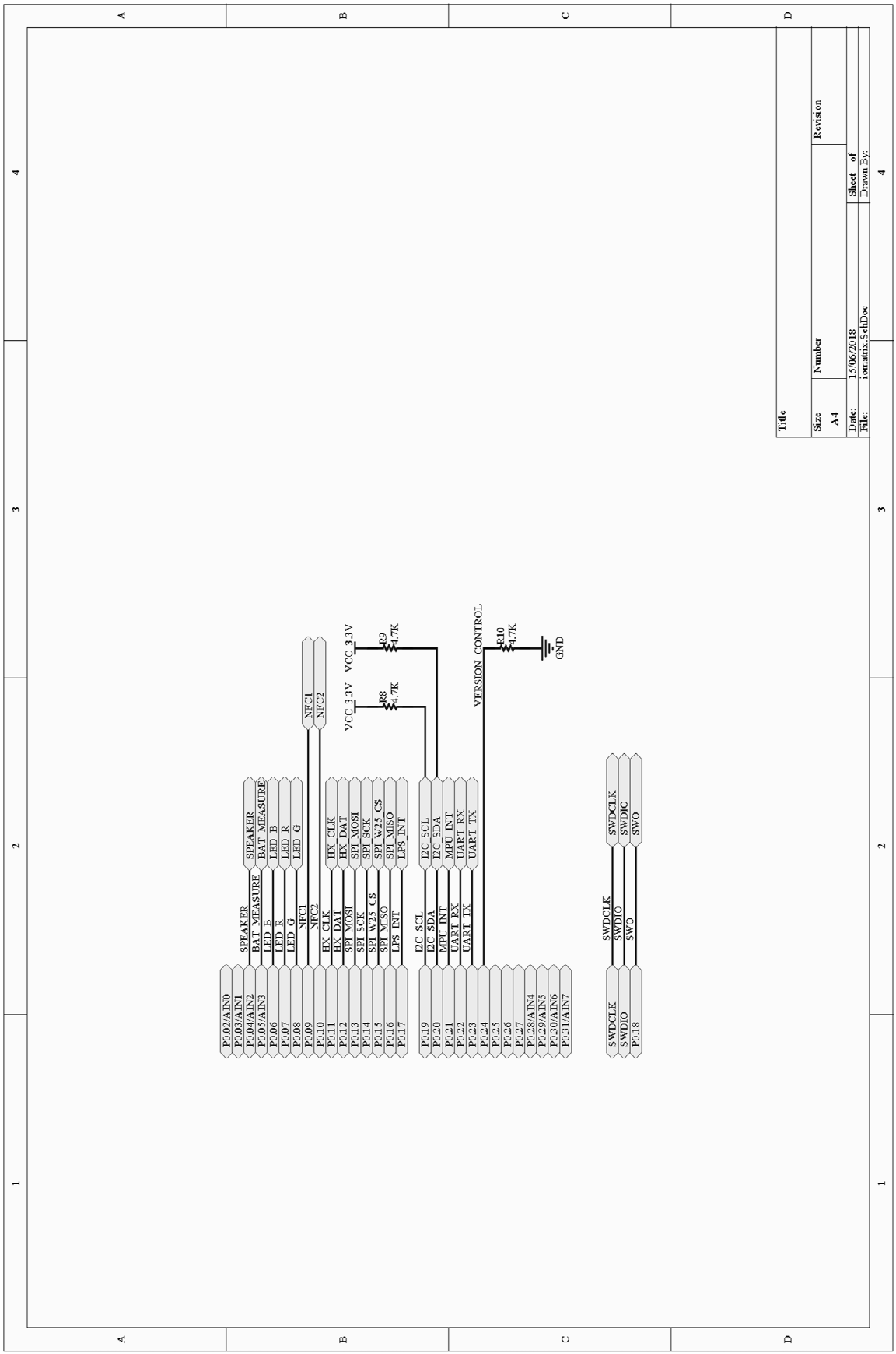
P0.02/AIN0
P0.03/AIN1
P0.04/AIN2
P0.05/AIN3
P0.06
P0.07
P0.08
P0.09
P0.10
P0.11
P0.12
P0.13
P0.14
P0.15
P0.16
P0.17
P0.19
P0.20
P0.21
P0.22
P0.23
P0.24
P0.25
P0.26
P0.27
P0.28/AIN4
P0.29/AIN5
P0.30/AIN6
P0.31/AIN7
SWDCLK
SWDIO
P0.18
SPEAKER
BAT_MEASURE
LED_B
LED_R
LED_G
NFC1
NFC2
HX_CLK
HX_DAT
SPI_MOSI
SPI_SCK
SPI_W25_CS
SPI_MISO
LPS_INT
I2C_SCL
I2C_SDA
MPU_INT
UART_RX
UART_TX
VERSION_CONTROL
SWDCLK
SWDIO
SWO
VCC_3.3V
R8
4.7K
VCC_3.3V
R9
4.7K
R10
4.7K
GND
Title
Size
A4
Number
Revision
Date:
15/06/2018
Sheet of
File:
iomatrix.SchDoc
Drawn By:

Figure E-2 Circuit schematics of WBR-SH2 motherboard (2/5).

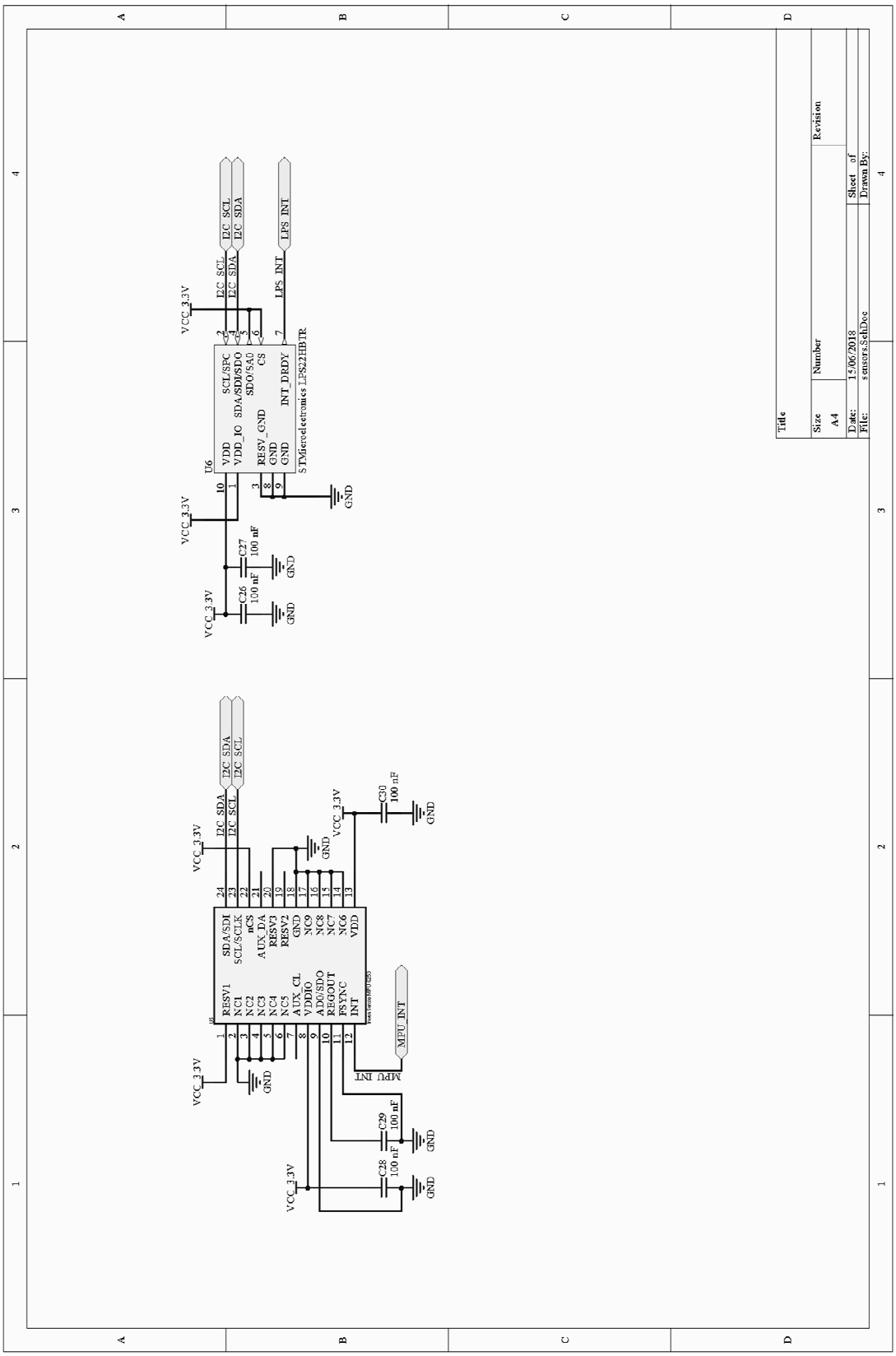

Figure E-3 Circuit schematics of WBR-SH2 motherboard (3/5).

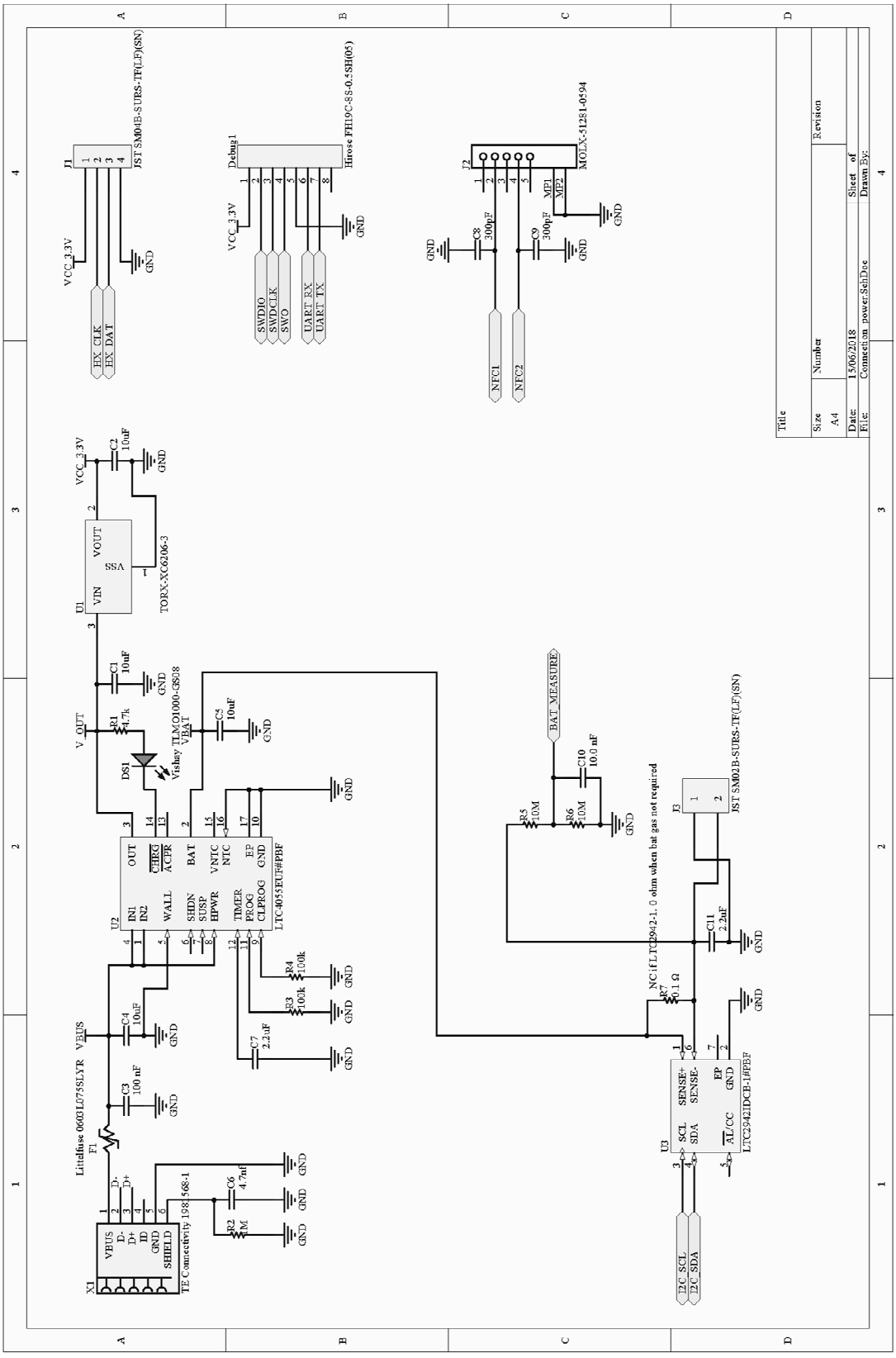

Figure E-4 Circuit schematics of WBR-SH2 motherboard (4/5).

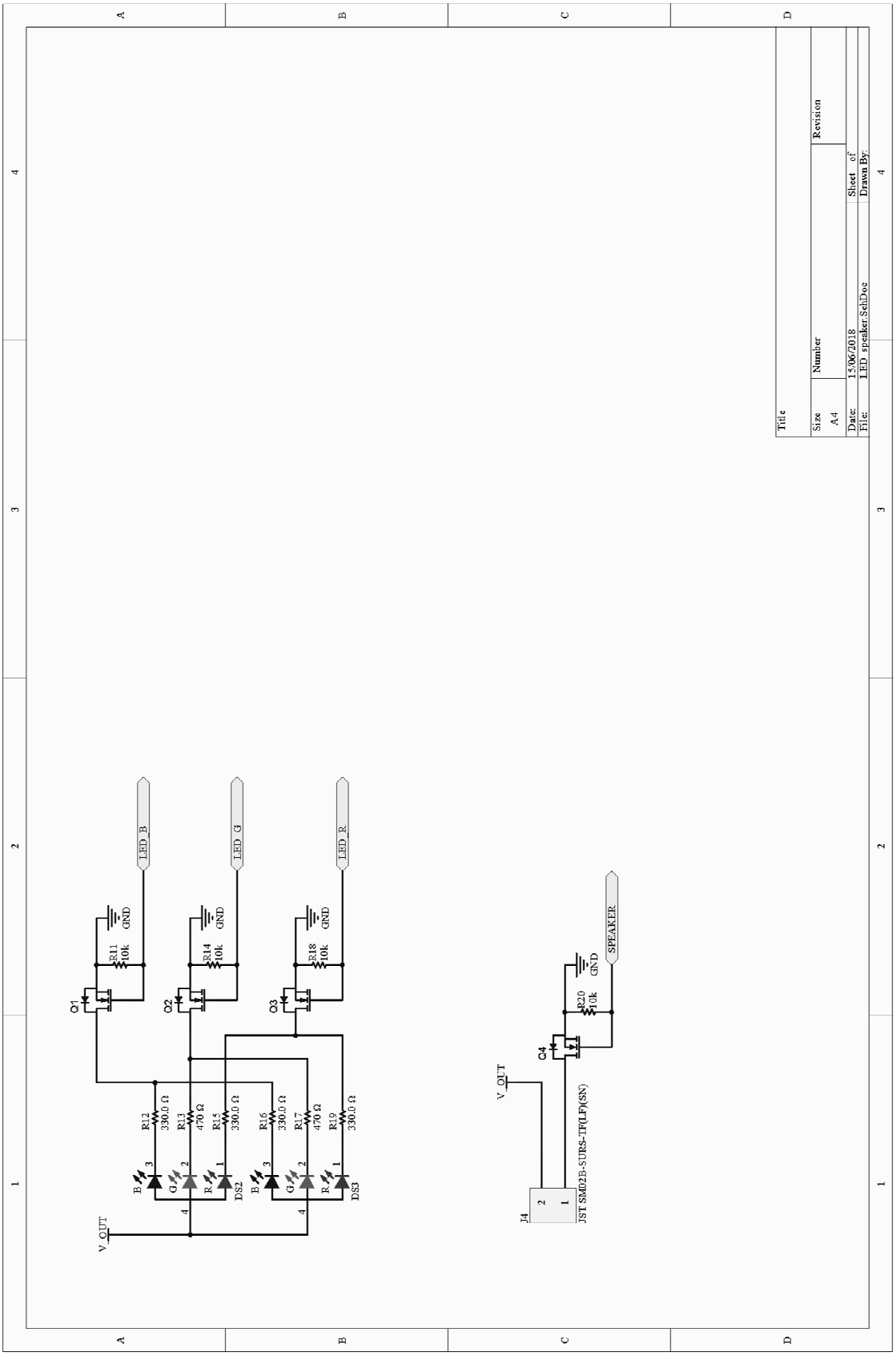
LED_B
LED_G
LED_R
SPEAKER
GND
R11 10k
R14 10k
R18 10k
R20 10k
Q1
Q2
Q3
Q4
R12 330.0 Ω
R13 470 Ω
R15 330.0 Ω
R16 330.0 Ω
R17 470 Ω
R19 330.0 Ω
DS2
DS3
V_OUT
J4
JST SM02B-SURS-TF(LF)(SN)
Title
Size A4
Number
Revision
Date: 15/06/2018
File: LED speaker.SchDoc
Sheet of
Drawn By:

Figure E-5 Circuit schematics of WBR-SH2 motherboard (5/5).

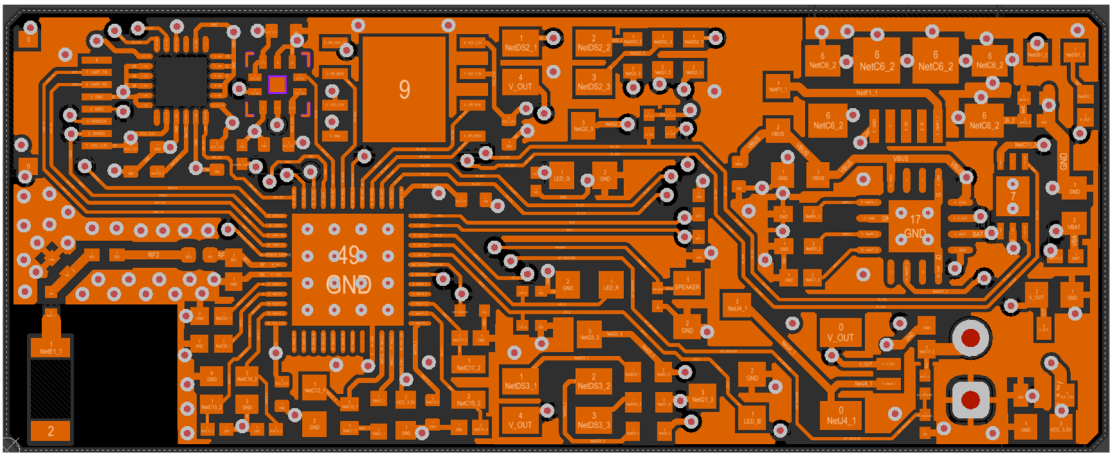

Figure E-6 Top-layer layout of WBR-SH2 motherboard.

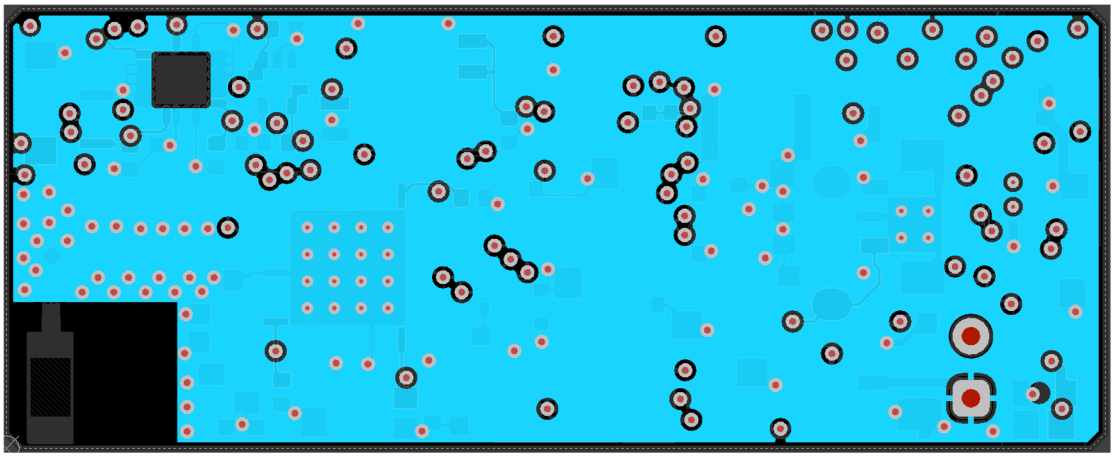

Figure E-7 Ground-layer layout of WBR-SH2 motherboard.

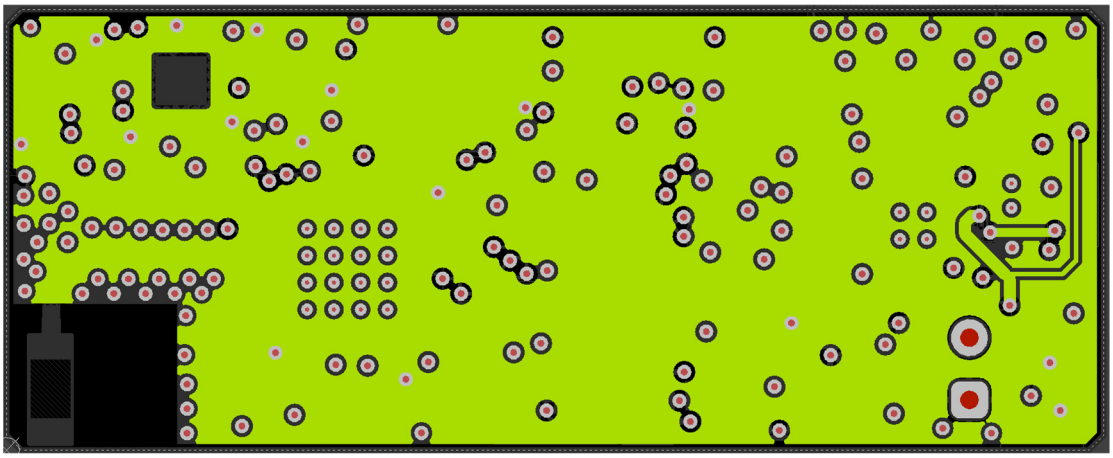

Figure E-8 Power-layer layout of WBR-SH2 motherboard.

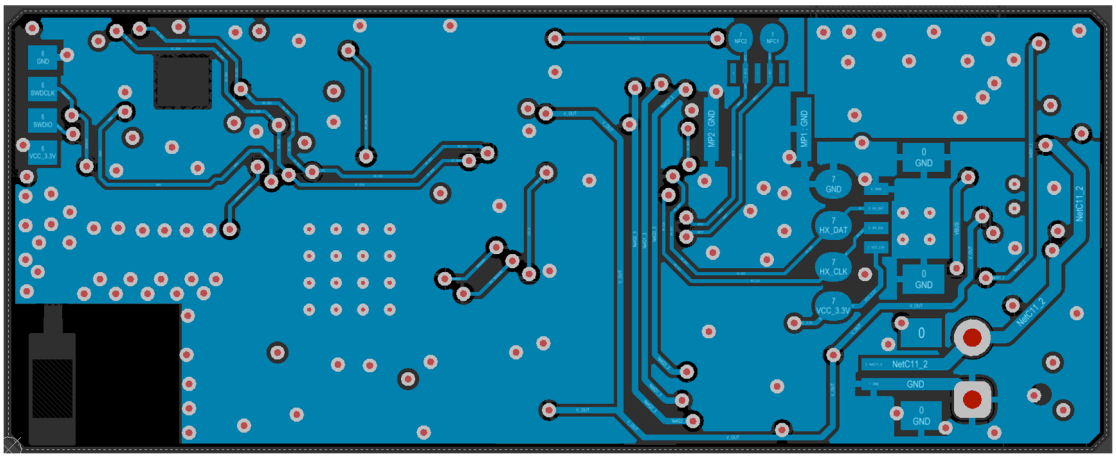

Figure E-9 Bottom-layer layout of WBR-SH2 motherboard.

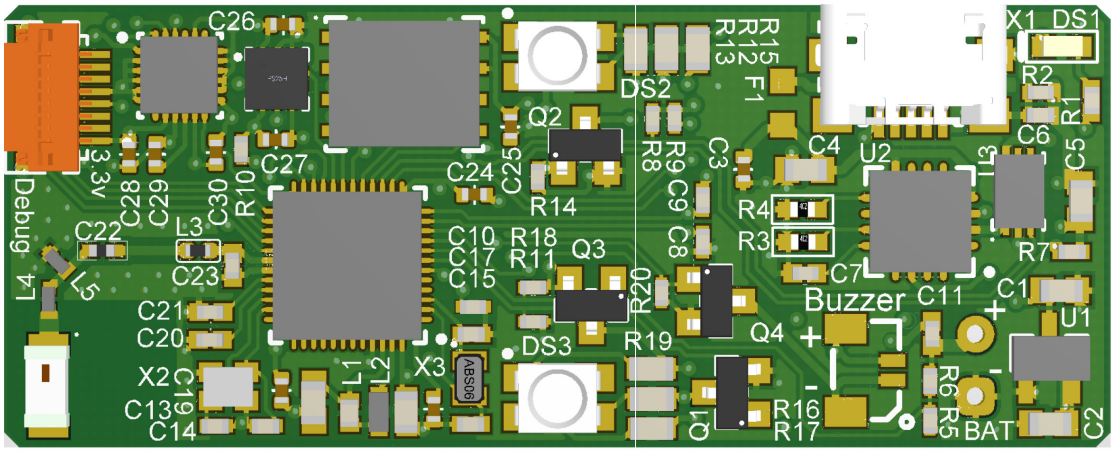

Figure E-10 Assembly of WBR-SH2 motherboard.

Appendix F User Feedback of WBR-SH2 and Resistance Band Exercise

Feedback for resistance band exercise

1. Elastico troppo lungo
2. Paura che scivoli da sotto il piede nell'ultimo esercizio
3. Le persone anziane tendono a modificare l'esercizio gli ultimi secondi di esecuzione
4. Negli anziani, non tutti, problemi nel ruotare il bacino a destra e sinistra nel primo esercizio, senza utilizzare le braccia
5. Terzo esercizio difficile da capire come esecuzione, dato che molti compiono il movimento per fare meno fatica
6. Esercizi complicati per anziani che non fanno attività fisica
7. Uomini più in difficoltà delle donne

English (translation)

1. Elastic too long
2. Fear that the band slips from under the foot in the last exercise
3. Older people tend to modify the exercise during the last seconds of execution
4. In some of the elderly, there are problems in rotating the pelvis right and left in the first exercise, without using the arms
5. The third exercise is difficult to understand in terms of execution, as many subjects perform the movement to make it less physically demanding
6. The exercises are complicated for elderly people who do not exercise
7. Men are in greater difficulty than women

Appendix G List of Publications

J. Ma, S. Ward, R. Sers and M. Zecca, “Introduction of an Open Source Compact Neural Network Framework on Microcontroller (NNoM)” (to be submitted to *Ad Hoc Networks*)

J. Ma, S. Ward, R. Sers, D. Magistro and M. Zecca, “Continuous Synchronisation of Connection-Oriented Bluetooth Low Energy Network with Stock Android Device” (to be submitted to *SoftwareX*)

J. Ma, E. Hogervorst, D. Magistro, V. Chouliaras, and M. Zecca, “Development of Sensorised Resistance Band for Objective Exercise Measurement: Activities Classification Trial,” in *Conf Proc IEEE Eng Med Biol Soc EMBC*2018, vol. 2018–July, pp. 3942–3945.

J. Ma, D. Magistro, and M. Zecca, “Distributed Sensor Synchronization using Bluetooth Low Energy with Unmodified Android Device,” in *International Conference on Neurorehabilitation*, 2018.

J. Ma and M. Zecca, “Development of a portable sensorised handle for the objective assessment of the effectiveness and concordance of intervention plans in dementia,” in *Conf Proc IEEE Eng Med Biol Soc EMBC2017*, 2017, pp. 2337–2340.

R. Sers, S. Forrester, E. Moss, S. Ward, **J. Ma** and M. Zecca, “Validity of the Perception Neuron Inertial Motion Capture System for Upper Body Motion Analysis”, *Measurement* (J. Ma contributed on data processing and visualisation)